

NASA  
TP  
1353  
c.1

# NASA Technical Paper 1353

LOAN COPY: RETURN TO  
AFWL TECHNICAL LIBRARY  
KIRTLAND AFB, N. M.  
0134390

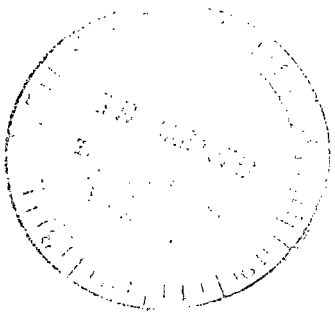


## An Experimental Wind-Tunnel Investigation of a Ram-Air-Spoiler Roll-Control Device on a Forward- Control Missile at Supersonic Speeds

A. B. Blair, Jr.

DECEMBER 1978

NASA





0134390

## NASA Technical Paper 1353

# An Experimental Wind-Tunnel Investigation of a Ram-Air-Spoiler Roll-Control Device on a Forward- Control Missile at Supersonic Speeds

A. B. Blair, Jr.  
*Langley Research Center  
Hampton, Virginia*



National Aeronautics  
and Space Administration

**Scientific and Technical  
Information Office**

1978

## SUMMARY

A parametric experimental wind-tunnel investigation has been made at supersonic Mach numbers to provide design data on a ram-air-spoiler roll-control device that is to be used on forward-control cruciform missile configurations.

The results indicate that the ram-air-spoiler tail fin is an effective roll-control device and that roll control is generally constant with vehicle attitude and Mach number unless direct canard and/or forebody shock impingement occurs. The addition of the ram-air-spoiler tail fins resulted in only small changes in aerodynamic-center location. For the ram-air-spoiler configurations tested, there are large axial-force coefficient effects associated with the increased fin thickness and ram-air momentum loss.

## INTRODUCTION

It is well documented that missile configurations which utilize forward surfaces to provide control experience the problem of induced rolling moments at supersonic Mach numbers. (See refs. 1 to 3.) The data from some of these configurations tend to indicate that the problem is associated with an interference effect of the deflected forward surface on one or more of the trailing fins. For these forward-control configurations, it is necessary either to reduce or eliminate the induced rolling moments or to provide an efficient system for their control.

One of several approaches to the solution of these problems has been studied and the preliminary aerodynamic results are encouraging. The approach, which is described in reference 4, uses a ram-air-spoiler roll-control device on a typical canard-controlled missile configuration to compensate for the unwanted induced rolling moments. The ram-air-spoiler concept evolved from earlier research of aerodynamic control devices with low actuator torque requirements; this work was performed by NASA and its predecessor, NACA. (See refs. 5 to 8.) In addition, the feasibility of interfacing a ram-air-spoiler system with an all fluidic-logic roll-control system has been investigated. (See refs. 9 and 10.)

A preliminary study has indicated that the ram-air-spoiler roll-control device is a feasible aerodynamic concept for providing roll stabilization on a canard-controlled missile. (See ref. 11.) In order to expand the technology base of the preliminary study and to provide the comprehensive aerodynamic data base required to confidently assess the merits of ram-air-spoiler systems, a parametric experimental wind-tunnel investigation has been conducted. The purpose of this paper is to present the results of that investigation. A summary of the significant findings can be found in reference 12. The study included model configurations which represented the ram-air-spoiler devices operating on a typical canard-controlled missile at zero and maximum roll control,

as well as a comparison with conventional aileron controls all at various missile maneuvering attitudes and Mach numbers.

The tests were conducted in the Langley Unitary Plan wind tunnel at Mach numbers from 1.60 to 4.63. The nominal angle-of-attack range was from  $-2^\circ$  to  $28^\circ$  at model roll angles of  $0^\circ$ ,  $22.5^\circ$ , and  $45^\circ$  for a Reynolds number of  $6.6 \times 10^6$  per meter ( $2.0 \times 10^6$  per foot).

#### SYMBOLS AND ABBREVIATIONS

The aerodynamic coefficient data are referred to the body axis system except for lift and drag which are referred to the stability axis system. The moment reference was located aft of the nose tip at 48.9 percent of the body length.

Measurements and calculations were made in the U.S. Customary Units. Measurements are presented in the International System of Units (SI), with the equivalent values given parenthetically in U.S. Customary Units. (See ref. 13.)

A	reference area, maximum cross-sectional area of model body, $0.004560 \text{ m}^2$ ( $0.049087 \text{ ft}^2$ )
$A_e$	total jet-exit slot area of one ram-air-spoiler tail fin, $\text{m}^2$ ( $\text{ft}^2$ )
$A_i$	cross-sectional area of one ram-air-spoiler inlet, $\text{m}^2$ ( $\text{ft}^2$ )
$C_A$	axial-force coefficient, $\frac{\text{Axial force}}{qA}$
$C_{A,c}$	balance-chamber axial-force coefficient, $\frac{\text{Chamber axial force}}{qA}$
$C_D$	drag coefficient, $\frac{\text{Drag}}{qA}$
$C_{D,c}$	balance-chamber drag coefficient, $C_{A,c} \cos \alpha$
$C_L$	lift coefficient, $\frac{\text{Lift}}{qA}$
$C_l$	rolling-moment coefficient, $\frac{\text{Rolling moment}}{qAd}$

$C_m$	pitching-moment coefficient, $\frac{\text{Pitching moment}}{qAl}$
$C_N$	normal-force coefficient, $\frac{\text{Normal force}}{qA}$
$C_n$	yawing-moment coefficient, $\frac{\text{Yawing moment}}{qAd}$
$C_Y$	side-force coefficient, $\frac{\text{Side force}}{qA}$
$d$	reference diameter, 7.620 cm (3.000 in.)
L.E.	leading edge
$l$	reference body length, 91.973 cm (36.210 in.)
M	free-stream Mach number
$P_{t,2}$	total pressure behind normal shock, Pa (psfa)
p	free-stream static pressure, Pa (psfa)
q	free-stream dynamic pressure, Pa (psfa)
$S_a/S_{exp}$	ratio of tail-fin aileron area to total exposed planform tail-fin area for one surface
T.E.	trailing edge
t/c	tail-fin thickness ratio at root chord
$x_{ac}/l$	aerodynamic-center location as fraction of model length, measured from nose tip
$\alpha$	angle of attack, deg
$\delta_j$	streamwise angle between center line of jet-exit slot and tail-fin surface, deg (see fig. 1(b))
$\Delta C_l$	incremental rolling-moment coefficient due to controls
$\delta_{roll}$	roll-control deflection of four tail-fin ailerons; positive to provide clockwise rotation as viewed from rear, deg

$\delta_{yaw}$	yaw-control deflection of canards; positive for leading edge right as viewed from rear; vertical canards deflected for $\phi = 0^\circ$ , deg
$\phi$	model roll angle; positive for clockwise roll angle when viewed from rear; for $\phi = 0^\circ$ , canards and tails are in vertical and horizontal planes, deg

## APPARATUS AND TESTS

### Wind Tunnel

Tests were conducted in both the low and high Mach number test sections of the Langley Unitary Plan wind tunnel, which is a variable-pressure, continuous-flow tunnel. The test sections are approximately 2.13 m (7 ft) long and 1.22 m (4 ft) square. The nozzles leading to the test sections are of the asymmetric sliding-block type, which permits continuous variations in Mach number from about 1.5 to 2.9 in the low Mach number test section and from about 2.3 to 4.7 in the high Mach number test section. (See ref. 14.)

### Model Concept

To simulate the concept of an operating control system, the ram-air-spoiler tail fins operated in the following manner. Free-stream air is directed into each tail-fin plenum by a tip-mounted normal-shock inlet and is expelled through slots on one side only near the trailing edge of the fin in a direction normal to the surface. The expelling air produces a jet normal force that interacts strongly with the local stream flow and results in a total force (reaction) that, at supersonic speeds, is several times larger than the pure reaction force of the jet. The aerodynamic jet interaction is physically similar to a ramp-wedge or step-induced turbulent boundary-layer separation on a flat plate at supersonic speeds. For the present investigation, the ram-air-spoiler tail fins were used only for roll control.

Details of the model are shown in figure 1. To evaluate the ram-air spoiler as a roll-control system, a general research missile model was chosen as the basic vehicle (fig. 1(a)). This model is a cruciform missile configuration that consists of a cylindrical body with a modified ogive nose, canards, and aft tail fins mounted in line. The canards and plain tail fins have trapezoidal planforms with beveled leading- and trailing-edge airfoil sections. For the major portion of these tests, the model had four ram-air-spoiler tail fins with generally the same planform geometry but with different thickness ratios  $t/c$  than the plain tail fins. Model photographs are presented in figure 2.

The ram-air-spoiler tail fins had nacelles mounted on the tip chord with simple normal-shock inlets and removable nacelle exit plugs. The most significant parameter of this investigation was inlet size. Three inlet areas ( $A_i/A = 0.028, 0.063$ , and  $0.111$ ) were tested to provide variations in mass flow (fig. 1(b)). With increases in inlet diameters, corresponding increases

in fin thickness ratios  $t/c$  were necessary to make the plenum entrance as large as possible in order to prevent internal flow restrictions (choked flow). Several ratios of exit area to inlet area ( $A_e/A_i = 0.50, 0.75, \text{ and } 0.90$ ) were investigated to produce positive rolling moment, with each ram-air-spoiler tail-fin configuration having plugged nacelle exits. (See fig. 1(b) and tables I and II.) For each configuration, these ratios were obtained from an arbitrary selection of different exit areas (by using interchangeable slotted cover plates) combined with a constant inlet cross-sectional area. For the majority of these tests, the plenum jet-exit slot angle was normal to the fin surface (e.g.,  $\delta_j = 90^\circ$ ); however, a limited amount of testing was done on the  $A_e/A = 0.028$  configuration with the slot angle inclined forward ( $\delta_j = 50^\circ$ ). Flow-through nacelle configurations were obtained by removing the nacelle exit plugs and substituting cover plates for slotted exit plates on the ram-air-spoiler tail fins.

The tests were conducted in the following sequence. To simulate an operating ram-air-spoiler system with closed control valves, ram-air-spoiler tail fins with three inlet diameters were investigated. Each of these configurations had plugged nacelle exits and utilized the most effective roll-control area ratios from reference 11 and unpublished data. The flow-through nacelle configuration simulated the nonoperating ram-air-spoiler control with an open control valve. For roll-control comparisons, plain tail fins were tested with conventional trailing-edge ailerons. (See fig. 1(c) and table I.) The aileron size was chosen to be approximately the same fin area as would nominally be affected by spoiler action of the ram-air-spoiler configurations ( $S_a/S_{exp} = 0.11$ ). Arbitrary deflection angles of  $0^\circ$  and  $10^\circ$  were made on each of the four fins to provide positive rolling moments for all comparisons made in the current study.

#### Test Conditions

Tests were performed at the following tunnel conditions:

Mach number	Stagnation temperature		Stagnation pressure		Reynolds number	
	K	°F	kPa	psfa	per meter	per foot
1.60	339	150	54.6	1141	$6.6 \times 10^6$	$2.0 \times 10^6$
1.80	339	150	58.5	1221	6.6	2.0
2.16	339	150	68.5	1430	6.6	2.0
2.96	339	150	103.9	2169	6.6	2.0
4.63	353	175	252.6	5275	6.6	2.0

The dewpoint temperature measured at stagnation pressure was maintained below 239 K ( $-30^\circ$  F) to assure negligible condensation effects. All tests were performed with boundary-layer transition strips measured streamwise on the outside of the nacelle inlets and on both sides of the canard and tail fin sur-

faces and placed on the body 3.05 cm (1.20 in.) aft of the nose and 1.02 cm (0.40 in.) aft of the leading edges. The transition strips were approximately 0.157 cm (0.062 in.) wide and were composed of No. 50 sand grains sprinkled in acrylic plastic for the tests at  $M = 1.60$  to  $M = 2.16$ . For the tests at higher Mach numbers, transition strips were composed of individual grains of No. 40 sand with a nominal height of 0.046 cm (0.018 in.) and were spaced about 0.184 cm (0.072 in.) between centers measured perpendicular to the airstream. (See ref. 15.) The model was tested over an angle-of-attack range from  $-2^\circ$  to  $28^\circ$  for roll angles of  $0^\circ$ ,  $22.5^\circ$ , and  $45^\circ$ .

### Measurements and Corrections

Aerodynamic forces and moments on the model were measured by means of a six-component electrical strain-gage balance which was housed within the model. The balance was attached to a sting which was, in turn, rigidly fastened to the model support system. Balance-chamber pressure was measured by means of a single static-pressure orifice located in the vicinity of the balance.

The angles of attack have been corrected for deflection of the balance and sting due to aerodynamic loads and tunnel-flow misalignment. The drag and axial-force coefficients have been adjusted to correspond to free-stream static pressure acting over the base of the model. Typical measured values of chamber axial-force and drag coefficients for the  $A_i/A = 0.063$  and plain tail-fin configurations are presented in figure 3.

### PRESENTATION OF RESULTS

Figure

Effect of ratio of plenum exit area to inlet area for roll control or lateral aerodynamic characteristics of model with ram-air-spoiler tail fins for $A_i/A = 0.028$ at -	
$\phi = 0^\circ$ . . . . .	4
$\phi = 22.5^\circ$ . . . . .	5
$\phi = 45^\circ$ . . . . .	6
Effect of ratio of plenum exit area to inlet area for roll control on lateral aerodynamic characteristics of model with ram-air-spoiler tail fins for $A_i/A = 0.063$ at -	
$\phi = 0^\circ$ . . . . .	7
$\phi = 22.5^\circ$ . . . . .	8
$\phi = 45^\circ$ . . . . .	9
Effect of ratio of plenum exit area to inlet area for roll control on lateral aerodynamic characteristics of model with ram-air-spoiler tail fins for $A_i/A = 0.111$ at -	
$\phi = 0^\circ$ . . . . .	10
$\phi = 22.5^\circ$ . . . . .	11
$\phi = 45^\circ$ . . . . .	12

Figure

Effect of four plain tail-fin ailerons on lateral aerodynamic characteristics of model at -	
$\phi = 0^\circ$ . . . . .	13
$\phi = 22.5^\circ$ . . . . .	14
$\phi = 45^\circ$ . . . . .	15
Summary of effects of ram-air-spoiler inlet and plenum exit size on roll control at $\phi = 45^\circ$ and $\alpha = 0^\circ$ . . . . .	16
Summary of angle-of-attack effects on ram-air-spoiler and plain tail-fin aileron roll control . . . . .	17
Summary of Mach number effects on ram-air-spoiler and plain tail-fin aileron roll control . . . . .	18
Effect of ram-air-spoiler roll control on lateral aerodynamic characteristics of model with canard yaw control . . . . .	19
Effect of plenum jet-exit slot angle on lateral aerodynamic characteristics of model with ram-air-spoiler tail fins for $A_i/A = 0.028$ and $A_e/A_i = 0.75$ at -	
$\phi = 0^\circ$ . . . . .	20
$\phi = 22.5^\circ$ . . . . .	21
$\phi = 45^\circ$ . . . . .	22
Effect of plenum jet-exit slot angle on longitudinal aerodynamic characteristics of model with ram-air-spoiler tail fins for $A_i/A = 0.028$ and $A_e/A_i = 0.75$ at -	
$\phi = 0^\circ$ . . . . .	23
$\phi = 45^\circ$ . . . . .	24
Effect of inlet size and fin thickness on longitudinal aerodynamic characteristics of model with flow-through nacelle ram-air spoiler and plain tail fins at -	
$\phi = 0^\circ$ . . . . .	25
$\phi = 45^\circ$ . . . . .	26
Effect of ratio of plenum exit area to inlet area for roll control on longitudinal aerodynamic characteristics of model with ram-air-spoiler tail fins for $A_i/A = 0.028$ at -	
$\phi = 0^\circ$ . . . . .	27
$\phi = 45^\circ$ . . . . .	28
Effect of ratio of plenum exit area to inlet area for roll control on longitudinal aerodynamic characteristics of model with ram-air-spoiler tail fins for $A_i/A = 0.063$ at -	
$\phi = 0^\circ$ . . . . .	29
$\phi = 45^\circ$ . . . . .	30

Figure

Effect of ratio of plenum exit area to inlet area for roll control on longitudinal aerodynamic characteristics of model with ram-air-spoiler tail fins for $A_e/A_i = 0.111$ at -	
$\phi = 0^\circ$ . . . . .	31
$\phi = 45^\circ$ . . . . .	32
Summary comparison of total axial-force coefficients and aerodynamic-center locations for each ram-air-spoiler and plain tail-fin configuration with and without roll control at $\phi = 0^\circ$ and $\alpha = 0^\circ$ . . . . .	33
Summary of Mach number effects on total axial-force coefficients and aerodynamic-center locations for each ram-air-spoiler and plain tail-fin configuration with and without roll control at $\phi = 0^\circ$ and $\alpha = 0^\circ$ . . . . .	34
Schlieren photographs of $A_e/A_i = 0.063$ ram-air-spoiler tail-fin configuration at $\phi = 0^\circ$ . . . . .	35

## DISCUSSION

The effect of  $A_e/A_i$  for roll control on the lateral aerodynamic characteristics of the model with each ram-air-spoiler tail-fin configuration tested at roll angles of  $0^\circ$ ,  $22.5^\circ$ , and  $45^\circ$  is presented in figures 4 to 12. In general, with increases in the ratio of exit area to inlet area for each ram-air-spoiler configuration ( $A_e/A_i$ ), there are increases in rolling-moment coefficients. These coefficients are usually accompanied by positive yawing-moment coefficients that increased in magnitude with increases in  $A_e/A_i$  and Mach number. Figures 13 to 15 present the effect of four plain tail-fin ailerons on the lateral aerodynamic characteristics of the model.

To present a more meaningful composite summary for evaluation of the ram-air-spoiler roll-control characteristics, summary cross plots were made from data presented in figures 4 to 15. Incremental roll values  $\Delta C_l$  were obtained by subtracting from the total rolling-moment coefficient of each configuration the rolling-moment coefficients of their respective baseline configurations (e.g.,  $0^\circ$  aileron-deflected data for the plain fin or flow-through nacelle data for the ram-air spoiler). These summary data cross-plot figures are presented and discussed in the following paragraphs.

The effect of inlet and plenum exit size on the roll control of the ram-air-spoiler tail fins for  $\alpha = 0^\circ$  is presented in figure 16. The ram-air-spoiler tail fins are effective roll-producing devices for any of the ratios of exit area to inlet area tested. For a constant inlet size ( $A_i/A$ ), roll control increases with exit-to-inlet area ratio and obtains a maximum test value at  $A_e/A_i = 0.90$ . Figure 16 also indicates that for a given ratio of exit area to inlet area, the rolling-moment coefficient produced by the ram-air spoiler is generally proportional to the inlet area or the mass flow of the spoiler jet.

A summary of the effects of angle of attack on the ram-air-spoiler roll-control characteristics is presented in figure 17. Each ram-air-spoiler tail-fin configuration is presented at  $\phi = 0^\circ$  and  $45^\circ$  with its most effective ratio of exit area to inlet area ( $A_e/A_i = 0.90$ ) for roll control. In addition, the roll control of four plain tail fins having 11-percent-area-ratio ailerons with an arbitrary deflection of  $10^\circ$  is shown to represent typical conventional roll control on a canard-controlled missile. In general, the ram-air-spoiler configurations produced more rolling-moment coefficient than the aileron system except at  $M = 1.60$ . The roll control of the ram-air spoilers is essentially constant both for model roll attitudes of  $0^\circ$  and  $45^\circ$  and over the angle-of-attack range up to about  $12^\circ$ . The angle-of-attack range for  $M = 1.60$  was reduced to prevent model forebody shock reflections off the tunnel wall from impinging on the ram-air-spoiler tail fins. At the higher Mach numbers, some gradual loss in rolling-moment capability would be expected with angle of attack at the higher attitudes as inlet mass flow reduces; however, sharp local losses may be produced when the forebody shock front passes over the lower inlets. Such a loss may be seen in figure 17(c) with the model at  $20^\circ$  angle of attack when strong forebody shocks (a coalescence of the canard and nose shocks) pass over both lower inlets at a model roll angle of  $45^\circ$ . While schlieren photographs portraying the  $45^\circ$  roll case are not available, some insight into the interference phenomena may be gained from schlieren photographs of the model at  $\phi = 0^\circ$ . These photographs are presented as figure 35 and show flow-field effects on the model when the  $A_i/A = 0.063$  ram-air-spoiler tail-fin configuration is operating ( $A_e/A_i = 0.90$ ) and when it is not (flow-through nacelle). It is evident that strong forebody shocks pass over the lower ram-air-spoiler inlet at the higher angles of attack, and shock impingement effects along with mass-flow losses result in the reductions in  $\Delta C_l$  that are shown in figure 17(c) for  $\phi = 0^\circ$ . The designer should be aware of these flow-field effects.

In general, the control effectiveness of any conventional aerodynamic control surface reduces in the supersonic speed range as Mach number increases. The effect of Mach number on the zero-lift ( $\alpha = 0^\circ$ ) roll-control characteristics of the plain tail fins with conventional ailerons and ram-air-spoiler tail fins is shown in figure 18. The roll control of the aileron is about the same as that of the ram-air spoiler with the small inlet ( $A_i/A = 0.028$ ) at  $M = 1.60$  but, as expected, decreases rapidly with increases in Mach number. In general, there is a small decrease in roll control at the lower Mach numbers for the ram-air spoilers with the larger inlets, but increases in Mach number lead to essentially constant control levels for each of the configurations.

To demonstrate the potential capability of the ram-air-spoiler roll control to negate adverse induced rolling moments on the model, a  $10^\circ$  canard yaw-control deflection was used in conjunction with an operating and nonoperating ram-air spoiler. Figure 19 presents the effect of ram-air-spoiler roll control on the lateral aerodynamic characteristics of the model with yaw control. The ram-air-spoiler tail fins are effective in producing rolling-moment coefficients in the presence of adverse flow fields generated by canard deflections.

The effect of plenum jet-exit slot angle on the lateral and longitudinal aerodynamic characteristics of the model with the  $A_i/A = 0.028$  ram-air-spoiler tail fins at  $\phi = 0^\circ$ ,  $22.5^\circ$ , and  $45^\circ$  is presented in figures 20 to 24. There

is a small increase in rolling-moment coefficient and axial-force coefficient when the jet-exit slot angle is inclined forward. (See also ref. 16.) Inclining the jet-exit slot angle forward has a favorable effect on the jet-interaction flow field by separating the boundary layer at a more forward location on the fin surface. An optimized jet angle determined by a trade-off between the increments of rolling moment and axial-force coefficient could result in a more efficient ram-air-spoiler system.

The effect of inlet size and fin thickness on the longitudinal aerodynamic characteristics of the model with plain and nonoperating ram-air-spoiler tail fins (flow-through nacelles) is presented in figures 25 and 26 for  $\phi = 0^\circ$  and  $45^\circ$ , respectively. There is a small increase in stability level and lift-curve slope which is accompanied by large increases in axial-force coefficient that occur with increases in inlet size and fin thickness.

The effect of the ratio of plenum exit area to inlet area for roll control on the longitudinal aerodynamic characteristics of the model with each of the ram-air-spoiler tail-fin configurations tested at  $\phi = 0^\circ$  and  $45^\circ$  is presented in figures 27 to 32. In general, for each  $A_i/A$  ram-air-spoiler configuration there is little difference between the longitudinal aerodynamic characteristics of the nonoperating (flow-through nacelle) and the operating ram-air spoiler except for an increase in axial-force coefficient. Comparisons of  $A_e/A_i$  for each operating ram-air-spoiler configuration ( $A_i/A$ ) indicate only negligible differences in total axial-force coefficients. However, with increases in  $A_i/A$ , a significant increase in axial-force coefficient, accompanied by a small decrease in lift-curve slope at the higher angles of attack, is indicated for the operating ram-air-spoiler configurations.

Figures 33 and 34 present a summary comparison of the total axial-force coefficients and aerodynamic-center locations for each ram-air-spoiler and plain tail-fin configuration with and without roll control. The solid symbols in figure 33 ( $A_i/A = 0$ ) indicate the plain fins with aileron controls at  $0^\circ$  and  $10^\circ$ . As the ram-air-spoiler inlet size increases, the wetted area and fin thickness increase; this tends to shift the aerodynamic center aft. The large increase in axial-force coefficient for the flow-through nacelle is a direct result of fin thickness, an increase in leading-edge bluntness, and cowling geometry. The axial-force coefficient increment between the flow-through and operating curves is due to the ram-air momentum loss in the inlet-duct-plenum manifolds. The dashed line in figure 33 shows that this increment can be accurately estimated by using free-stream tunnel conditions and applying the total pressure behind the normal shock to the inlet area according to the following equation:

$$\Delta C_A = 4A_i(p_{t,2} - p)/qA$$

This equation generally holds true except for the  $A_i/A = 0.111$  configuration ( $t/c = 0.11$ ) at the lower Mach numbers where the tail-fin leading edges are subsonic with standoff shocks. There is a decrease in axial-force coefficient with Mach number for the ram-air spoiler and for plain tail fins with and without roll control (fig. 34). A very small forward shift in aerodynamic center at the lower Mach numbers can also be seen.

The large axial-force penalty associated with the ram-air spoiler could be a serious deficiency when compared with the axial force associated with an aileron. For example, the ram-air spoiler with  $A_1/A = 0.028$  produced about the same roll control at  $M = 1.60$  as the aileron (shown in fig. 18) but had a 36-percent increase in axial-force coefficient, of which 16 percent is attributed just to the flow-through nacelle (nonoperating condition). For a missile system where axial force is of prime importance (longer range), the advantages of lower actuator torque requirements and better roll control at higher numbers might not offset the axial-force penalty of the ram-air spoiler. However, for short-range applications, which are generally thrust dominated, axial force is usually of secondary importance compared with other control characteristics.

For long-range applications at a cruise Mach number, matched inlet design could be obtained for the ram-air spoiler by using oblique lip or spiked inlets to improve total pressure recovery and to reduce axial force at the higher Mach numbers. Careful attention must be given to the overall missile geometry (e.g., nose shape, body fineness ratio, canard and tail-fin planforms) to obtain optimized roll-control performance from ram-air-spoiler tail fins on a canard-controlled missile configuration.

#### CONCLUSIONS

A parametric experimental wind-tunnel investigation has been made at supersonic Mach numbers to provide design data on a ram-air-spoiler roll-control device that is to be used on forward-control cruciform missile configurations. The results of the investigation are as follows:

1. The ram-air-spoiler tail fin is an effective roll-control device and the roll control is generally constant with vehicle attitude and Mach number unless direct canard and/or forebody shock impingement occurs.
2. The addition of the ram-air-spoiler tail fins resulted in only small changes in aerodynamic-center location.
3. For the ram-air-spoiler configurations tested, there are large axial-force coefficient effects associated with the increased fin thickness and ram-air momentum loss.

Langley Research Center  
National Aeronautics and Space Administration  
Hampton, VA 23665  
September 26, 1978

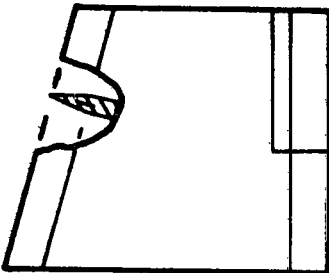
## REFERENCES

1. Corlett, William A.; and Howell, Dorothy T.: Aerodynamic Characteristics at Mach 0.60 to 4.63 of Two Cruciform Missile Models, One Having Trapezoidal Wings With Canard Controls and the Other Having Delta Wings With Tail Controls. NASA TM X-2780, 1978.
2. Blair, A. B., Jr.: Aerodynamic Characteristics of a Tandem-Canard Missile at Mach Numbers From 1.83 to 4.63. NASA TM X-3040, 1974.
3. Burt, James R., Jr.: The Effectiveness of Canards for Roll Control. Tech. Rep. RD-77-8, U.S. Army, Nov. 1976. (Available from DDC as AD A037 077.)
4. Sawyer, Wallace C.; Jackson, Charlie M., Jr.; and Blair A. B., Jr.: Aerodynamic Technologies for the Next Generation of Missiles. Paper presented at the AIAA/ADPA Tactical Missile Conference (Gaithersburg, Maryland), April 27-28, 1977.
5. Turner, Thomas R.; and Vogler, Raymond D.: Wind-Tunnel Investigation at Transonic Speeds of a Jet Control on an 80° Delta-Wing Missile. NACA RM L55H22, 1955.
6. Lowry, John G.: Recent Control Studies. NACA RM L55L22a, 1956.
7. Schult, Eugene D.: Free-Flight Roll Performance of a Steady-Flow Jet-Spoiler Control on an 80° Delta-Wing Missile Between Mach Numbers of 0.6 and 1.8. NACA RM L57J28, 1958.
8. Schult, Eugene D.: Free-Flight Investigation at Mach Numbers Between 0.5 and 1.7 of the Zero-Lift Rolling Effectiveness and Drag of Various Surface, Spoiler, and Jet Controls on an 80° Delta-Wing Missile. NASA TN D-205, 1960.
9. Durham, Mark: Feasibility of a "Fluidic Rolleron" for Application to the Chaparral Missile. NWC Tech. Note 4063-224, U.S. Navy, Nov. 1970.
10. Young, R.: Final Report. Fluidic Roll Rate Damping System. Doc. No. 73SD2110, Gen. Elec. Co., July 1973. (Available from DDC as AD B007 800L.)
11. Blair, A. B., Jr.: Wind-Tunnel Investigation at Mach Numbers From 1.90 to 2.86 of a Canard-Controlled Missile With Ram-Air-Jet Spoiler Roll Control. NASA TP-1124, 1978.
12. Blair, A. B., Jr.; Sawyer, Wallace C.; and Jackson, Charlie M., Jr.: A Ram-Air-Spoiler Roll Stabilization Device for Forward Control Cruciform Missiles. AIAA Paper 78-24, Jan. 1978.
13. Mechtly, E. A.: The International System of Units - Physical Constants and Conversion Factors (Second Revision). NASA SP-7012, 1973.

14. Schaefer, William T., Jr.: Characteristics of Major Active Wind Tunnels at the Langley Research Center. NASA TM X-1130, 1965.
15. Stallings, Robert L., Jr.; and Lamb, Milton: Effects of Roughness Size on the Position of Boundary-Layer Transition and on the Aerodynamic Characteristics of a 55° Swept Delta Wing at Supersonic Speeds. NASA TP-1027, 1977.
16. Lord, Douglas R.. Aerodynamic Characteristics of Several Jet-Spoiler Controls on a 45° Sweptback Wing at Mach Numbers of 1.61 and 2.01. NACA RM L58D18, 1958.

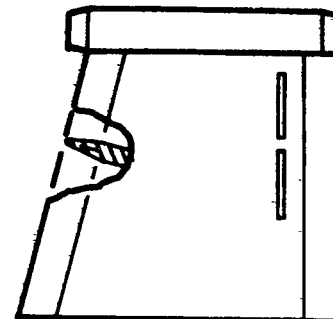
TABLE I.- TAIL-FIN GEOMETRY AND TEST PARAMETERS

$S_a/S_{exp} = 0.11$   
 $t/c = 0.04$



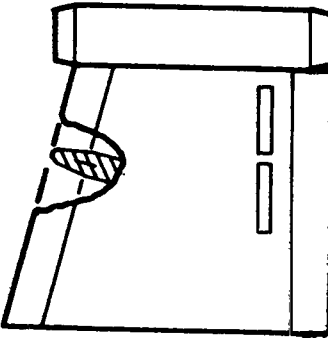
Plain fin with aileron

$A_i/A = 0.028$   
 $t/c = 0.05$



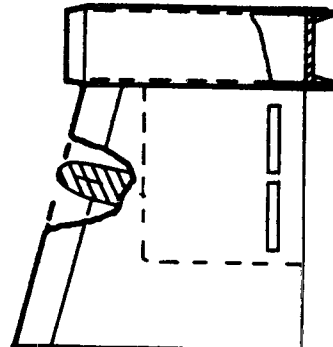
$A_e/A_i = 0.50, 0.75, \text{ and } 0.90$

$A_i/A = 0.063$   
 $t/c = 0.08$



$A_e/A_i = 0.50, 0.75, \text{ and } 0.90$

$A_i/A = 0.111$   
 $t/c = 0.11$



$A_e/A_i = 0.50, 0.75, \text{ and } 0.90$

TABLE II.- GEOMETRIC CONSTANTS FOR RAM-AIR-SPOILER  
TAIL-FIN CONFIGURATIONS<sup>a</sup>

(a)  $A_i/A = 0.028$ ;  $t/c = 0.05$

Inlet diameter, cm (in.) . . . . .	1.270 (0.500)
Inlet area $A_i$ , $\text{cm}^2$ ( $\text{in}^2$ ) . . . . .	1.265 (0.196)
Plenum entrance area, $\text{cm}^2$ ( $\text{in}^2$ ) . . . . .	1.815 (0.281)
Nozzle block . . . . .	None
$A_e$ for -	
$A_e/A_i = 0.50$ and $\delta_j = 90^\circ$ , $\text{cm}^2$ ( $\text{in}^2$ ) . . . . .	0.632 (0.098)
$A_e/A_i = 0.75$ and $\delta_j = 90^\circ$ , $\text{cm}^2$ ( $\text{in}^2$ ) . . . . .	0.942 (0.146)
$A_e/A_i = 0.75$ and $\delta_j = 50^\circ$ , $\text{cm}^2$ ( $\text{in}^2$ ) . . . . .	0.942 (0.146)
$A_e/A_i = 0.90$ and $\delta_j = 90^\circ$ , $\text{cm}^2$ ( $\text{in}^2$ ) . . . . .	1.136 (0.176)

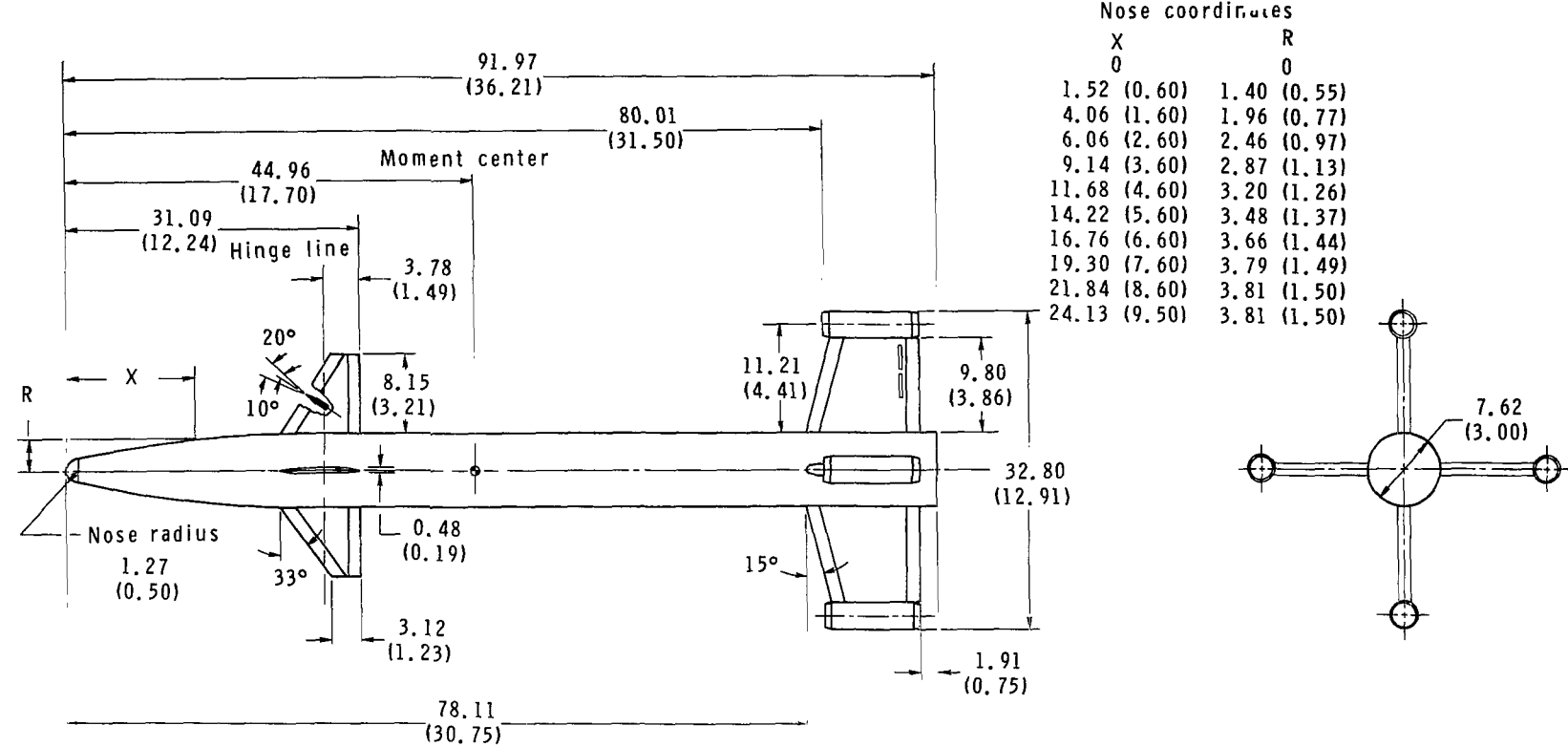
(b)  $A_i/A = 0.063$ ;  $t/c = 0.08$

Inlet diameter, cm (in.) . . . . .	1.905 (0.750)
Inlet area $A_i$ , $\text{cm}^2$ ( $\text{in}^2$ ) . . . . .	2.852 (0.442)
Plenum entrance area, $\text{cm}^2$ ( $\text{in}^2$ ) . . . . .	3.632 (0.563)
Nozzle block . . . . .	None
$A_e$ for -	
$A_e/A_i = 0.50$ and $\delta_j = 90^\circ$ , $\text{cm}^2$ ( $\text{in}^2$ ) . . . . .	1.432 (0.222)
$A_e/A_i = 0.75$ and $\delta_j = 90^\circ$ , $\text{cm}^2$ ( $\text{in}^2$ ) . . . . .	2.142 (0.332)
$A_e/A_i = 0.90$ and $\delta_j = 90^\circ$ , $\text{cm}^2$ ( $\text{in}^2$ ) . . . . .	2.568 (0.398)

(c)  $A_i/A = 0.111$ ;  $t/c = 0.11$

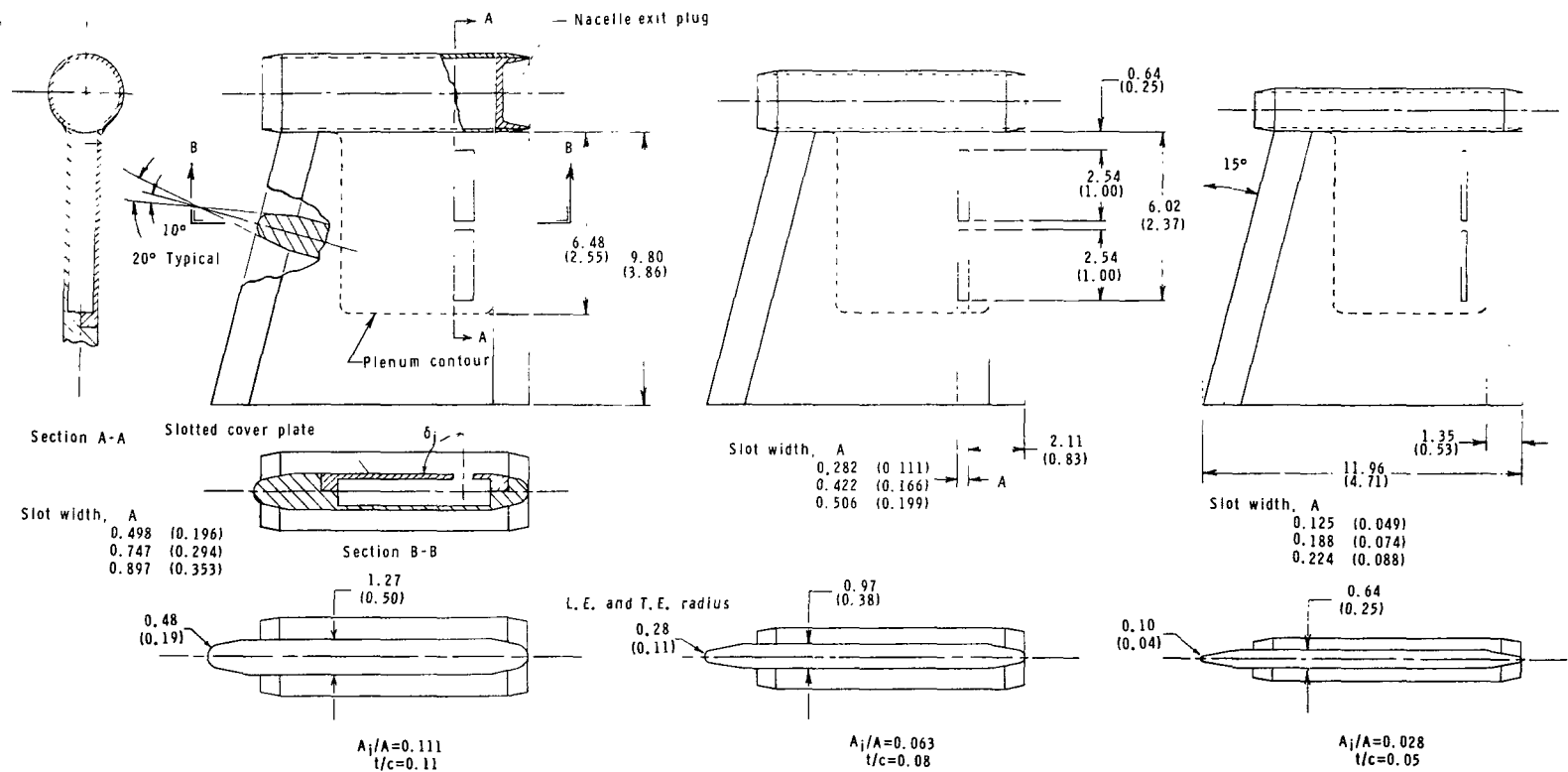
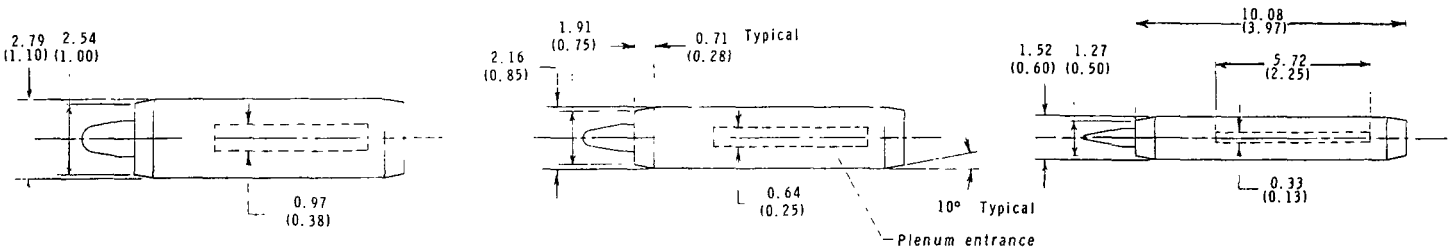
Inlet diameter, cm (in.) . . . . .	2.540 (1.000)
Inlet area $A_i$ , $\text{cm}^2$ ( $\text{in}^2$ ) . . . . .	5.065 (0.785)
Plenum entrance area, $\text{cm}^2$ ( $\text{in}^2$ ) . . . . .	5.445 (0.844)
Nozzle block . . . . .	None
$A_e$ for -	
$A_e/A_i = 0.50$ and $\delta_j = 90^\circ$ , $\text{cm}^2$ ( $\text{in}^2$ ) . . . . .	2.529 (0.392)
$A_e/A_i = 0.75$ and $\delta_j = 90^\circ$ , $\text{cm}^2$ ( $\text{in}^2$ ) . . . . .	3.794 (0.588)
$A_e/A_i = 0.90$ and $\delta_j = 90^\circ$ , $\text{cm}^2$ ( $\text{in}^2$ ) . . . . .	4.555 (0.706)

<sup>a</sup>Per fin.



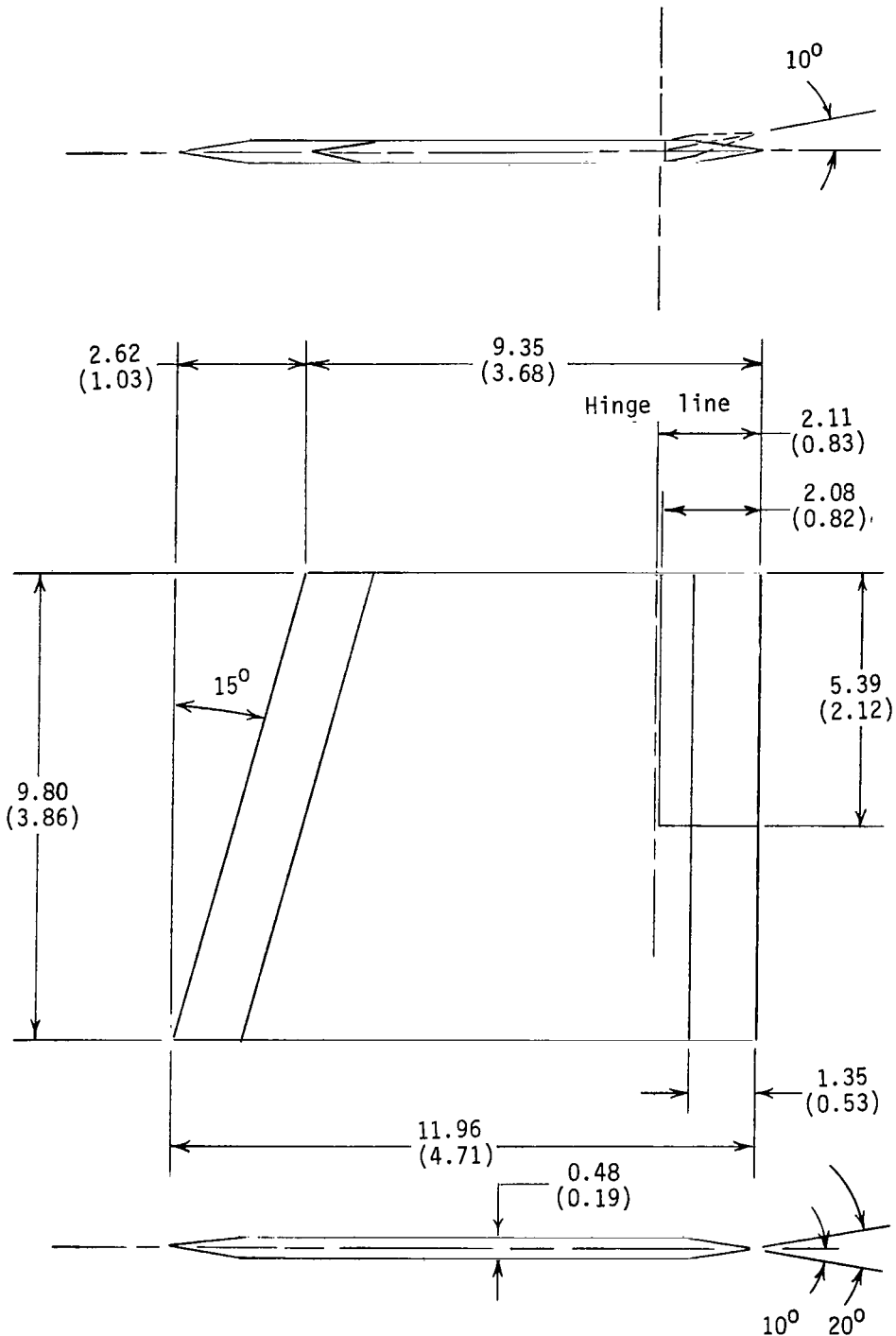
(a) Complete model with  $A_i/A = 0.111$  ram-air-spoiler tail fins.

Figure 1.- Model details. All dimensions in centimeters (inches) unless otherwise indicated.



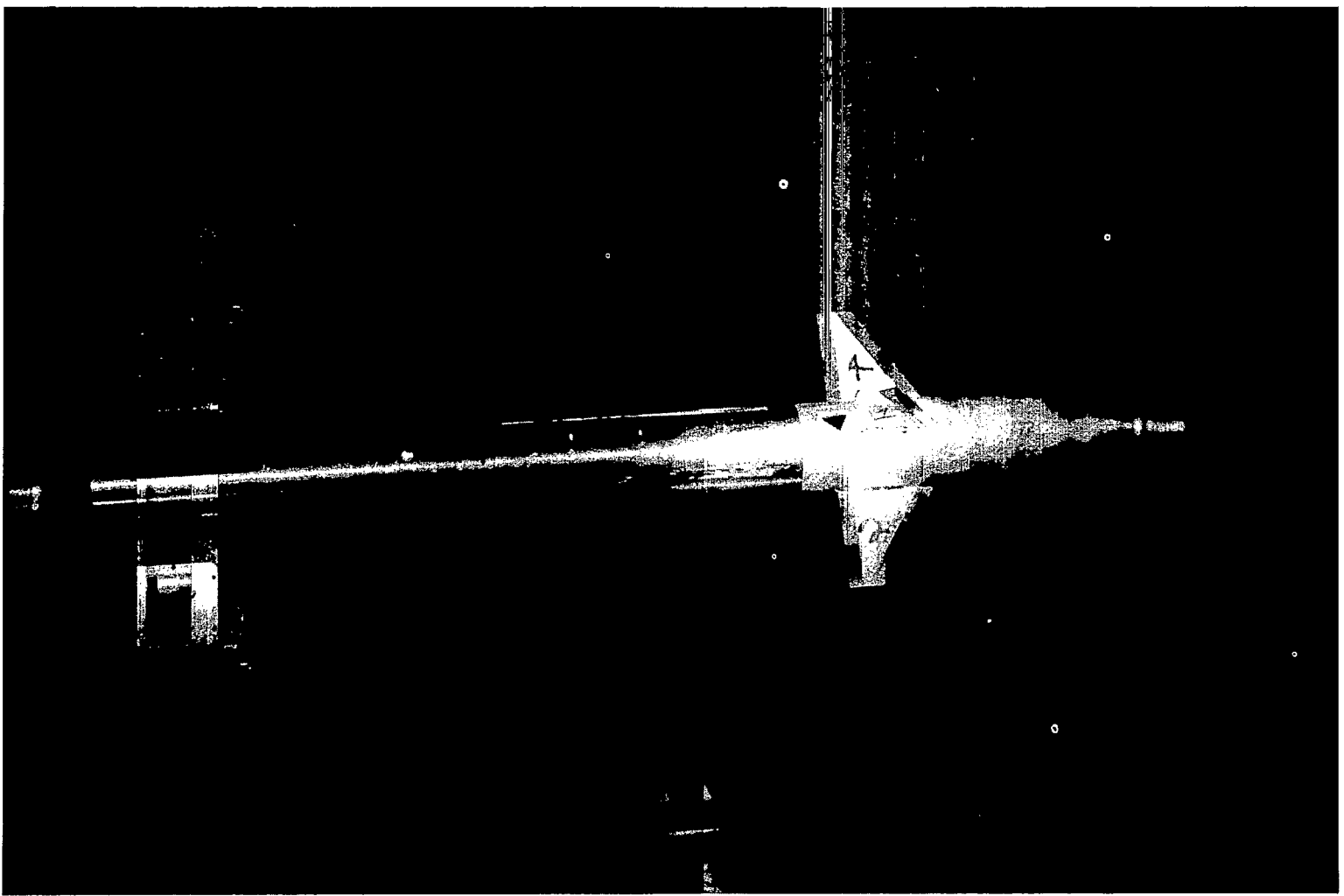
(b) Ram-air-spoiler tail fins.

Figure 1.- Continued.



(c) Plain tail fin with aileron.

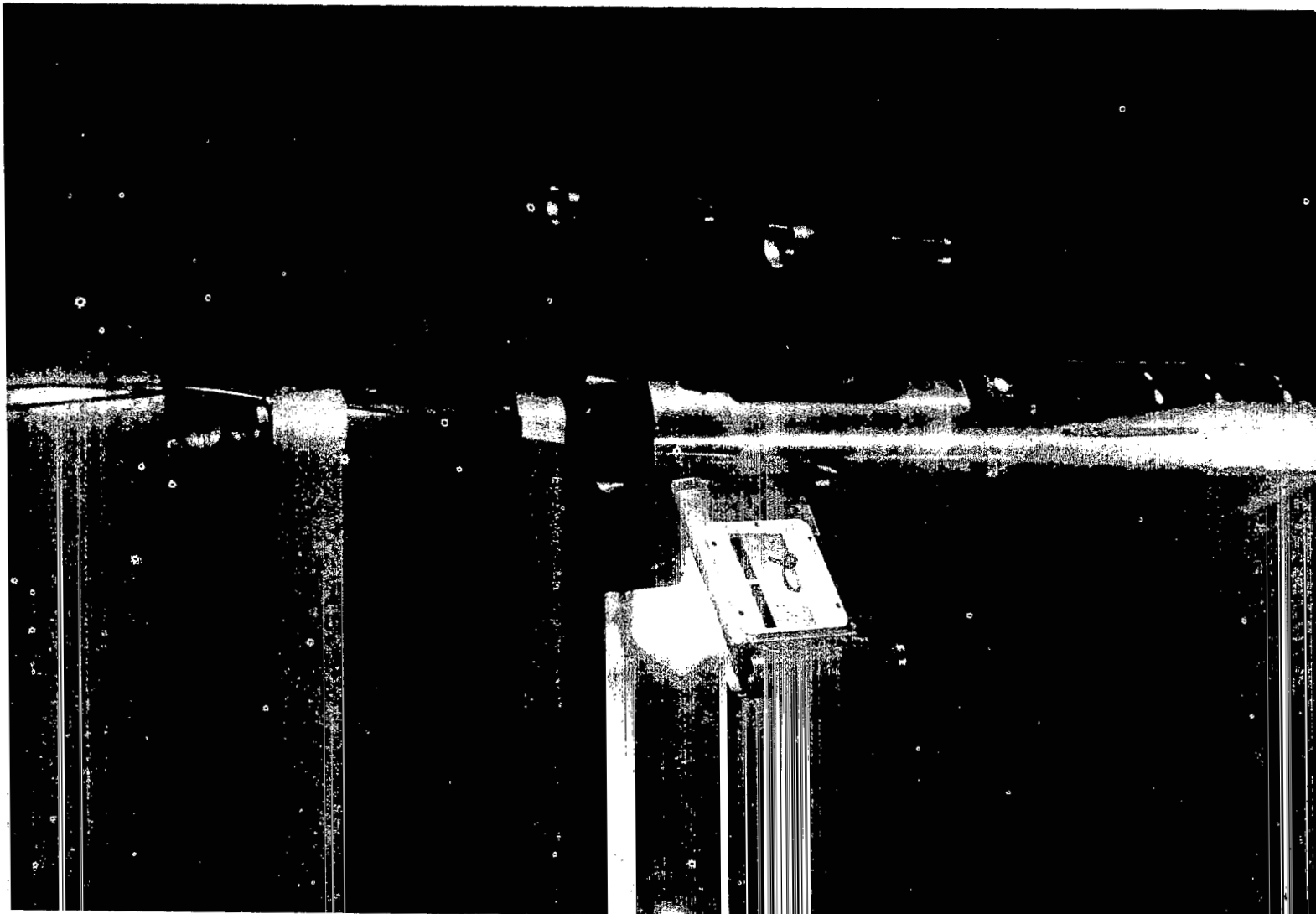
Figure 1.- Concluded.



L-77-6358

(a) Model with  $A_i/A = 0.111$  ram-air-spoiler tail fins for  $A_e/A_i = 0.75$ .

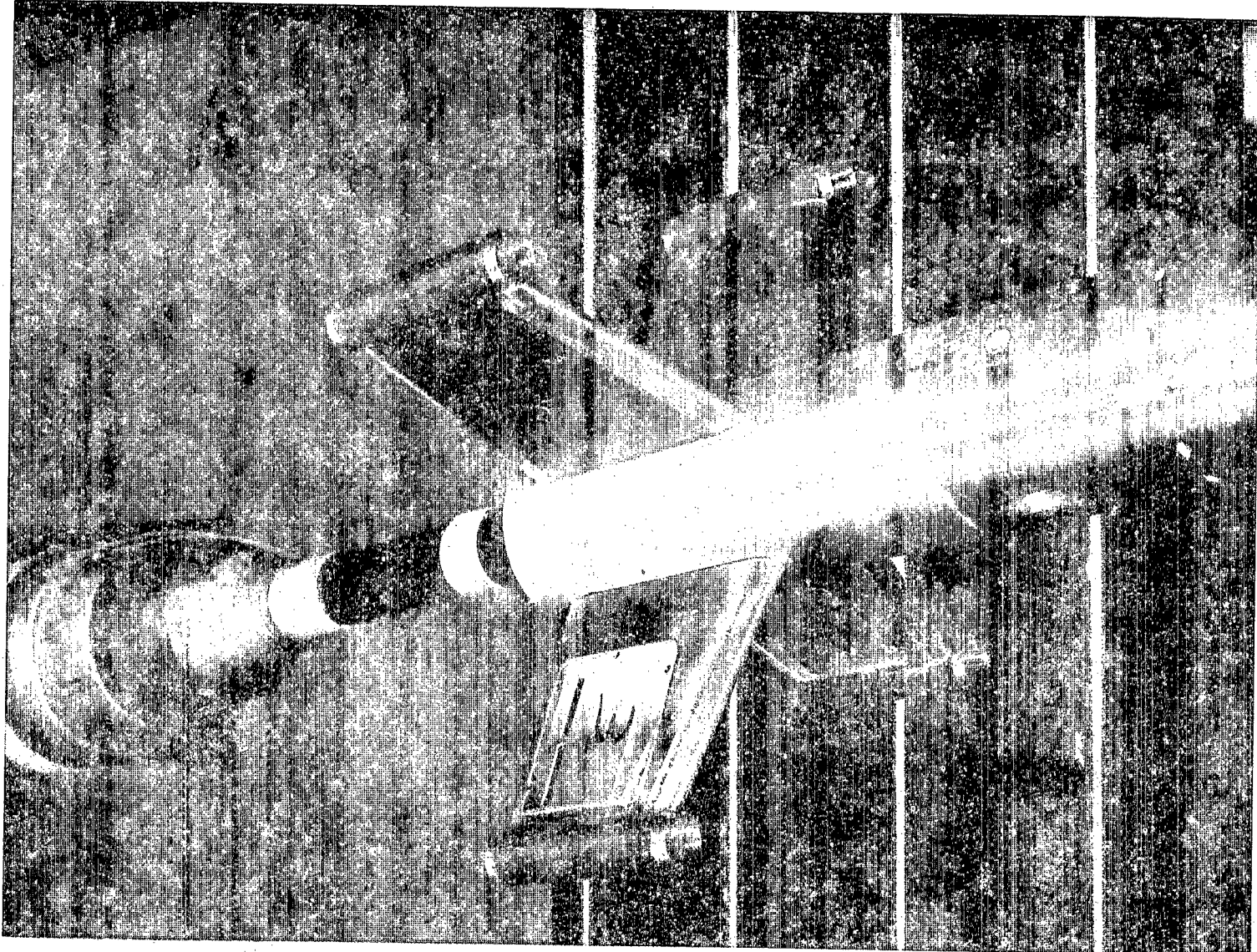
Figure 2.- Model.



L-77-6359

(a) Concluded.

Figure 2.- Continued.

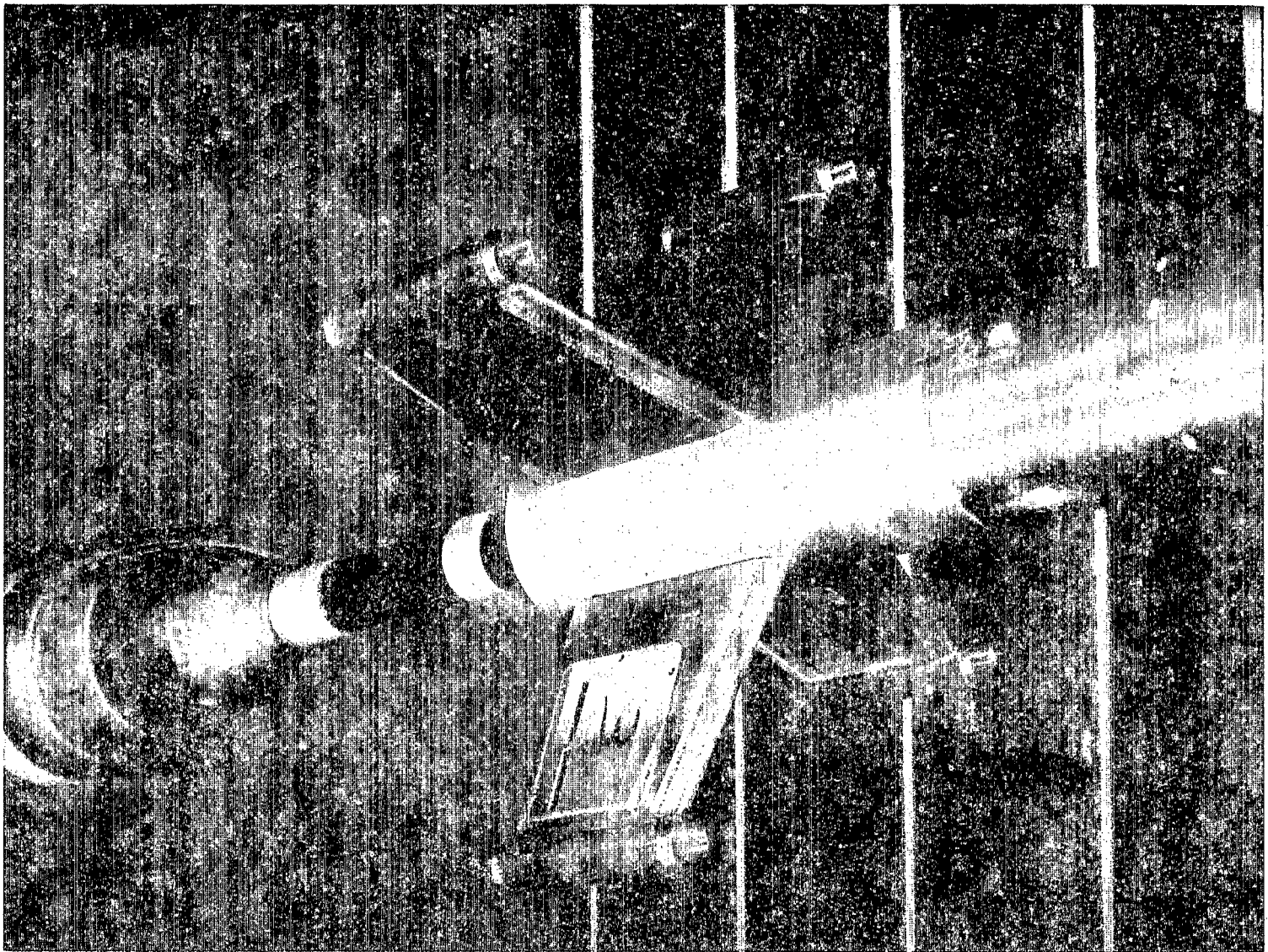


L-77-6412

(b) Model with  $A_i/A = 0.063$  ram-air-spoiler tail fins for  $A_e/A_i = 0.50$ .

21

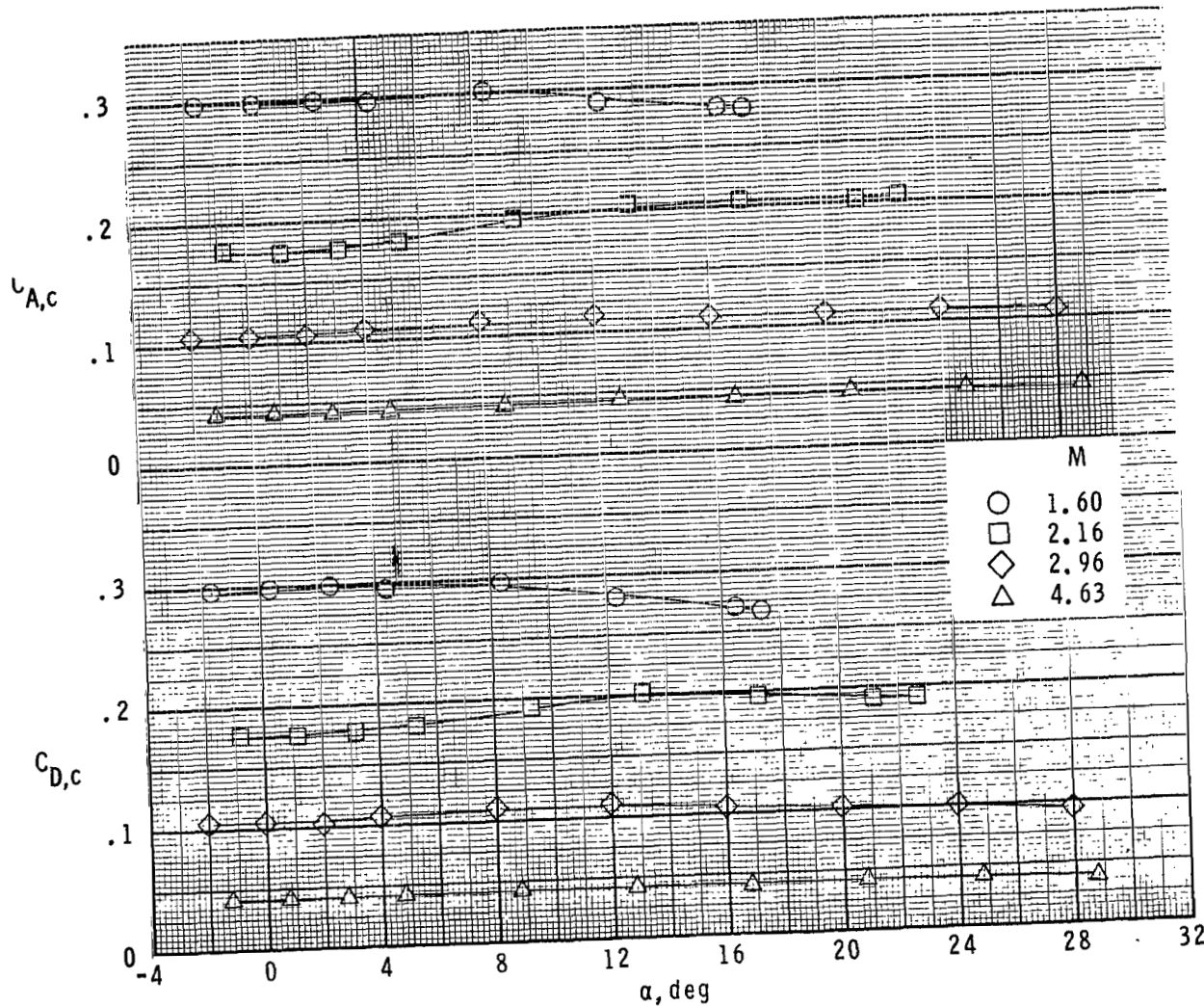
Figure 2.- Continued.



L-77-6412

(b) Model with  $A_i/A = 0.063$  ram-air-spoiler tail fins for  $A_e/A_i = 0.50$ .

Figure 2.- Continued.



(a) Flow-through nacelle.

Figure 3.- Typical variation of measured  $C_{A,c}$  and  $C_{D,c}$  with angle of attack.

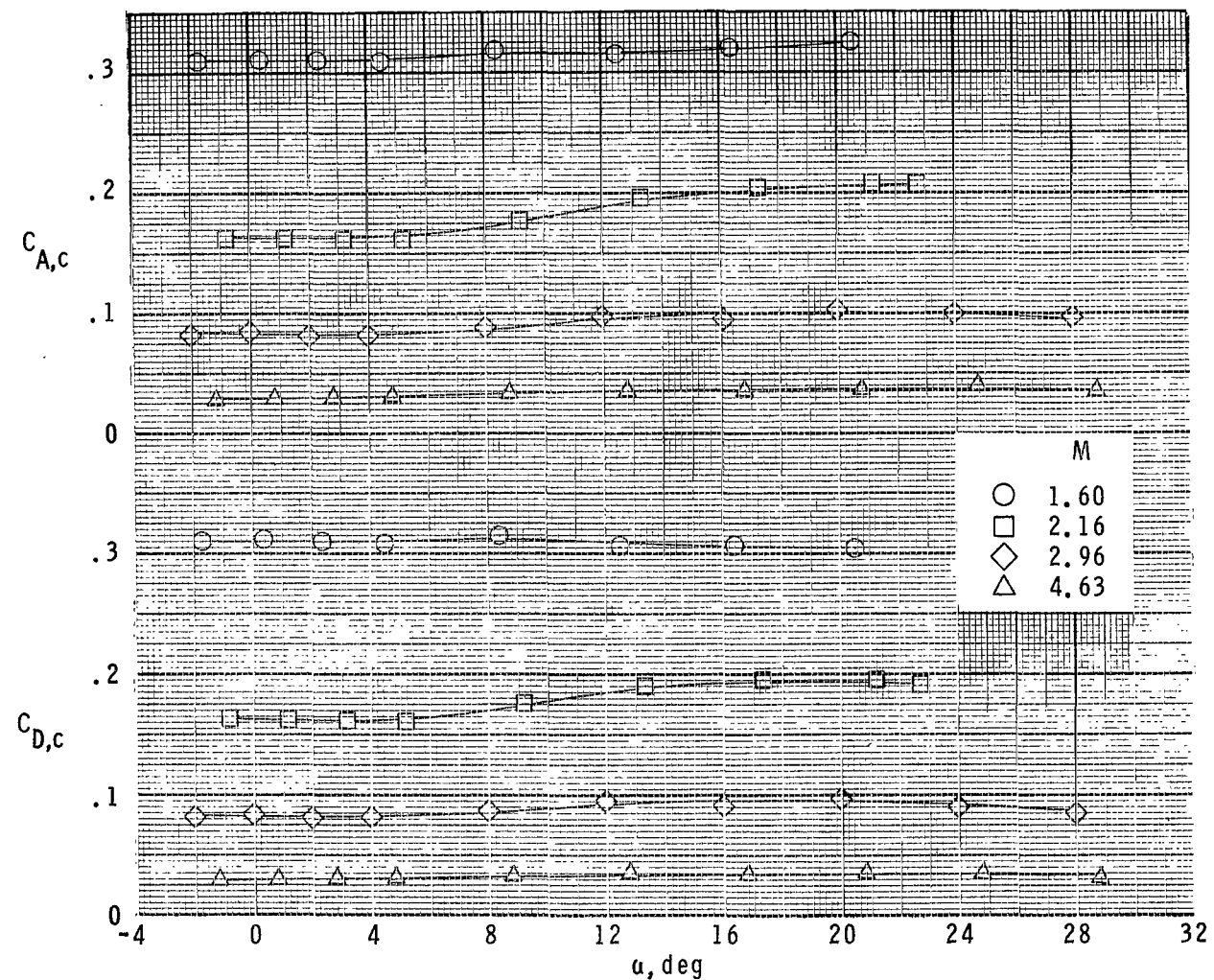
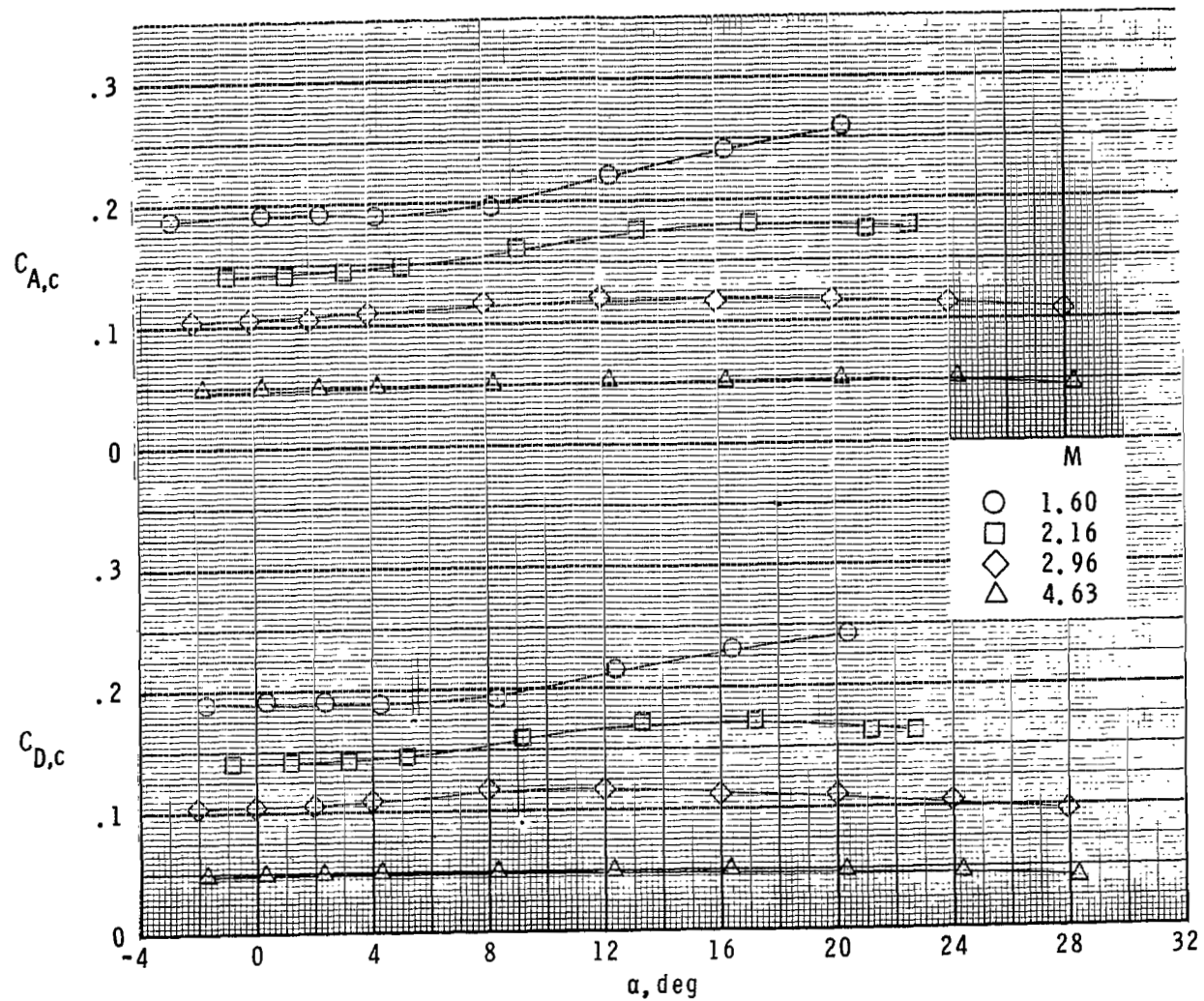
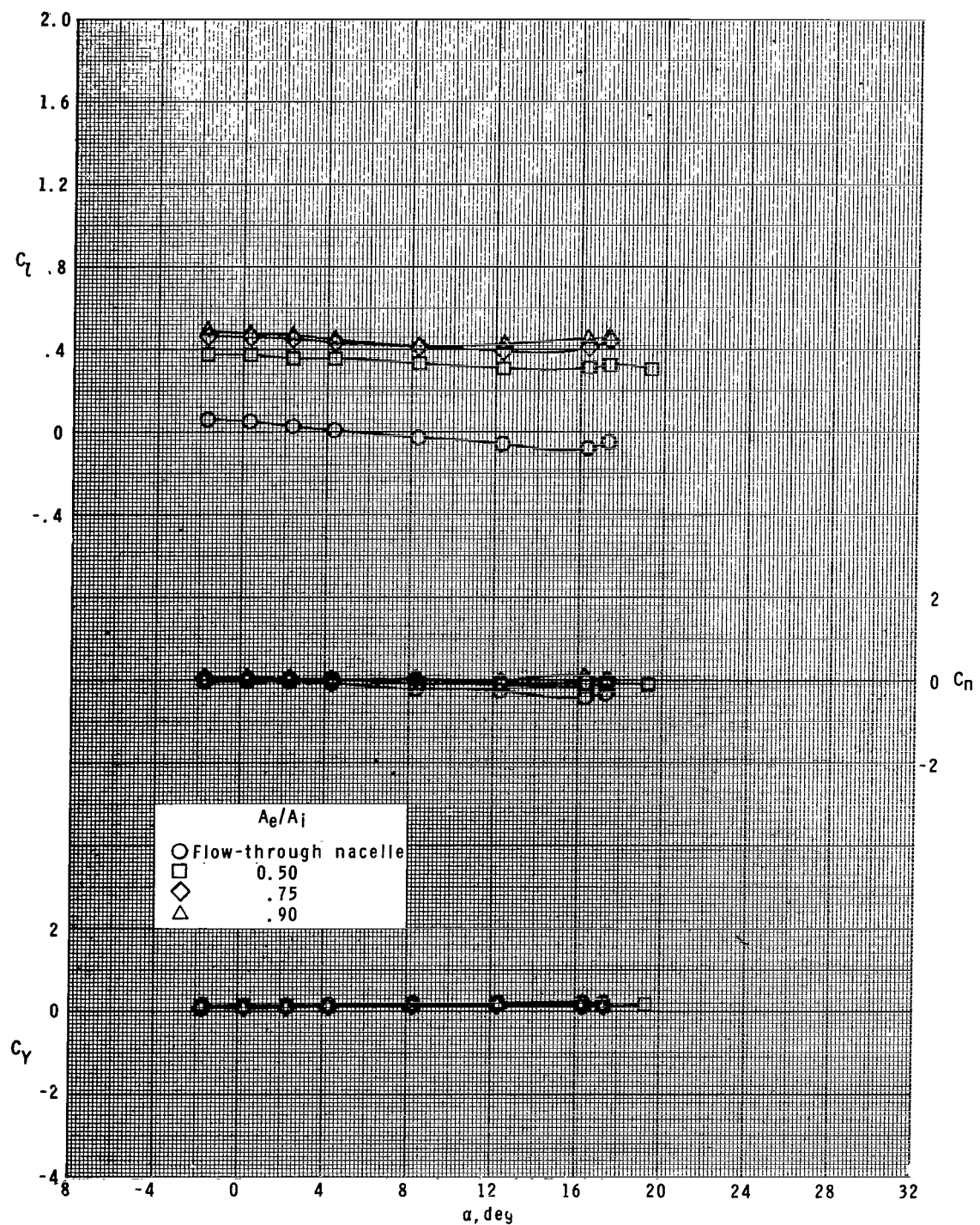
(b)  $A_e/A_i = 0.90.$ 

Figure 3.- Continued.



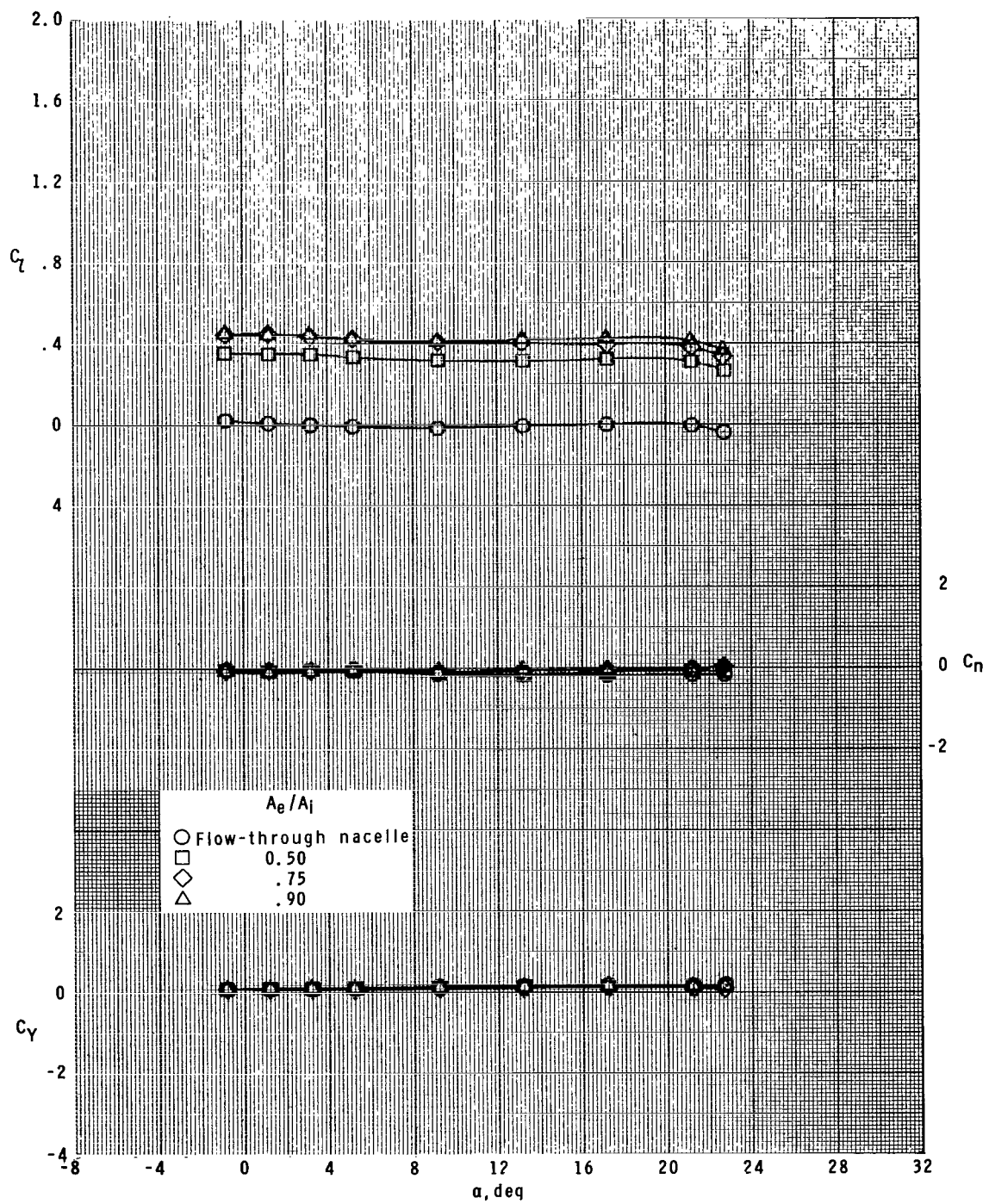
(c) Plain tail fin.

Figure 3.- Concluded.



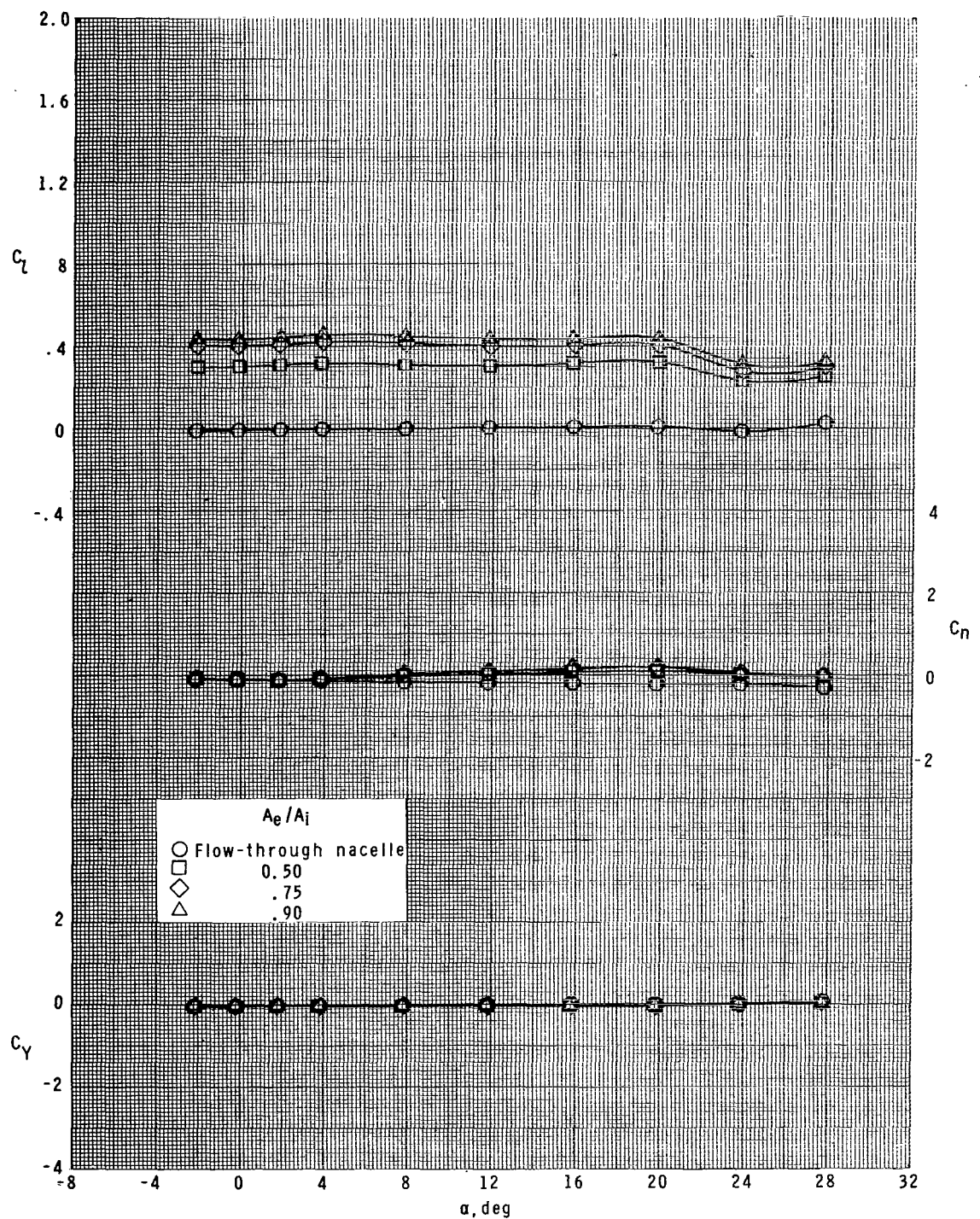
(a)  $M = 1.60.$

**Figure 4.- Effect of ratio of plenum exit area to inlet area for roll control on lateral aerodynamic characteristics of model with ram-air-spoiler tail fins for  $A_i/A = 0.028$  at  $\phi = 0^\circ$ .**



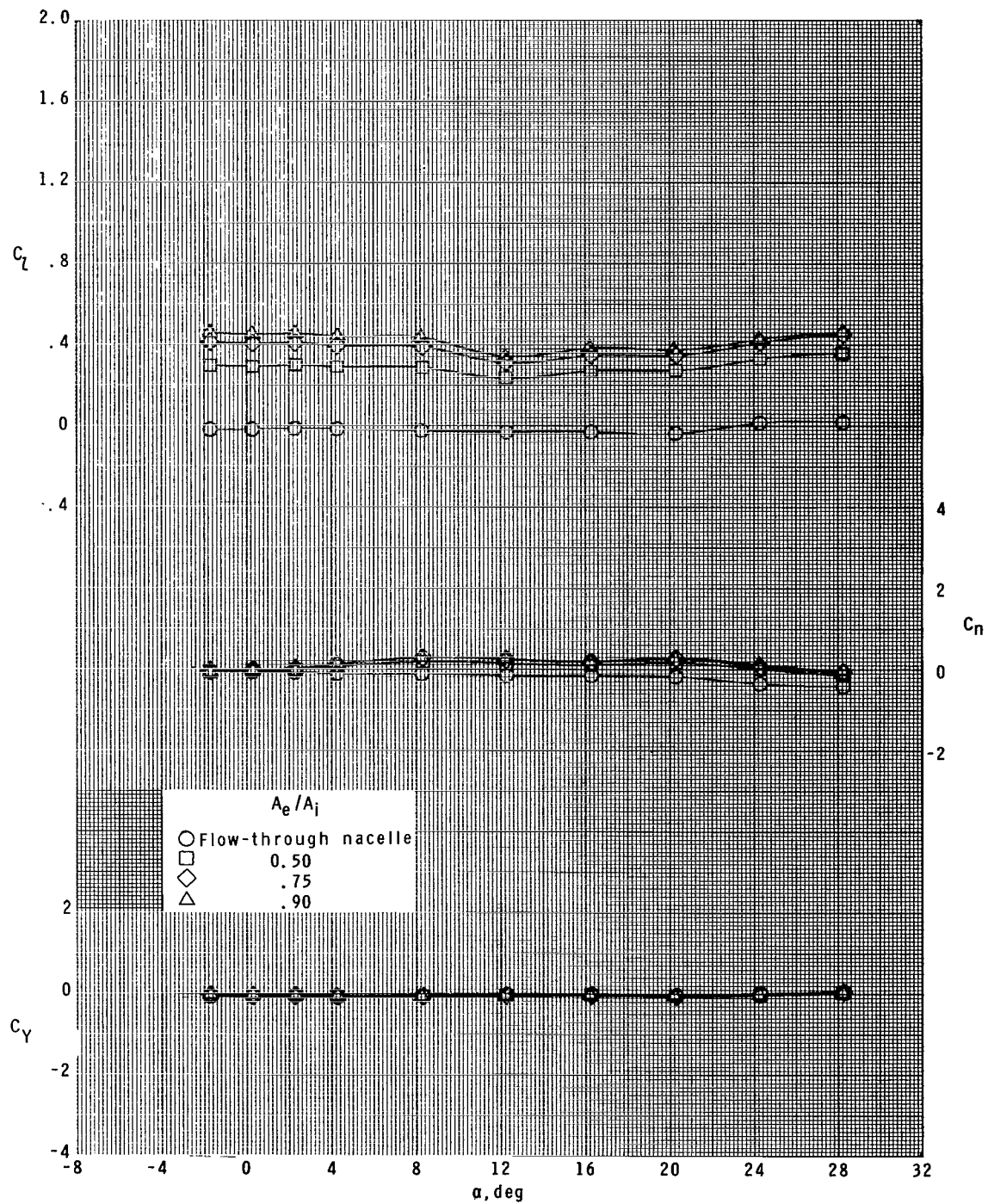
(b)  $M = 2.16$ .

Figure 4.- Continued.



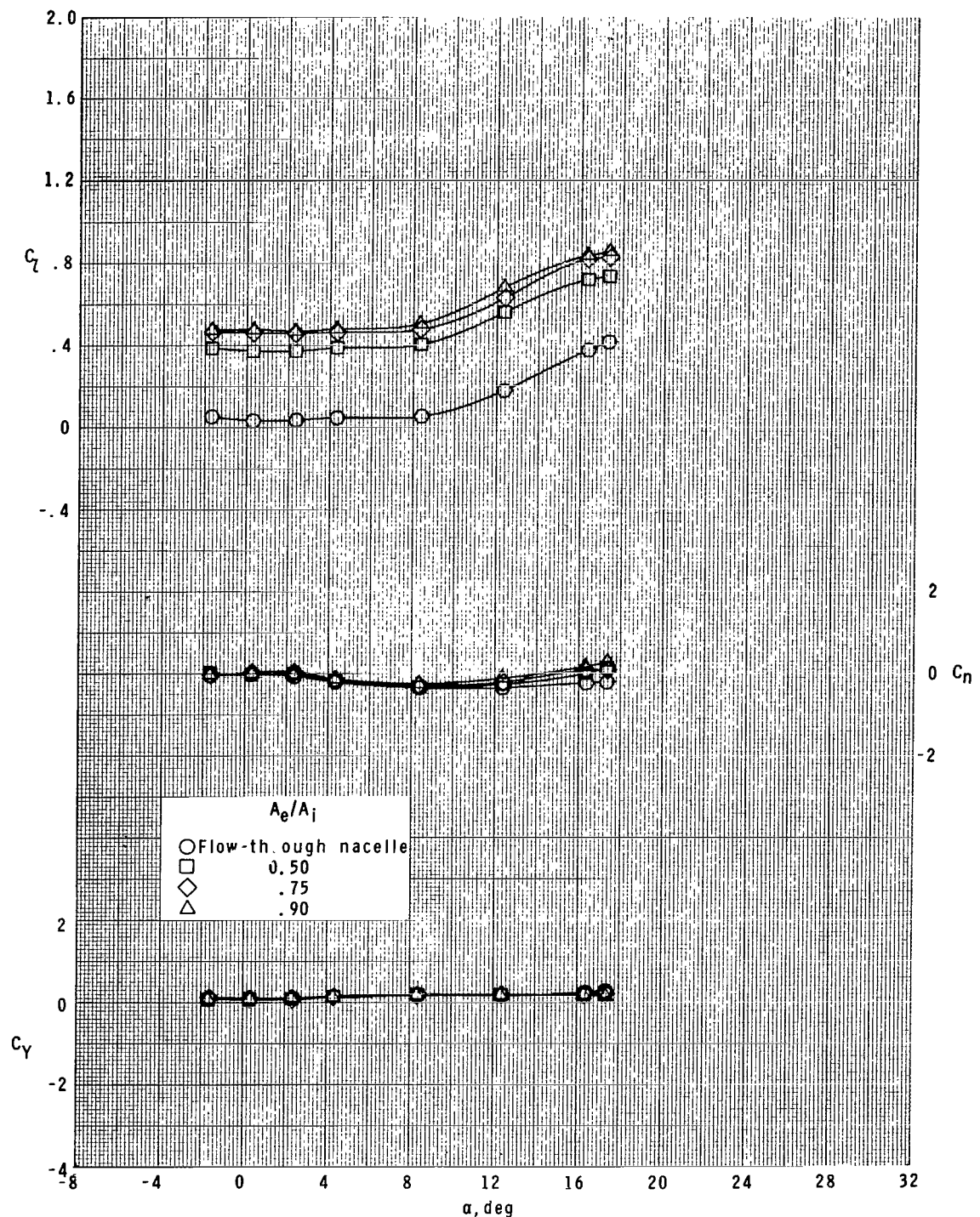
(c)  $M = 2.96.$

Figure 4.- Continued.



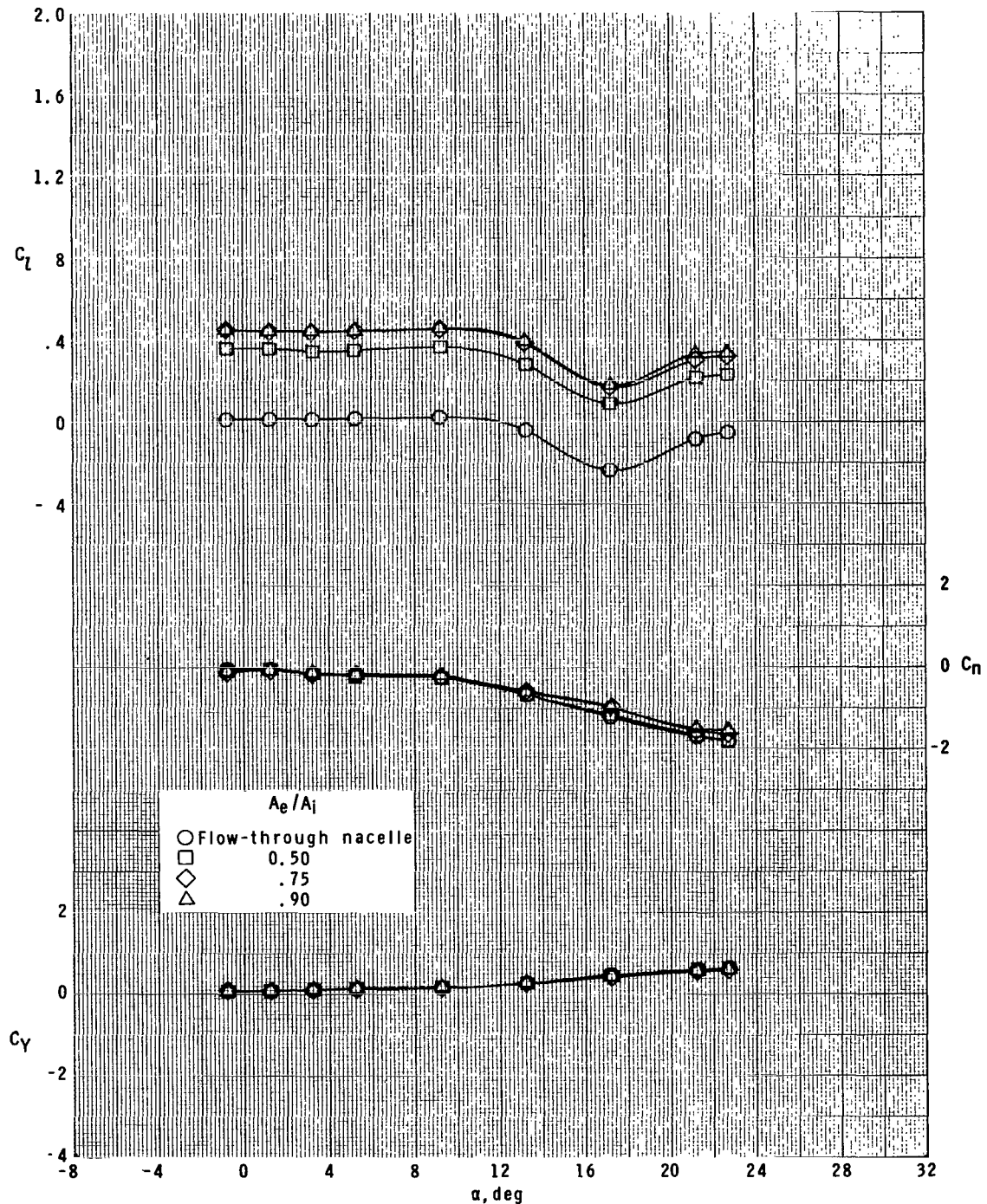
(d)  $M = 4.63.$

Figure 4.- Concluded.



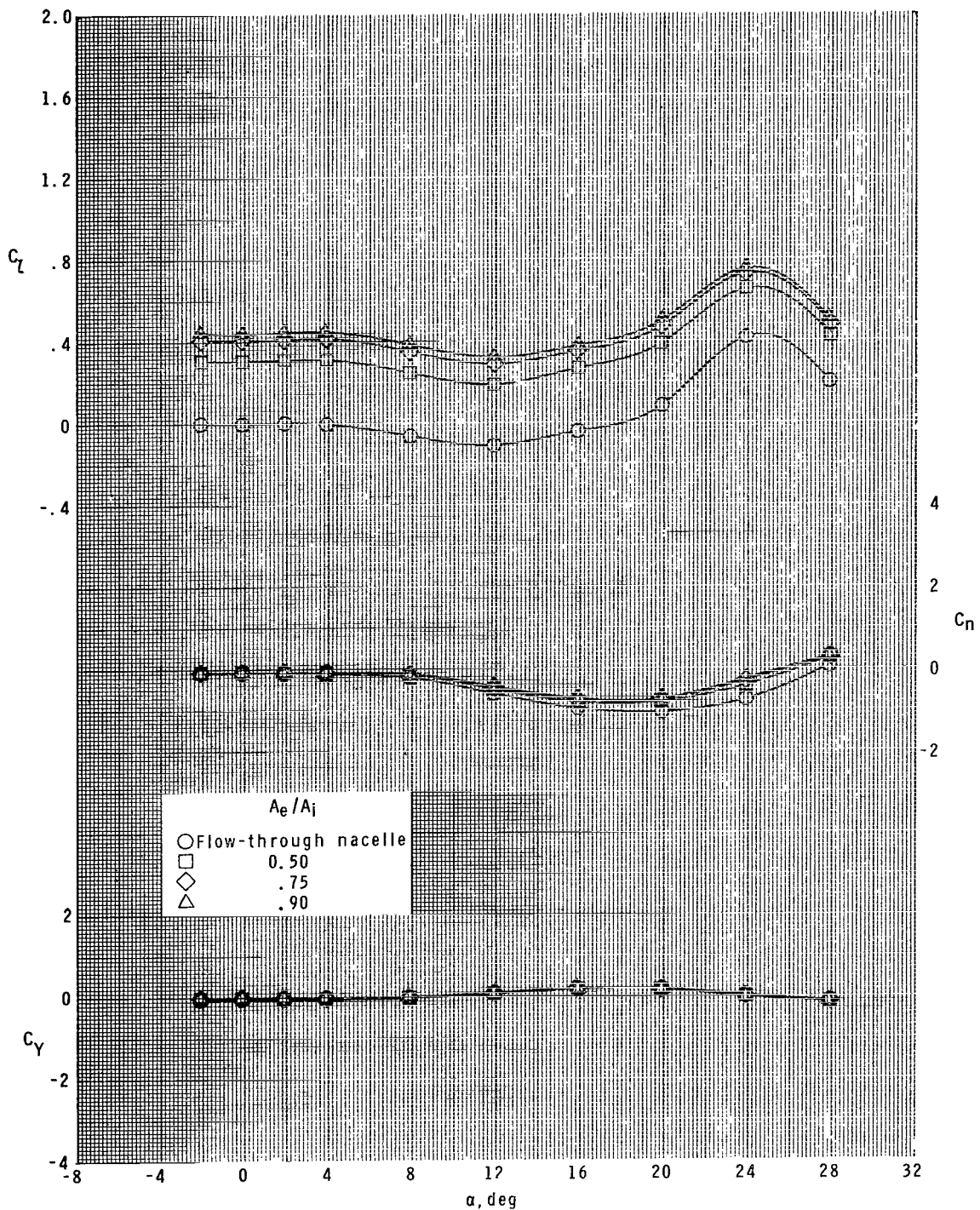
(a)  $M = 1.60.$

Figure 5.- Effect of ratio of plenum exit area to inlet area for roll control on lateral aerodynamic characteristics of model with ram-air-spoiler tail fins for  $A_i/A = 0.028$  at  $\phi = 22.5^\circ$ .



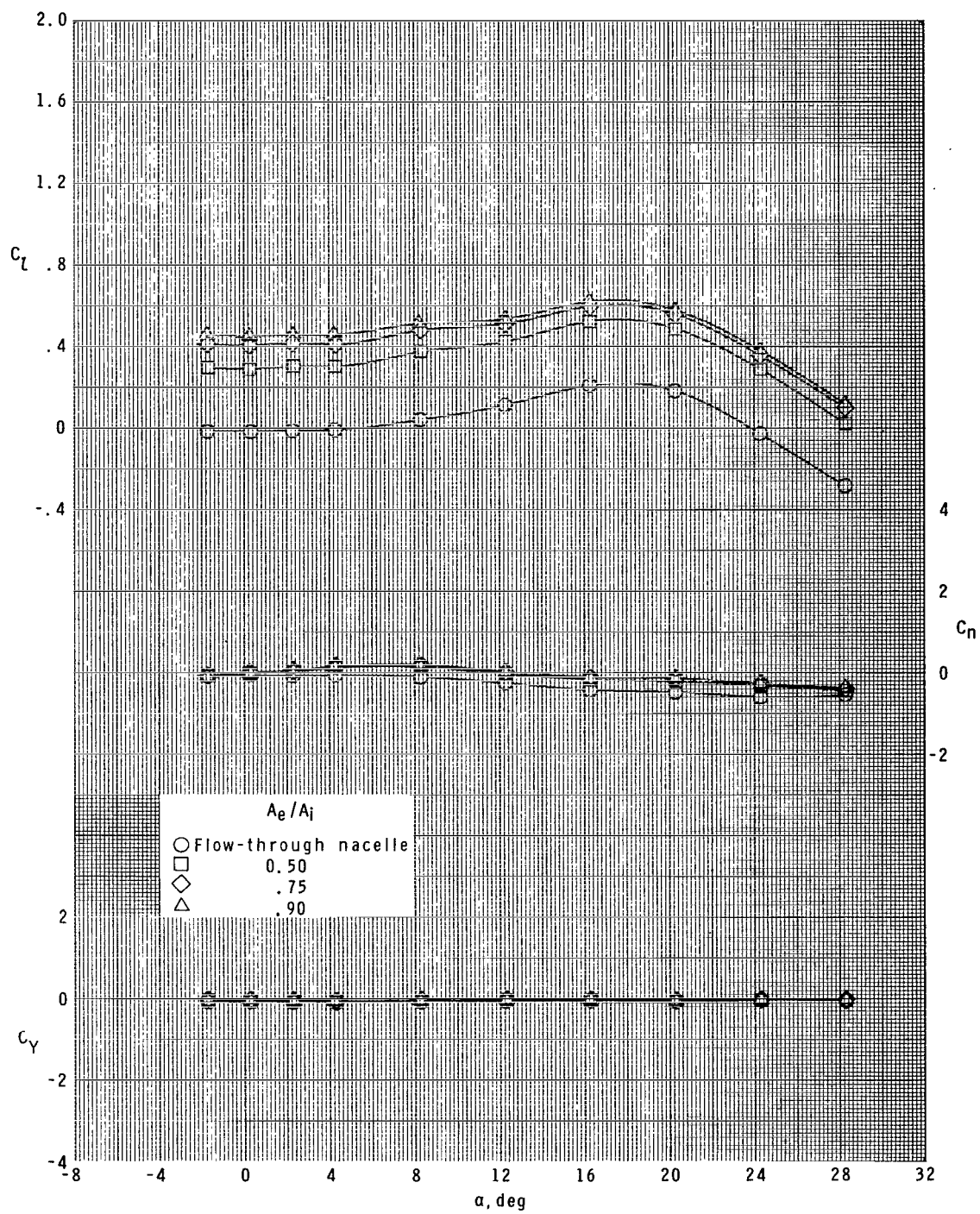
(b)  $M = 2.16$ .

Figure 5.- Continued.



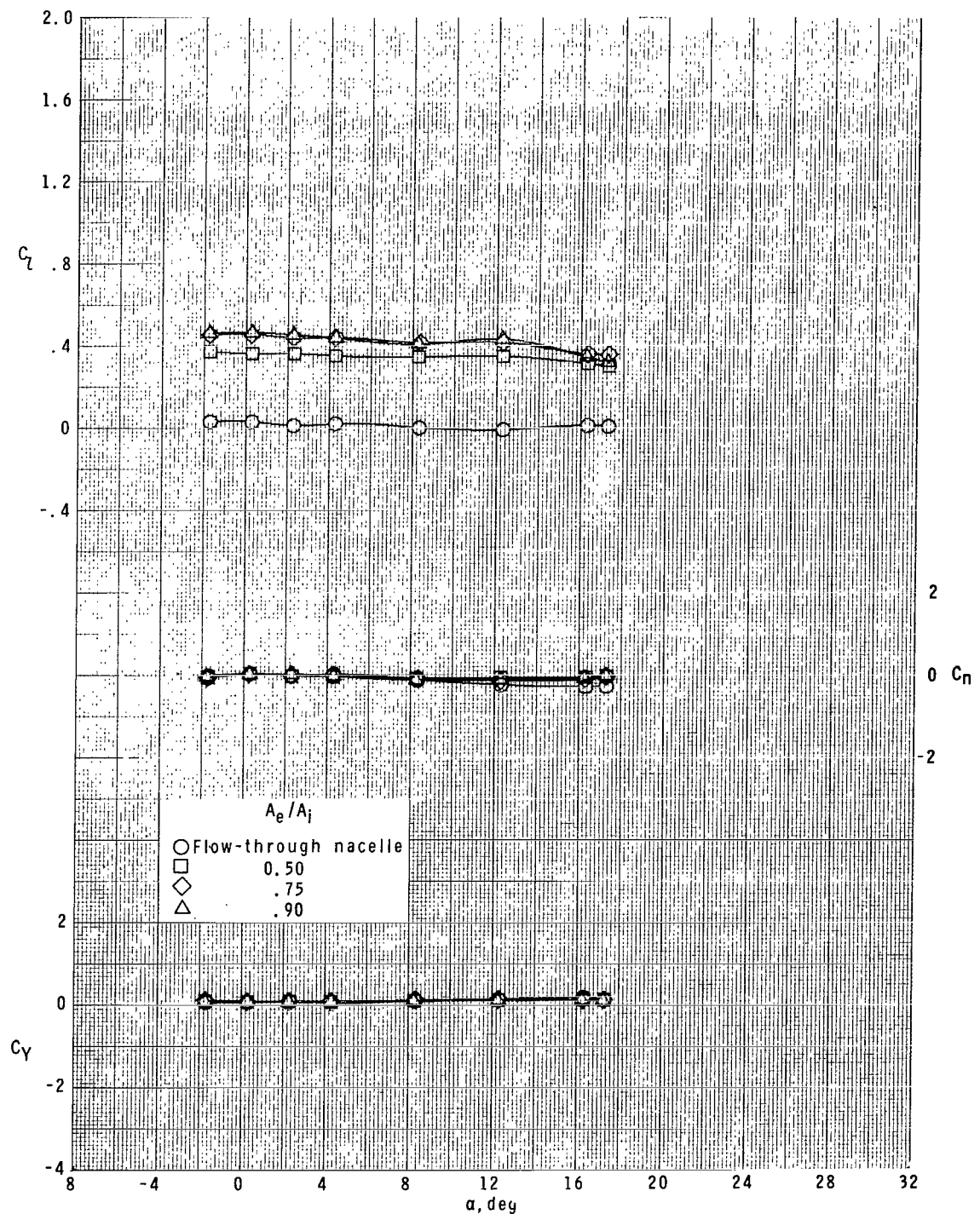
(c)  $M = 2.96.$

Figure 5.- Continued.



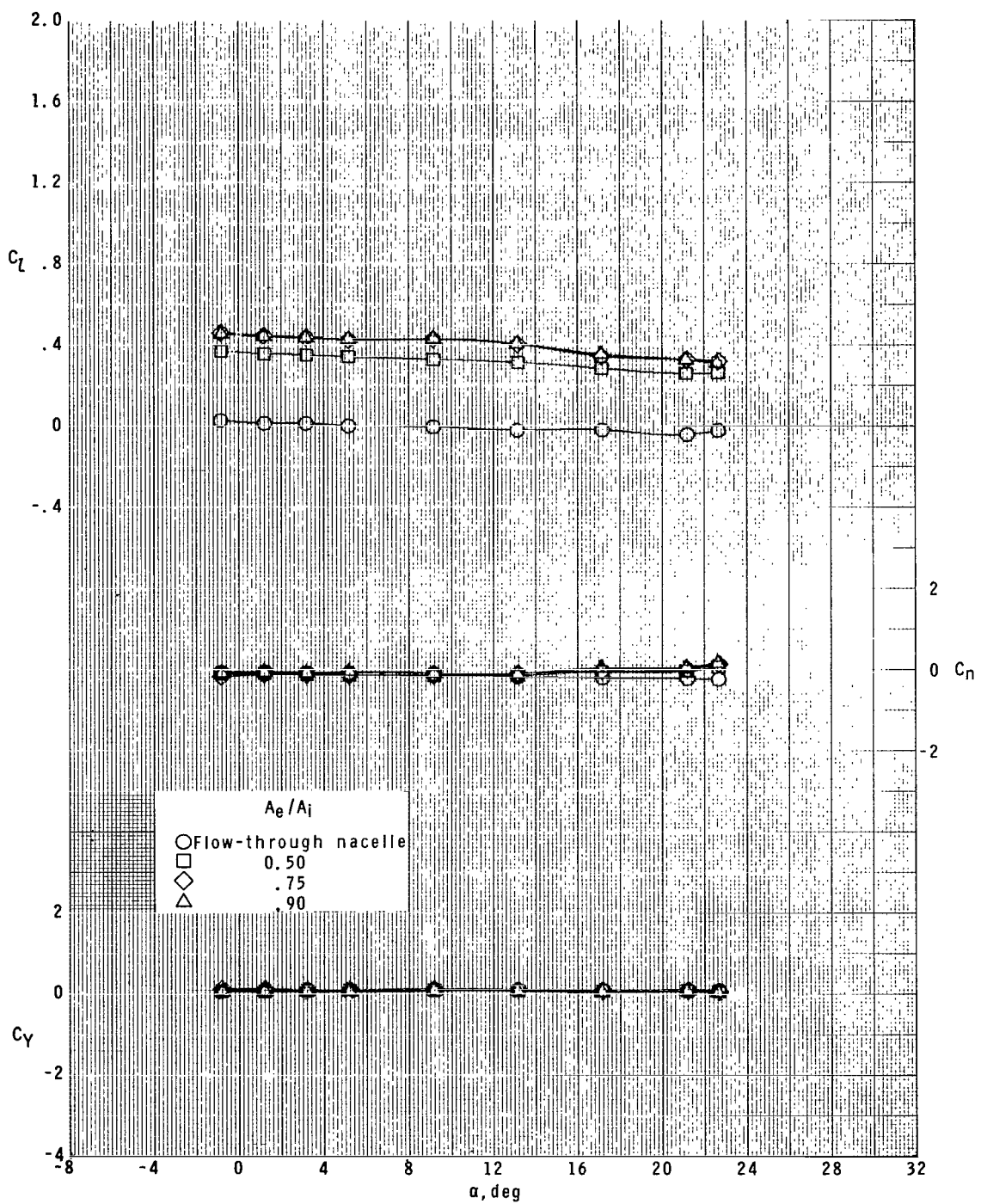
(d)  $M = 4.63.$

Figure 5.- Concluded.



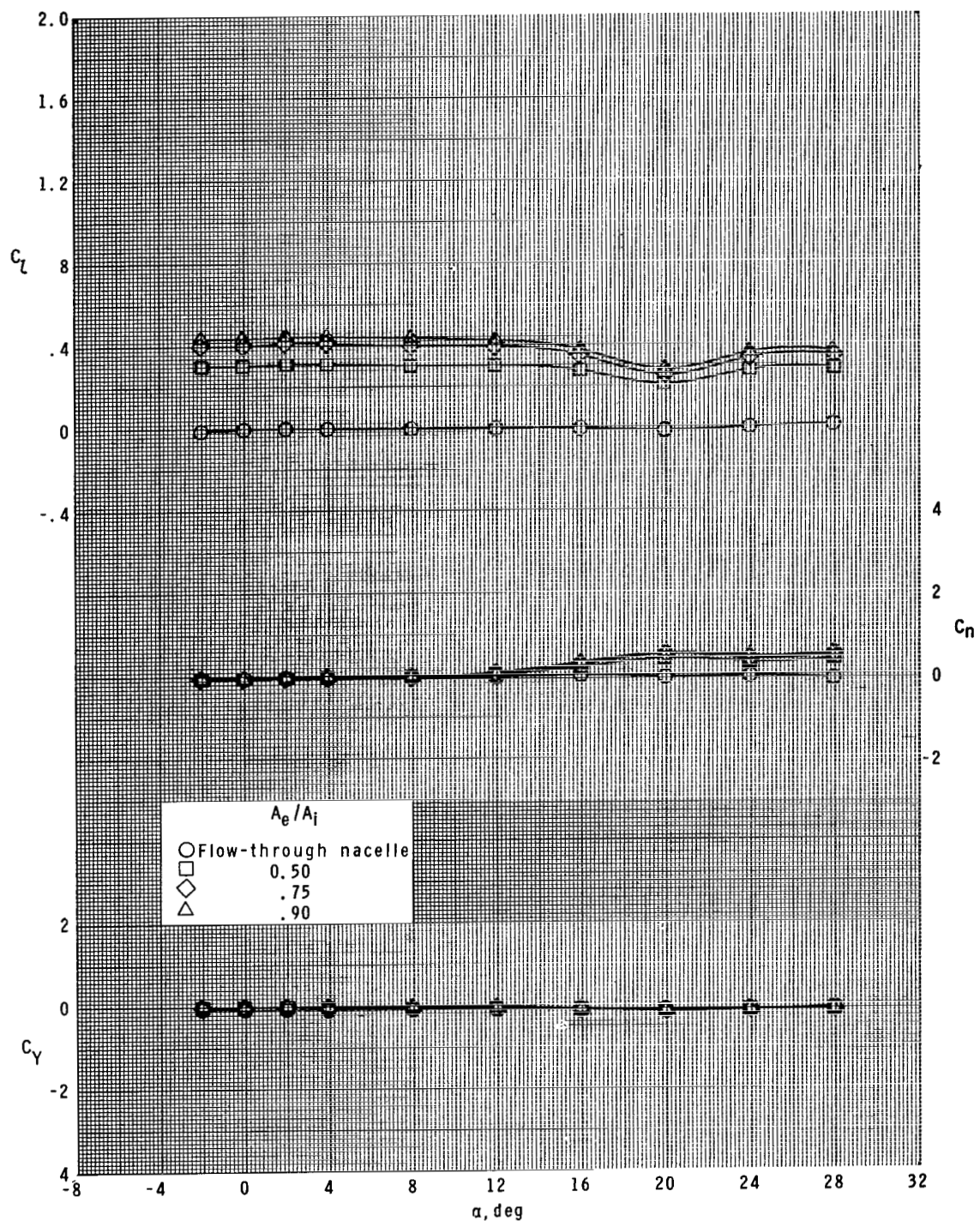
(a)  $M = 1.60.$

Figure 6.- Effect of ratio of plenum exit area to inlet area for roll control on lateral aerodynamic characteristics of model with ram-air-spoiler tail fins for  $A_i/A = 0.028$  at  $\phi = 45^\circ$ .



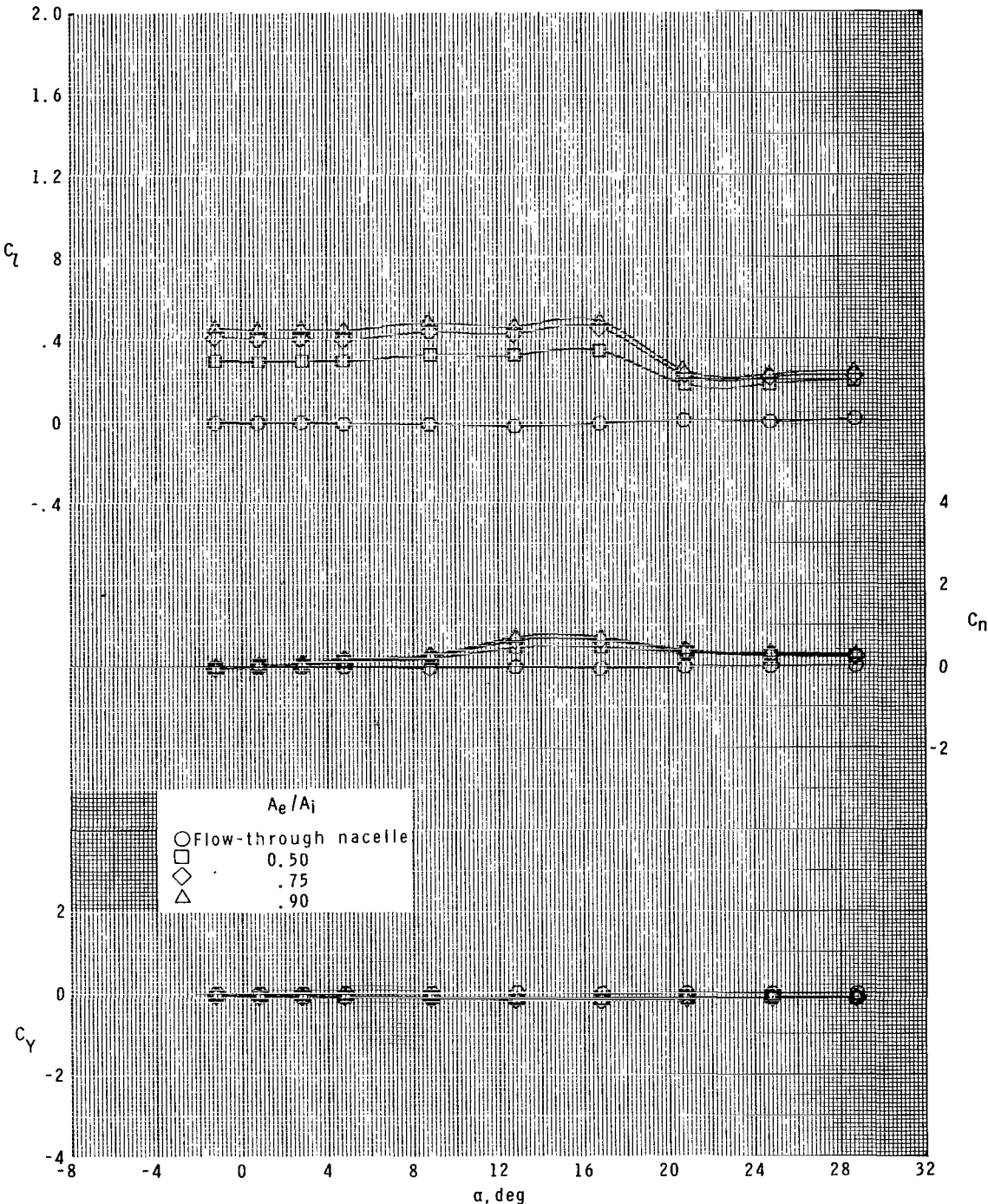
(b)  $M = 2.16.$

Figure 6.-- Continued.



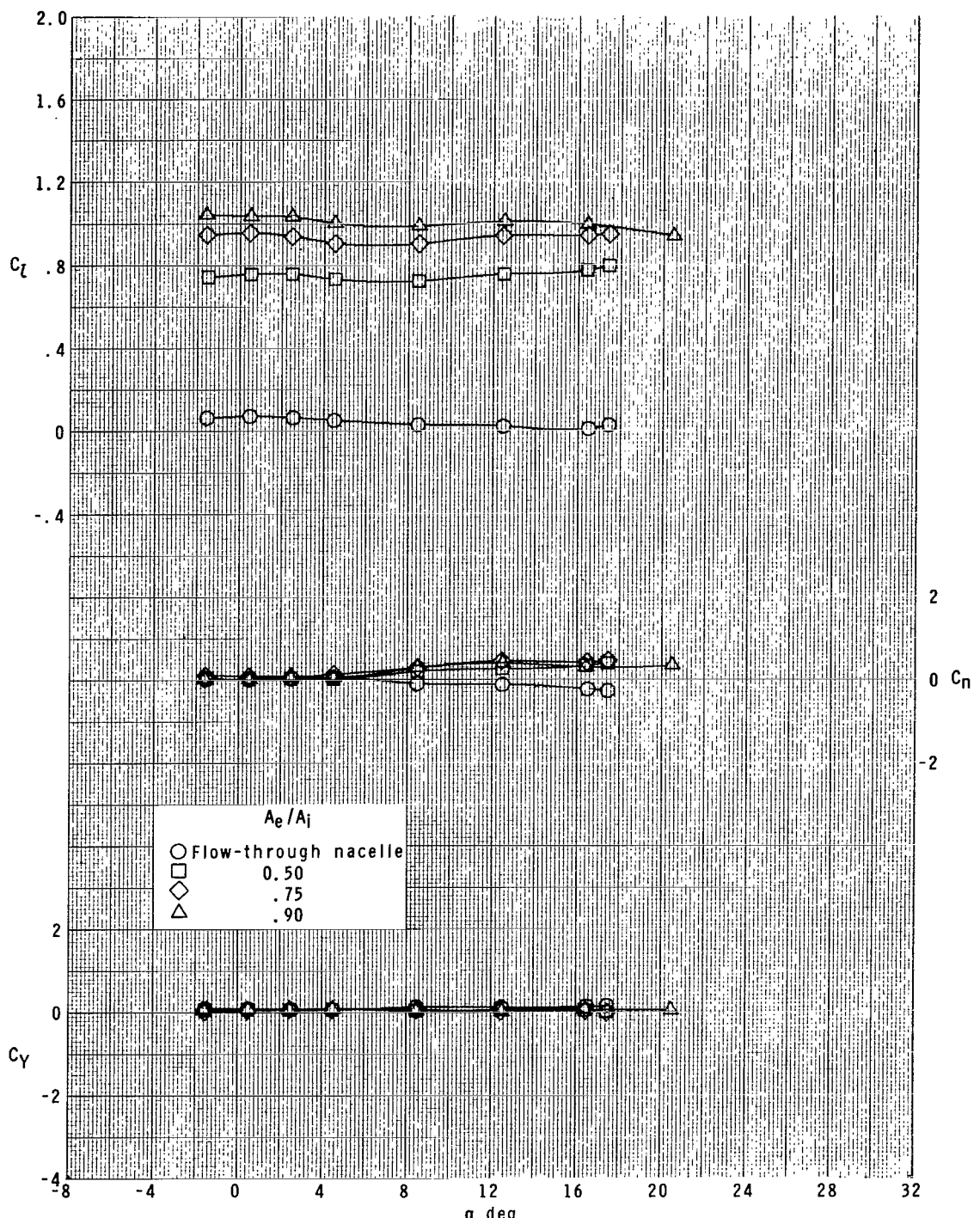
(c)  $M = 2.96.$

Figure 6.- Continued.



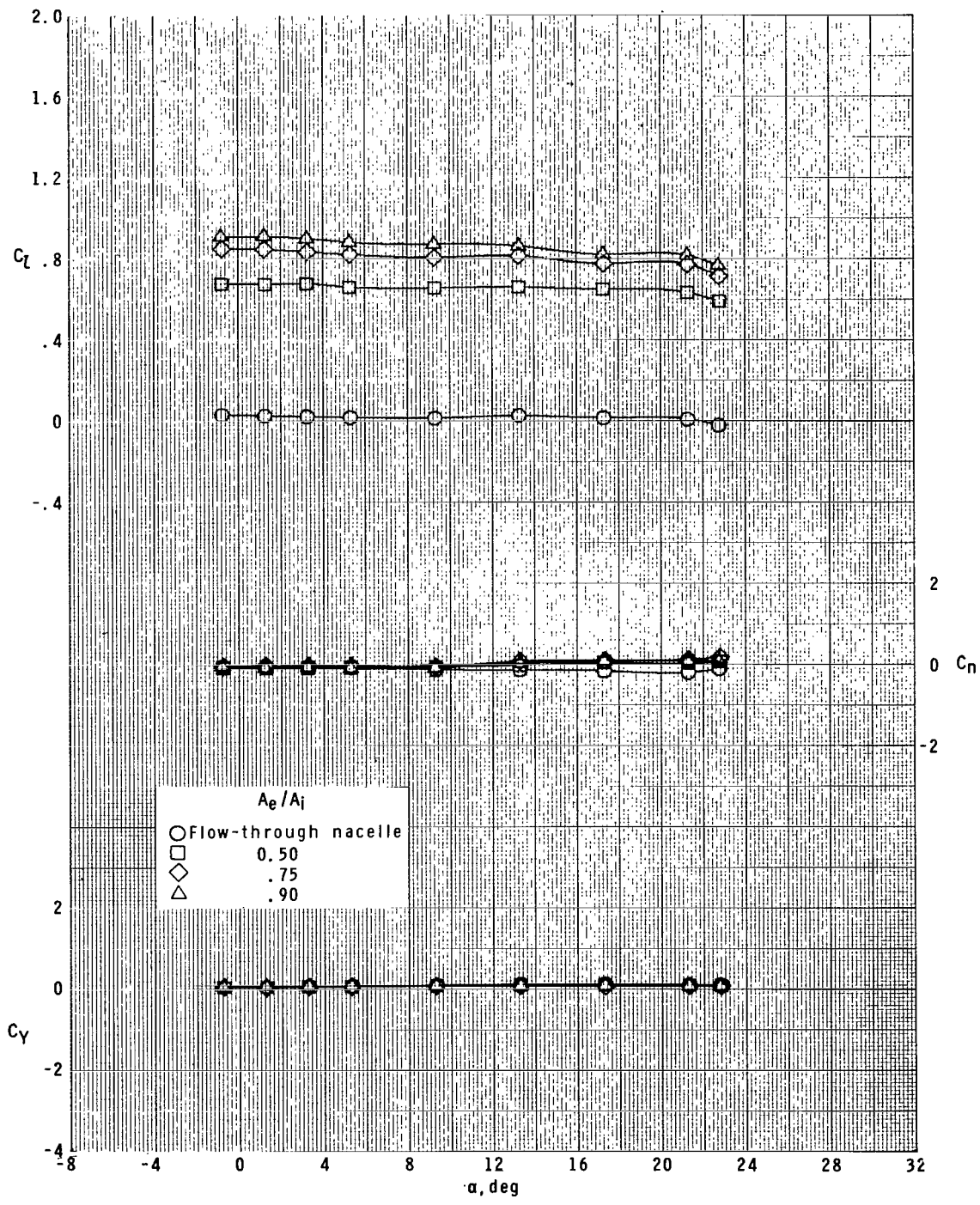
(d)  $M = 4.63.$

Figure 6.- Concluded.



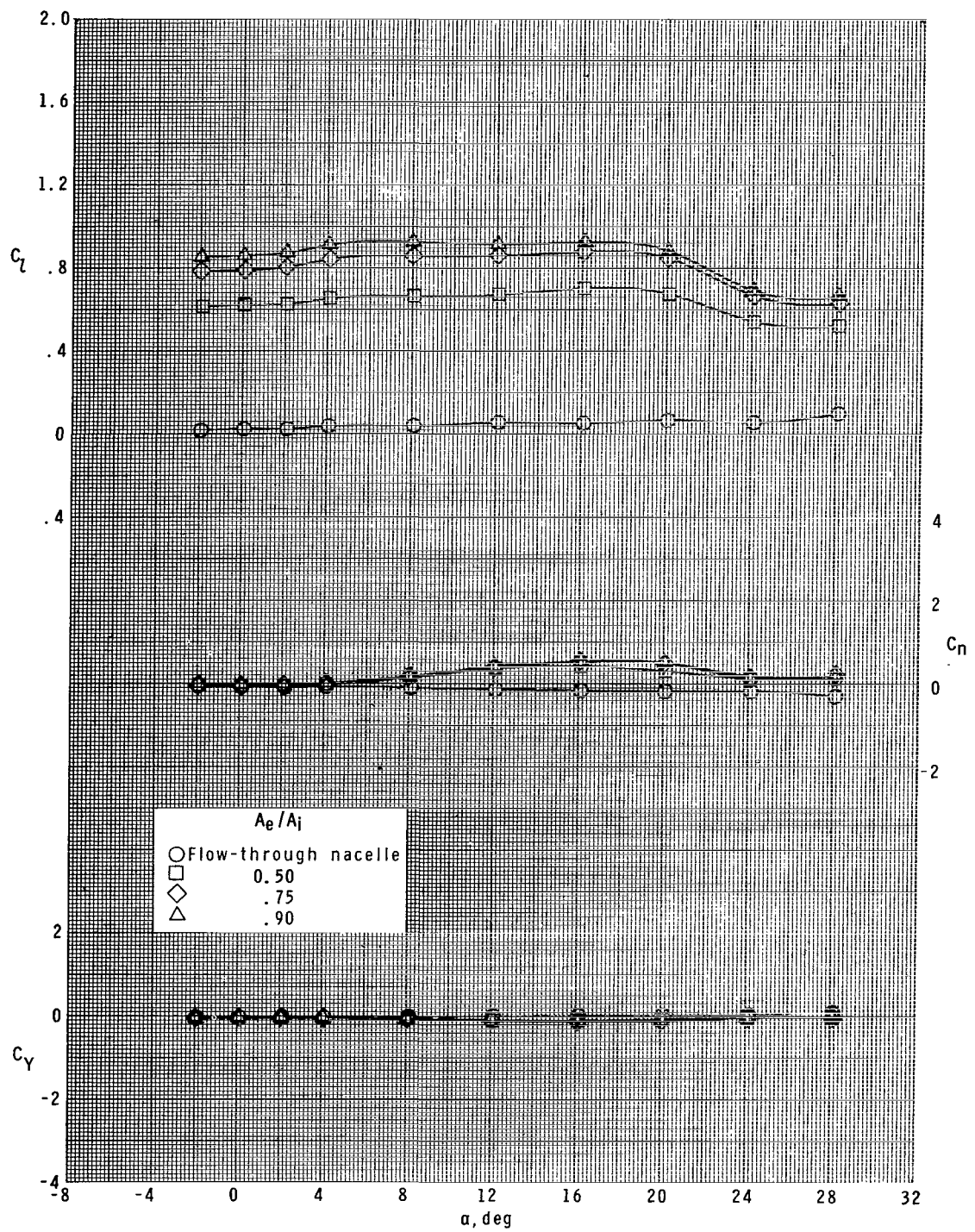
(a)  $M = 1.60$ .

Figure 7.- Effect of ratio of plenum exit area to inlet area for roll control on lateral aerodynamic characteristics of model with ram-air-spoiler tail fins for  $A_i/A = 0.063$  at  $\phi = 0^\circ$ .



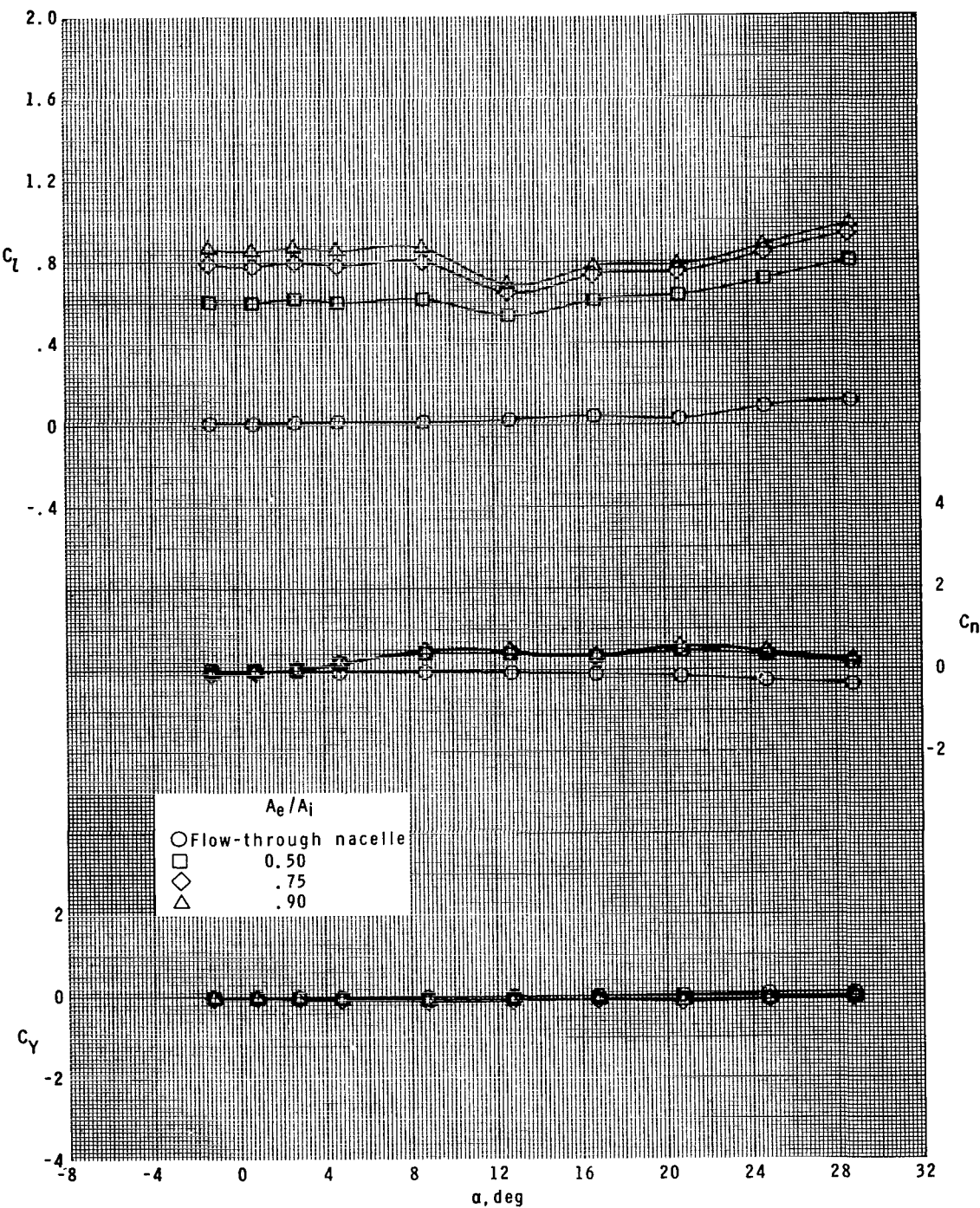
(b)  $M = 2.16.$

Figure 7.- Continued.



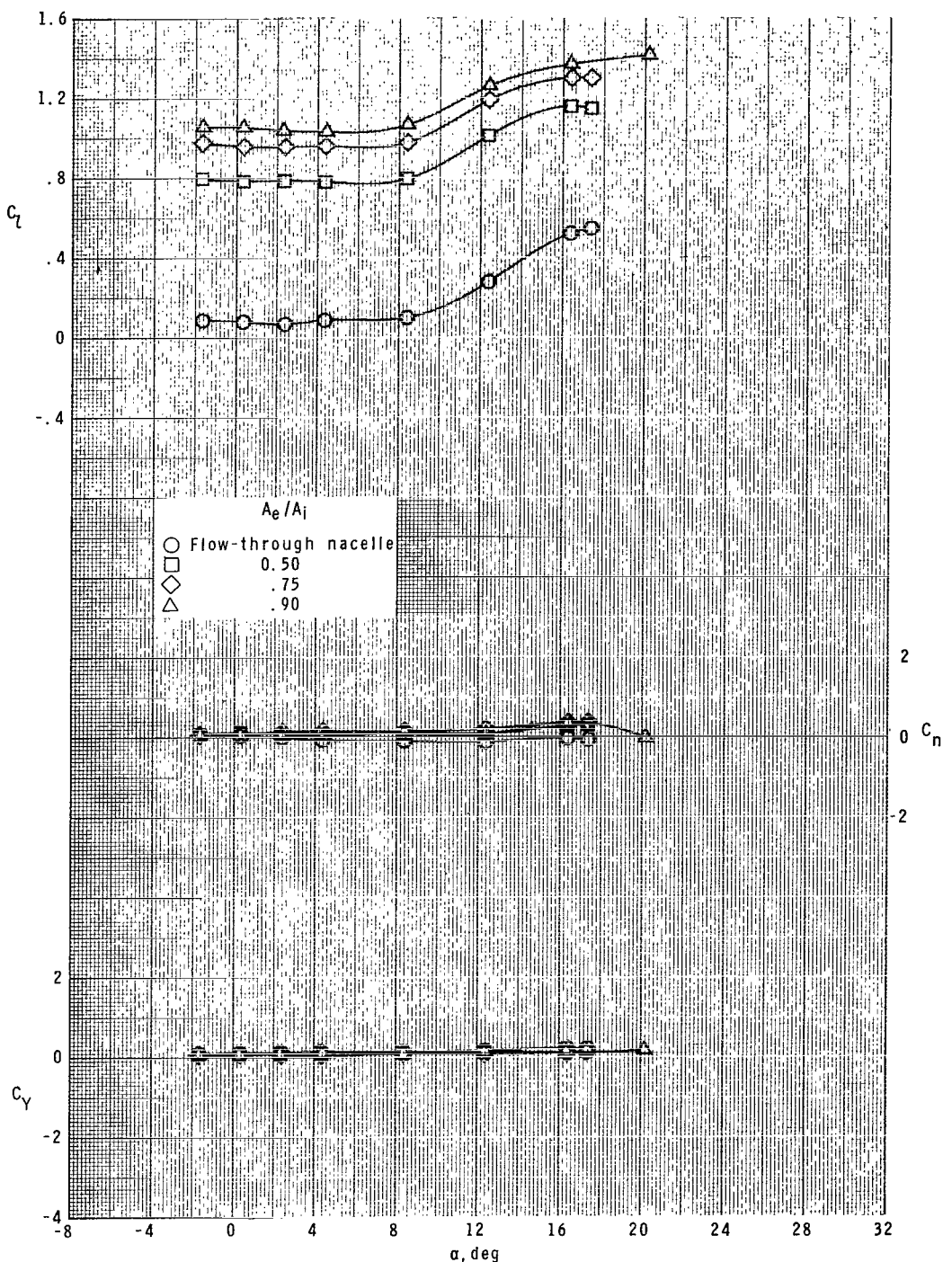
(c)  $M = 2.96.$

Figure 7.- Continued.



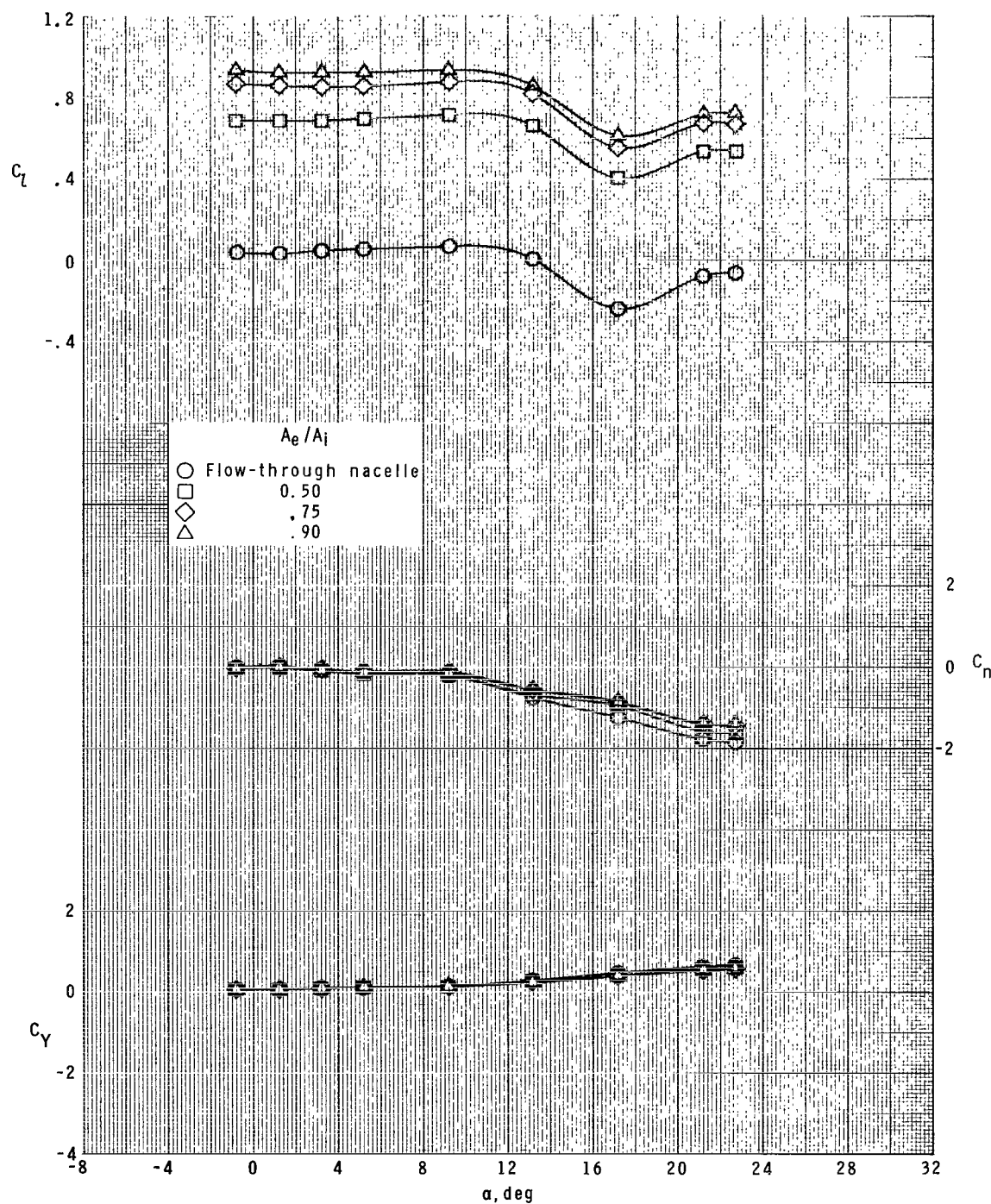
(d)  $M = 4.63.$

Figure 7.-- Concluded.



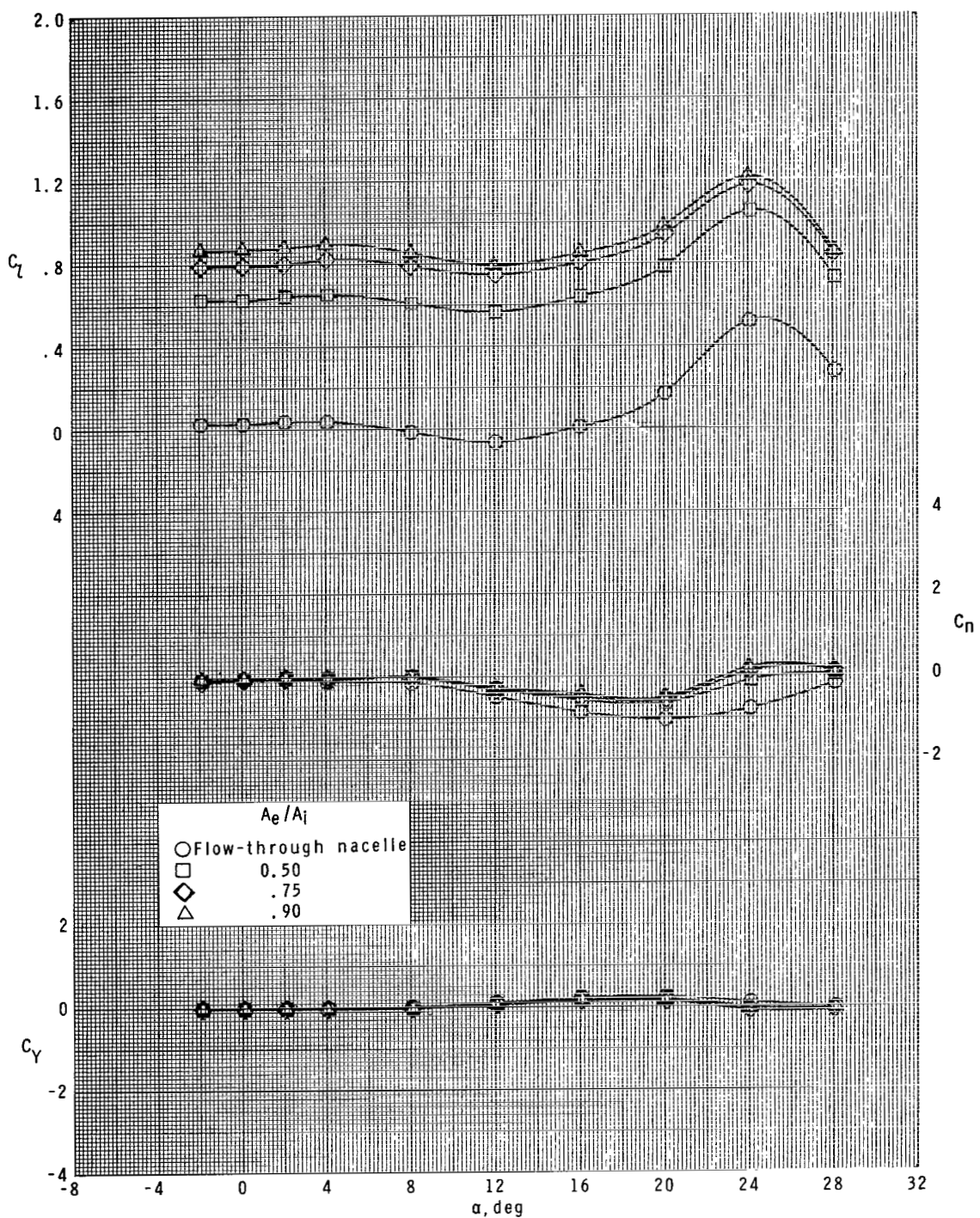
(a)  $M = 1.60.$

Figure 8.- Effect of ratio of plenum exit area to inlet area for roll control on lateral aerodynamic characteristics of model with ram-air-spoiler tail fins for  $A_i/A = 0.063$  at  $\phi = 22.5^\circ$ .



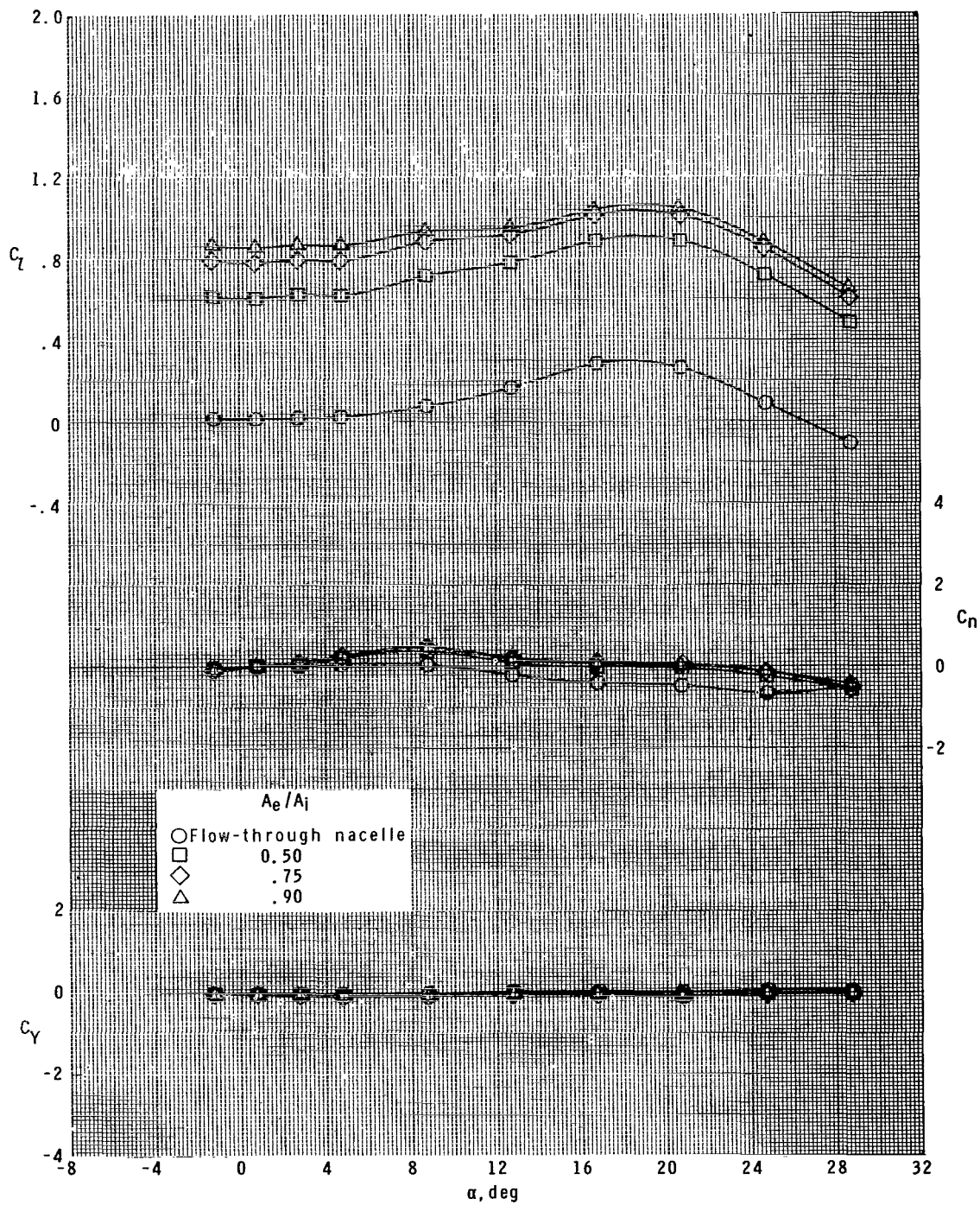
(b)  $M = 2.16.$

Figure 8.- Continued.



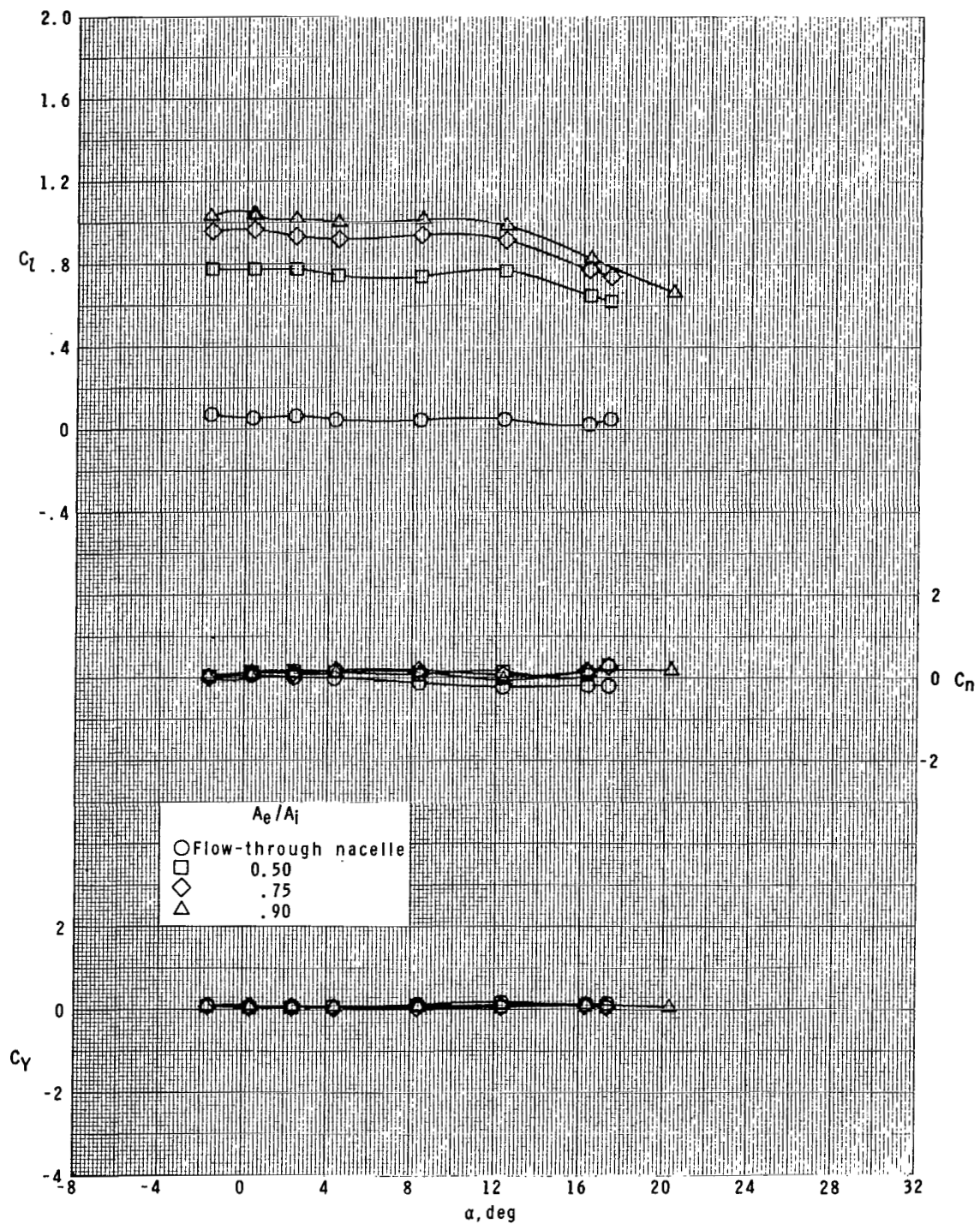
(c)  $M = 2.96.$

Figure 8.- Continued.



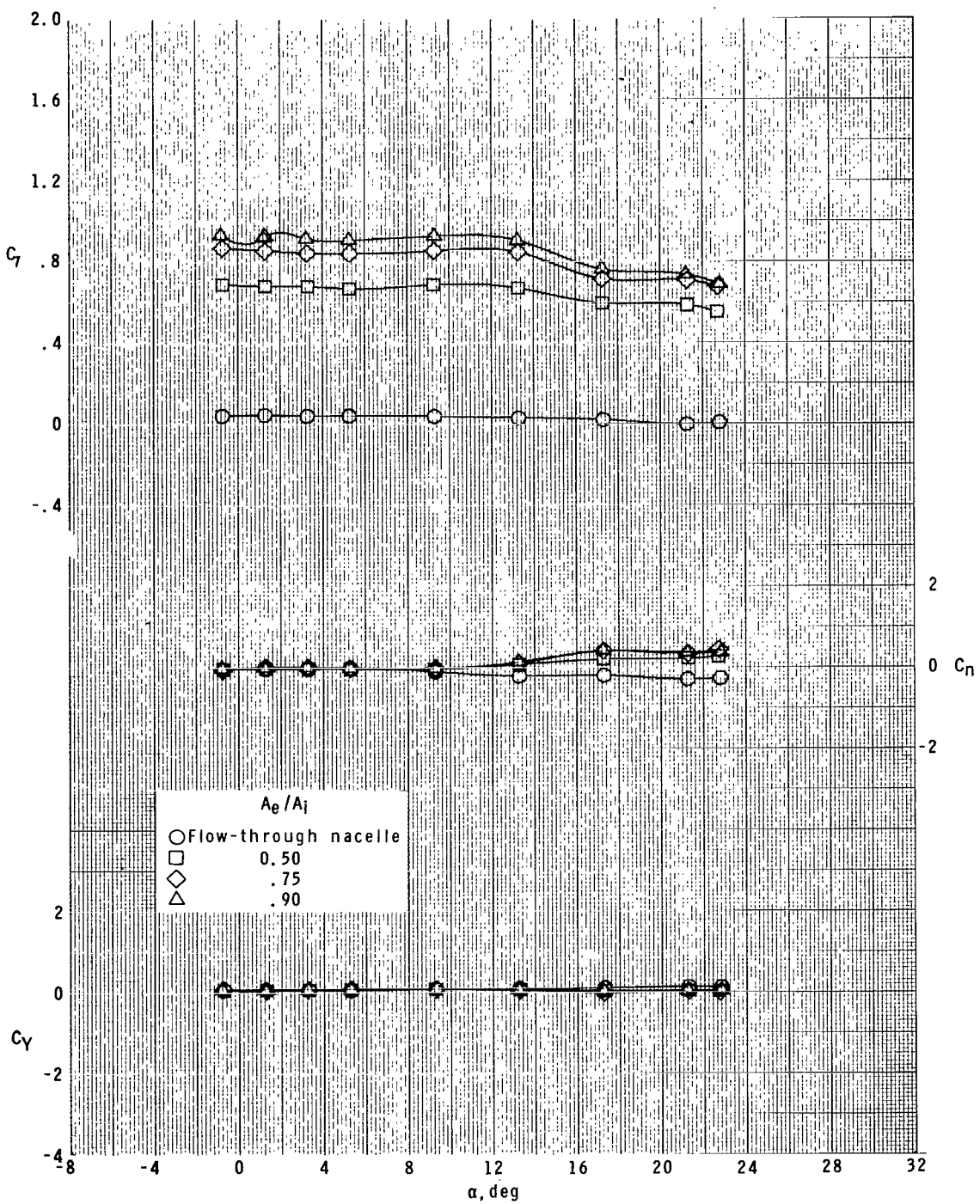
(d)  $M = 4.63.$

Figure 8.- Concluded.



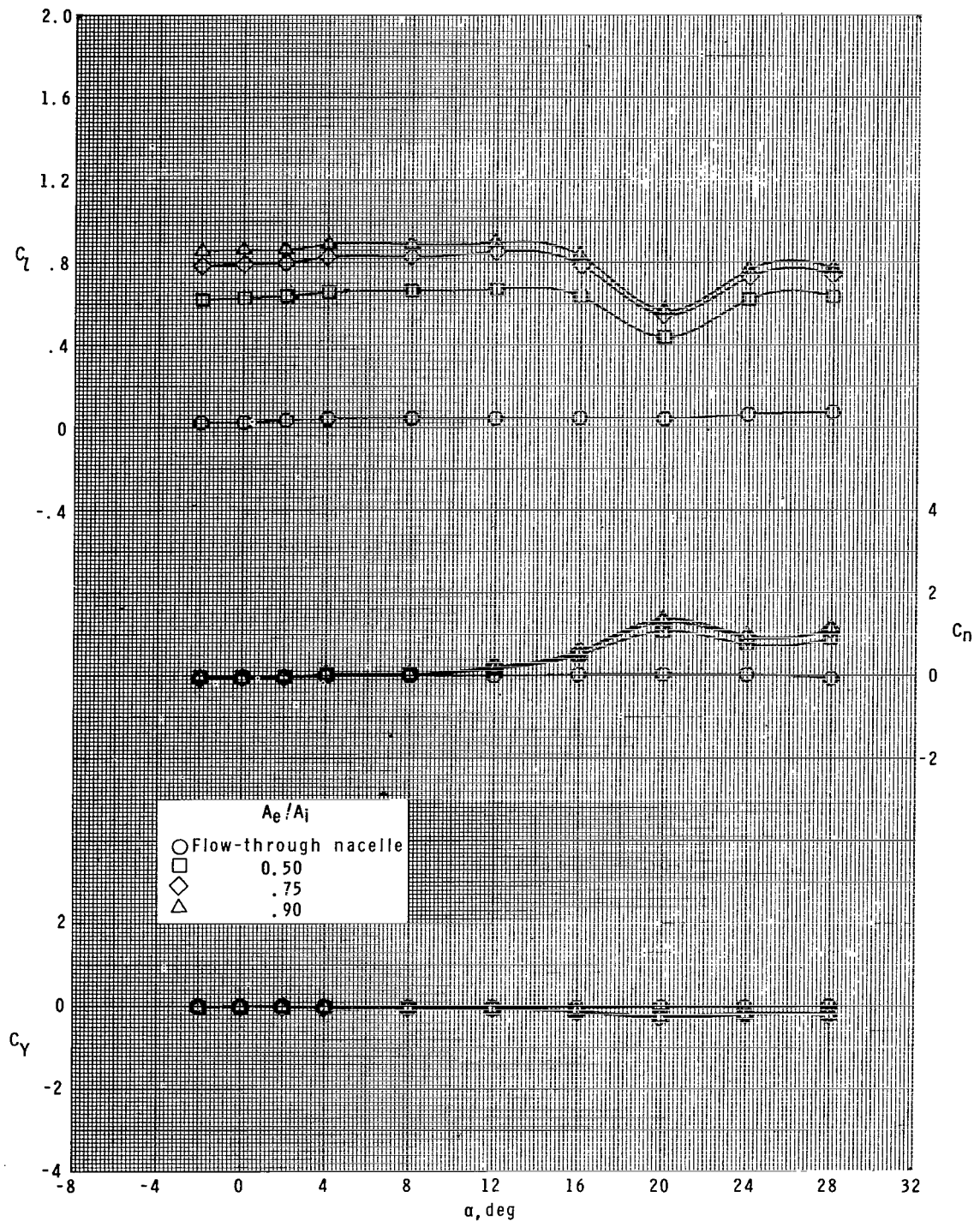
(a)  $M = 1.60.$

Figure 9.- Effect of ratio of plenum exit area to inlet area for roll control on lateral aerodynamic characteristics of model with ram-air-spoiler tail fins for  $A_i/A = 0.063$  at  $\phi = 45^\circ$ .



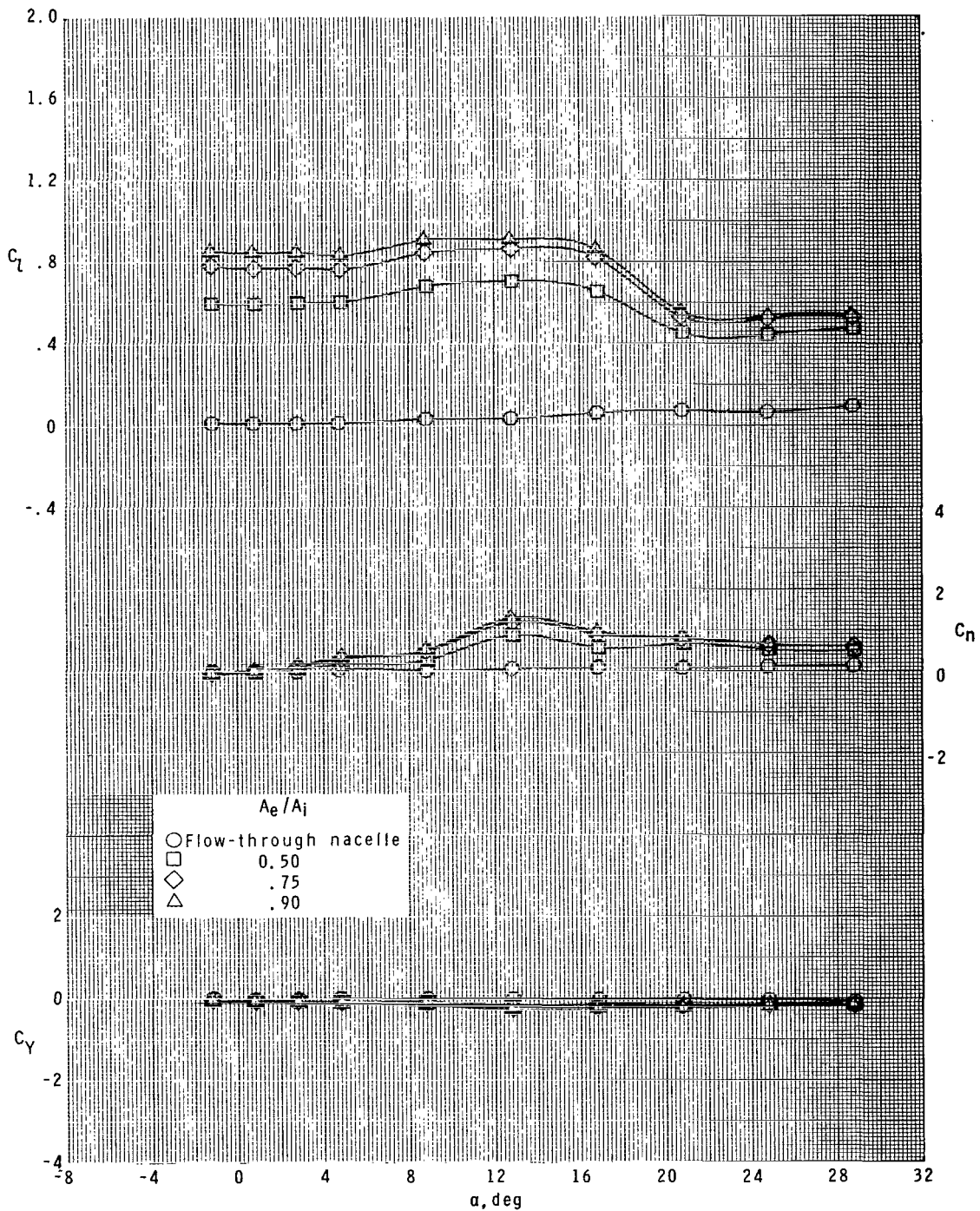
(b)  $M = 2.16.$

Figure 9.- Continued.



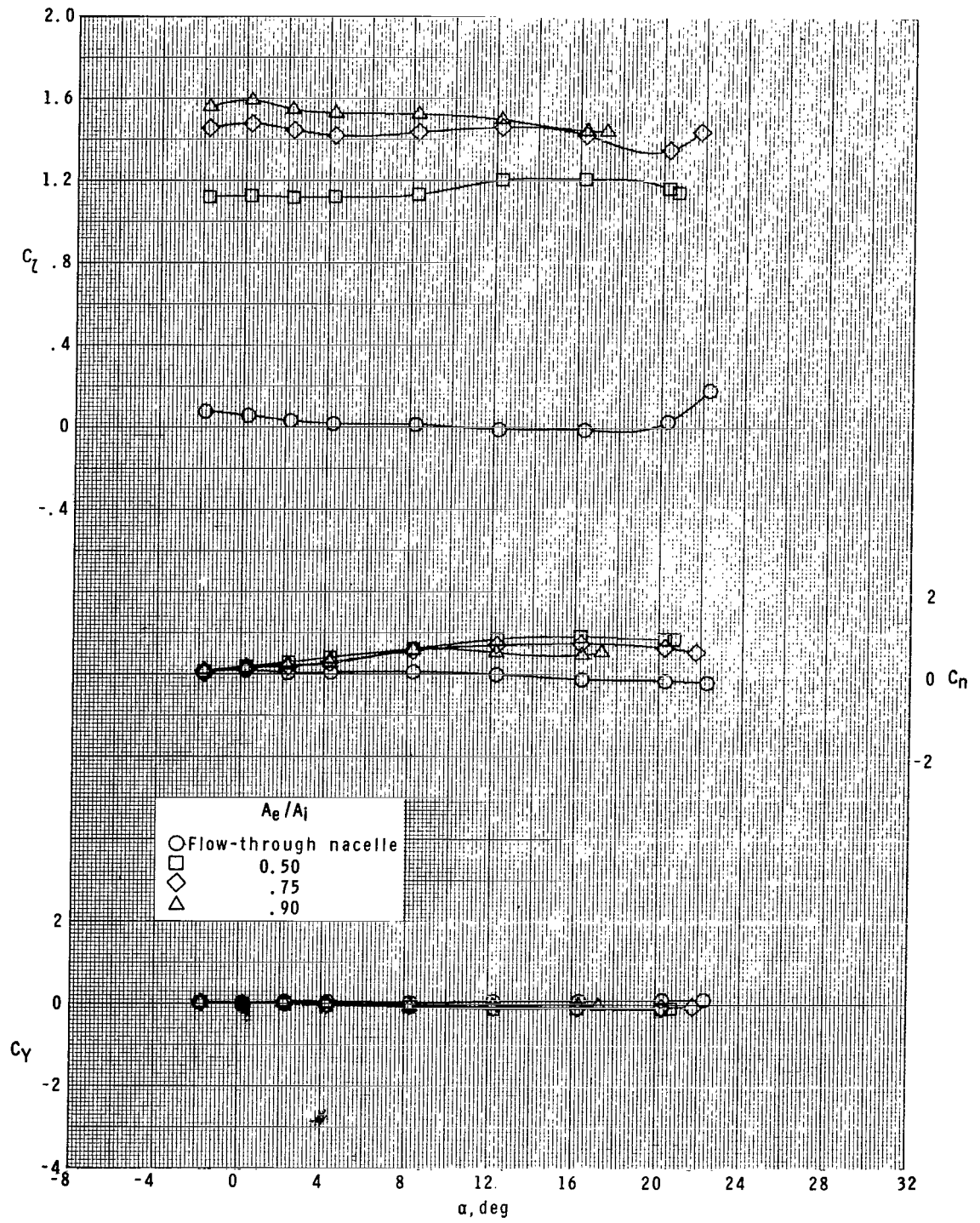
(c)  $M = 2.96.$

Figure 9.- Continued.



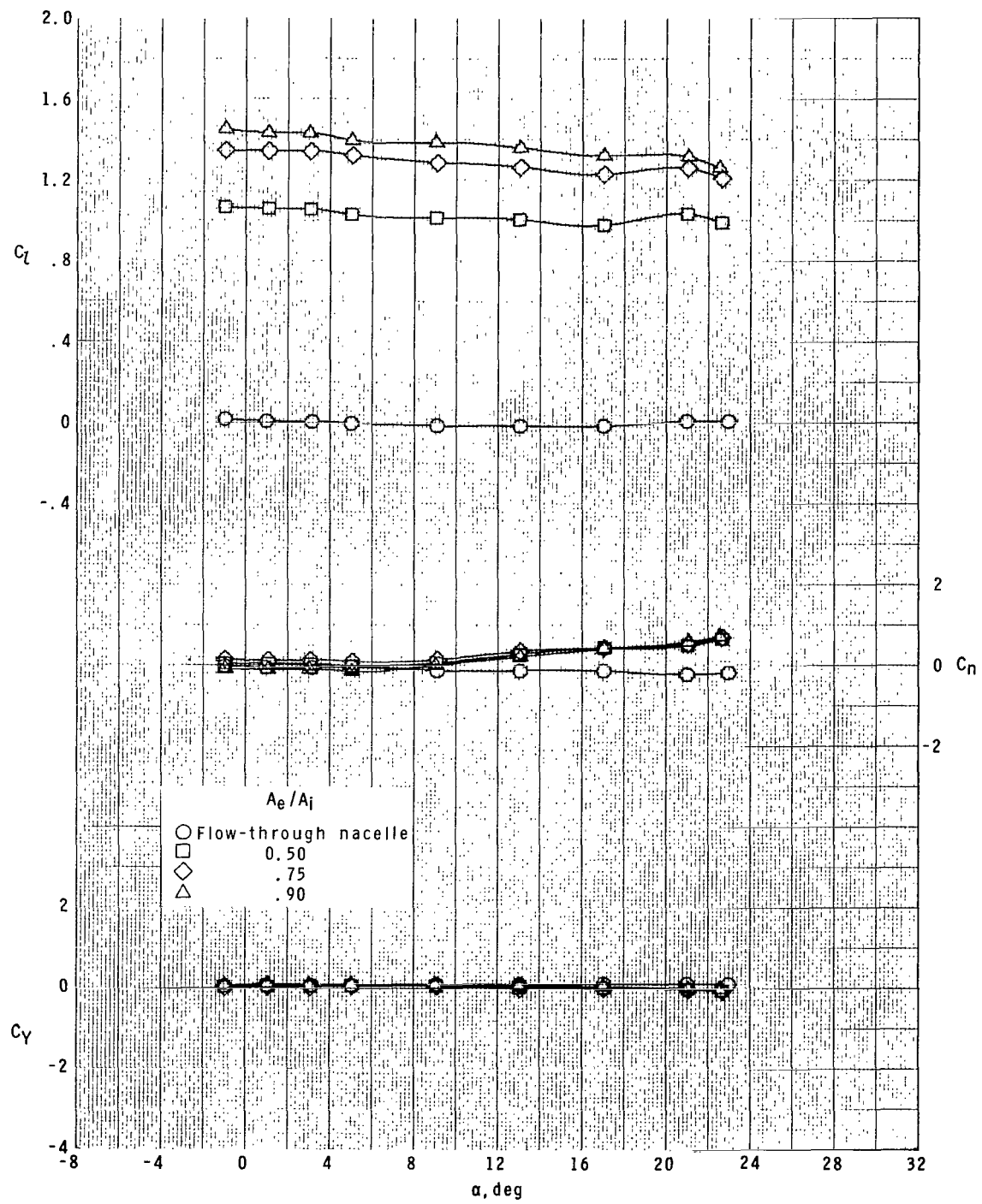
(d)  $M = 4.63.$

Figure 9.- Concluded.



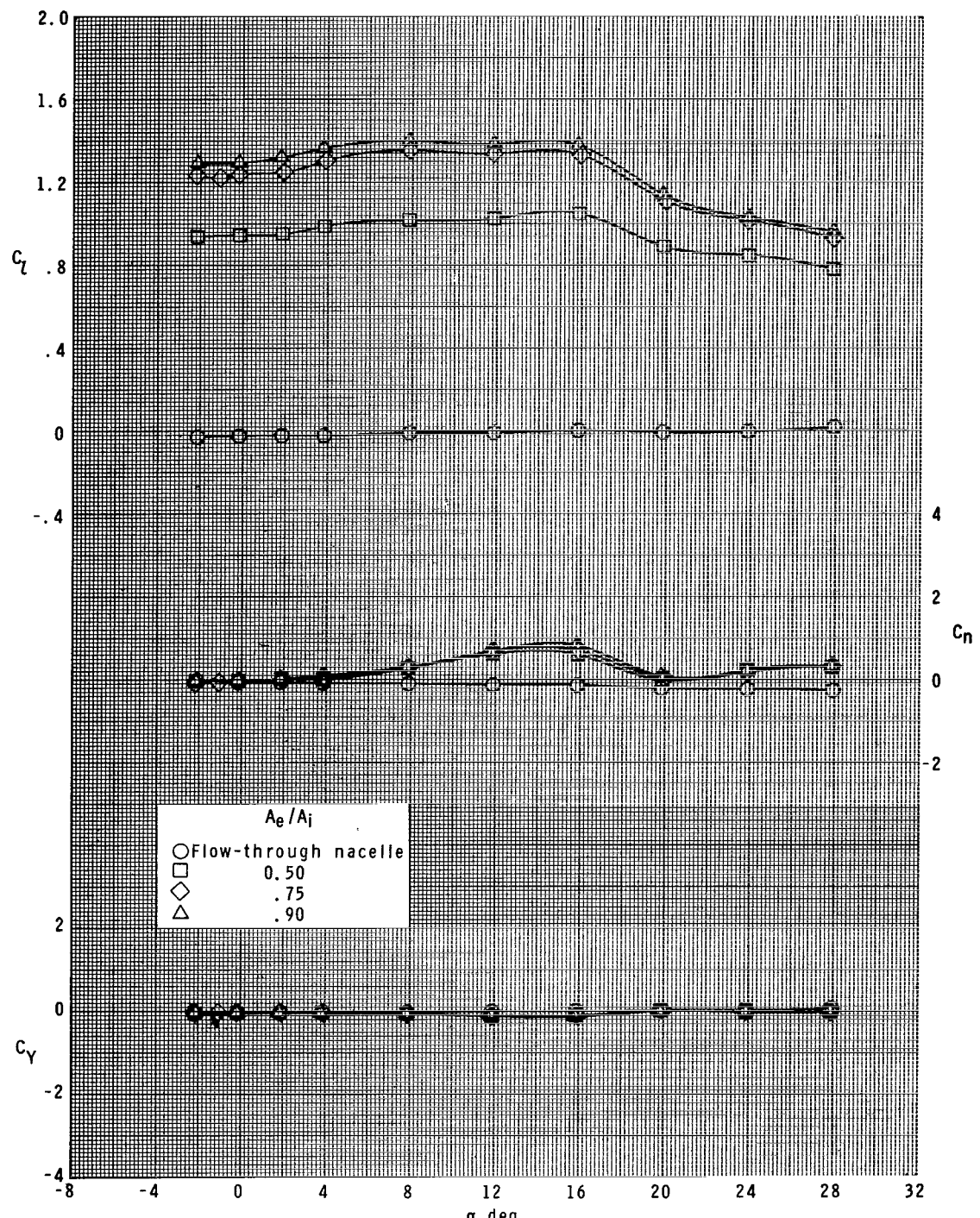
(a)  $M = 1.60$ .

Figure 10.- Effect of ratio of plenum exit area to inlet area for roll control on lateral aerodynamic characteristics of model with ram-air-spoiler tail fins for  $A_i/A = 0.111$  at  $\phi = 0^\circ$ .



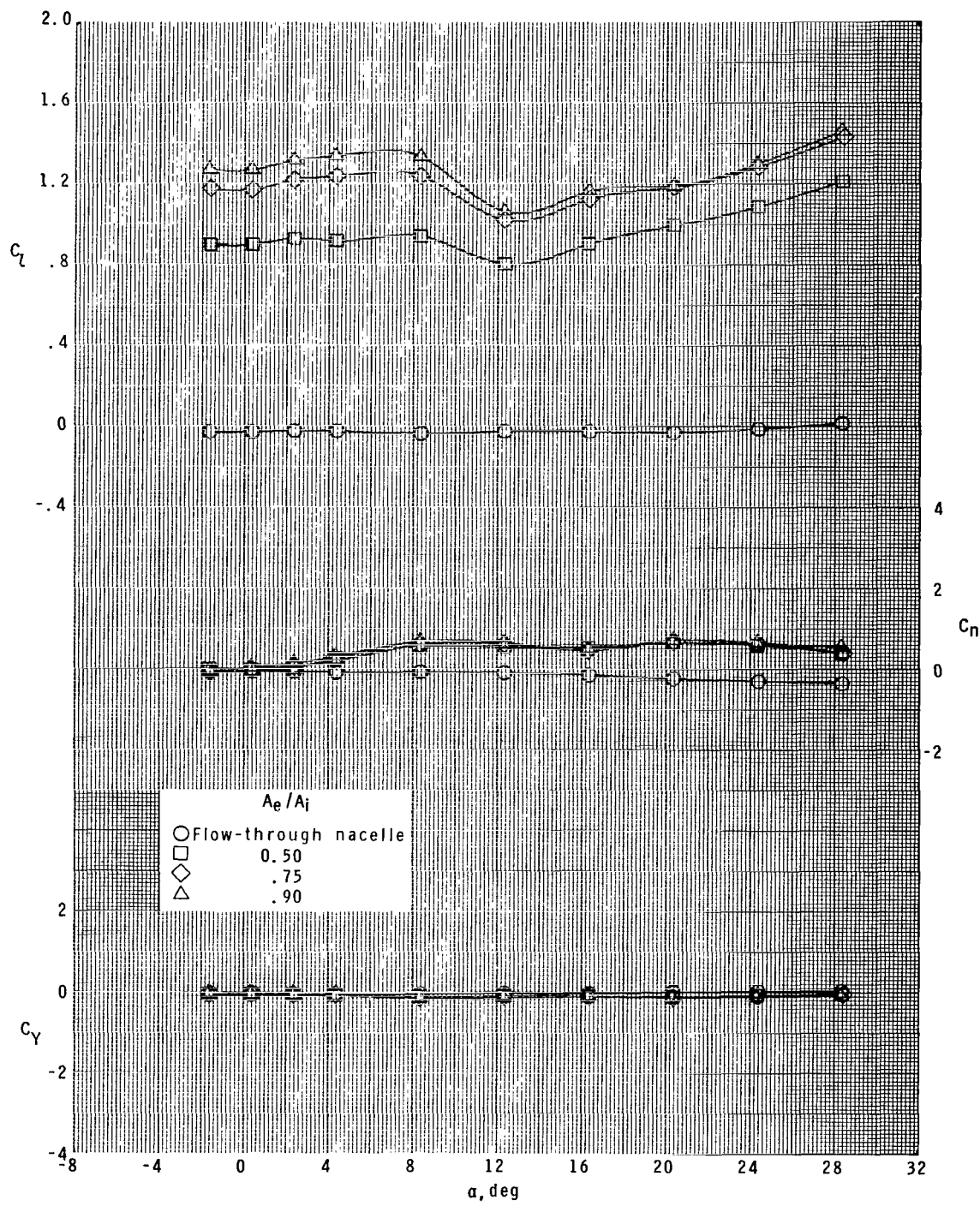
(b)  $M = 2.16.$

Figure 10.- Continued.



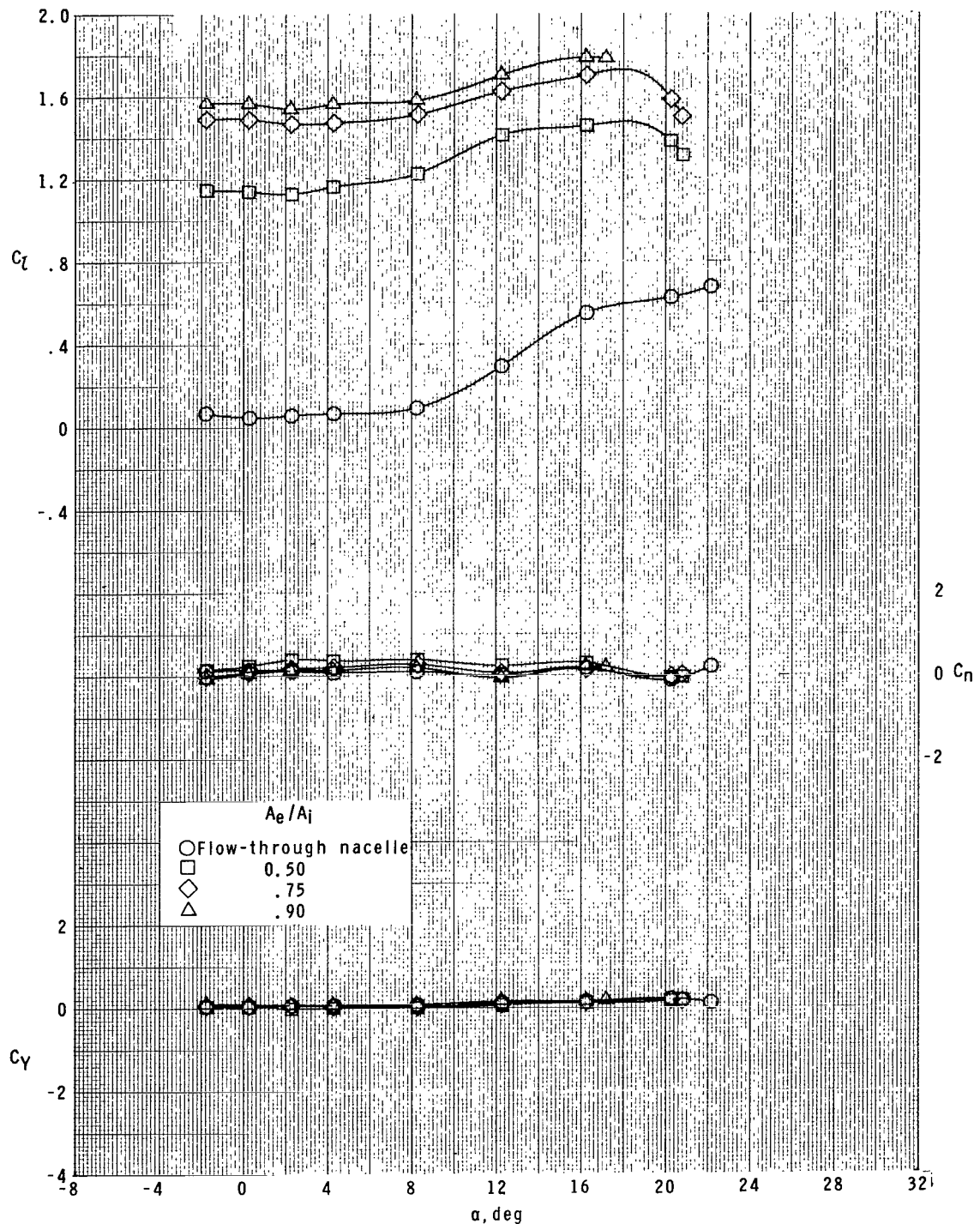
(c)  $M = 2.96$ .

Figure 10.- Continued.



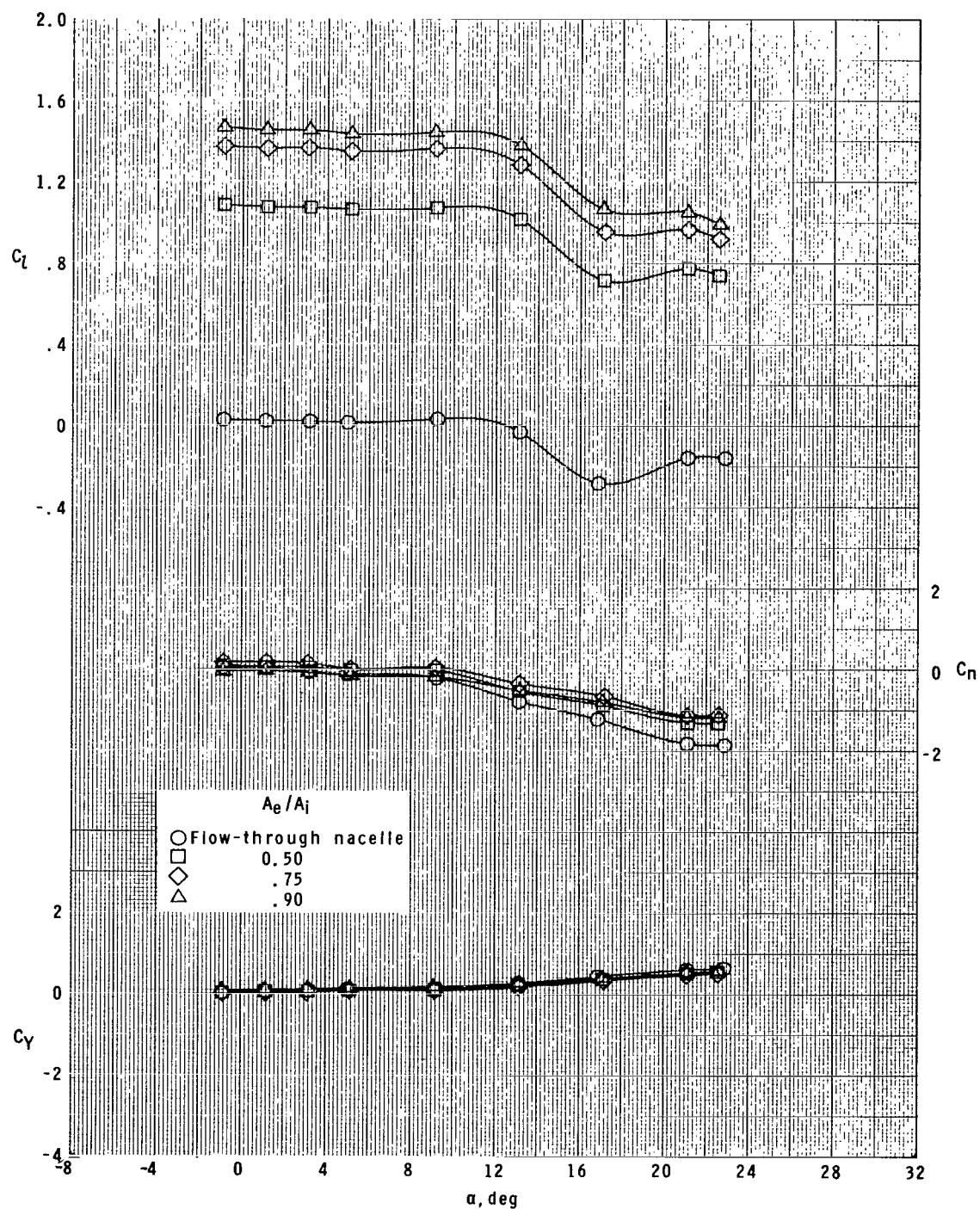
(d)  $M = 4.63.$

Figure 10.- Concluded.



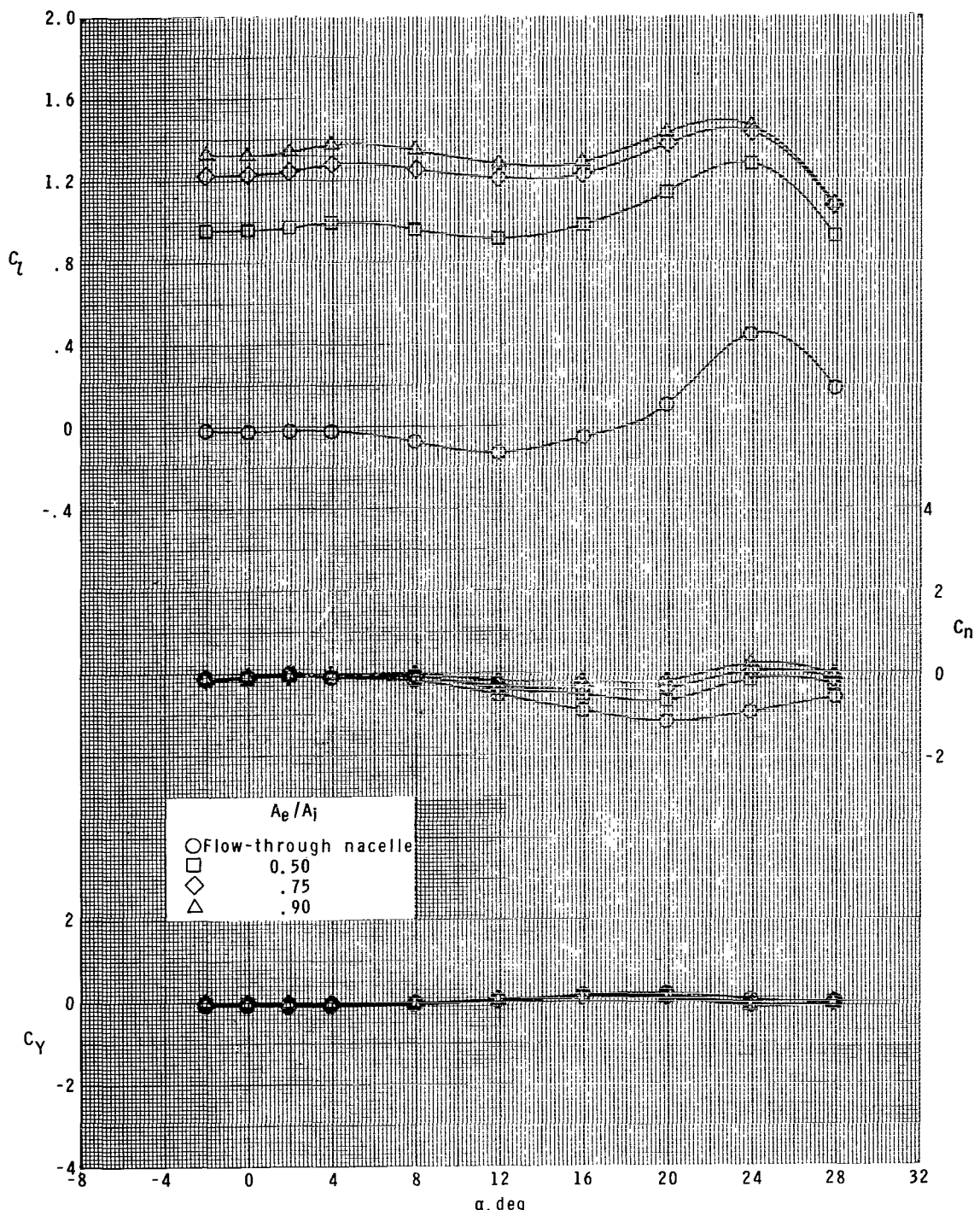
(a)  $M = 1.60$ .

Figure 11.- Effect of ratio of plenum exit area to inlet area for roll control on lateral aerodynamic characteristics of model with ram-air-spoiler tail fins for  $A_e/A_i = 0.111$  at  $\phi = 22.5^\circ$ .



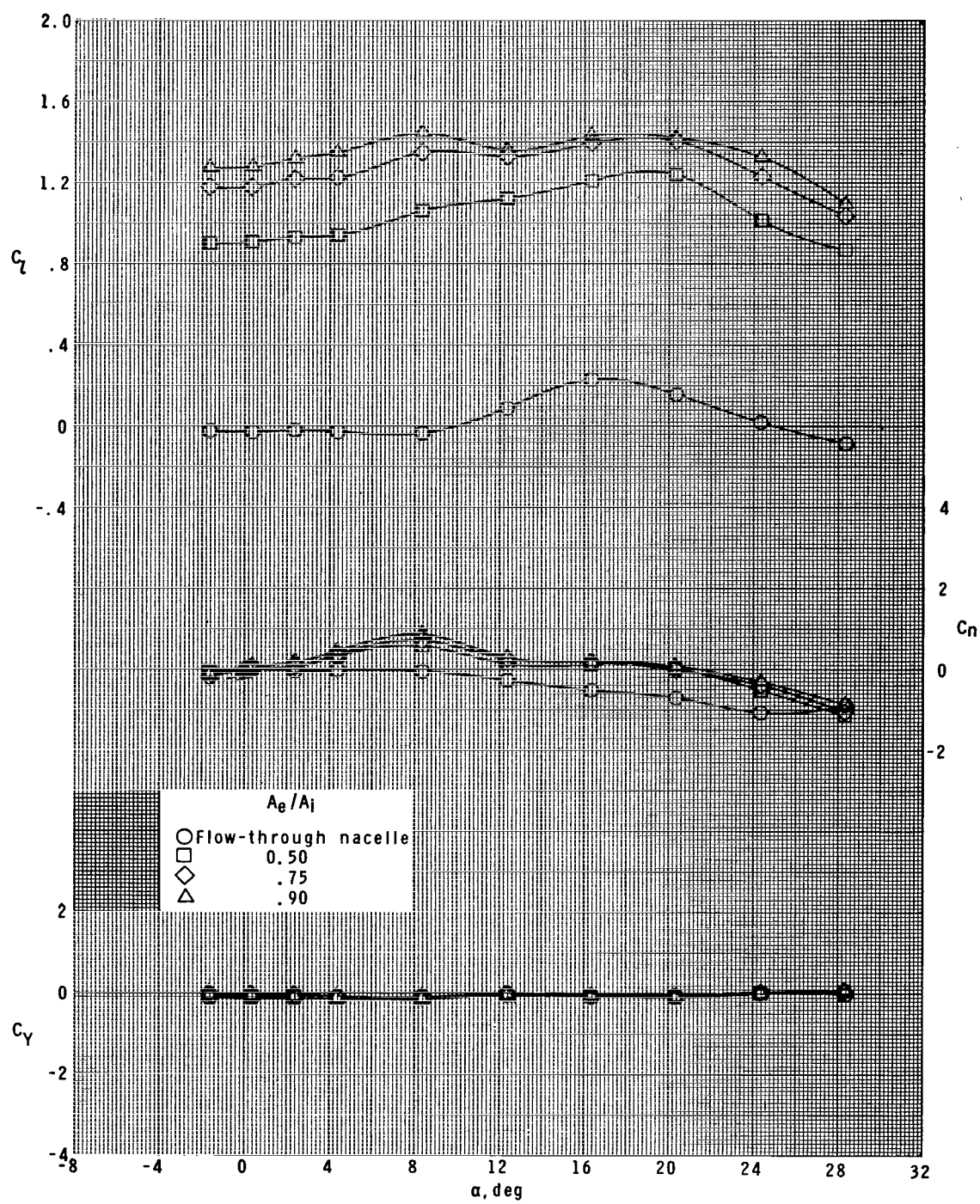
(b)  $M = 2.16.$

Figure 11.- Continued.



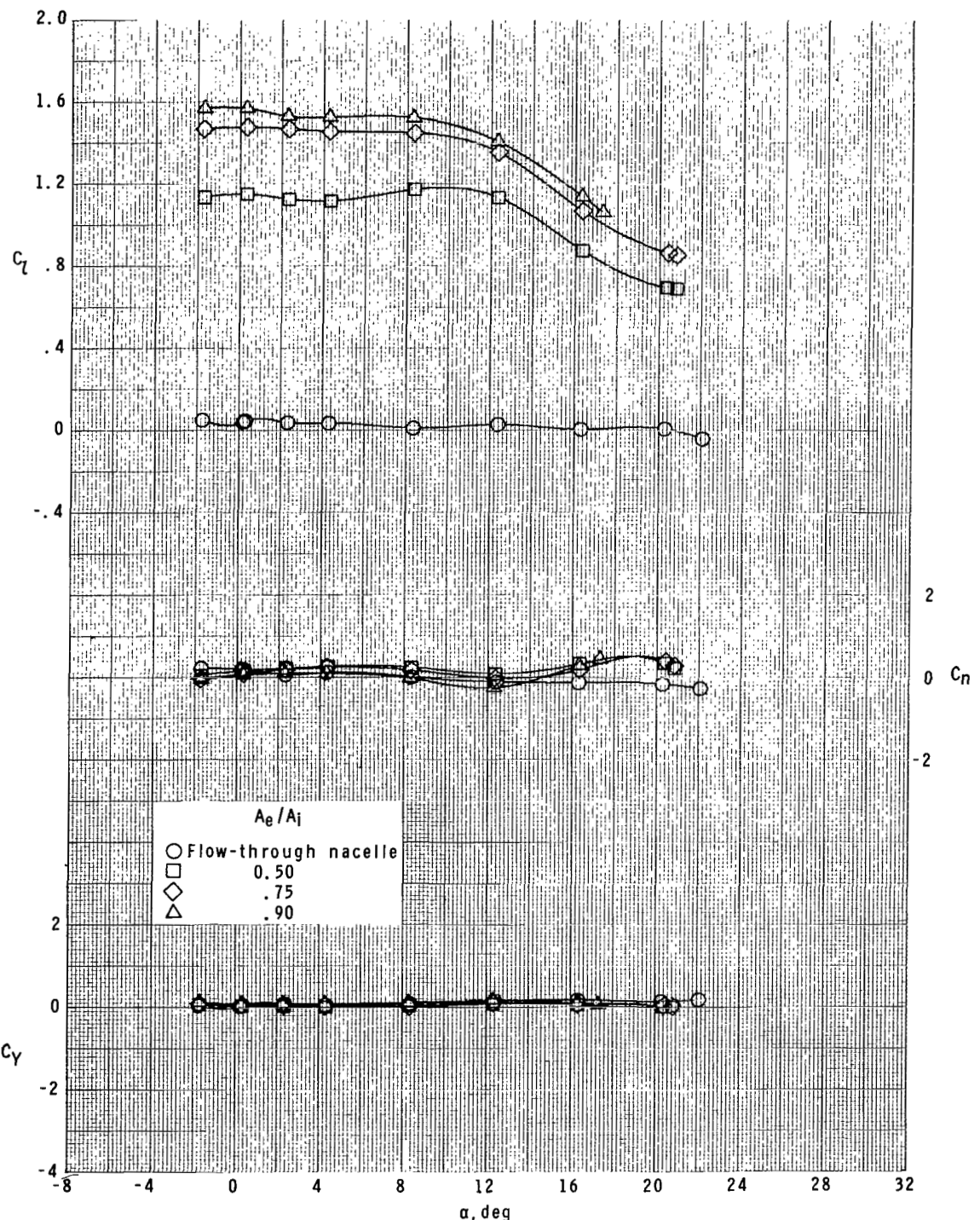
(c)  $M = 2.96$ .

Figure 11.- Continued.



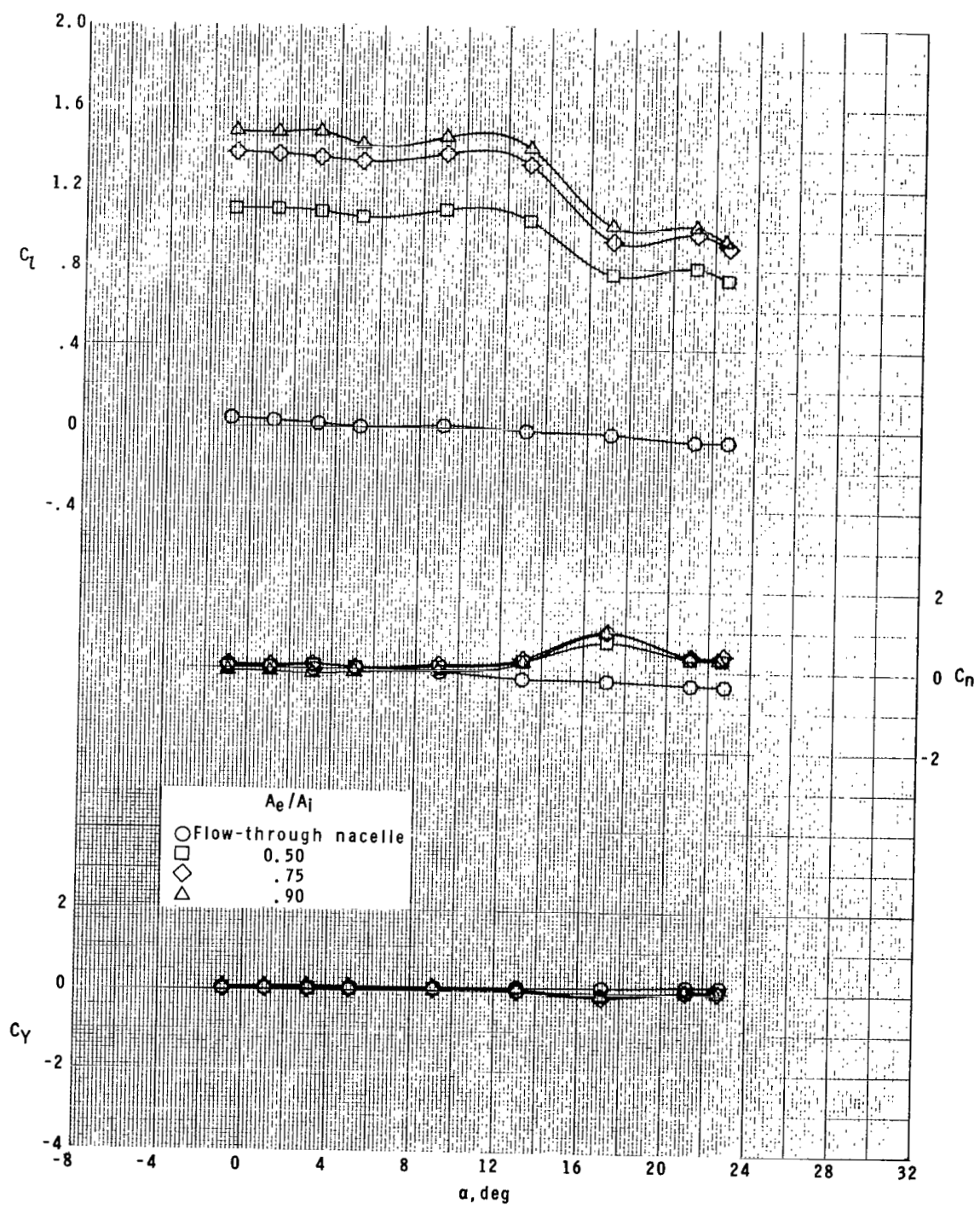
(d)  $M = 4.63.$

Figure 11.- Concluded.



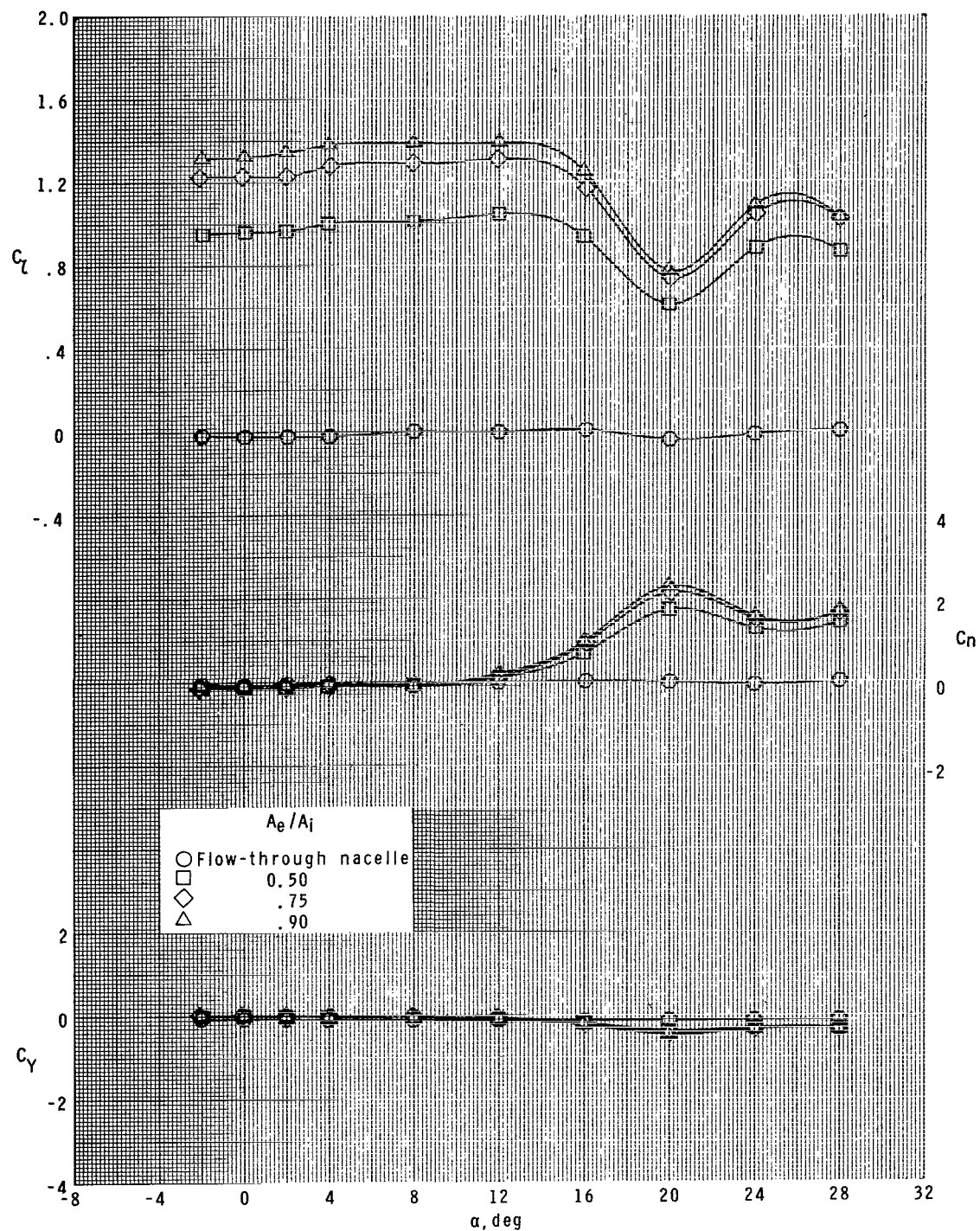
(a)  $M = 1.60.$

Figure 12.- Effect of ratio of plenum exit area to inlet area for roll control on lateral aerodynamic characteristics of model with ram-air-spoiler tail fins for  $A_i/A = 0.111$  at  $\phi = 45^\circ$ .



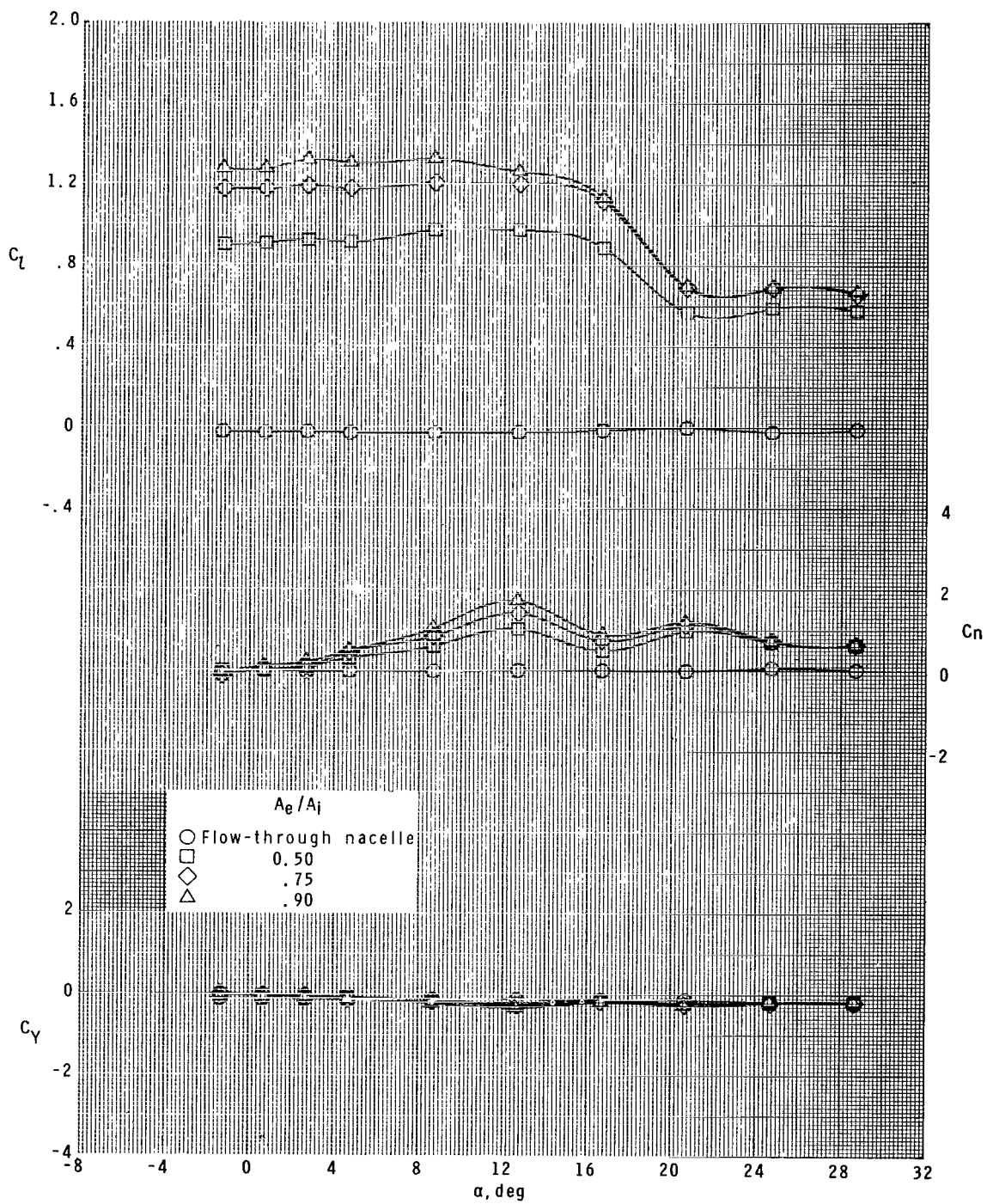
(b)  $M = 2.16.$

Figure 12.- Continued.



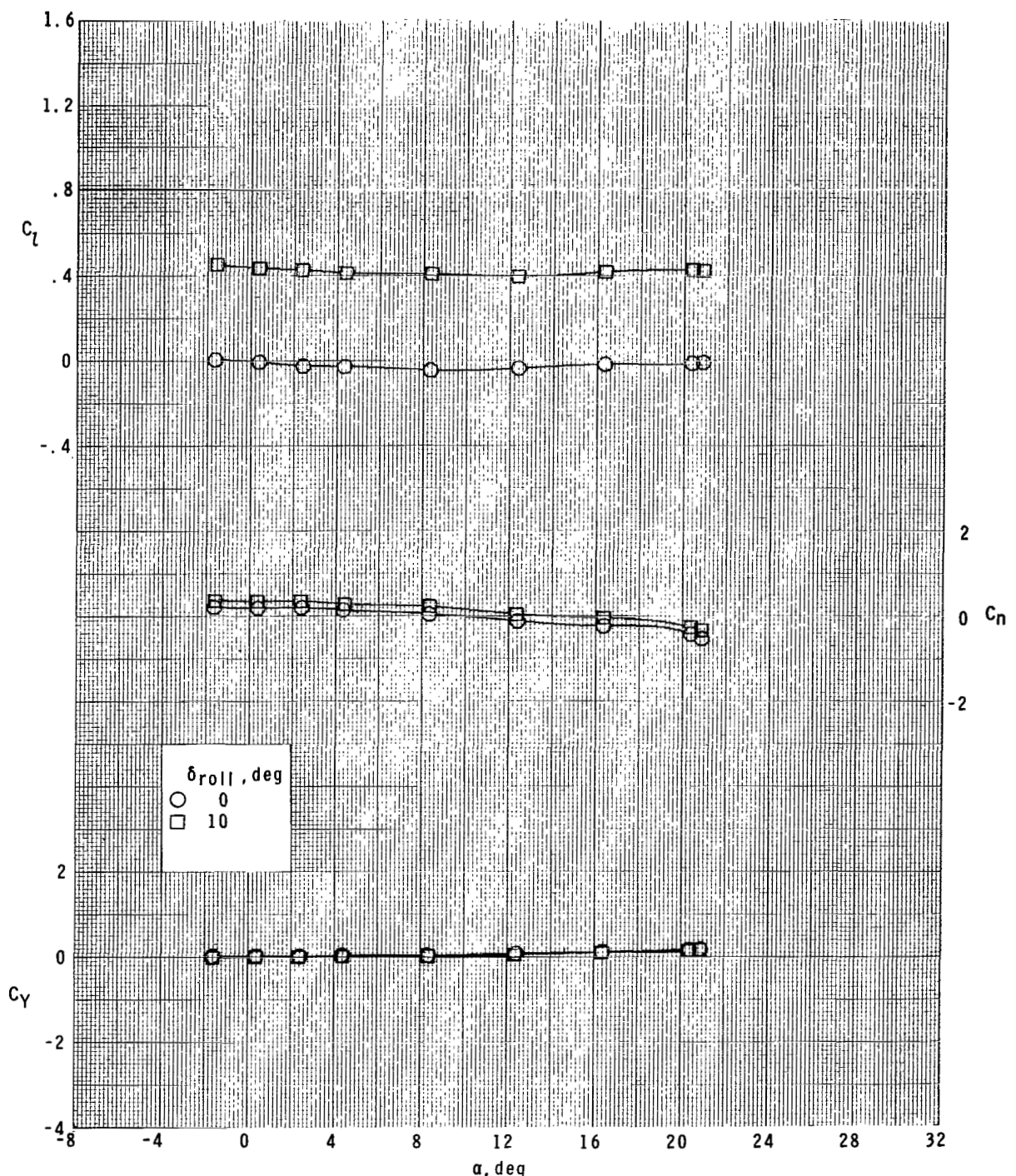
(c)  $M = 2.96.$

Figure 12.- Continued.



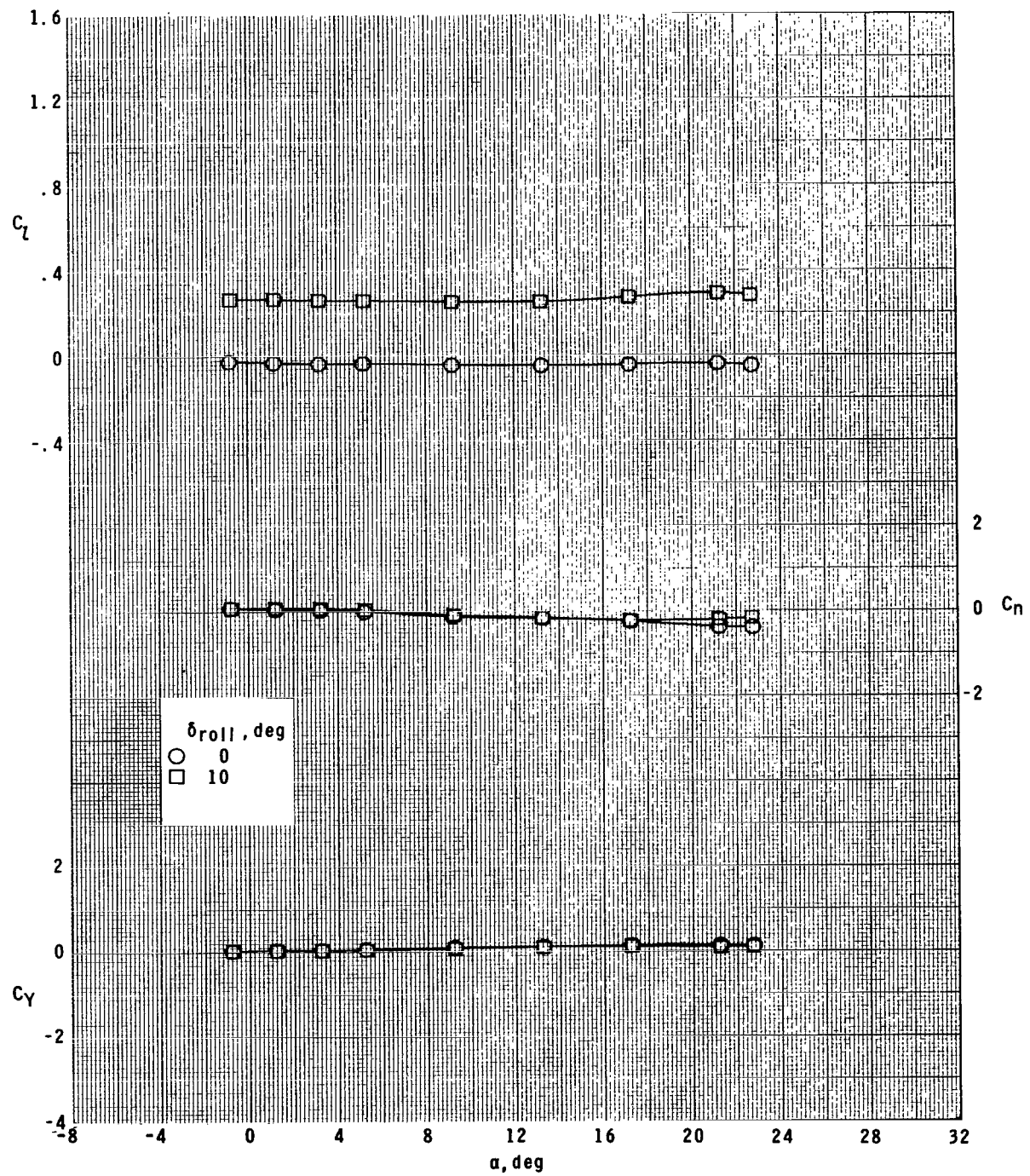
(d)  $M = 4.63.$

Figure 12.- Concluded.



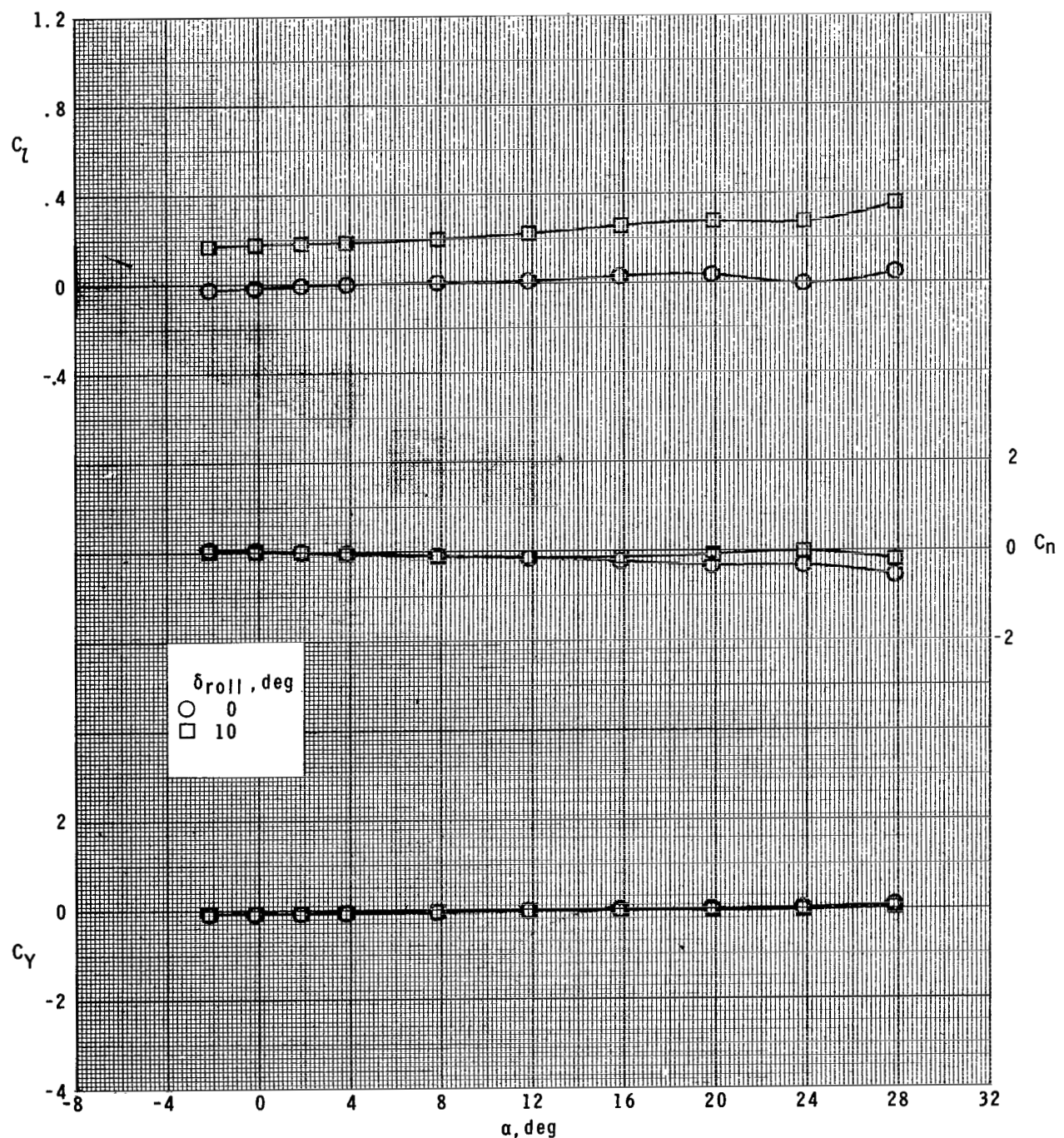
(a)  $M = 1.60$ .

Figure 13.- Effect of four plain tail-fin ailerons on lateral aerodynamic characteristics of model at  $\phi = 0^\circ$ .



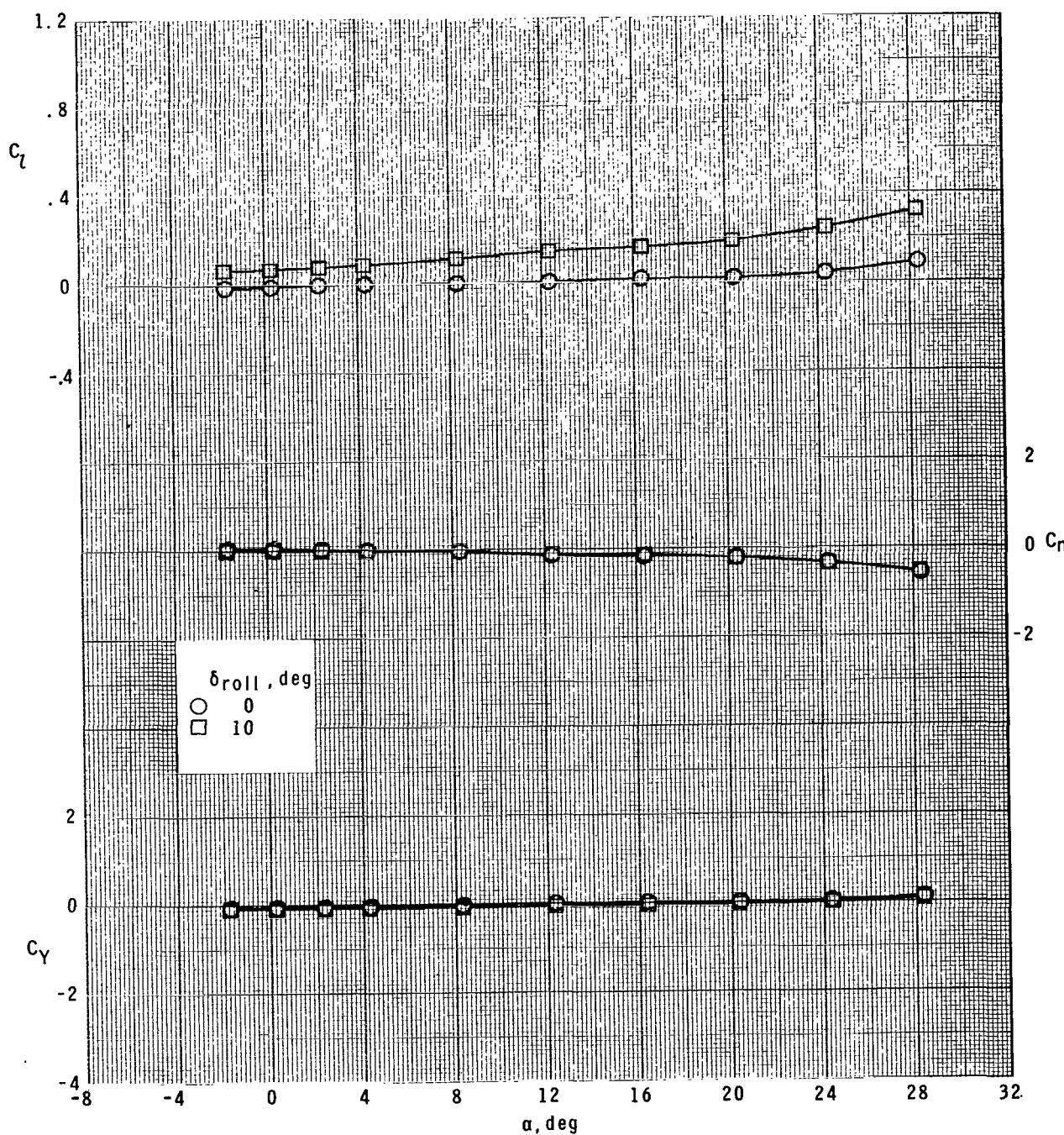
(b)  $M = 2.16.$

Figure 13.- Continued.



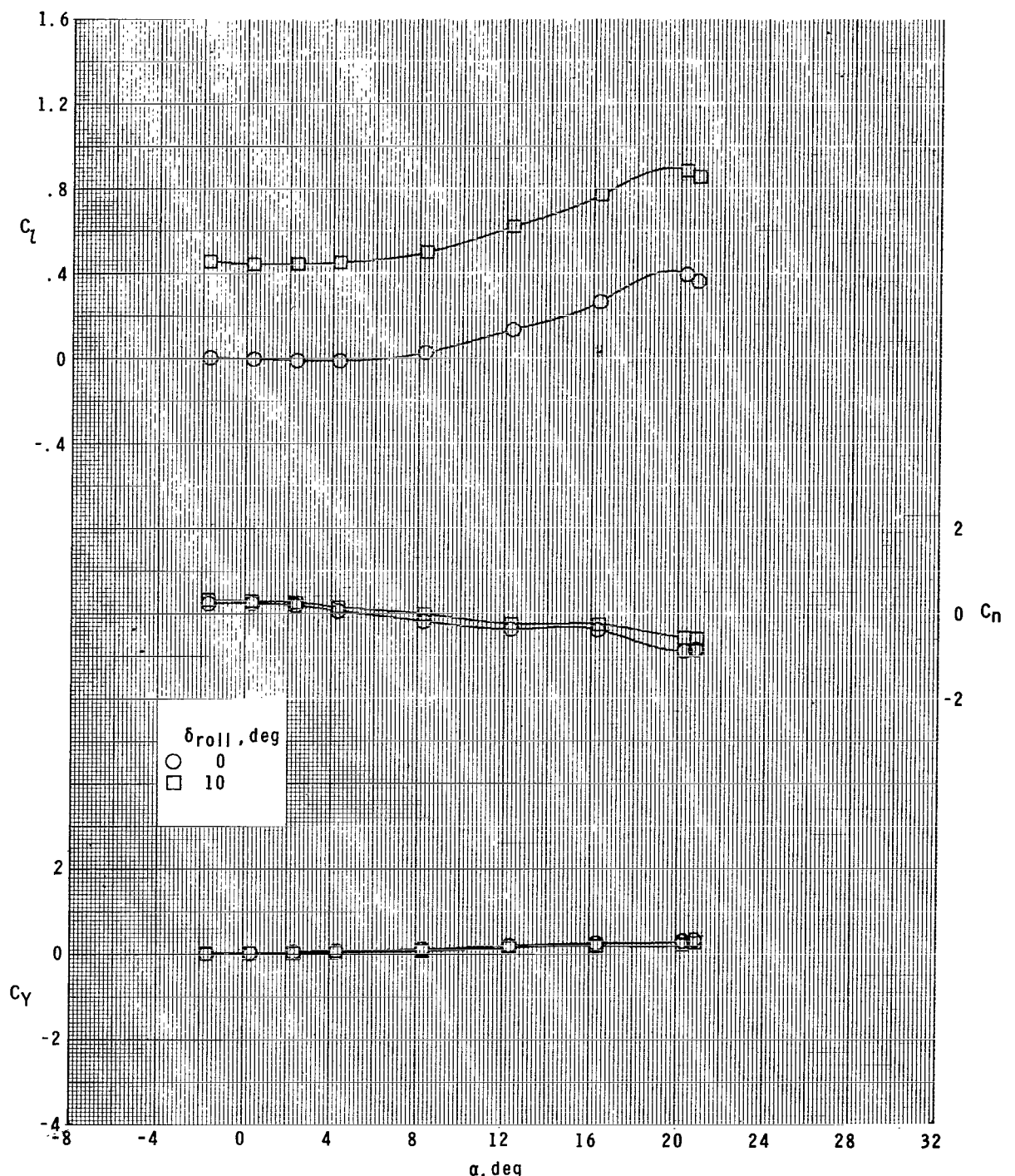
(c)  $M = 2.96.$

Figure 13.- Continued.



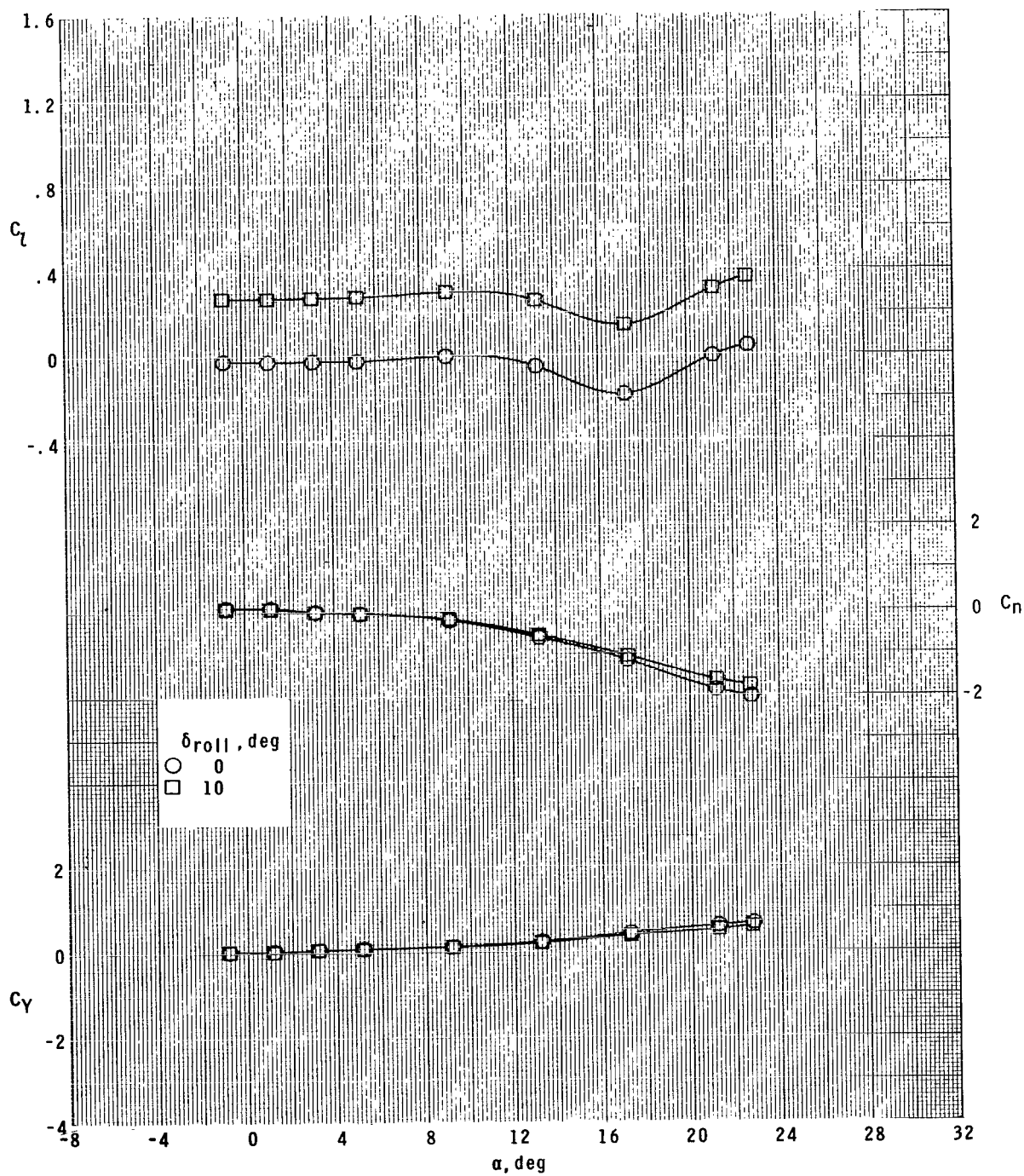
(d)  $M = 4.63.$

Figure 13.- Concluded.



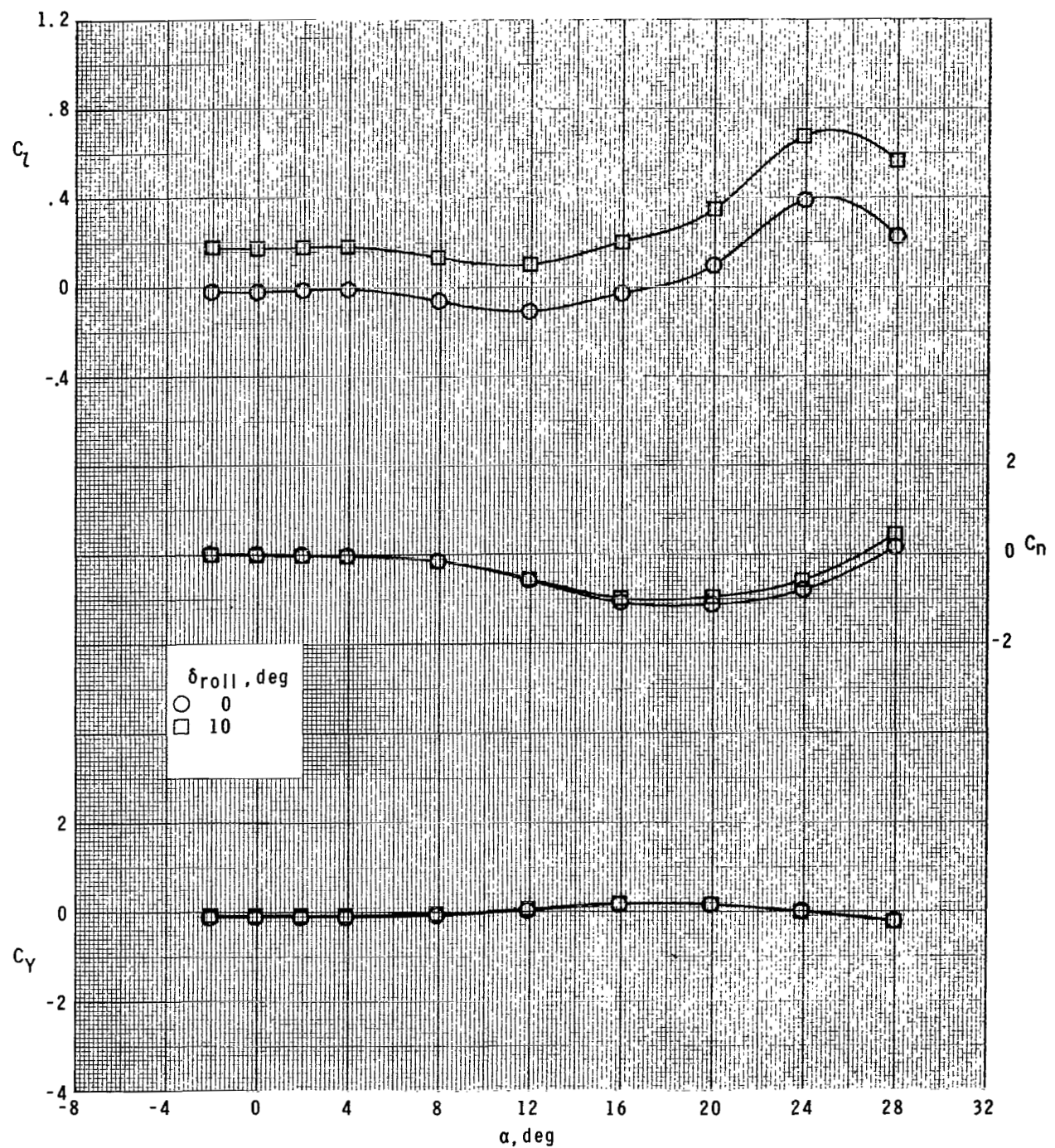
(a)  $M = 1.60$ .

Figure 14.- Effect of four plain tail-fin ailerons on lateral aerodynamic characteristics of model at  $\phi = 22.5^\circ$ .



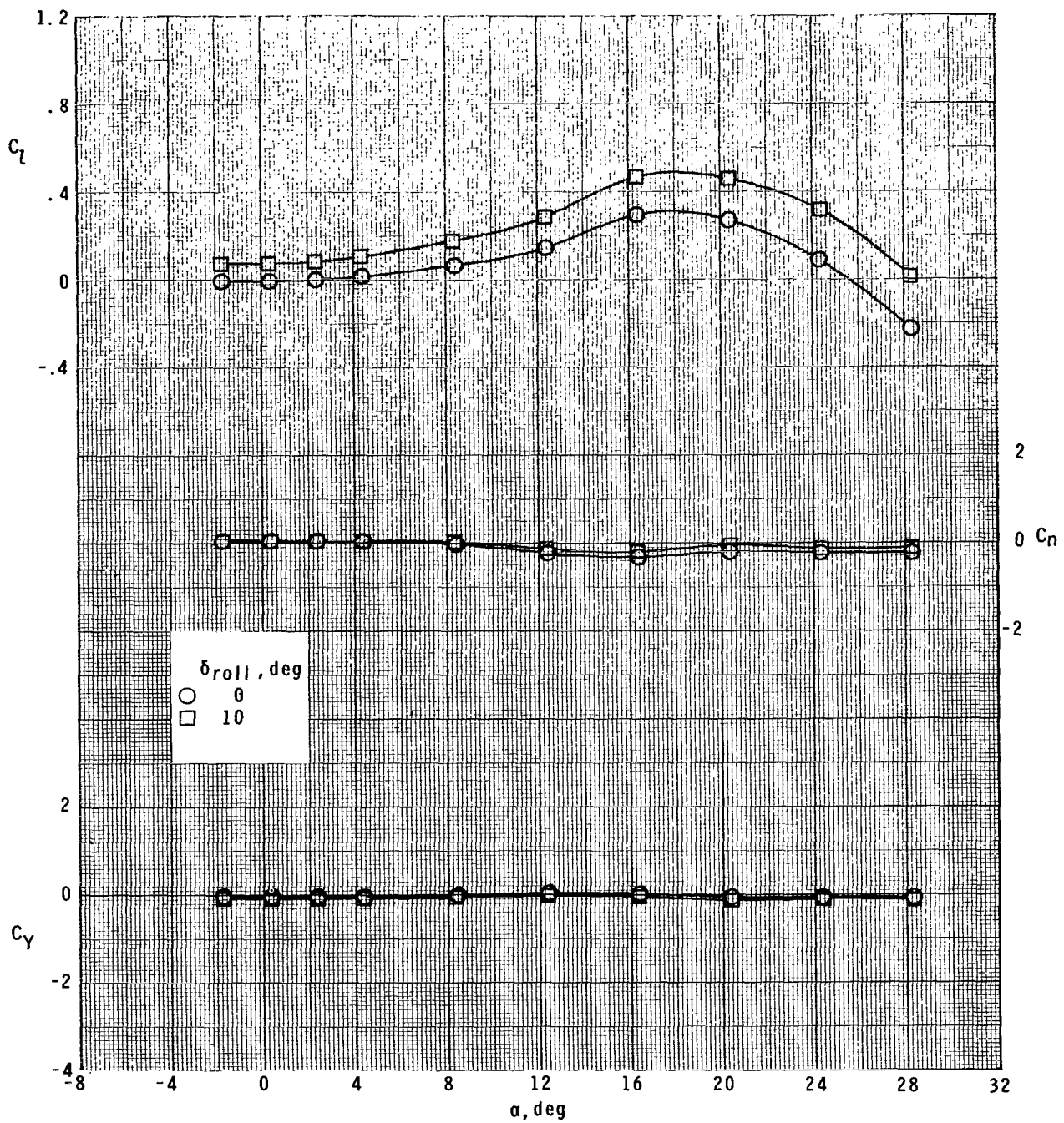
(b)  $M = 2.16.$

Figure 14.- Continued.



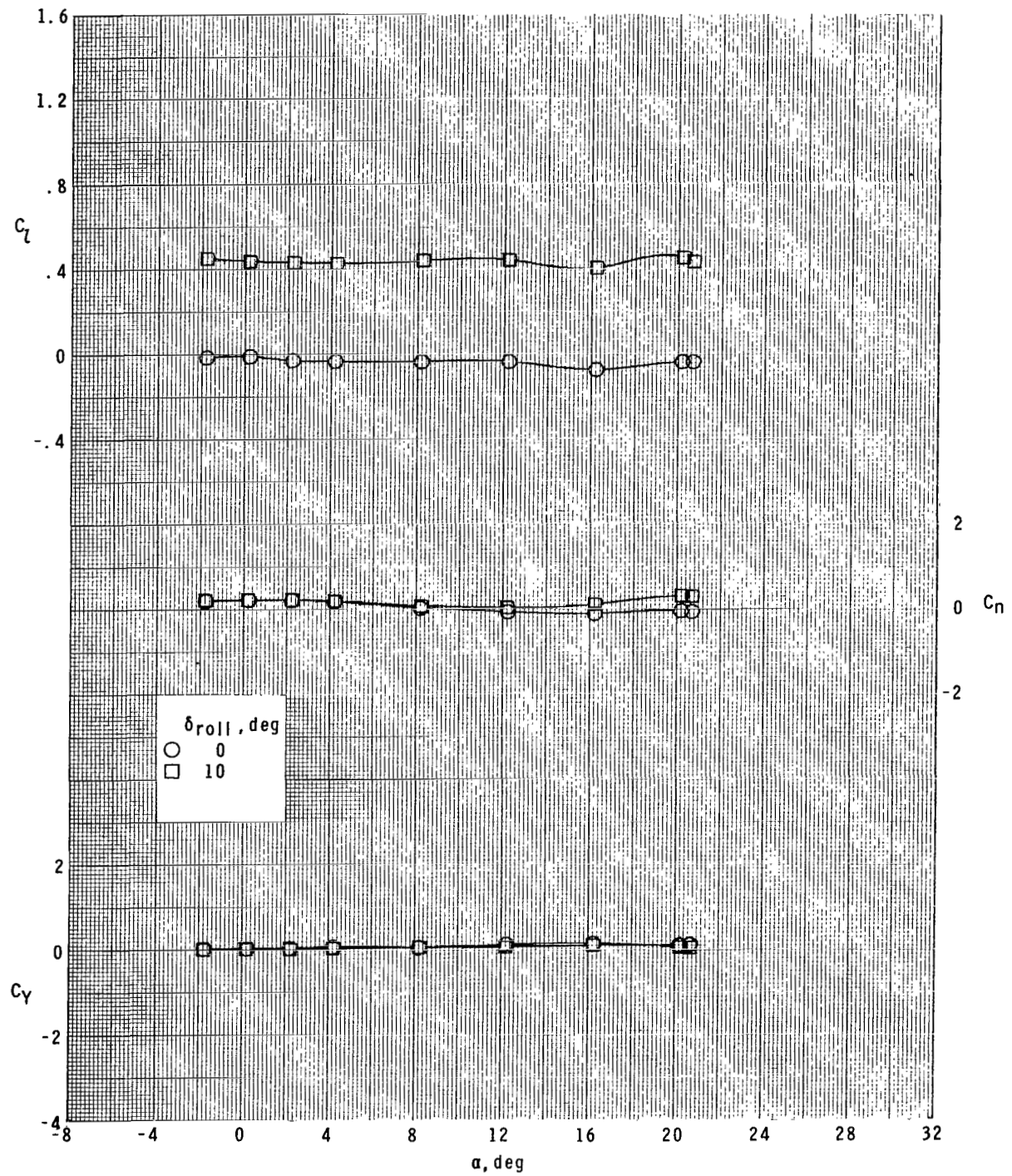
(c)  $M = 2.96.$

Figure 14.- Continued.



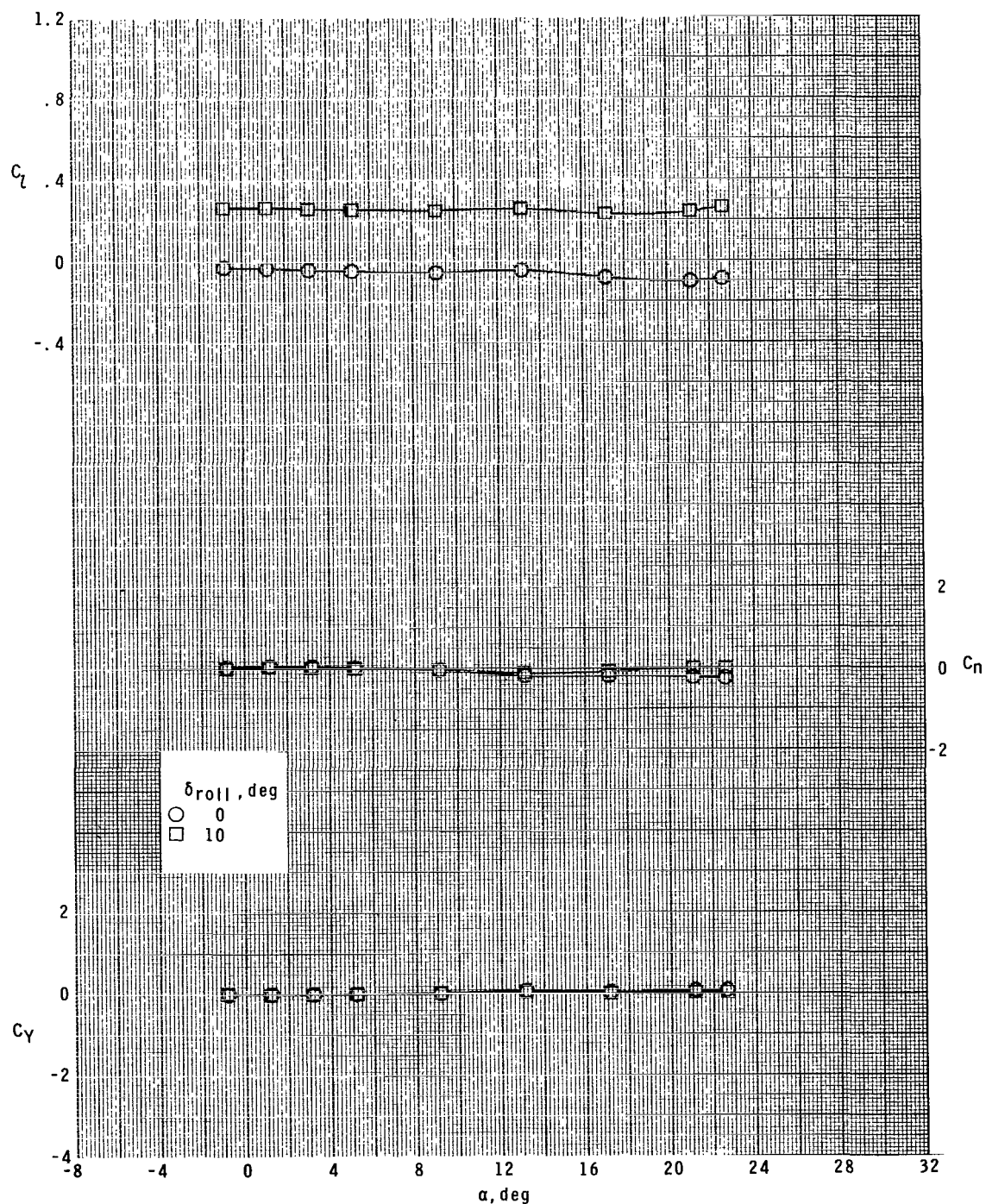
(d)  $M = 4.63.$

Figure 14.- Concluded.



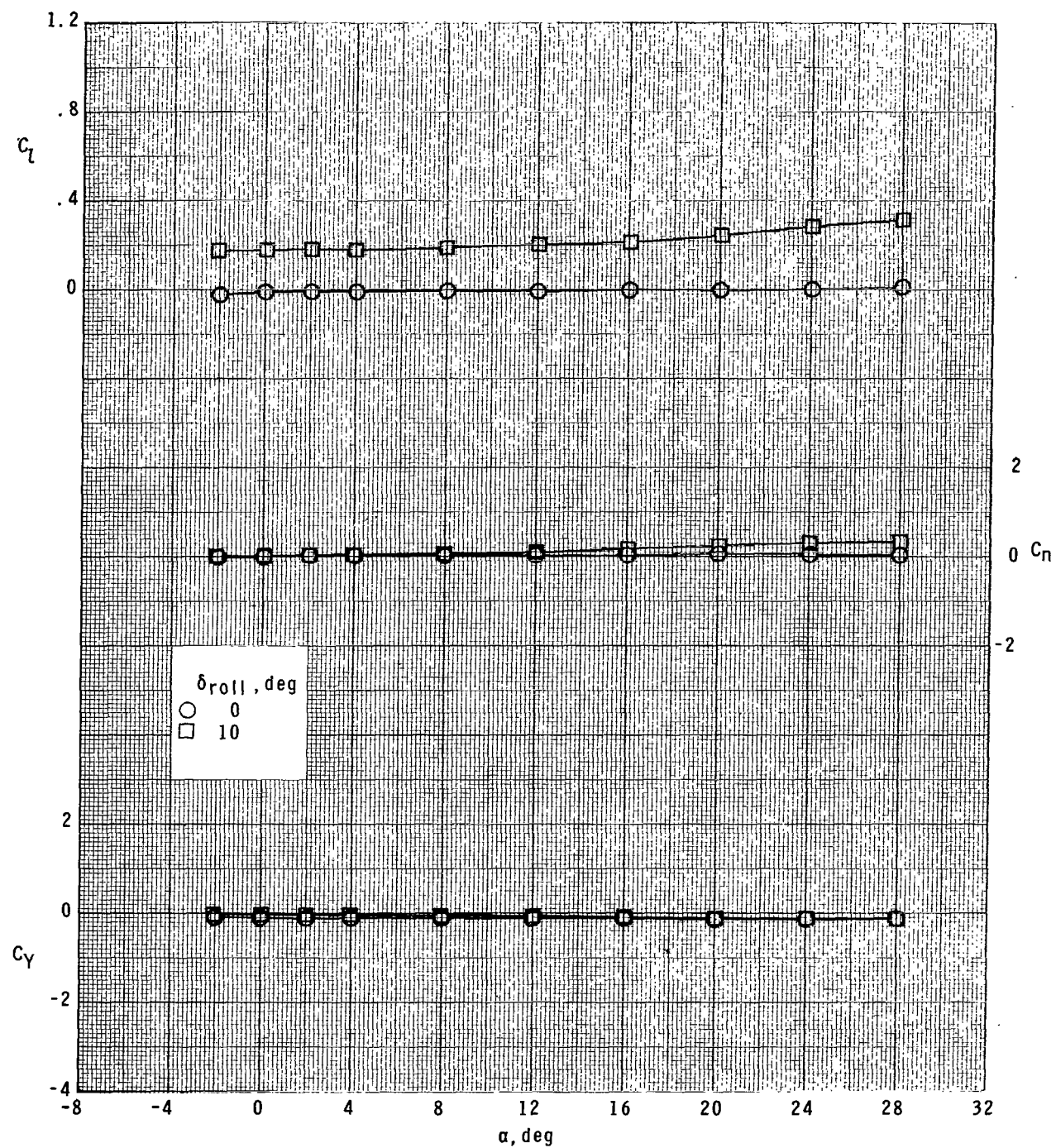
(a)  $M = 1.60.$

Figure 15.- Effect of four plain tail-fin ailerons on lateral aerodynamic characteristics of model at  $\phi = 45^\circ$ .



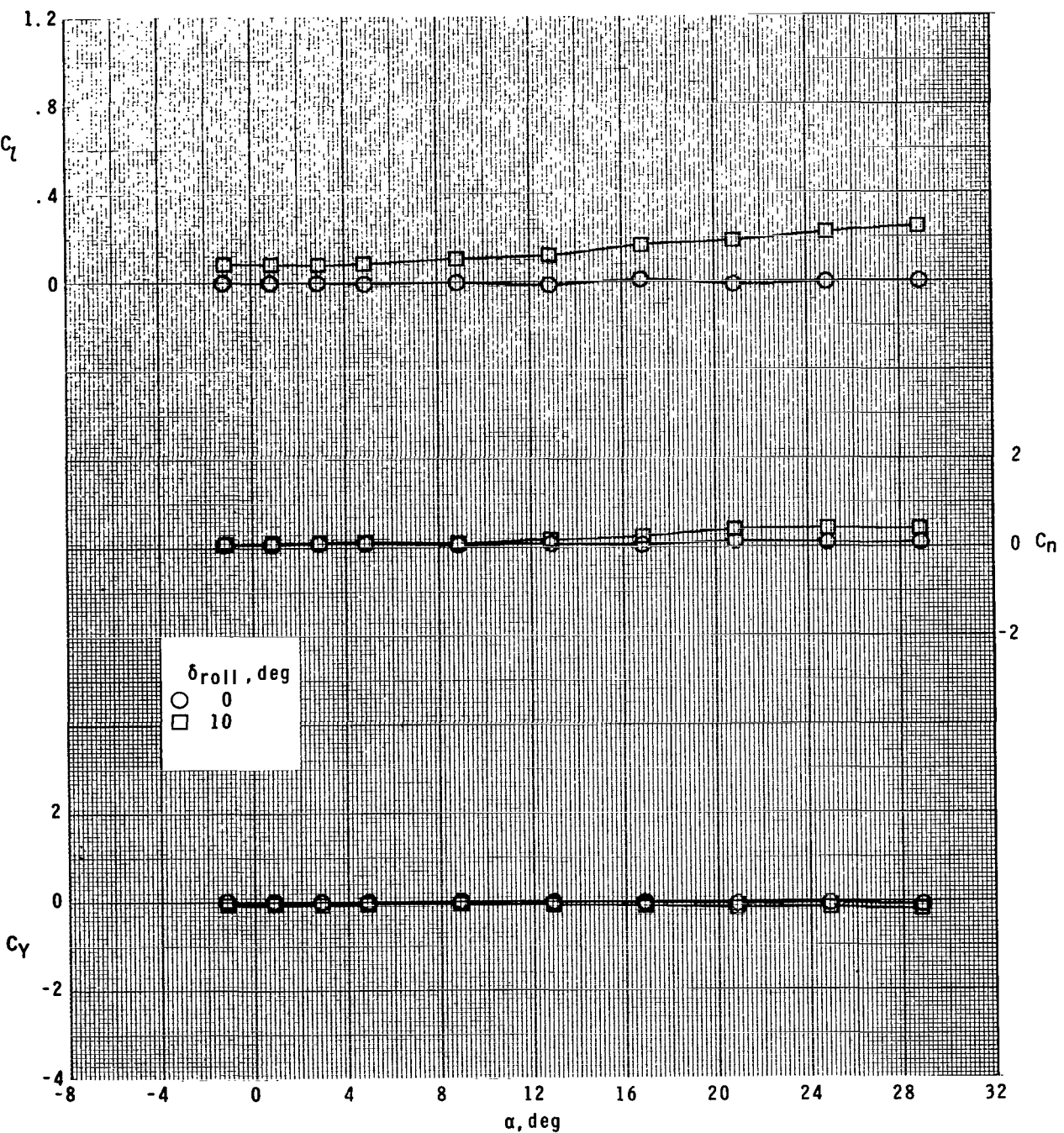
(b)  $M = 2.16.$

Figure 15.- Continued.



(c)  $M = 2.96$ .

Figure 15.- Continued.



(d)  $M = 4.63.$

Figure 15.- Concluded.

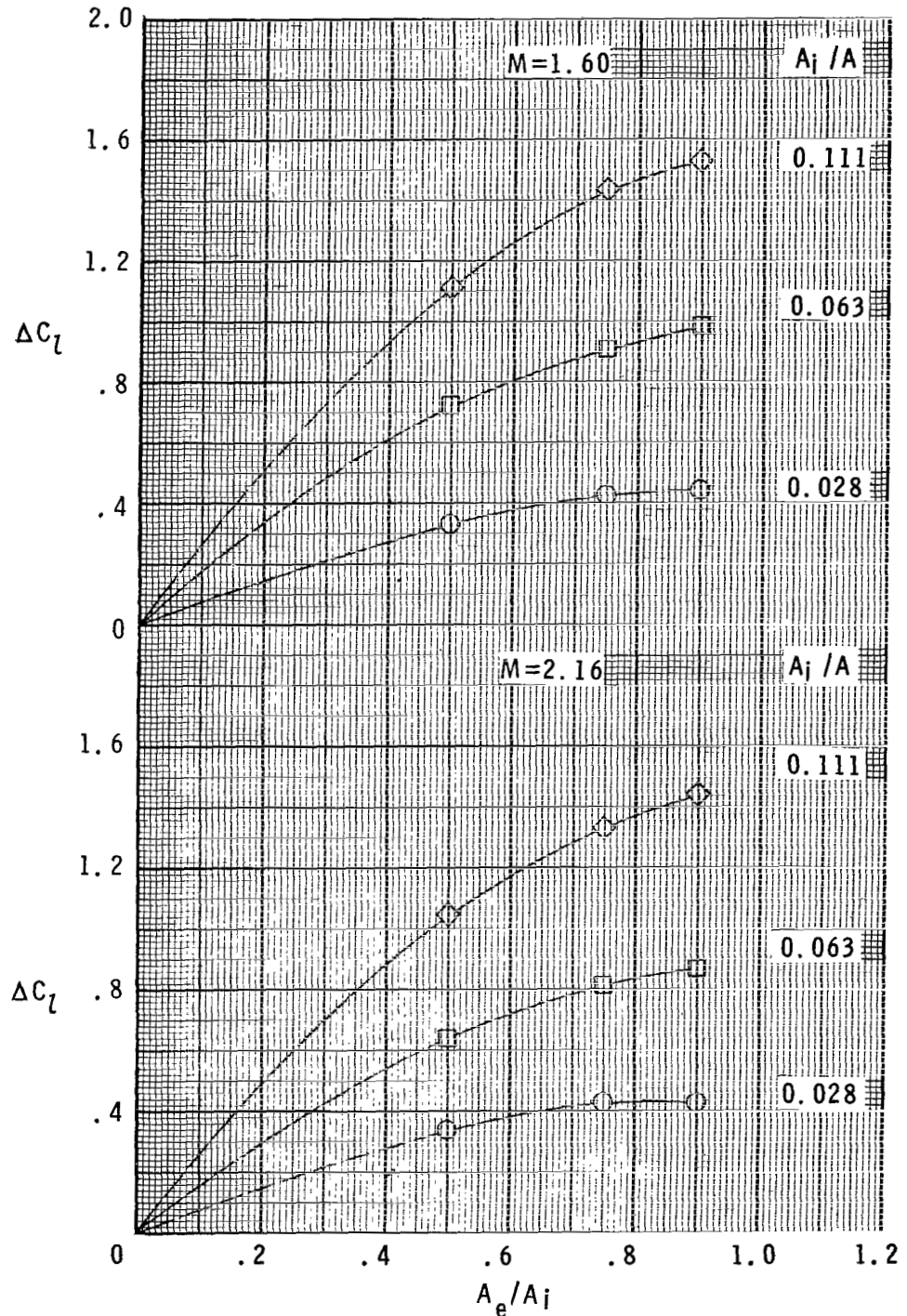
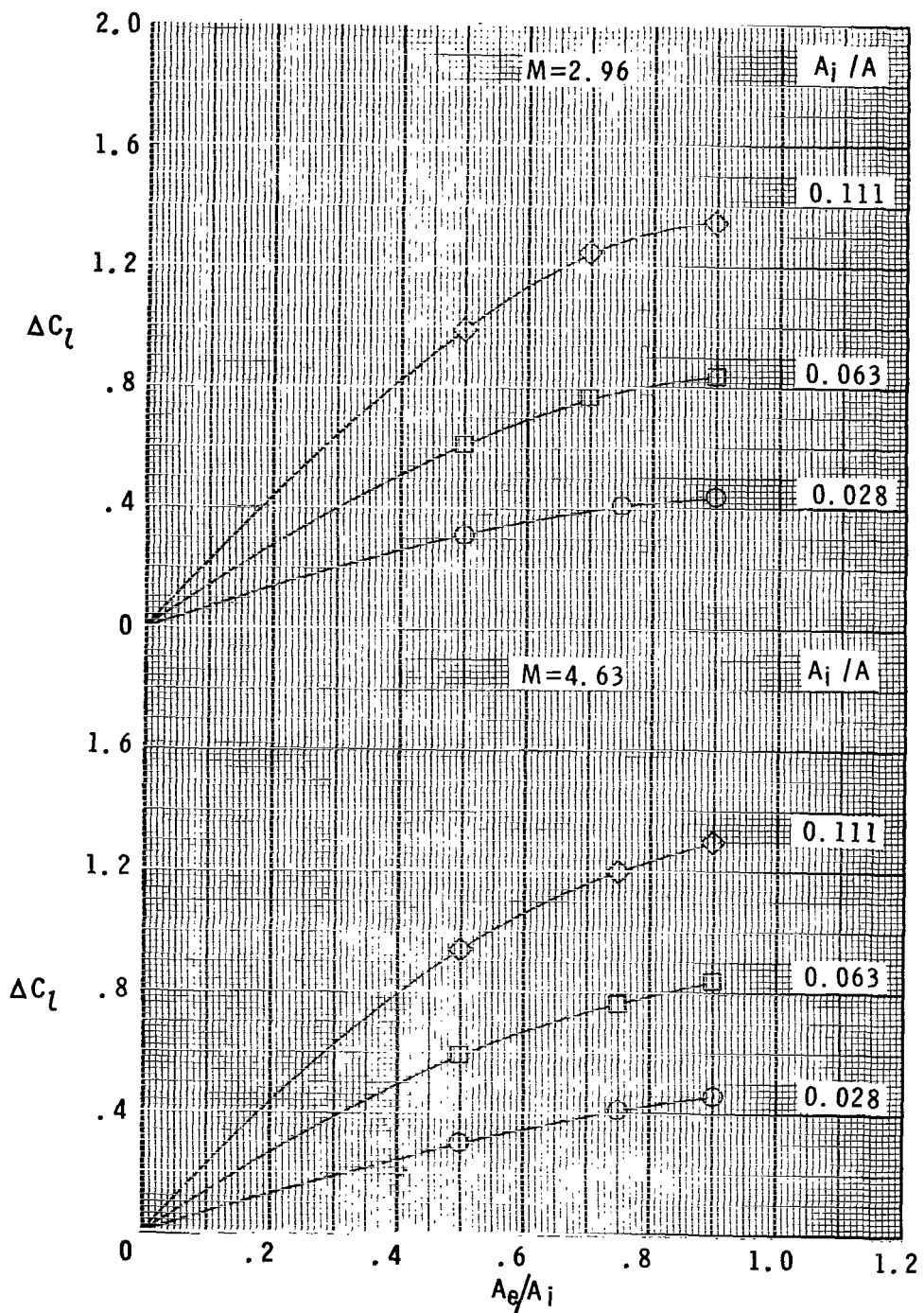
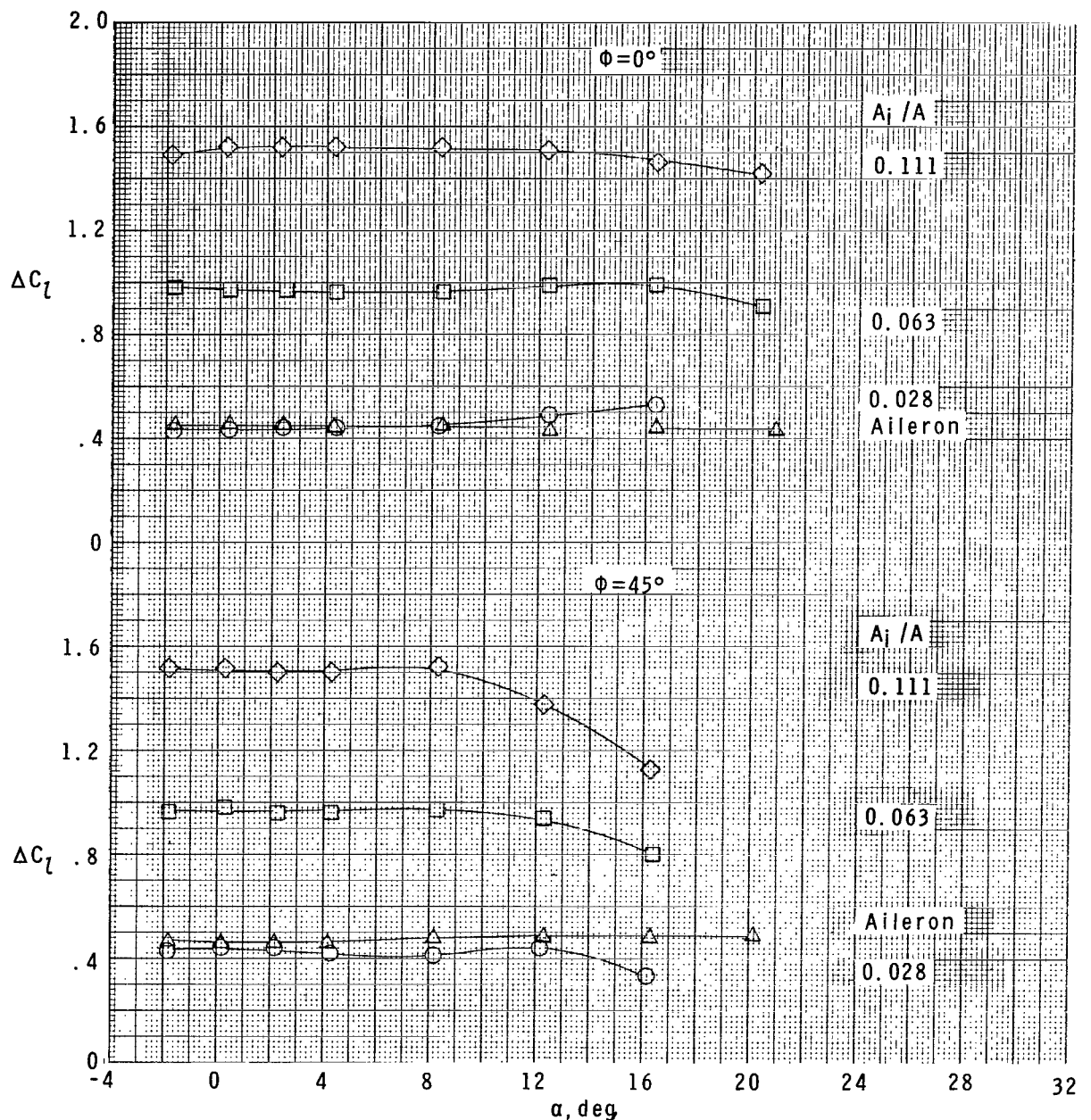


Figure 16.- Summary of effects of ram-air-spoiler inlet and plenum exit size on roll control at  $\phi = 45^\circ$  and  $\alpha = 0^\circ$ . (Dashed line indicates extrapolated data.)

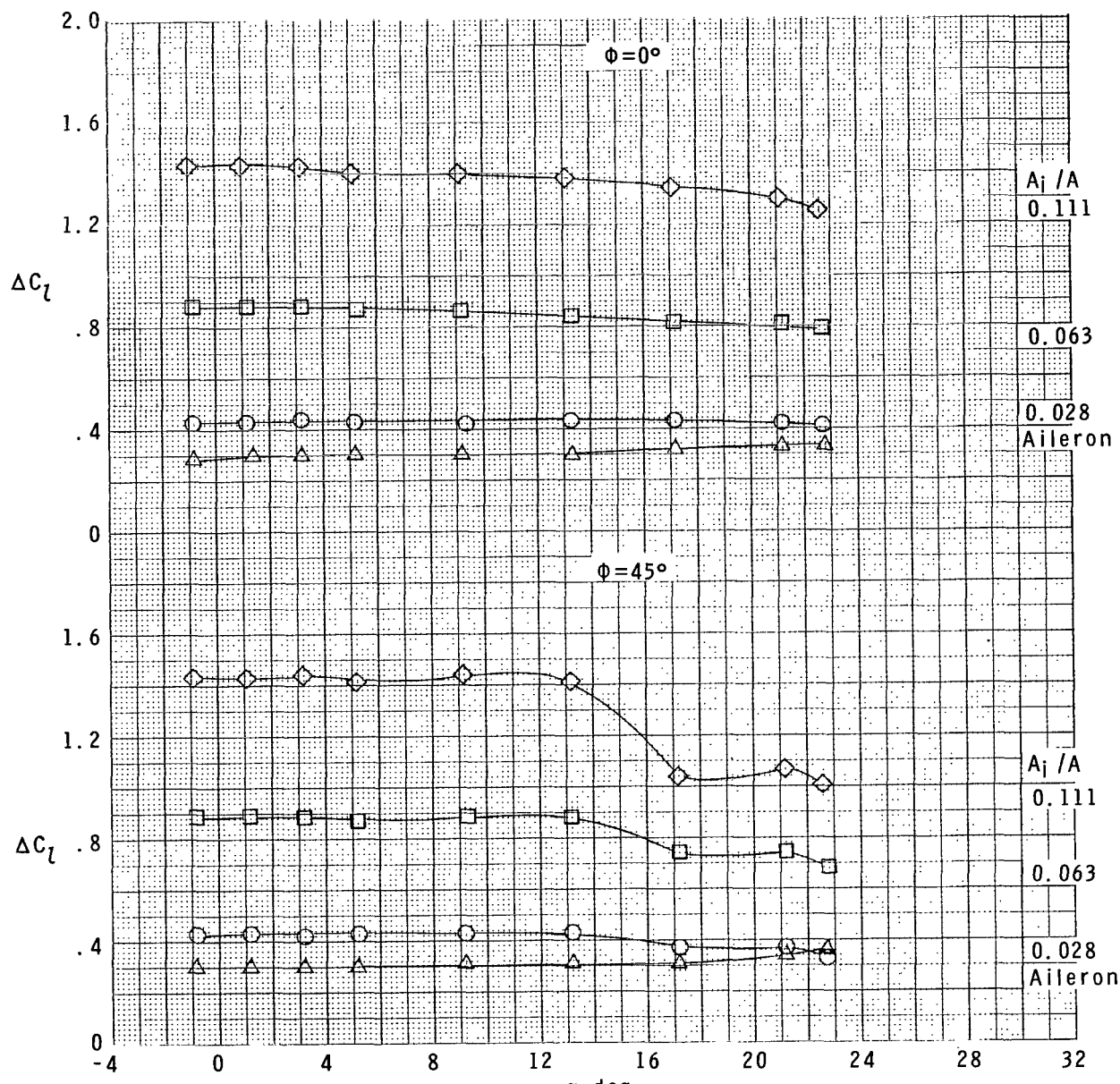


**Figure 16.- Concluded.**



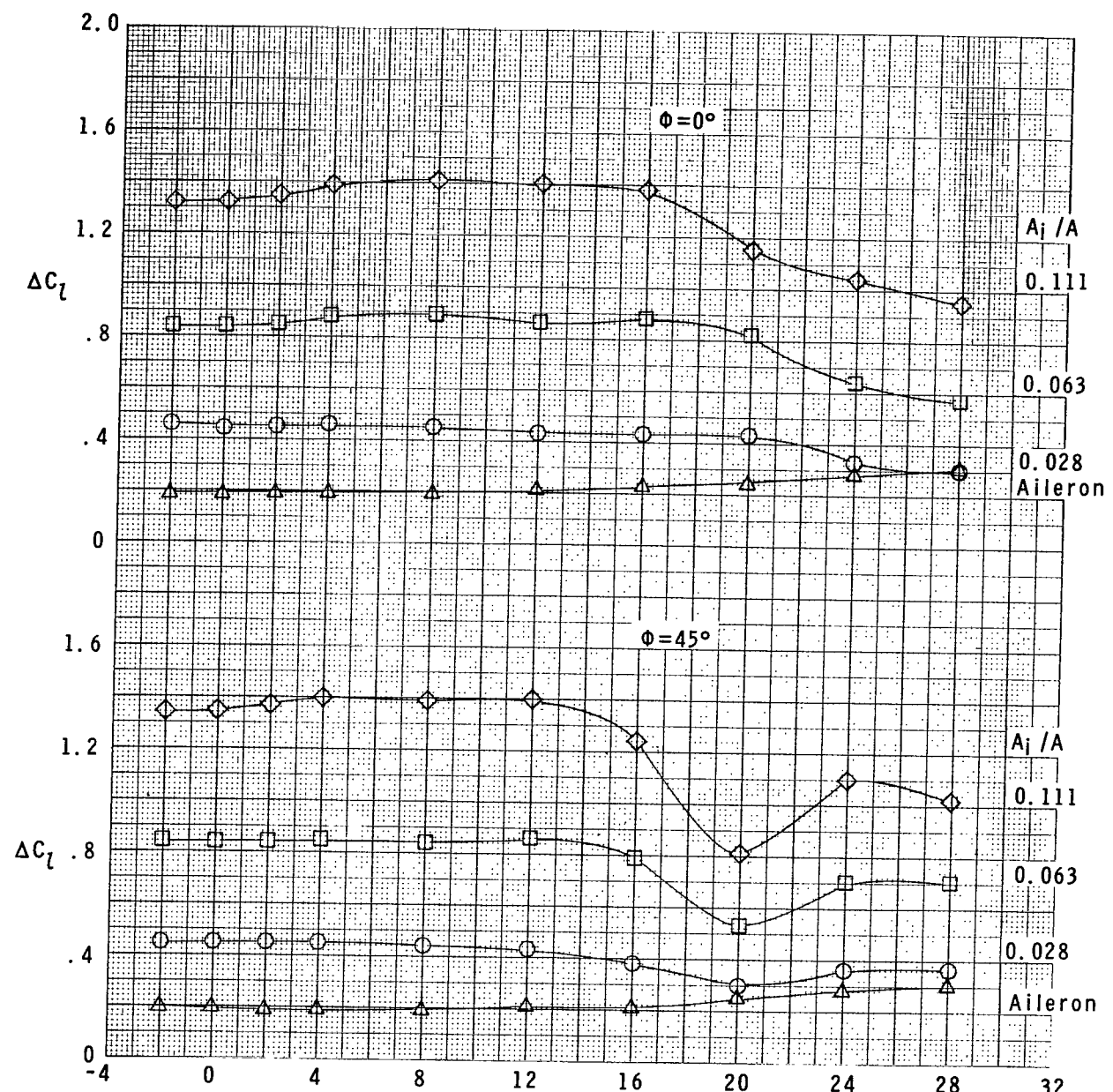
(a)  $M = 1.60$ .

Figure 17.- Summary of angle-of-attack effects on ram-air-spoiler and plain tail-fin aileron roll control.  $A_e/A_i = 0.90$  and  $\delta_{roll} = 10^\circ$ .



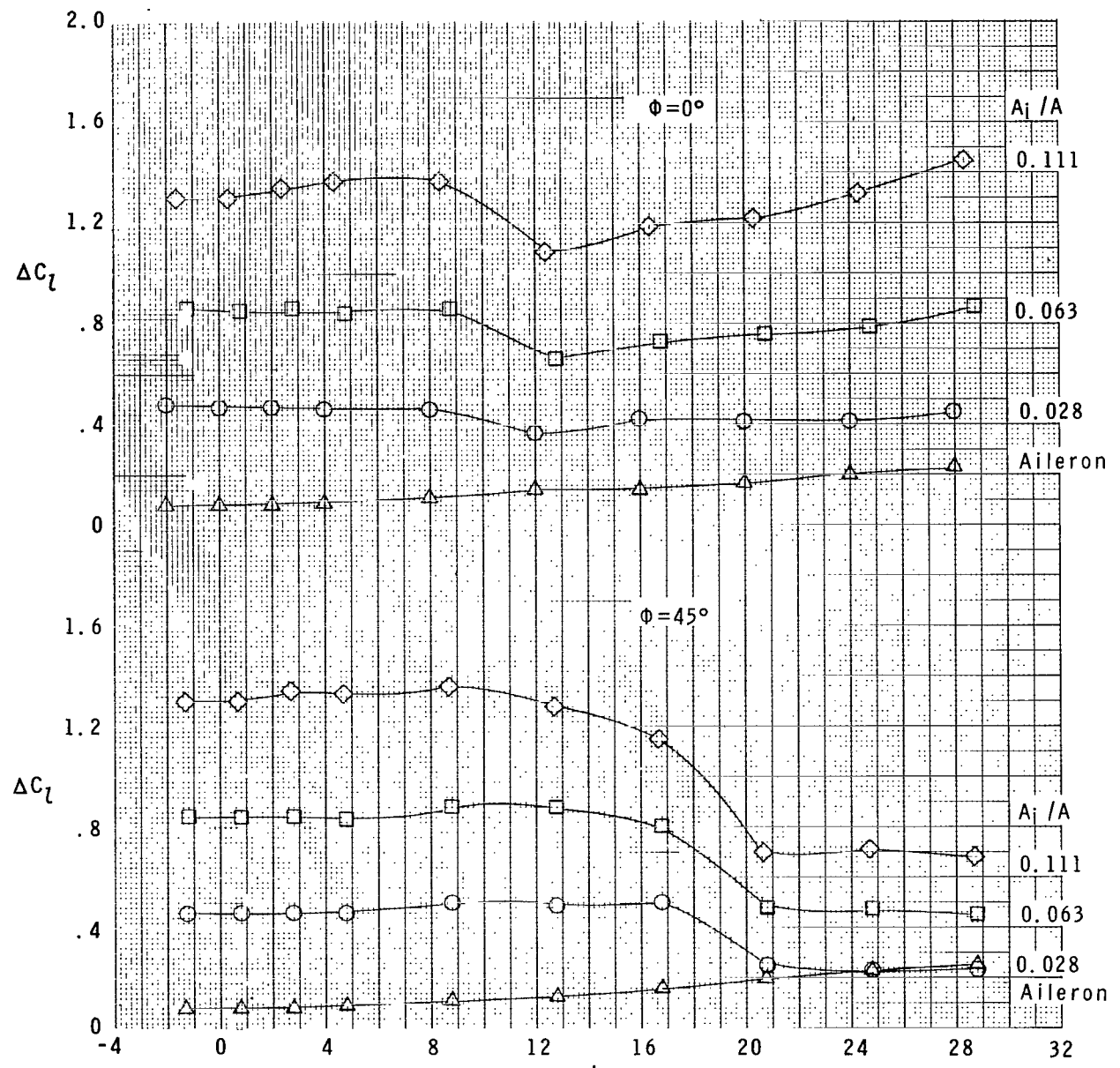
(b)  $M = 2.16.$

Figure 17.- Continued.



(c)  $M = 2.96.$

Figure 17.- Continued.



(d)  $M = 4.63.$

Figure 17.- Concluded.

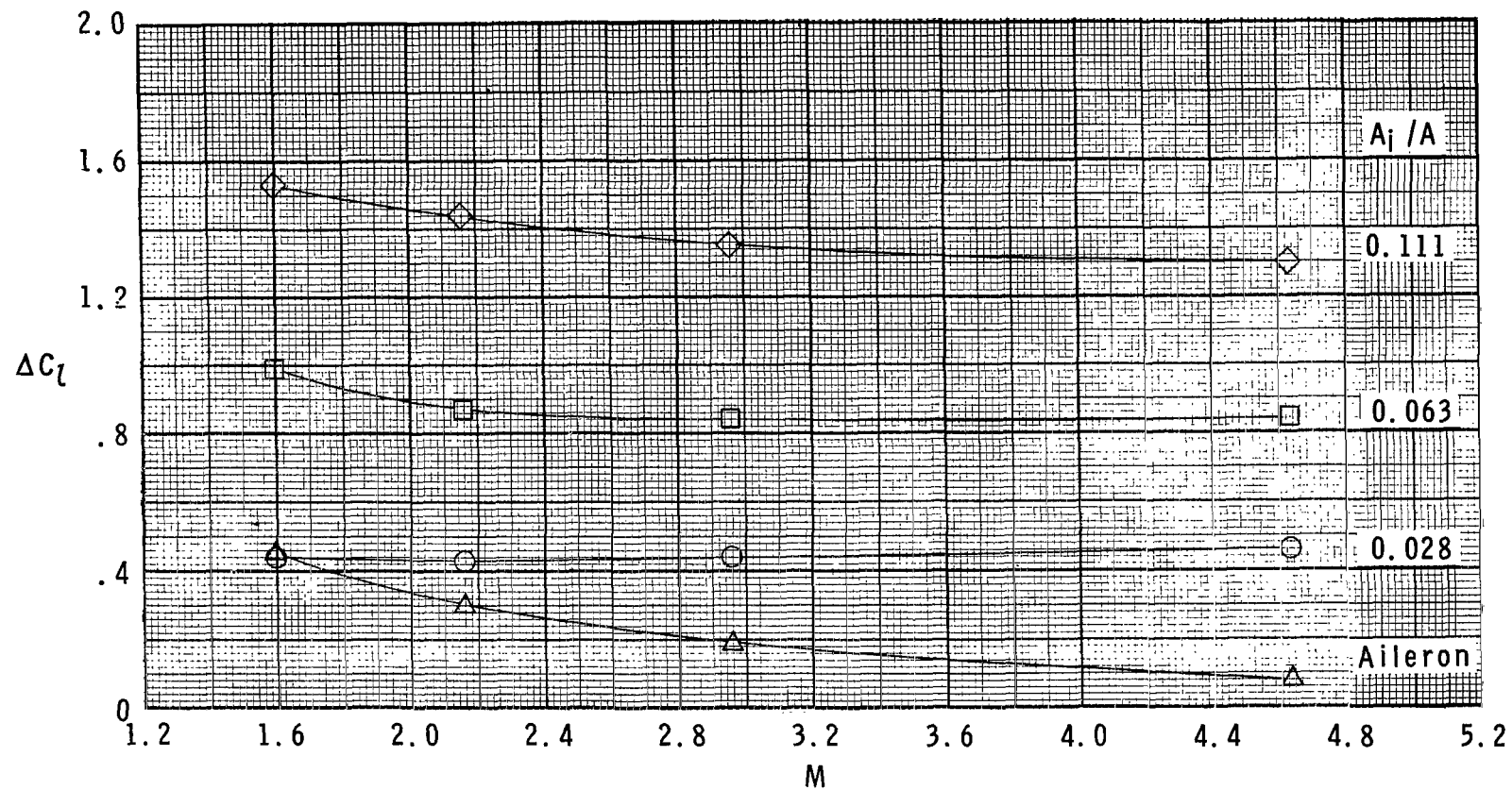
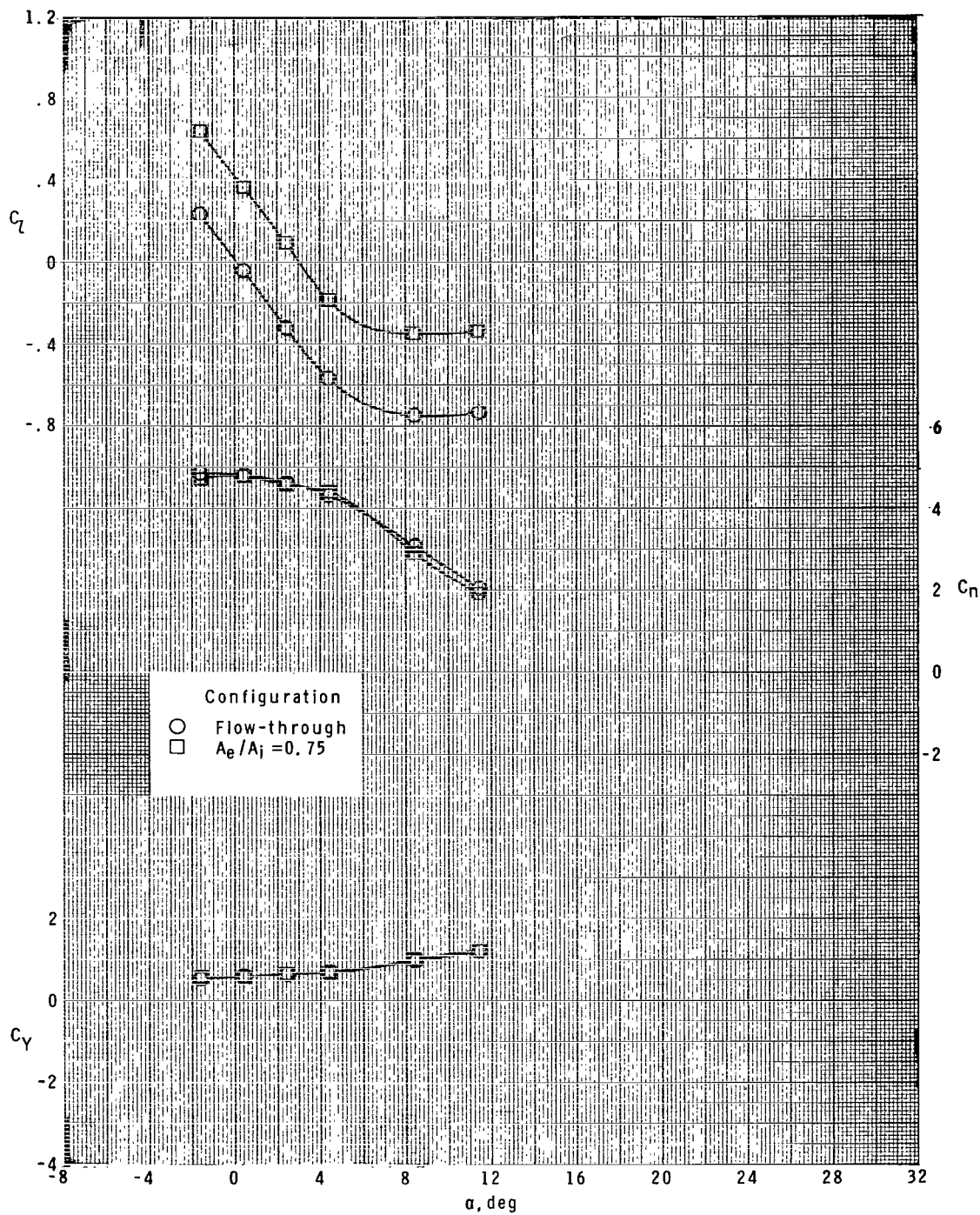
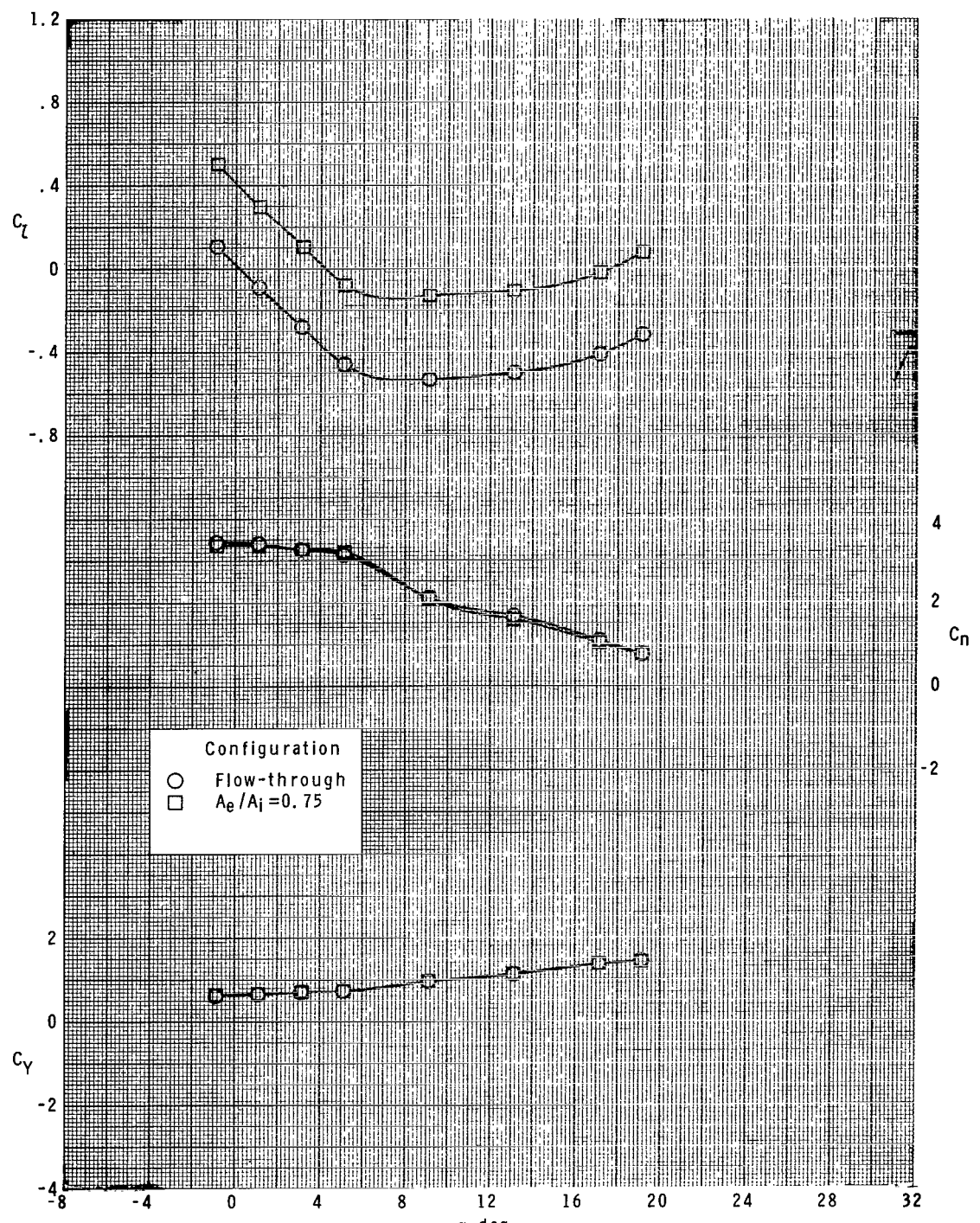


Figure 18.- Summary of Mach number effects on ram-air-spoiler and plain tail-fin aileron roll control at  $\alpha = 0^\circ$ .  $A_e/A_j = 0.90$  and  $\delta_{roll} = 10^\circ$ .



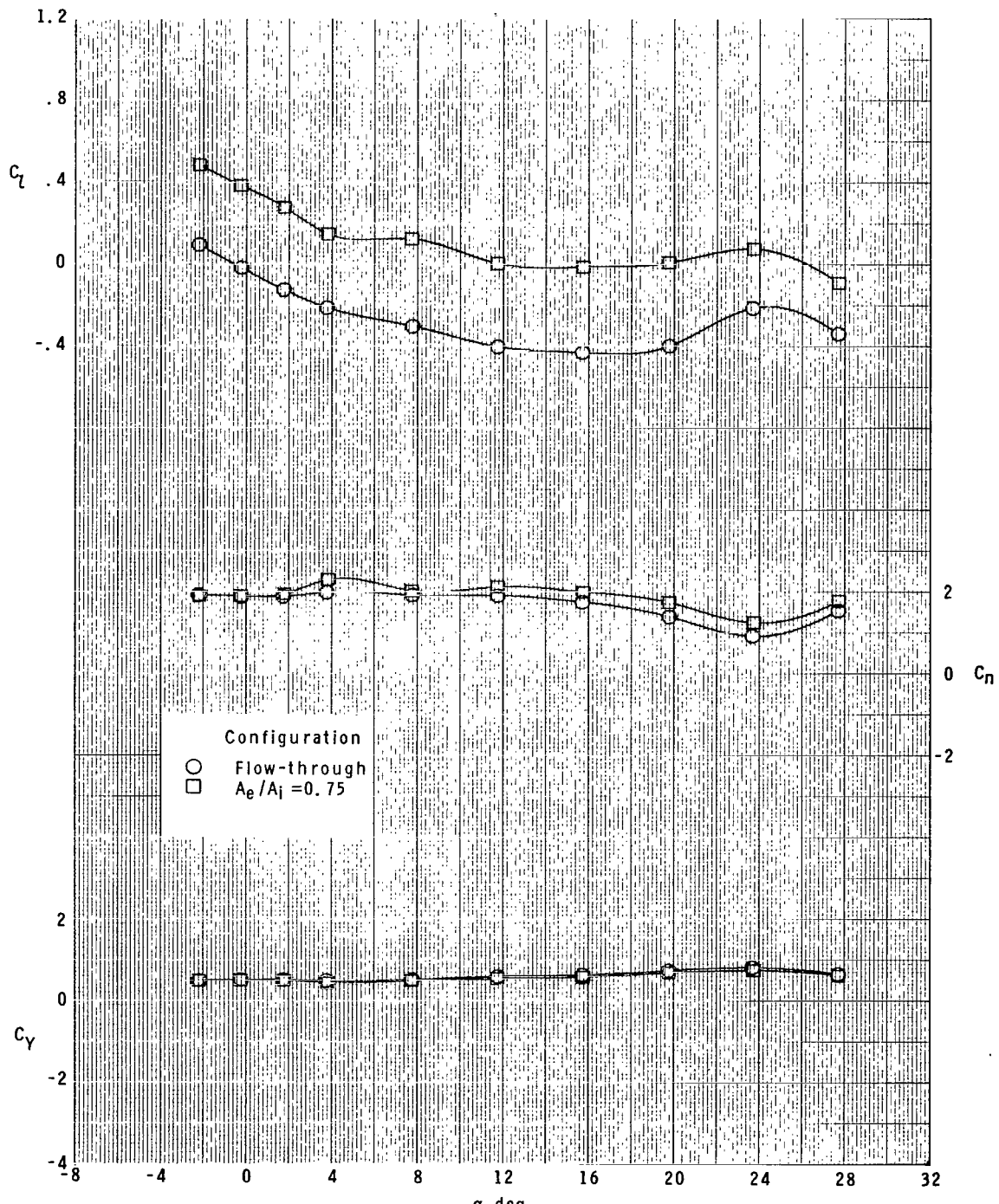
(a)  $M = 1.80.$

Figure 19.- Effect of ram-air-spoiler roll control on lateral aerodynamic characteristics of model with canard yaw control.  $A_i/A = 0.028$ ,  $\phi = 0^\circ$ , and  $\delta_{yaw} = 10^\circ$ .



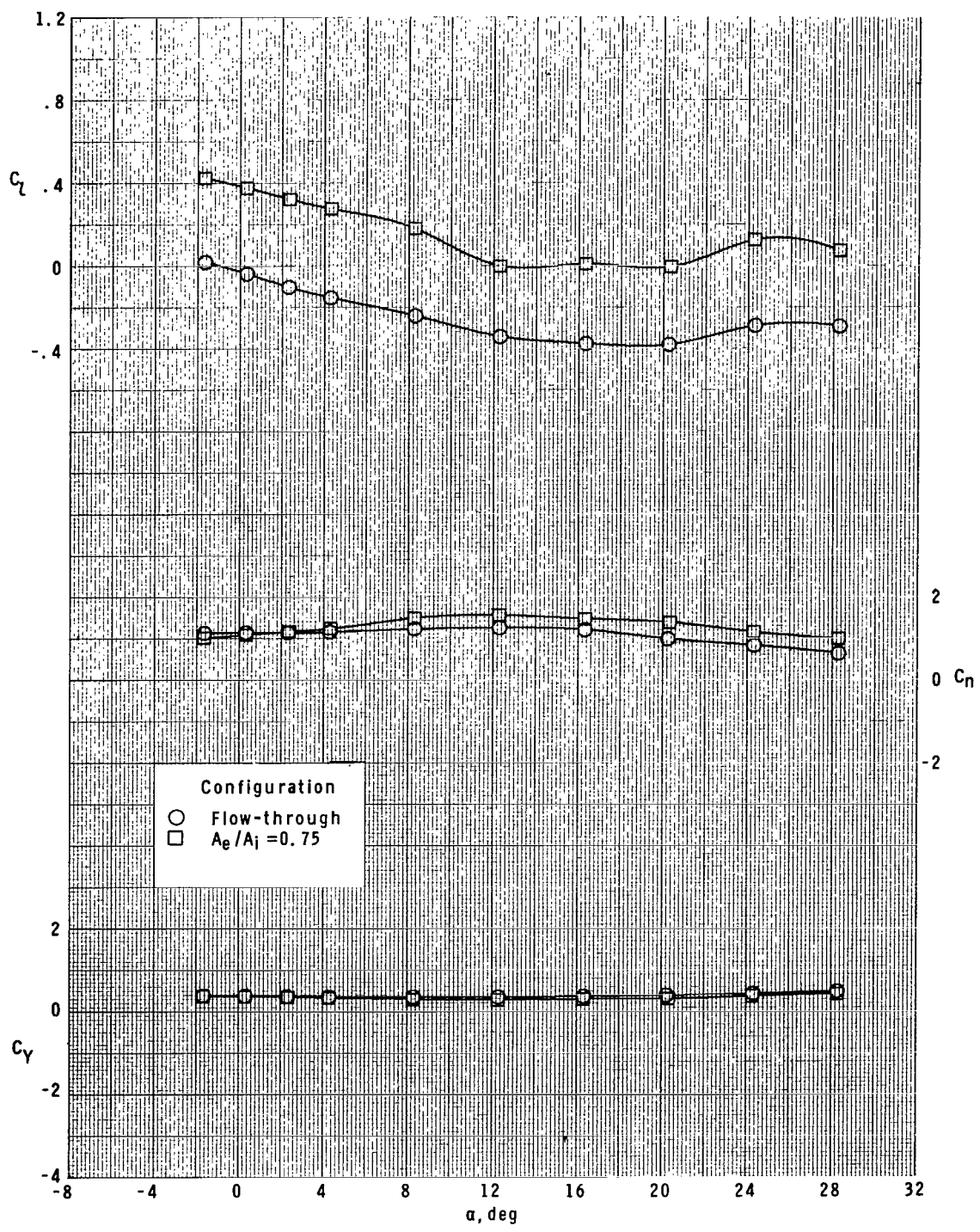
(b)  $M = 2.16.$

Figure 19.- Continued.



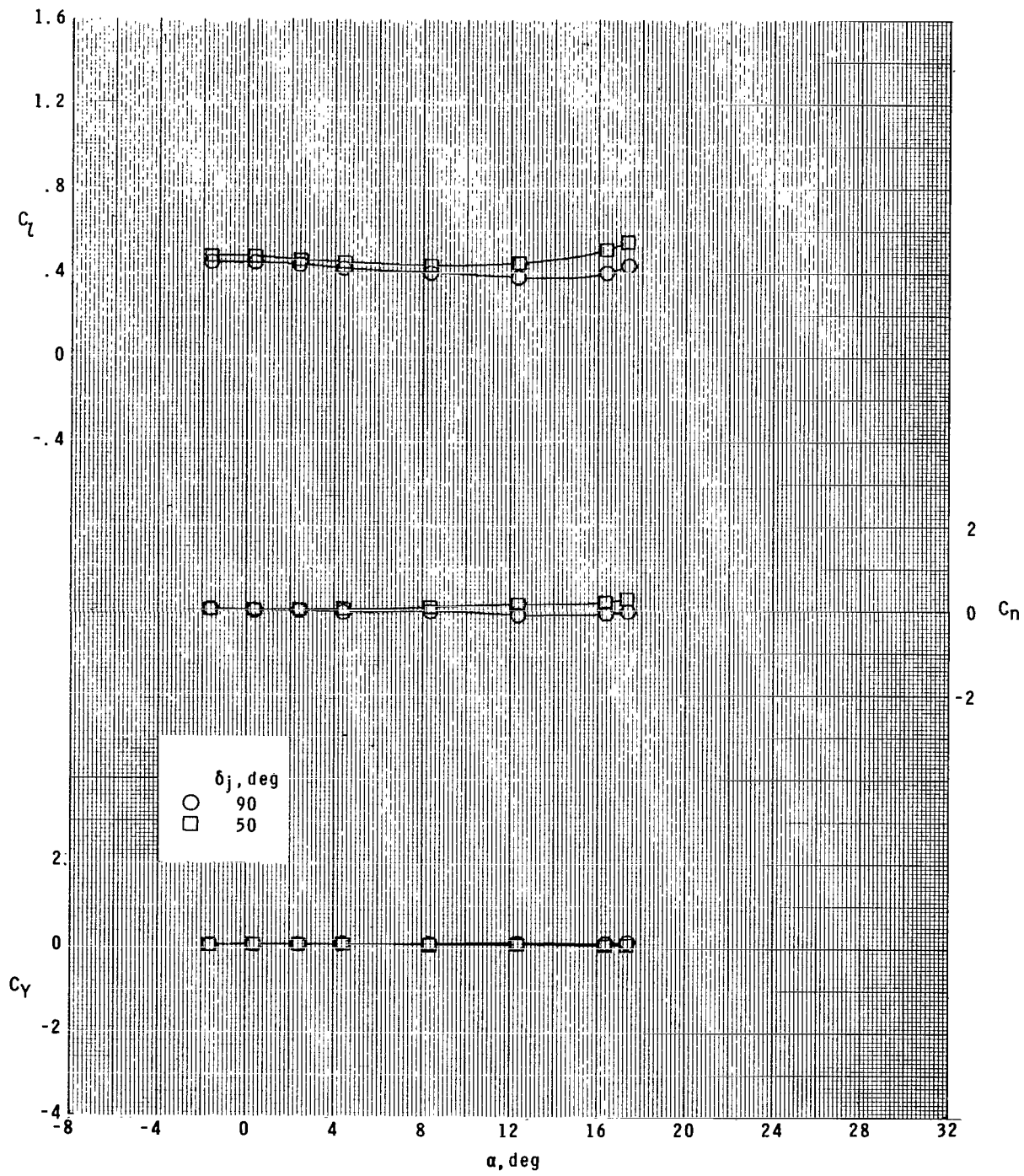
(c)  $M = 2.96.$

Figure 19.- Continued.



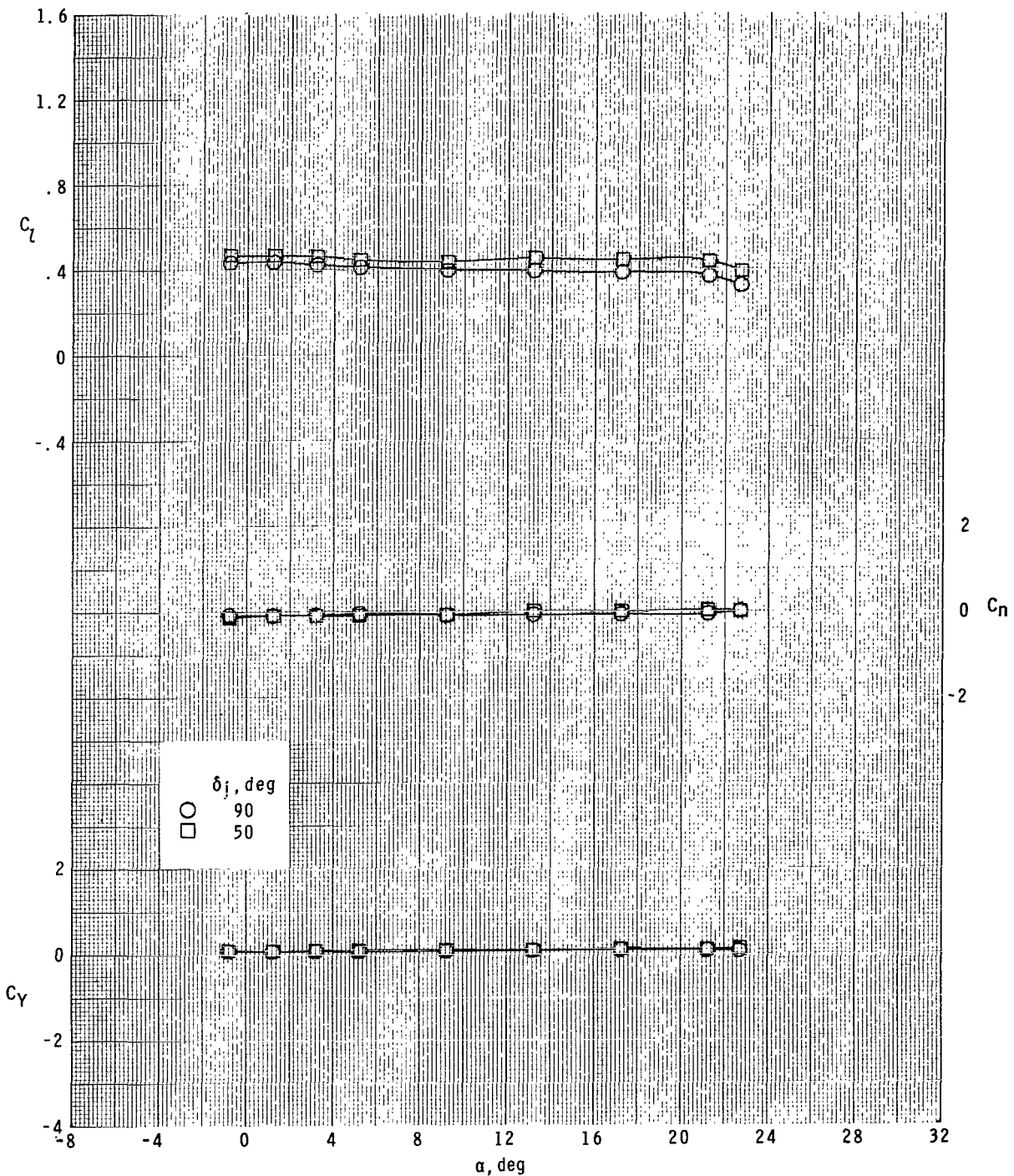
(d)  $M = 4.63.$

Figure 19.- Concluded.



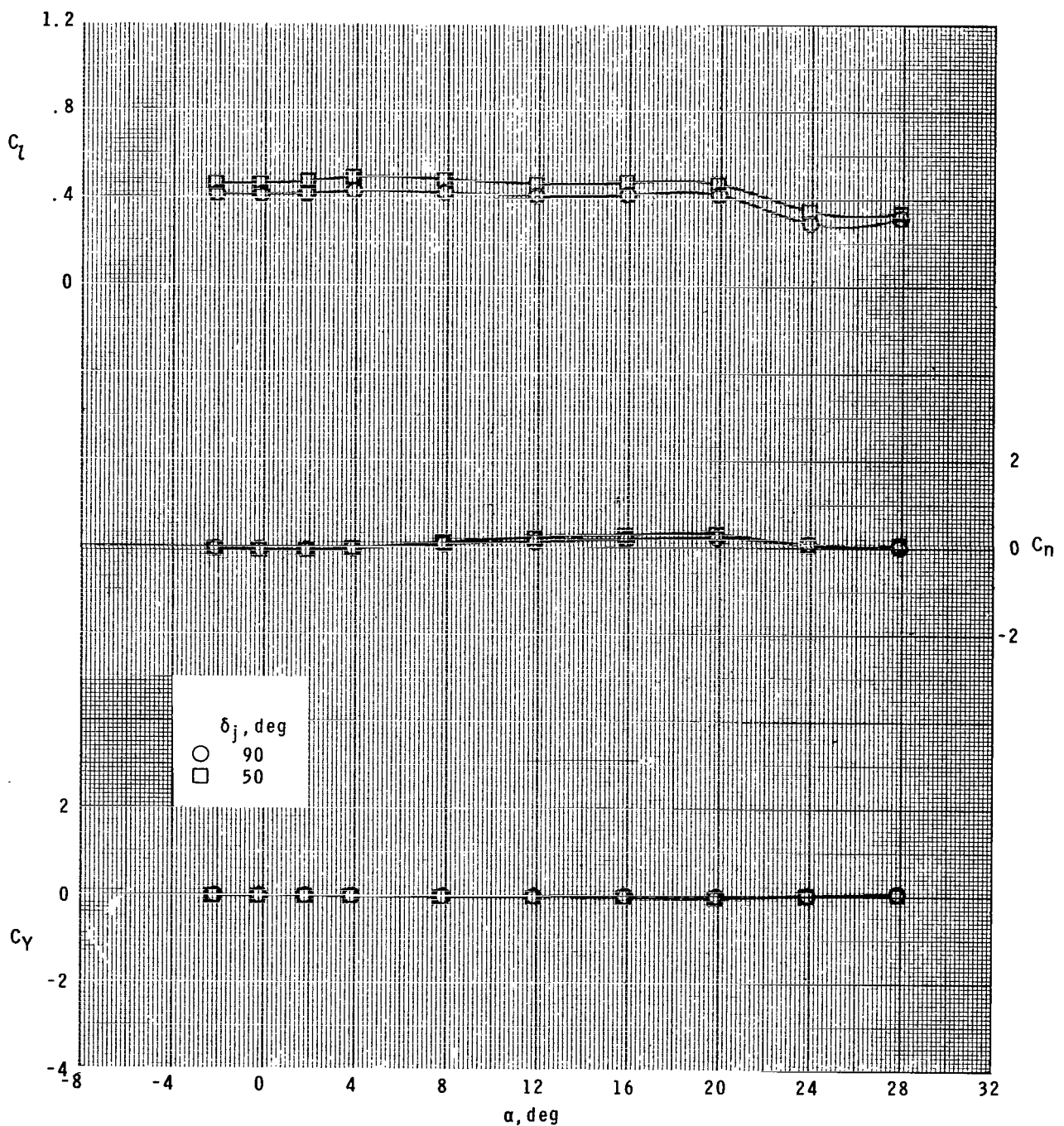
(a)  $M = 1.60.$

Figure 20.- Effect of plenum jet-exit slot angle on lateral aerodynamic characteristics of model with ram-air-spoiler tail fins for  $A_i/A = 0.028$  and  $A_e/A_i = 0.75$  at  $\phi = 0^\circ$ .



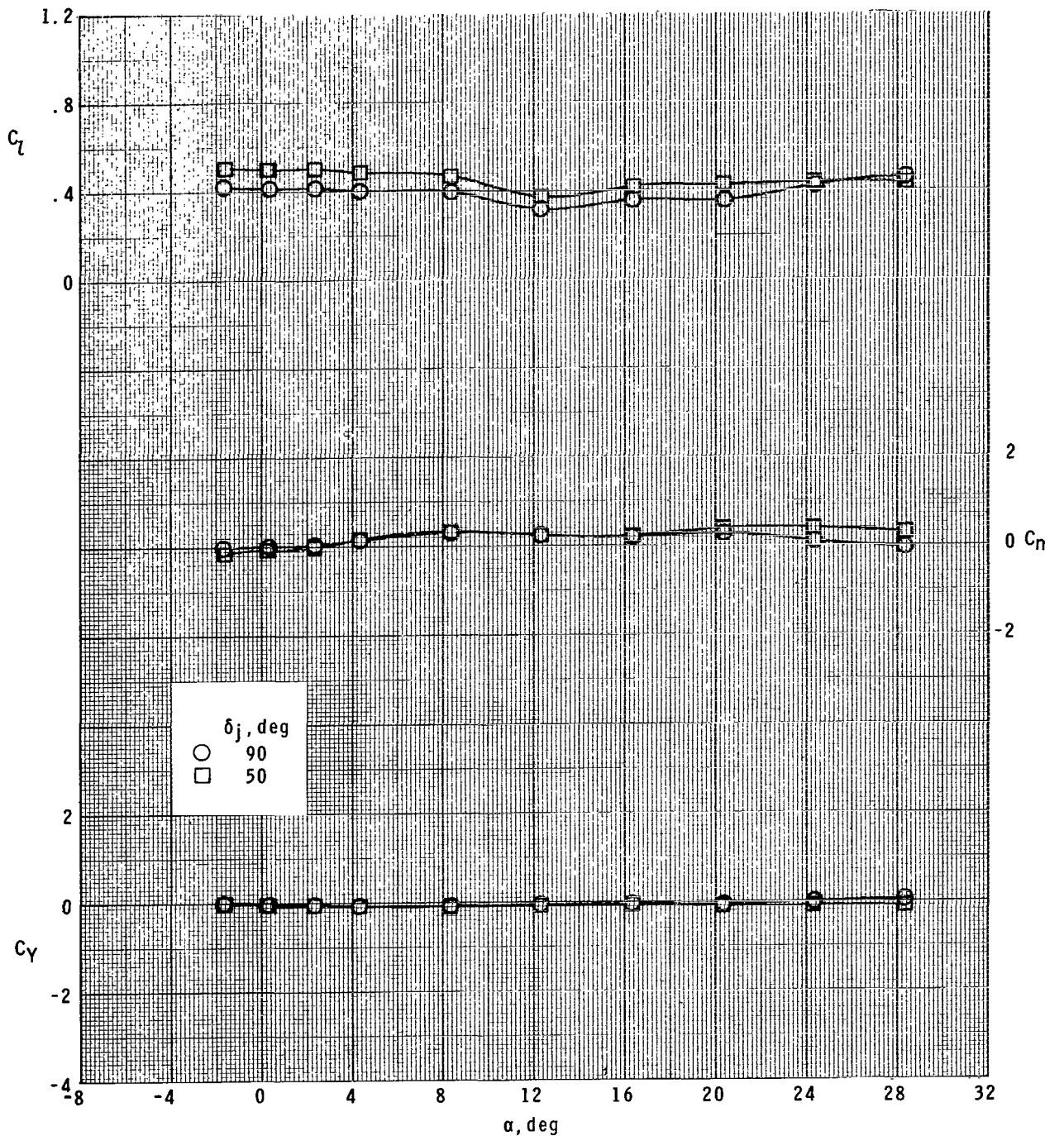
(b)  $M = 2.16.$

Figure 20.- Continued.



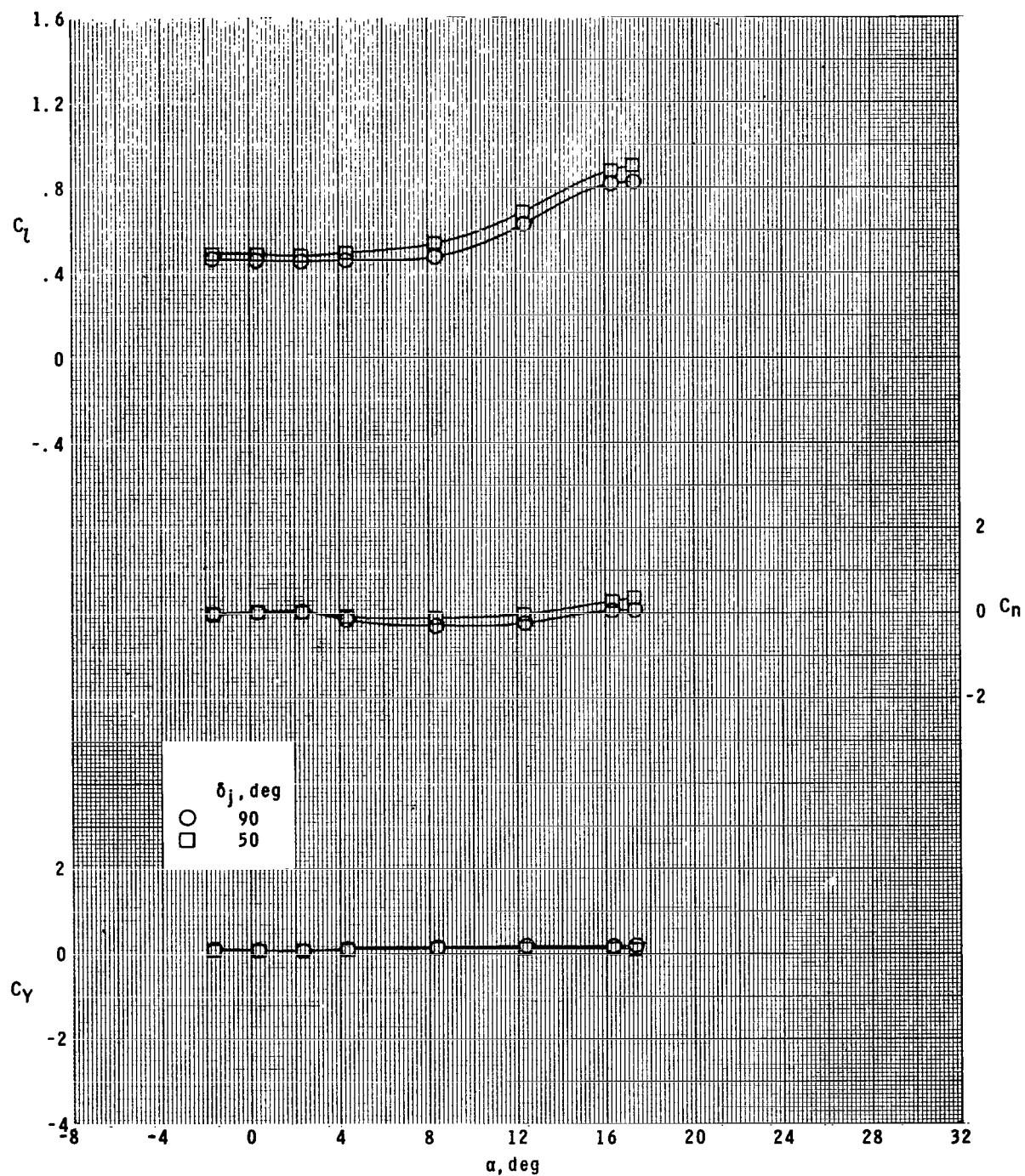
(c)  $M = 2.96$ .

Figure 20.- Continued.



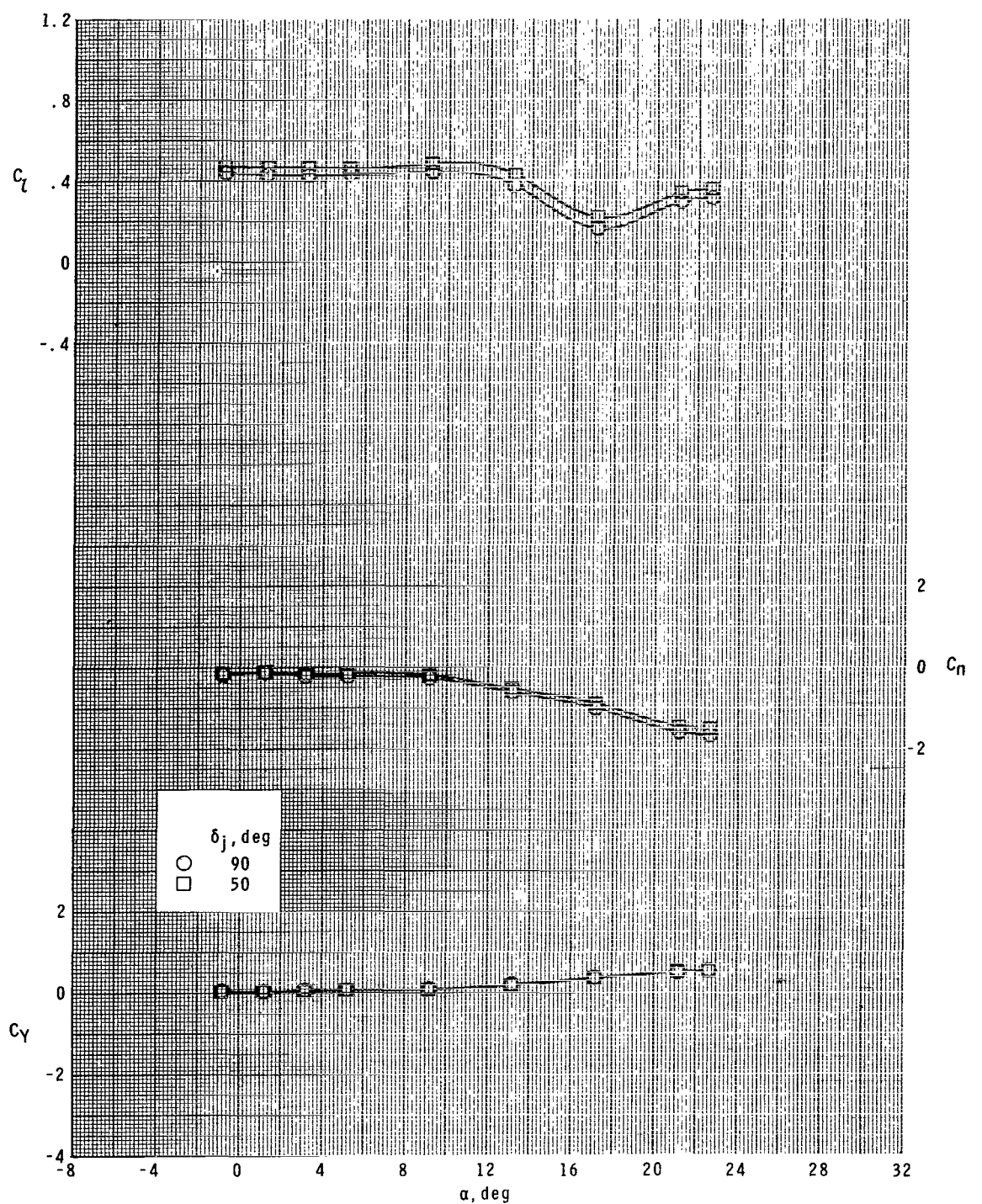
(d)  $M = 4.63.$

Figure 20.- Concluded.



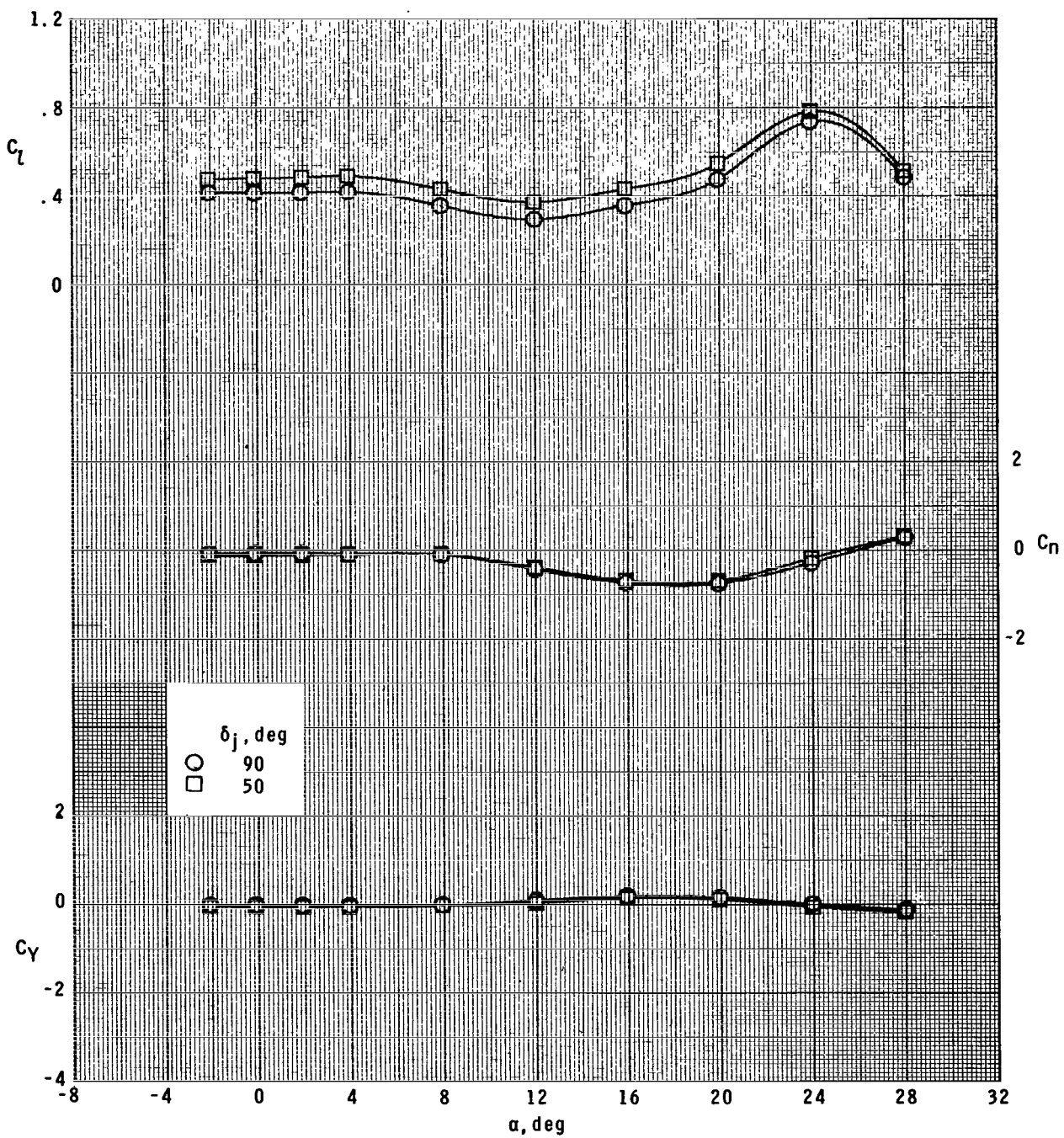
(a)  $M = 1.60.$

Figure 21.- Effect of plenum jet-exit slot angle on lateral aerodynamic characteristics of model with ram-air-spoiler tail fins for  $A_i/A = 0.028$  and  $A_e/A_i = 0.75$  at  $\phi = 22.5^\circ$ .



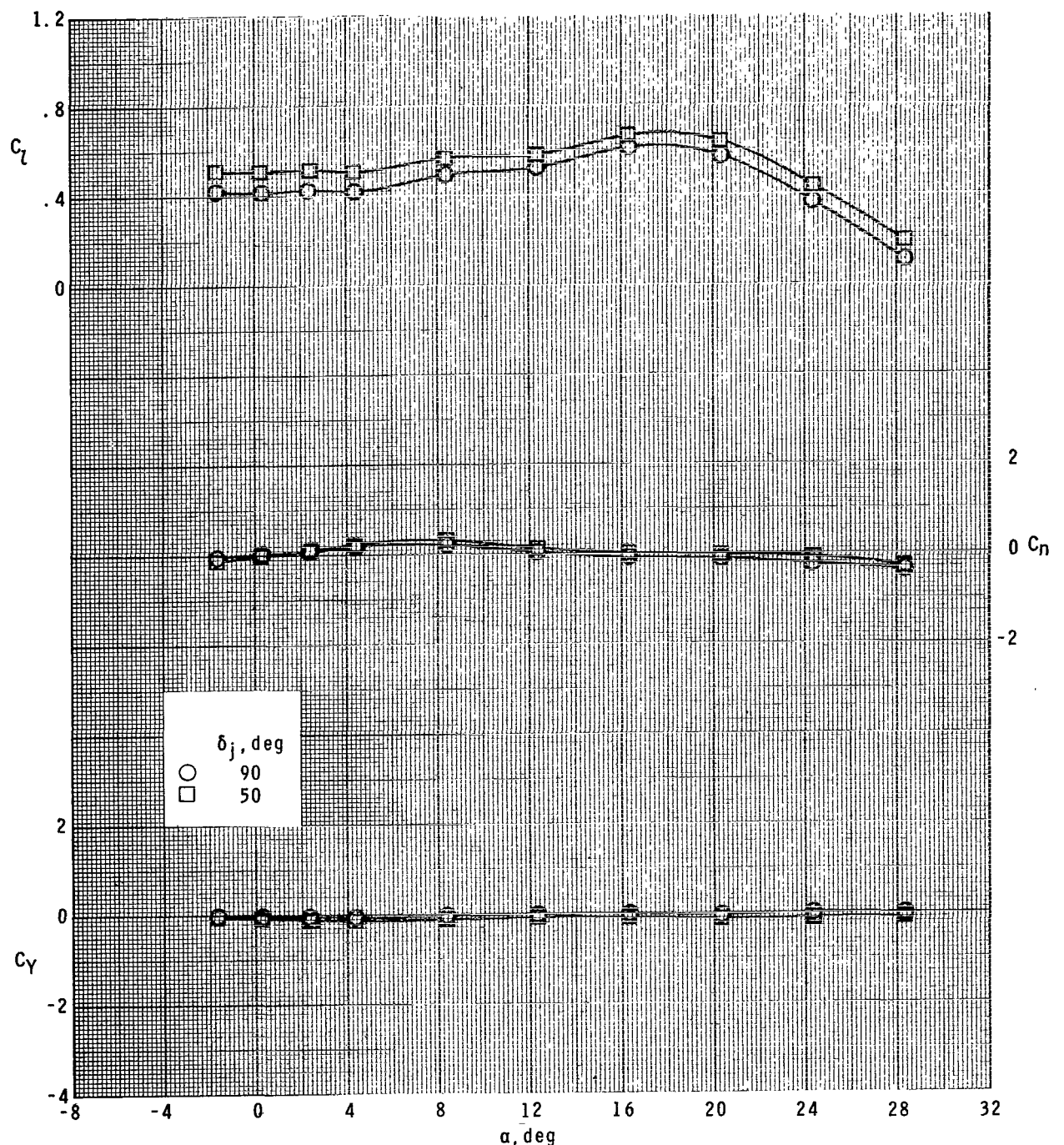
(b)  $M = 2.16$ .

Figure 21.- Continued.



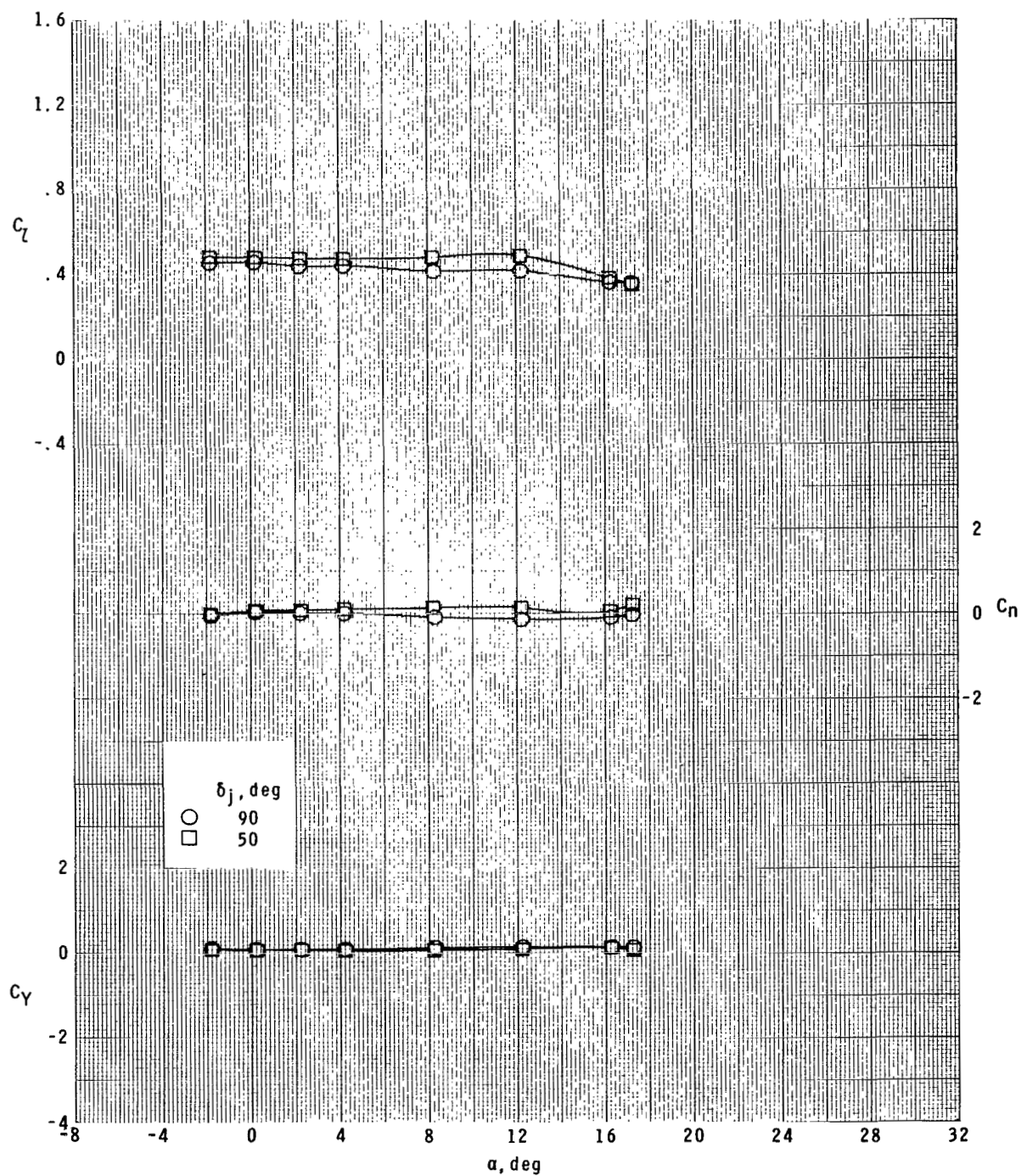
(c)  $M = 2.96$ .

Figure 21.- Continued.



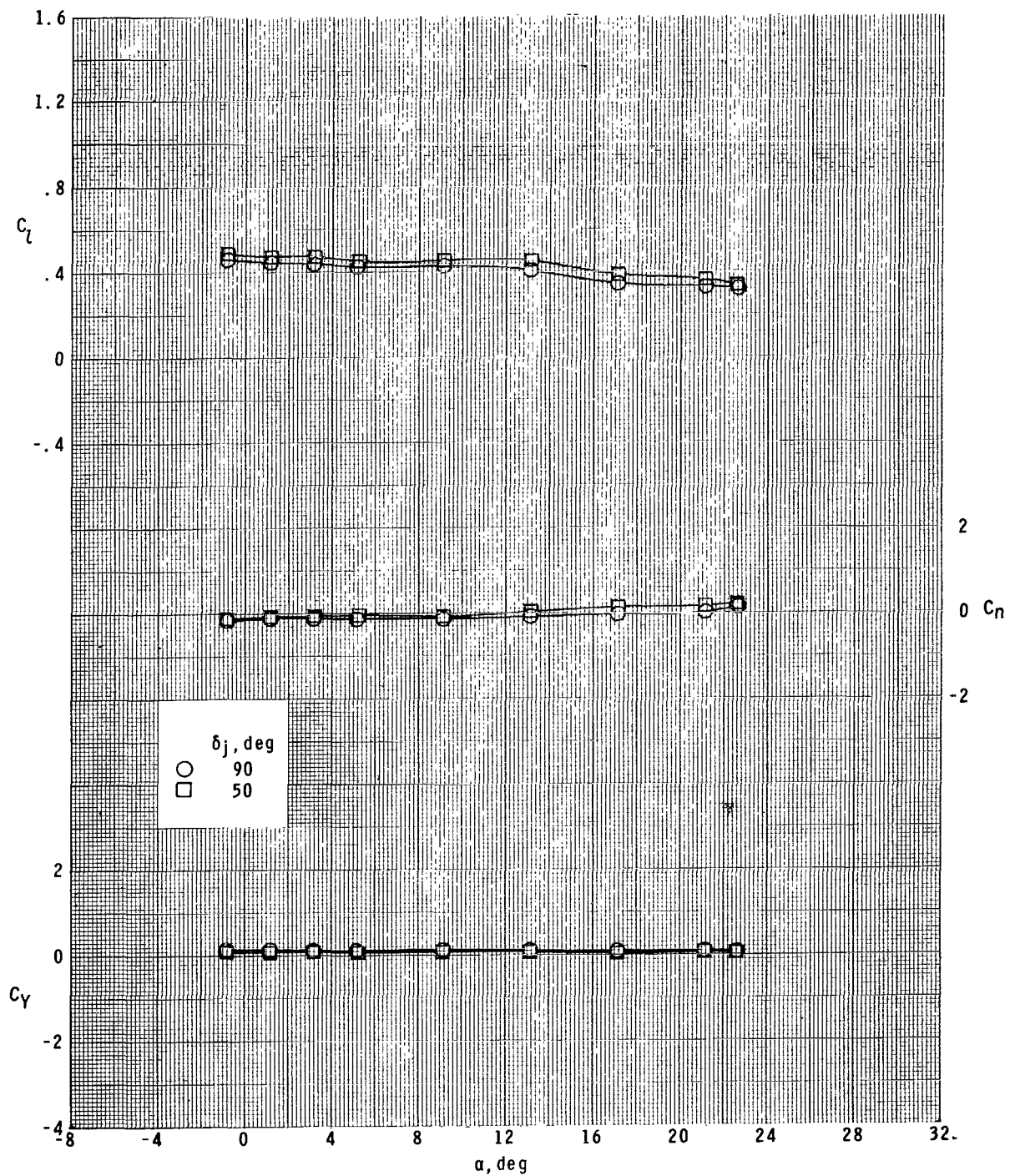
(d)  $M = 4.63$ .

Figure 21.- Concluded.



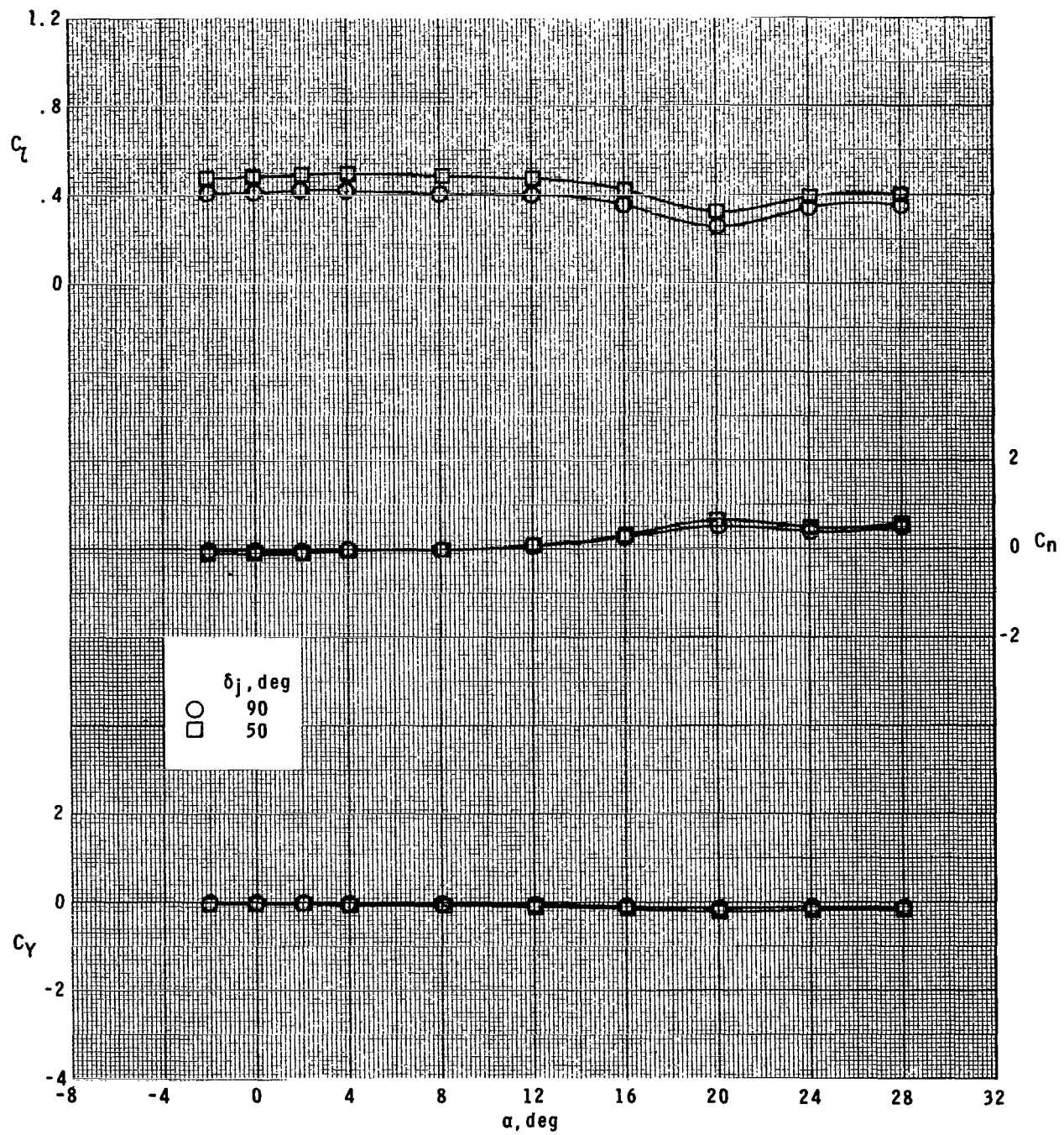
(a)  $M = 1.60$ .

Figure 22.- Effect of plenum jet-exit slot angle on lateral aerodynamic characteristics of model with ram-air-spoiler tail fins for  $A_j/A_i = 0.028$  and  $A_e/A_i = 0.75$  at  $\phi = 45^\circ$ .



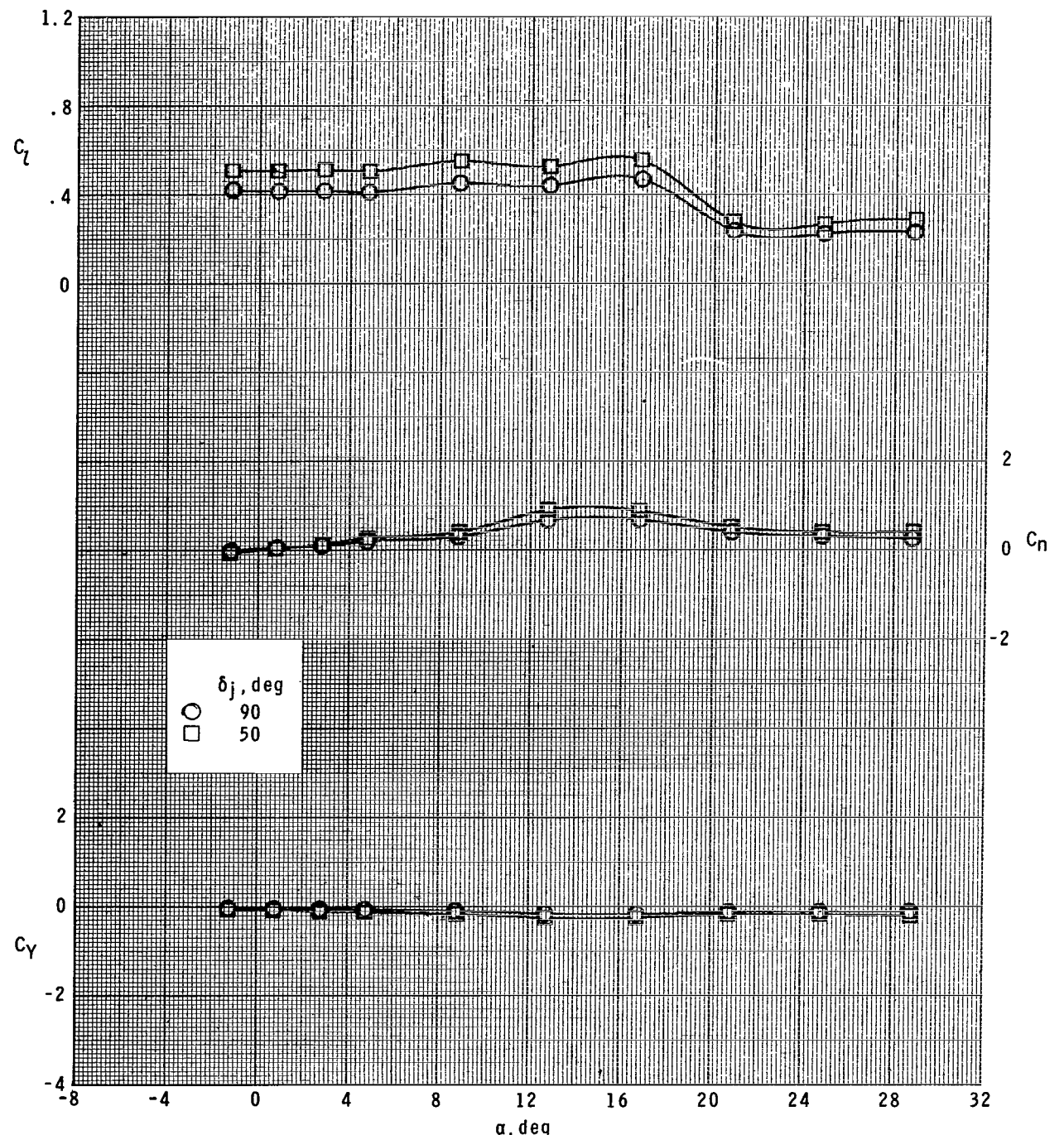
(b)  $M = 2.16.$

Figure 22.- Continued.



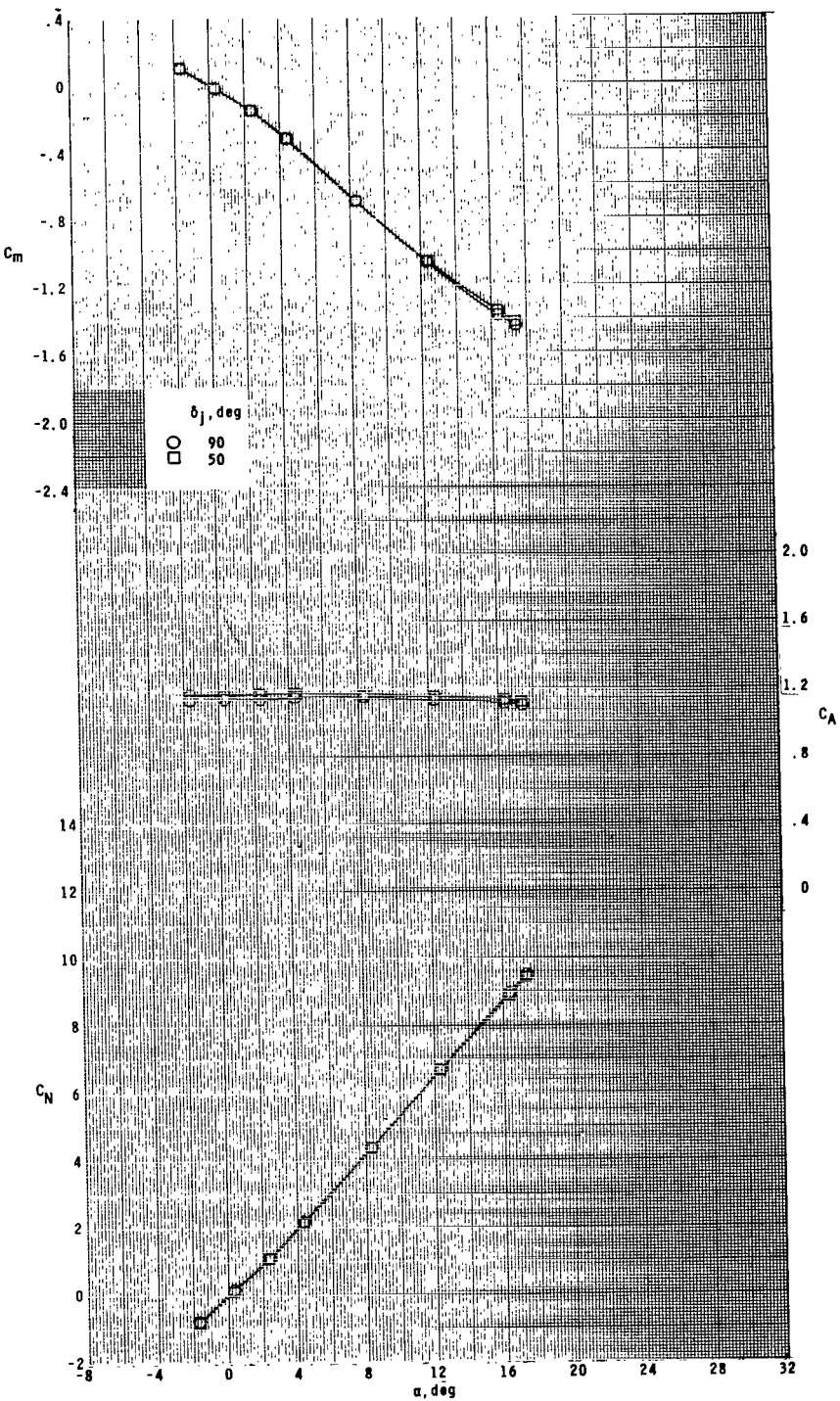
(c)  $M = 2.96.$

Figure 22.- Continued.



(d)  $M = 4.63.$

Figure 22.- Concluded.



(a)  $M = 1.60.$

Figure 23.- Effect of plenum jet-exit slot angle on longitudinal aerodynamic characteristics of model with ram-air-spoiler tail fins for  $A_i/A = 0.028$  and  $A_e/A_i = 0.75$  at  $\phi = 0^\circ$ .

# **Error**

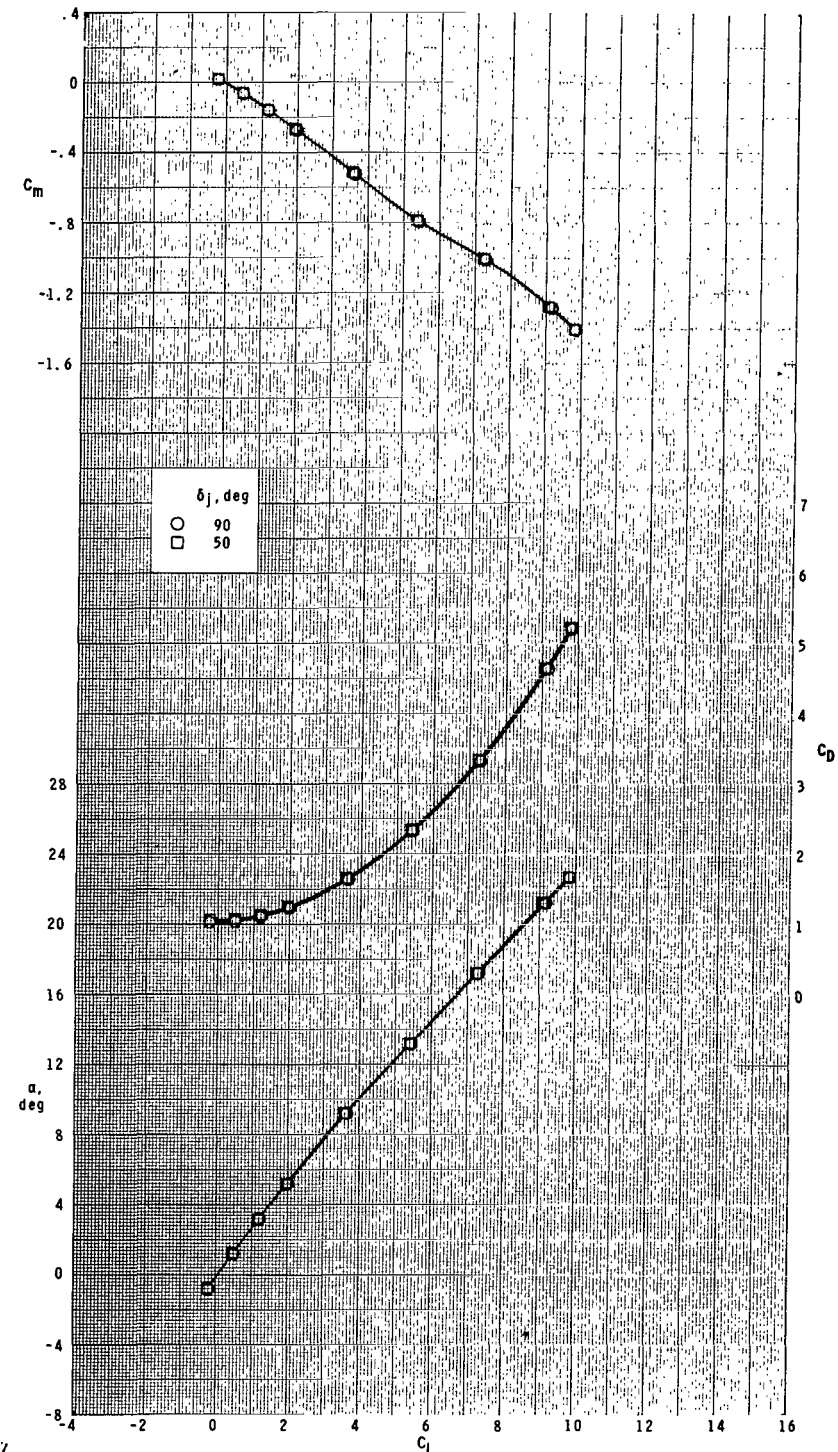
---

An error occurred while processing this page. See the system log for more details.

# **Error**

---

An error occurred while processing this page. See the system log for more details.



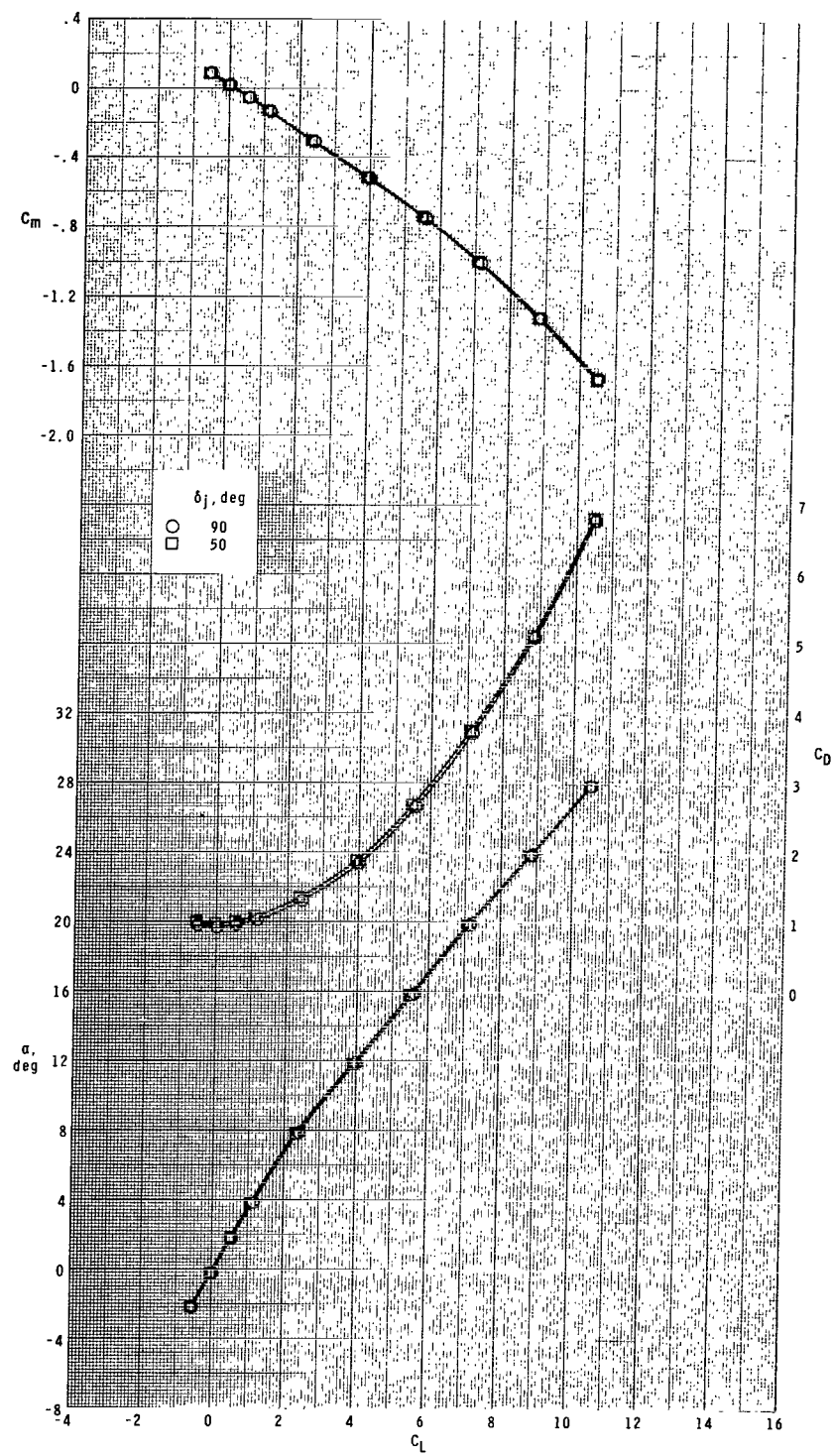
(b) Concluded.

Figure 23.- Continued.

# **Error**

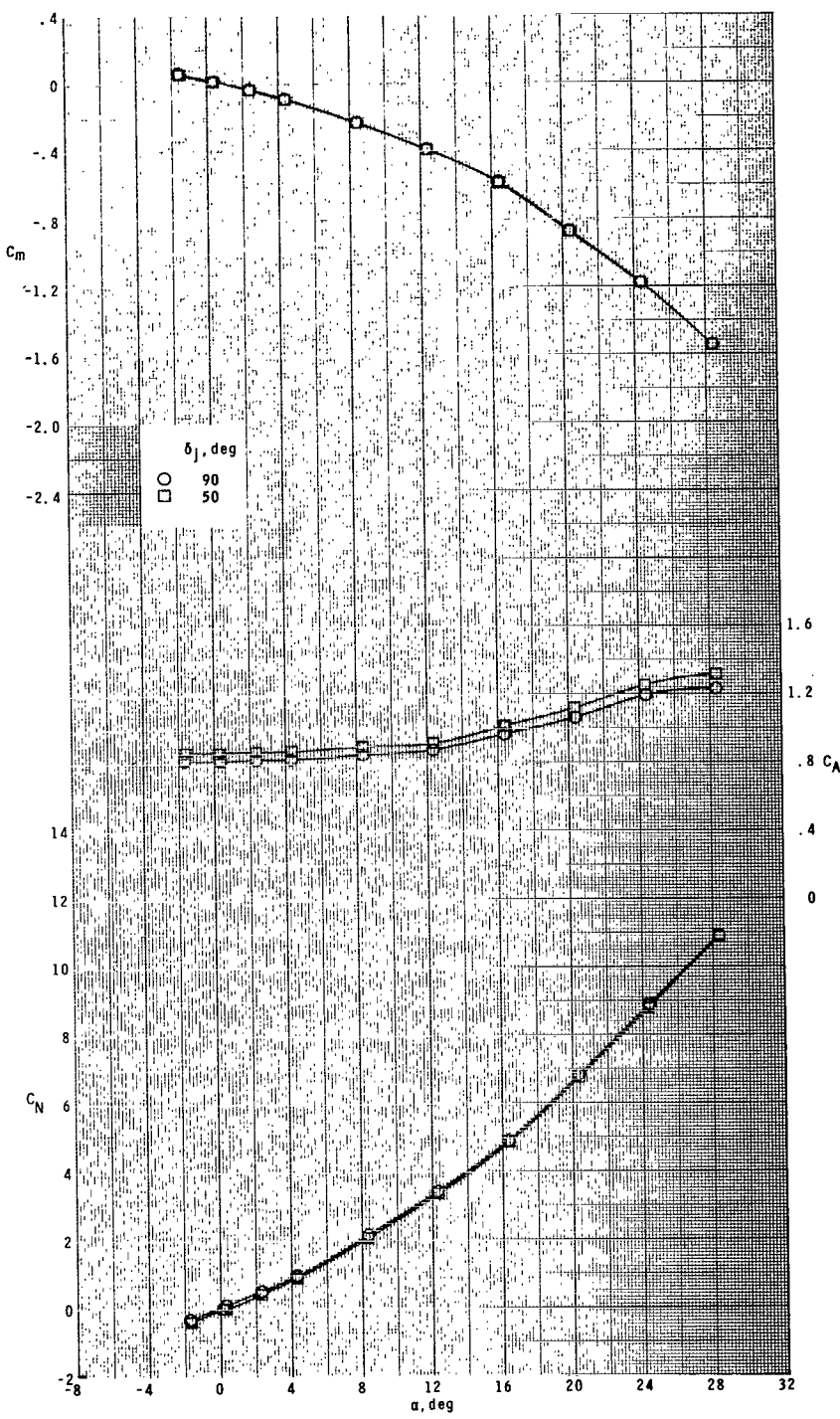
---

An error occurred while processing this page. See the system log for more details.



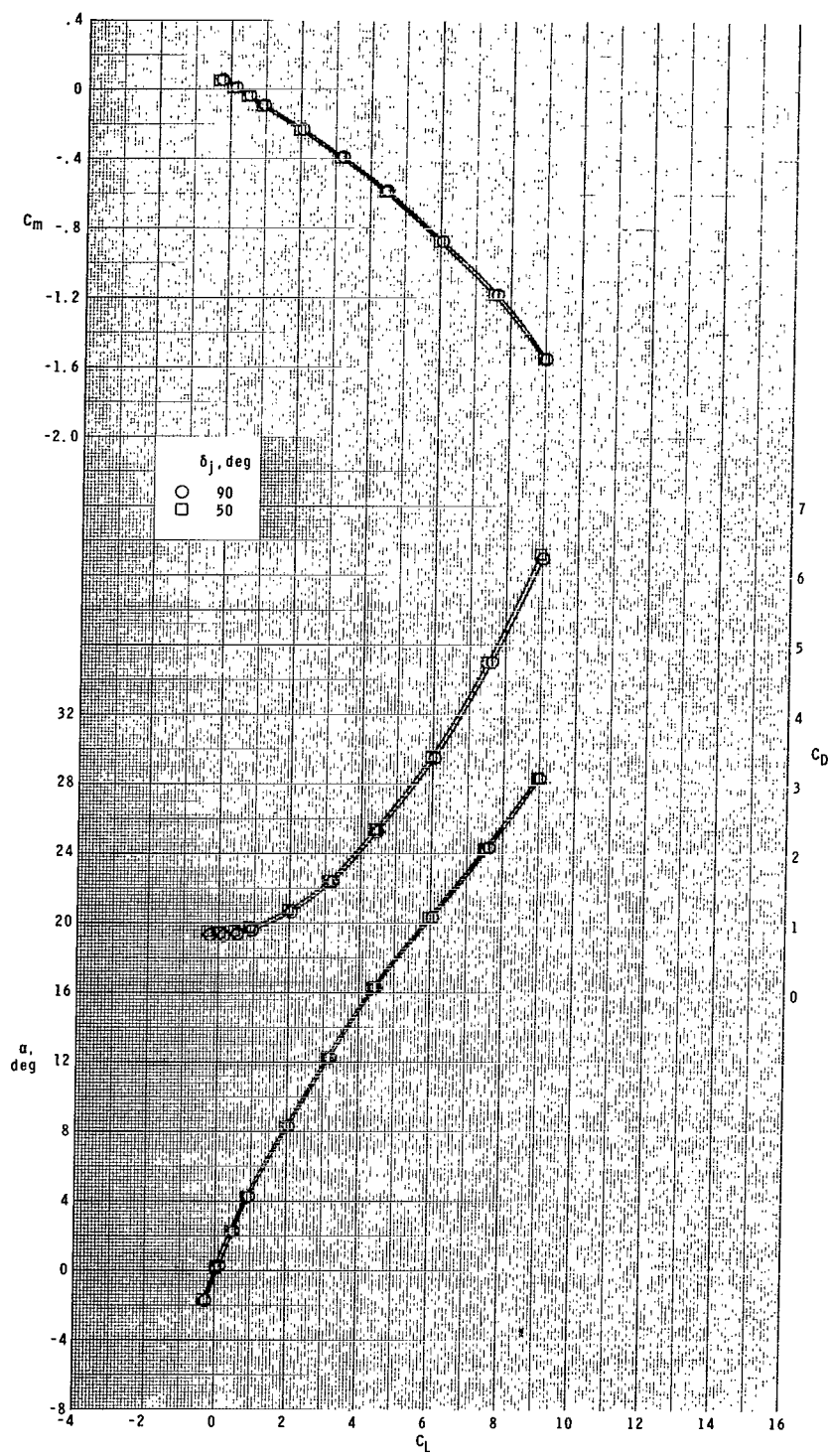
(c) Concluded.

Figure 23.- Continued.



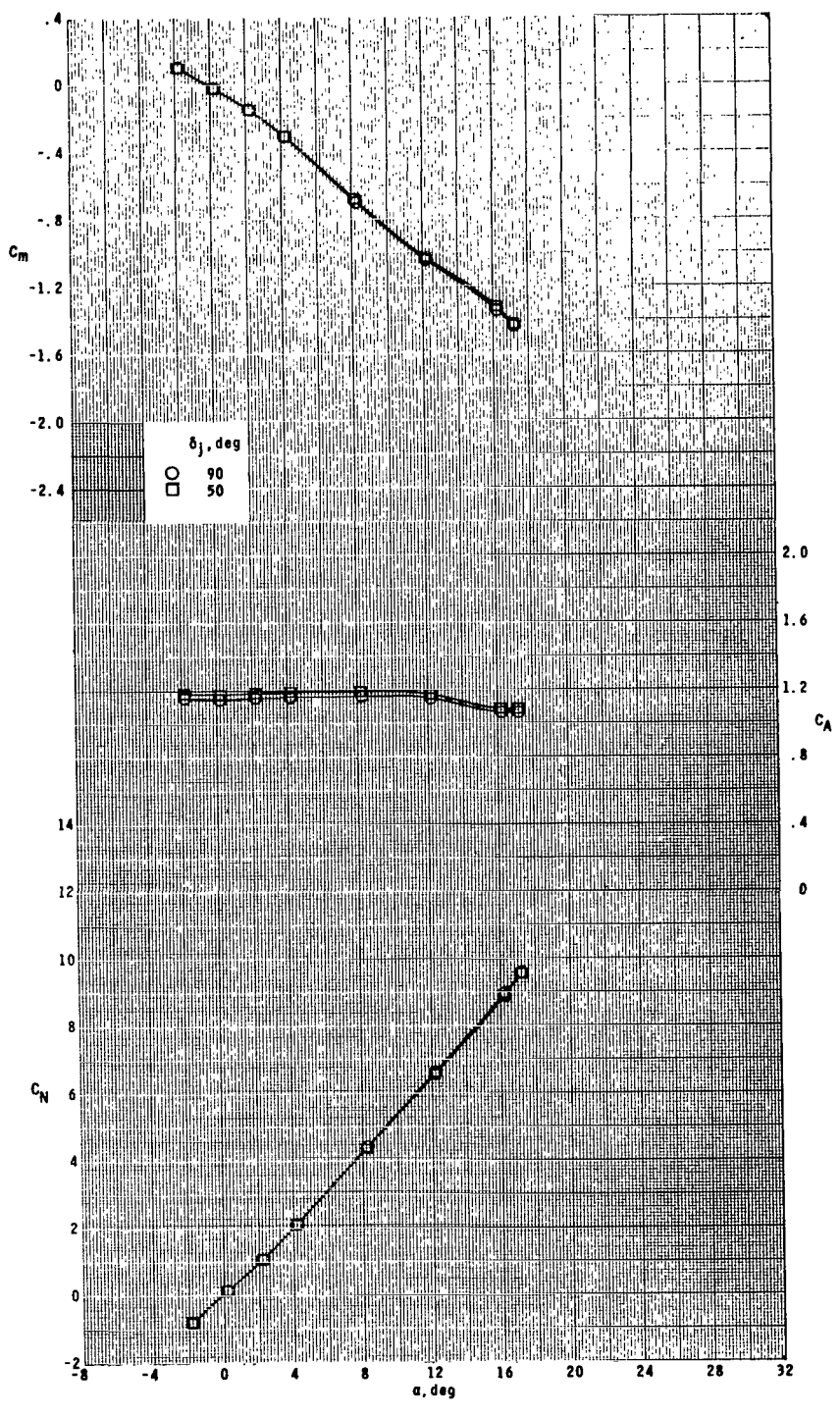
(d)  $M = 4.63.$

Figure 23.- Continued.



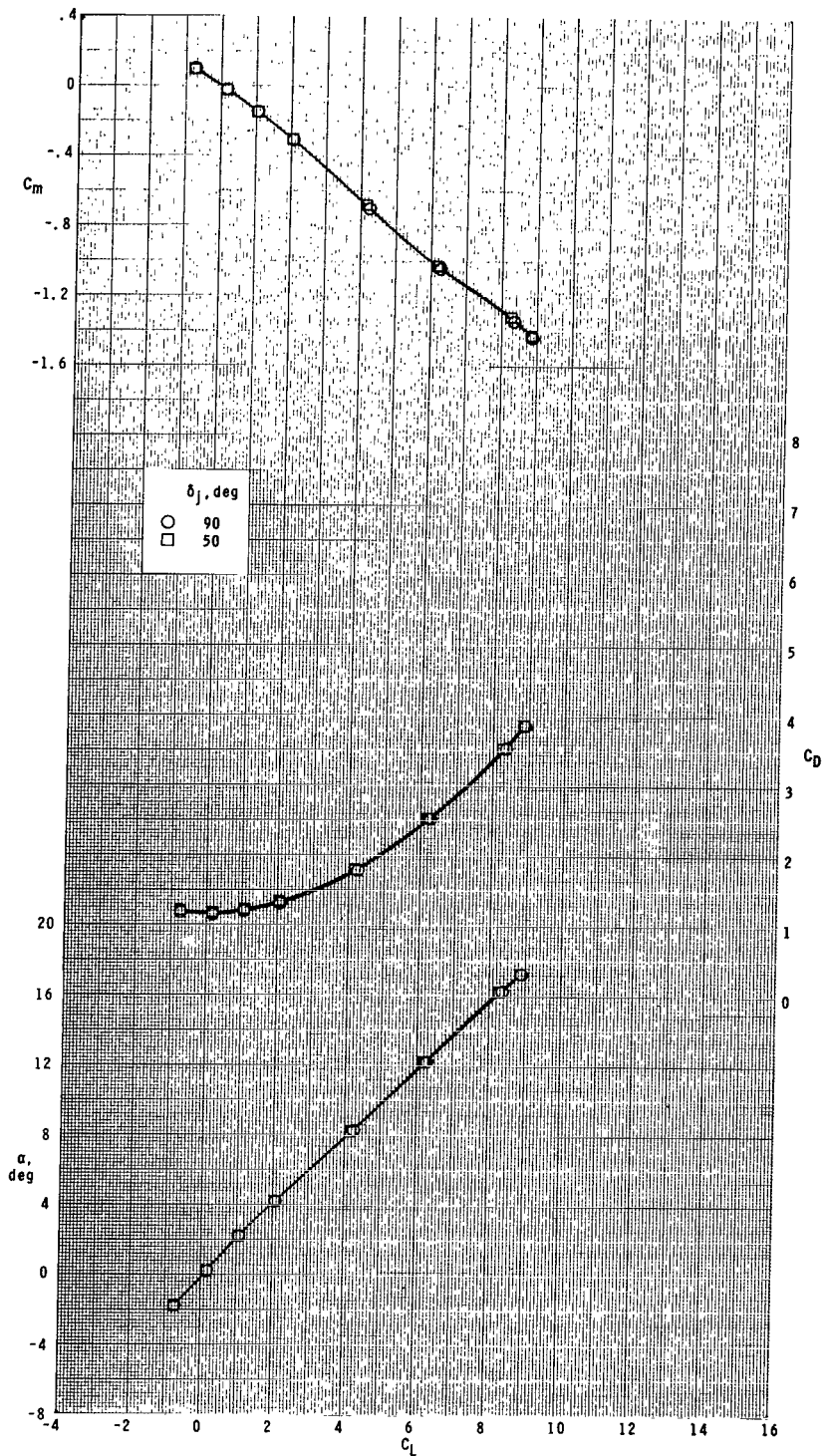
(d) Concluded.

Figure 23.- Concluded.



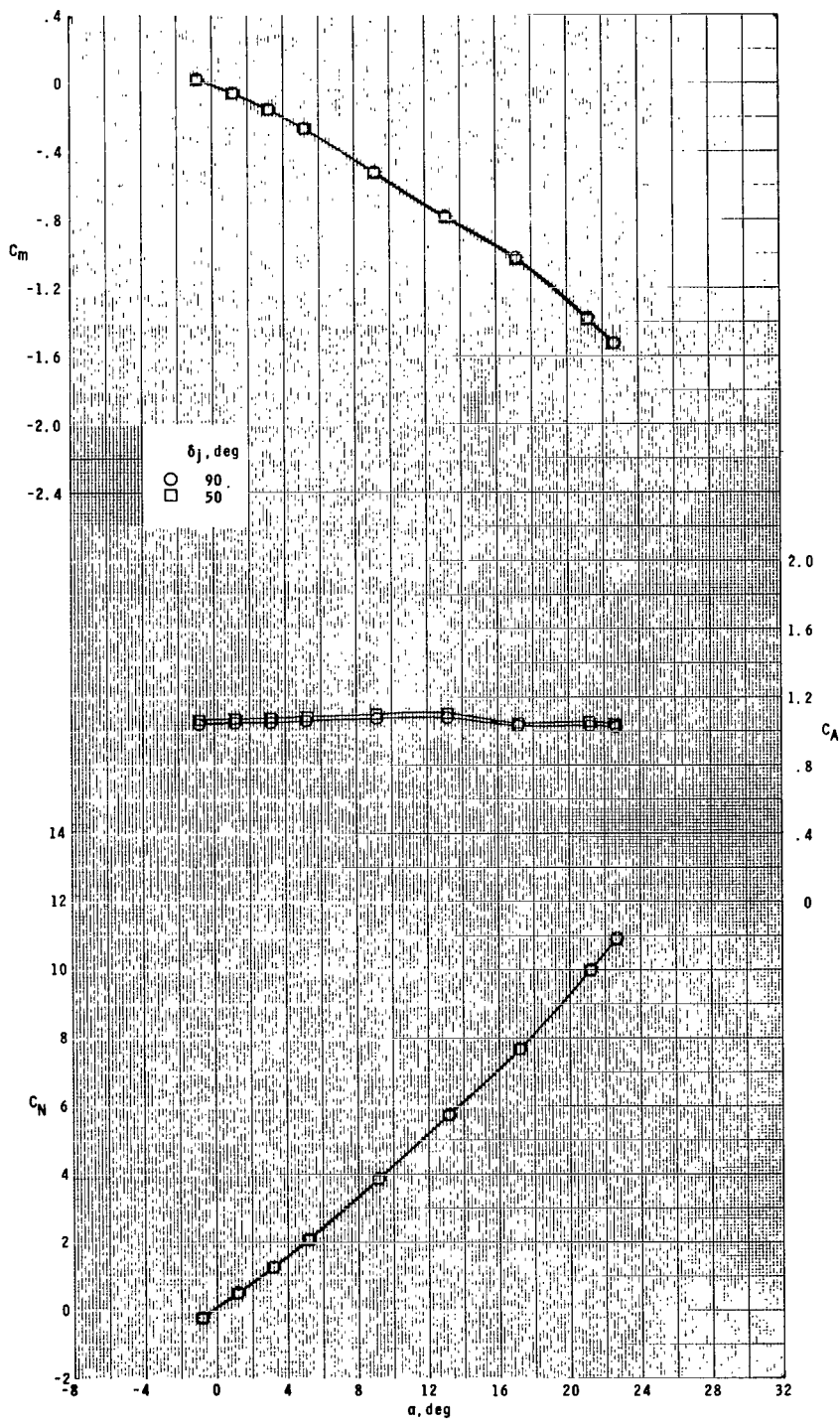
(a)  $M = 1.60.$

Figure 24.- Effect of plenum jet-exit slot angle on longitudinal aerodynamic characteristics of model with ram-air-spoiler tail fins for  $A_i/A = 0.028$  and  $A_e/A_i = 0.75$  at  $\phi = 45^\circ$ .



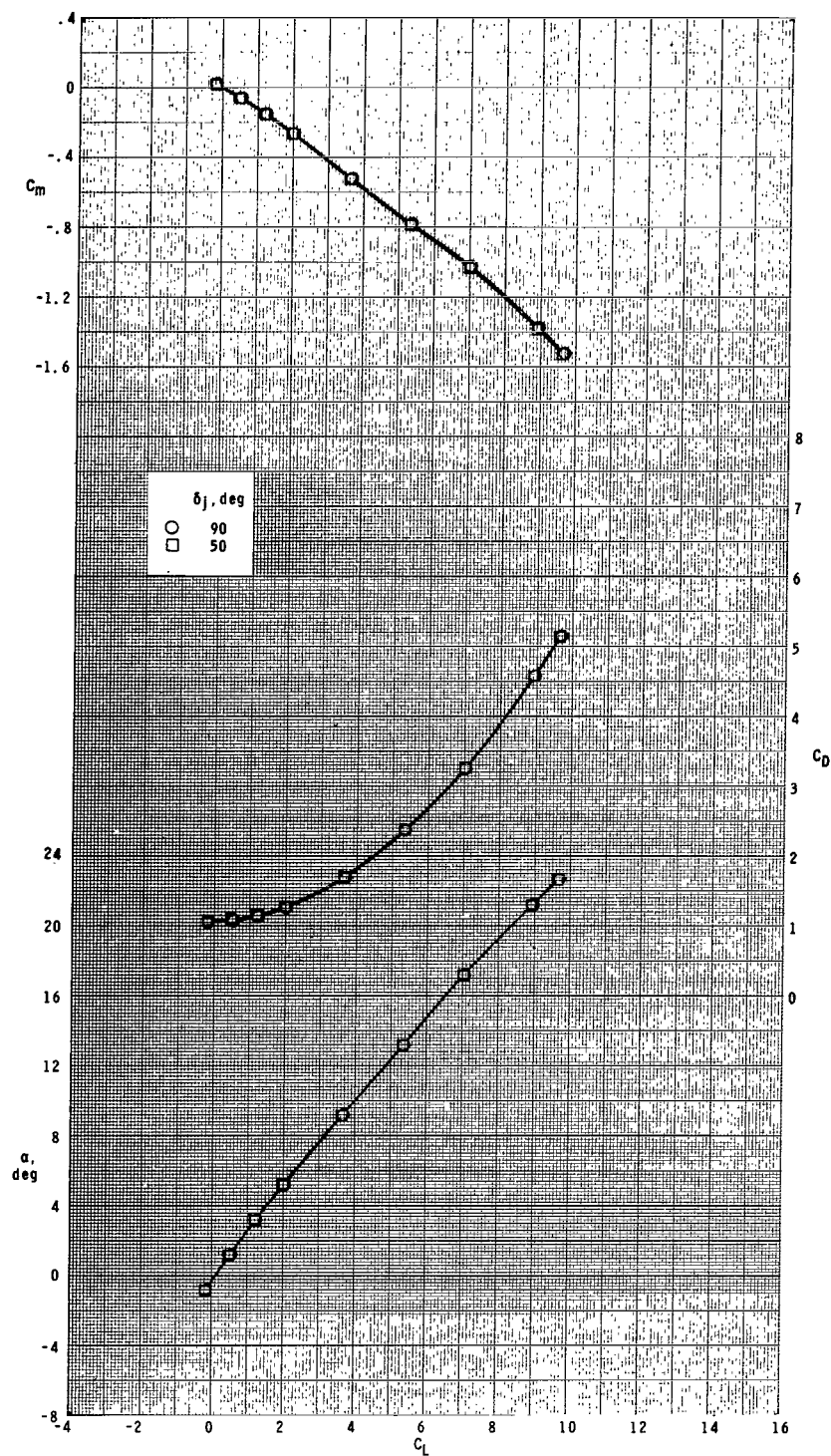
(a) Concluded.

Figure 24.- Continued.



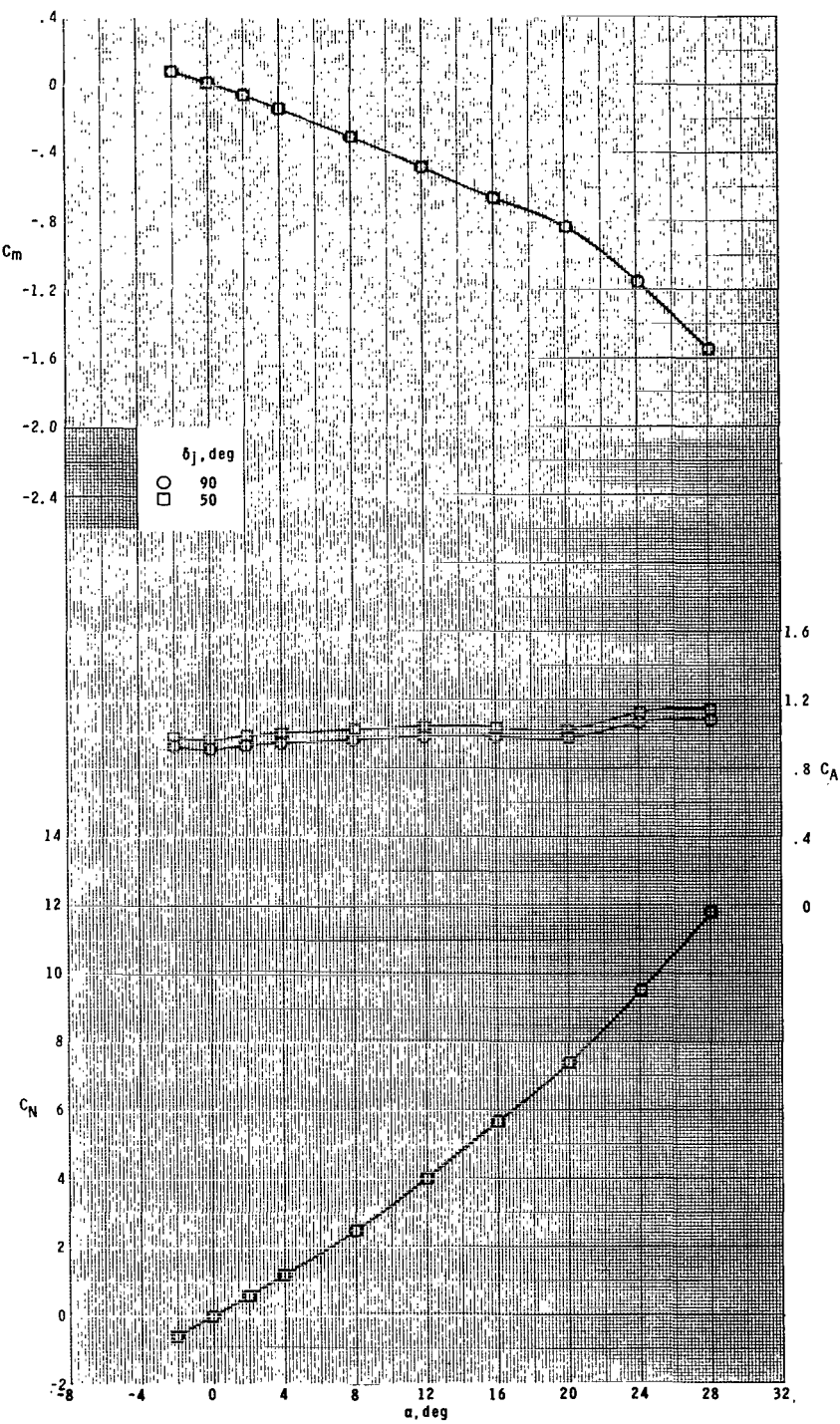
(b)  $M = 2.16.$

Figure 24.- Continued.



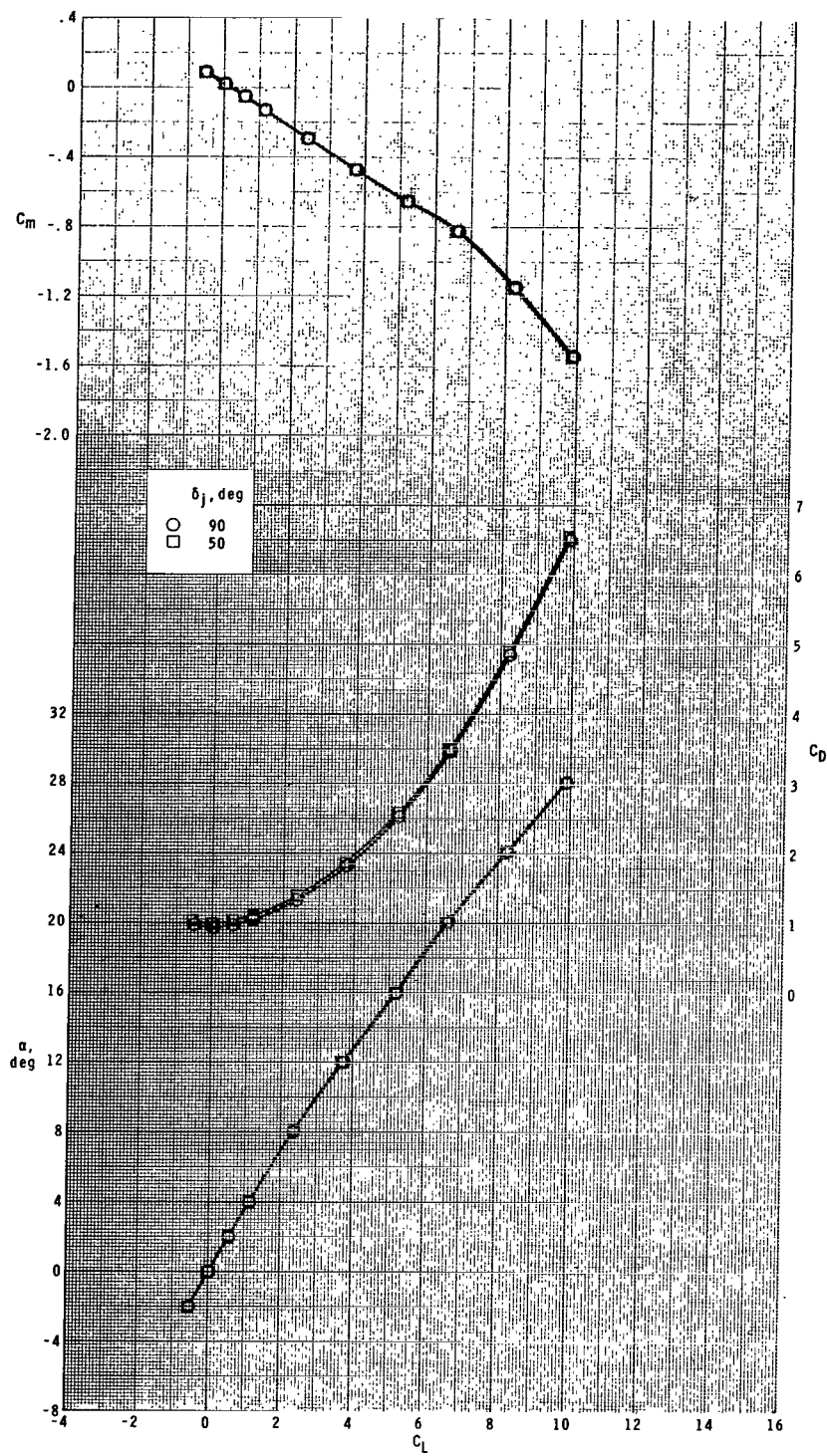
(b) Concluded.

Figure 24.- Continued.



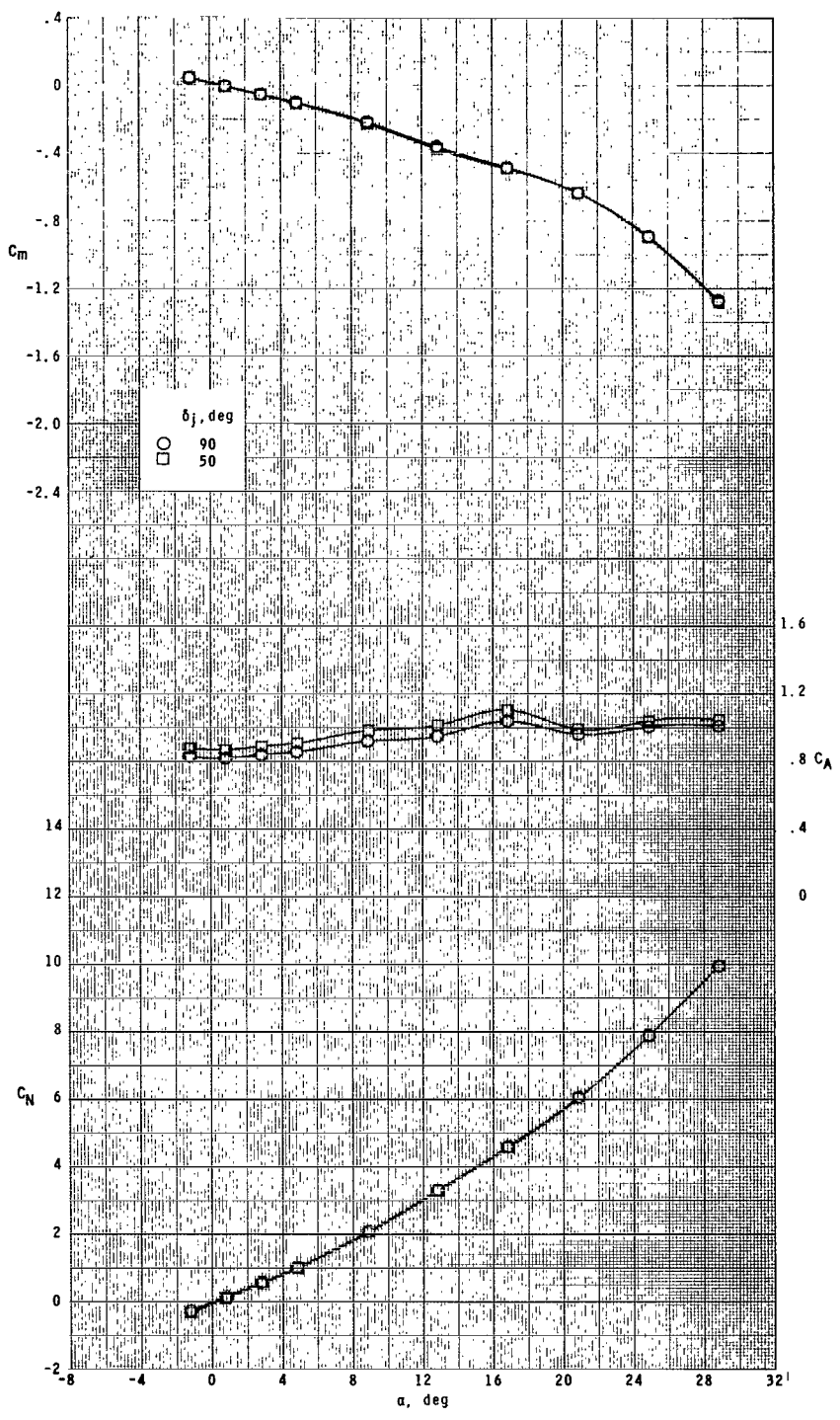
(c)  $M = 2.96$ .

Figure 24.- Continued.



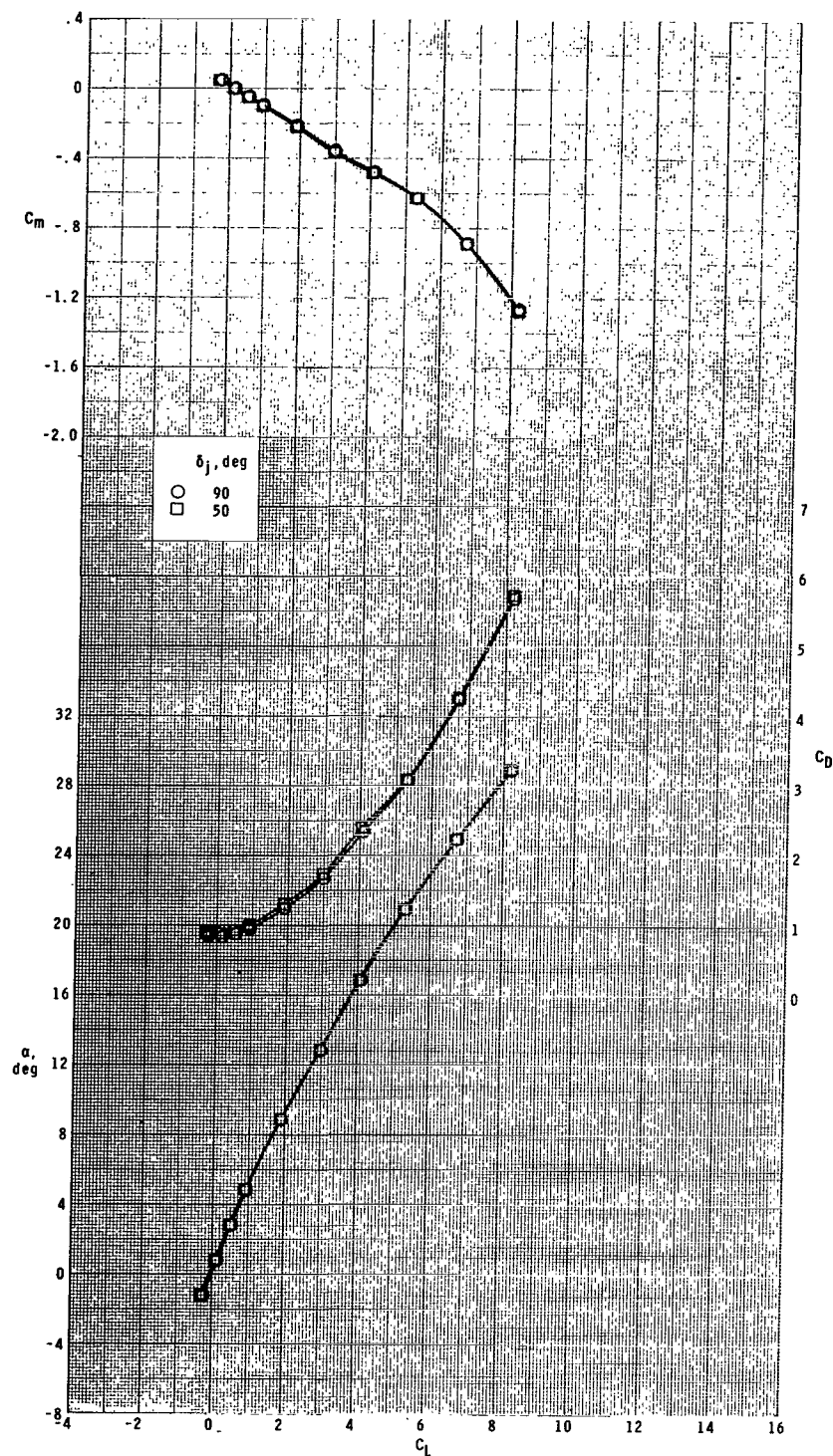
(c) Concluded.

Figure 24.- Continued.



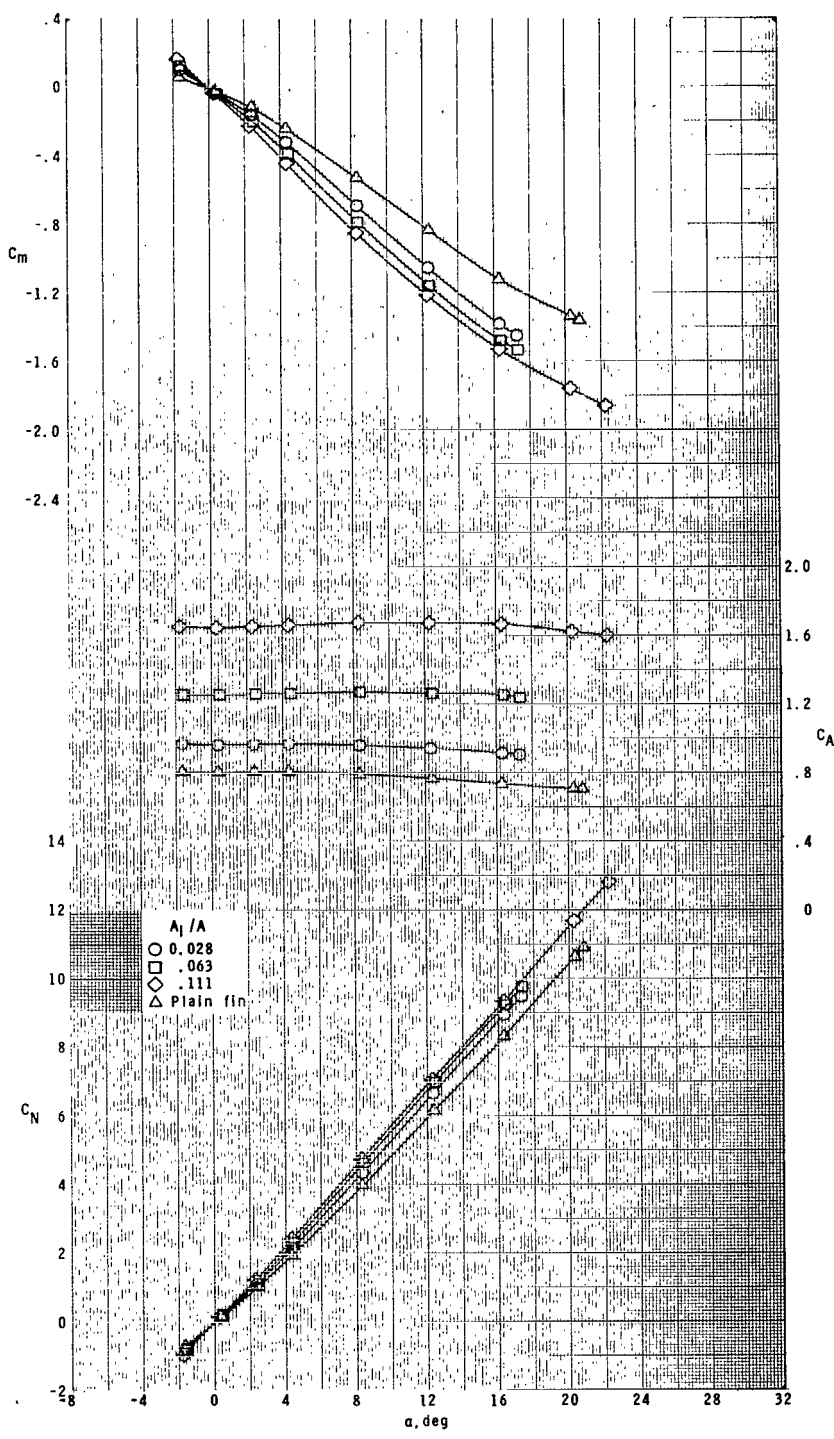
(d)  $M = 4.63.$

Figure 24.- Continued.



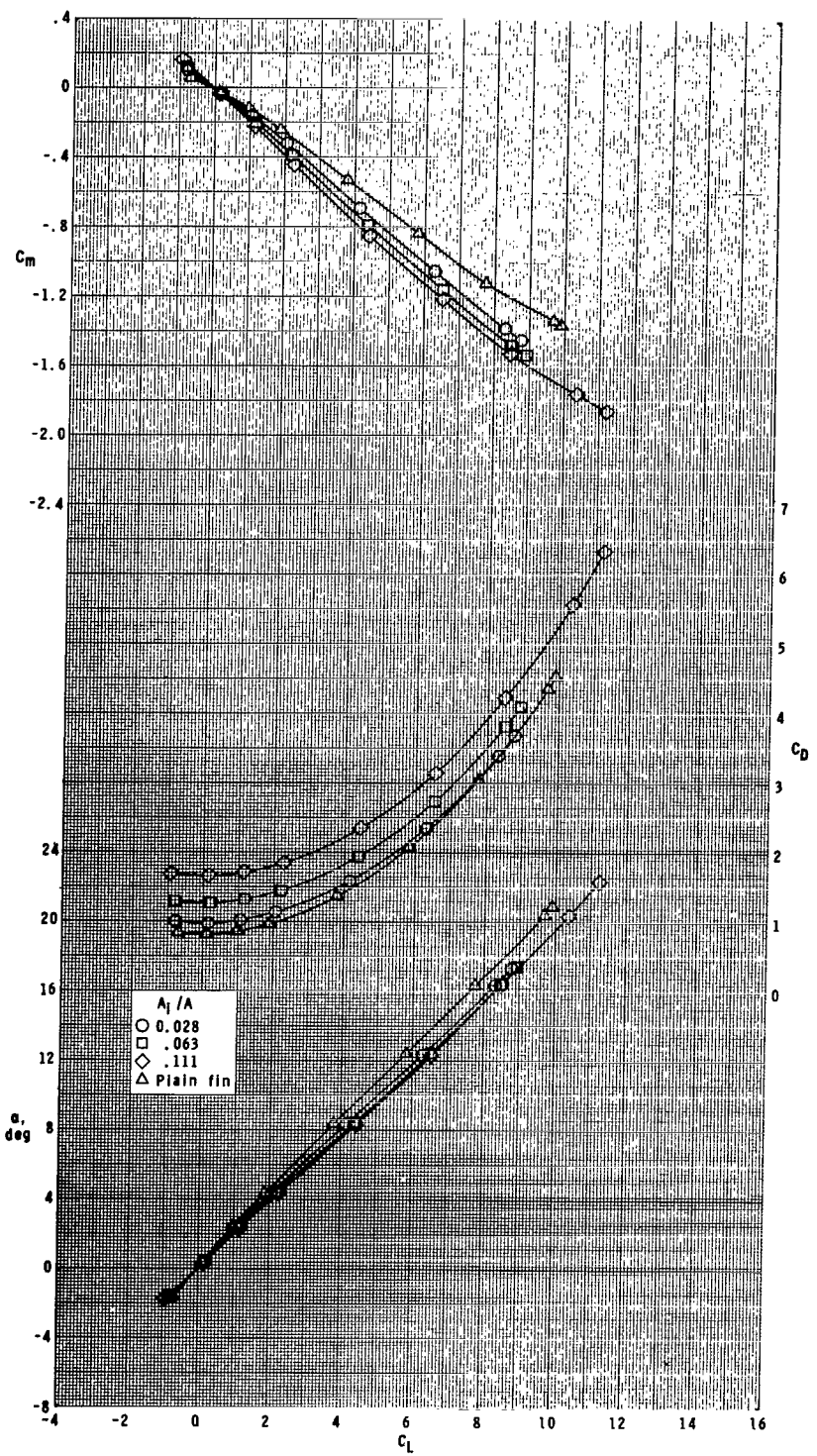
(d) Concluded.

Figure 24.- Concluded.



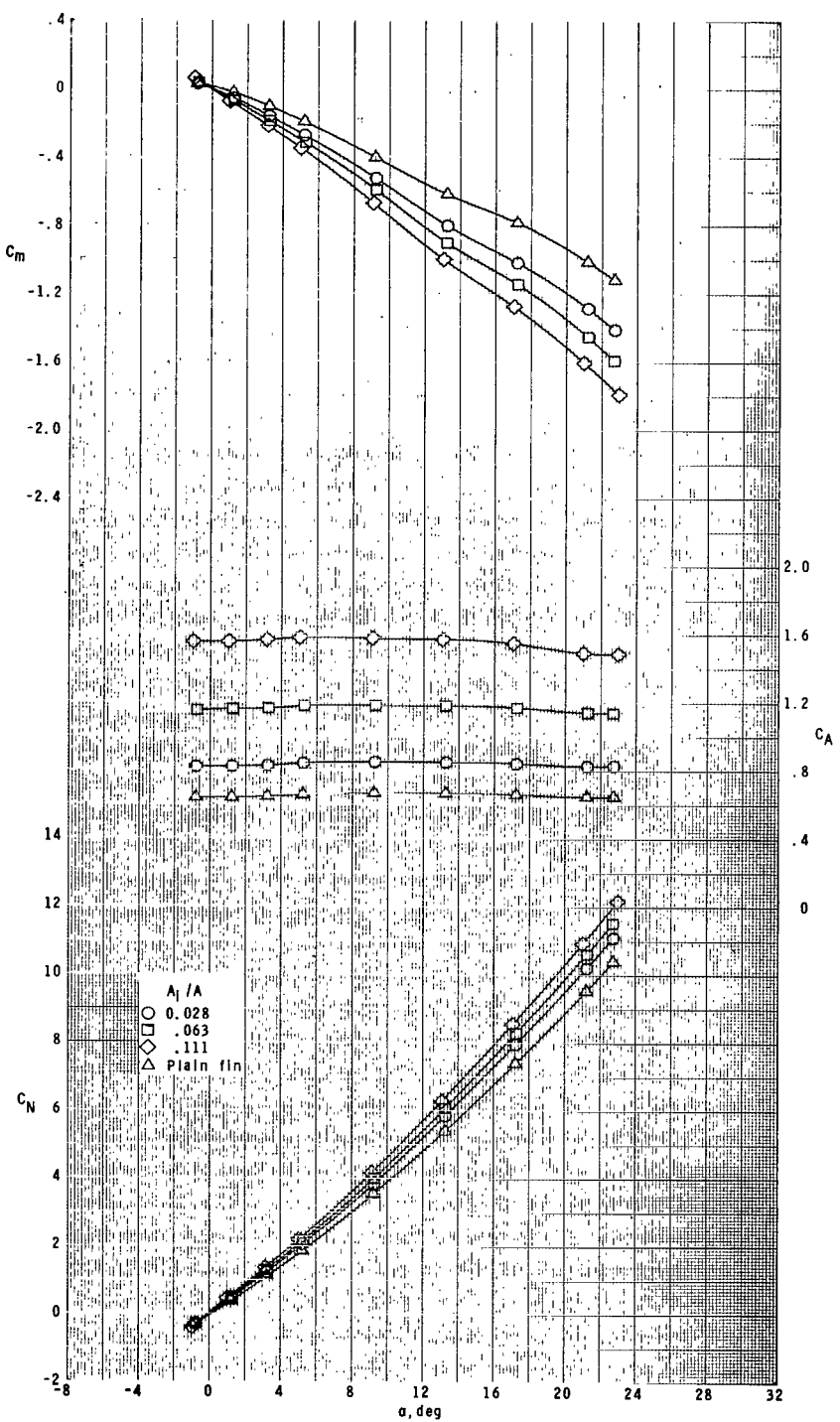
(a)  $M = 1.60$ .

Figure 25.- Effect of inlet size and fin thickness on longitudinal aerodynamic characteristics of model with flow-through nacelle ram-air spoiler and plain tail fins at  $\phi = 0^\circ$ .



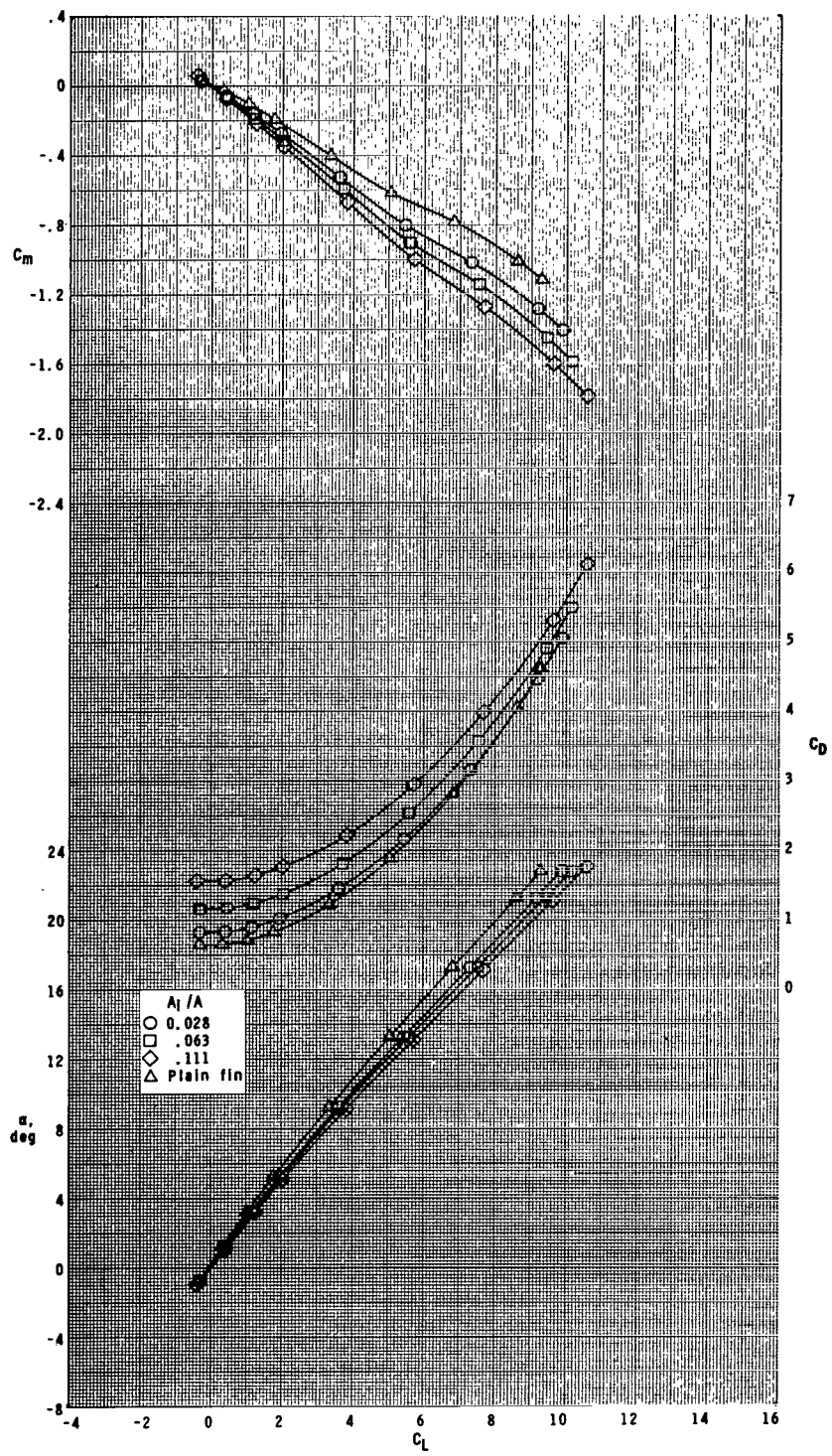
(a) Concluded.

Figure 25.- Continued.



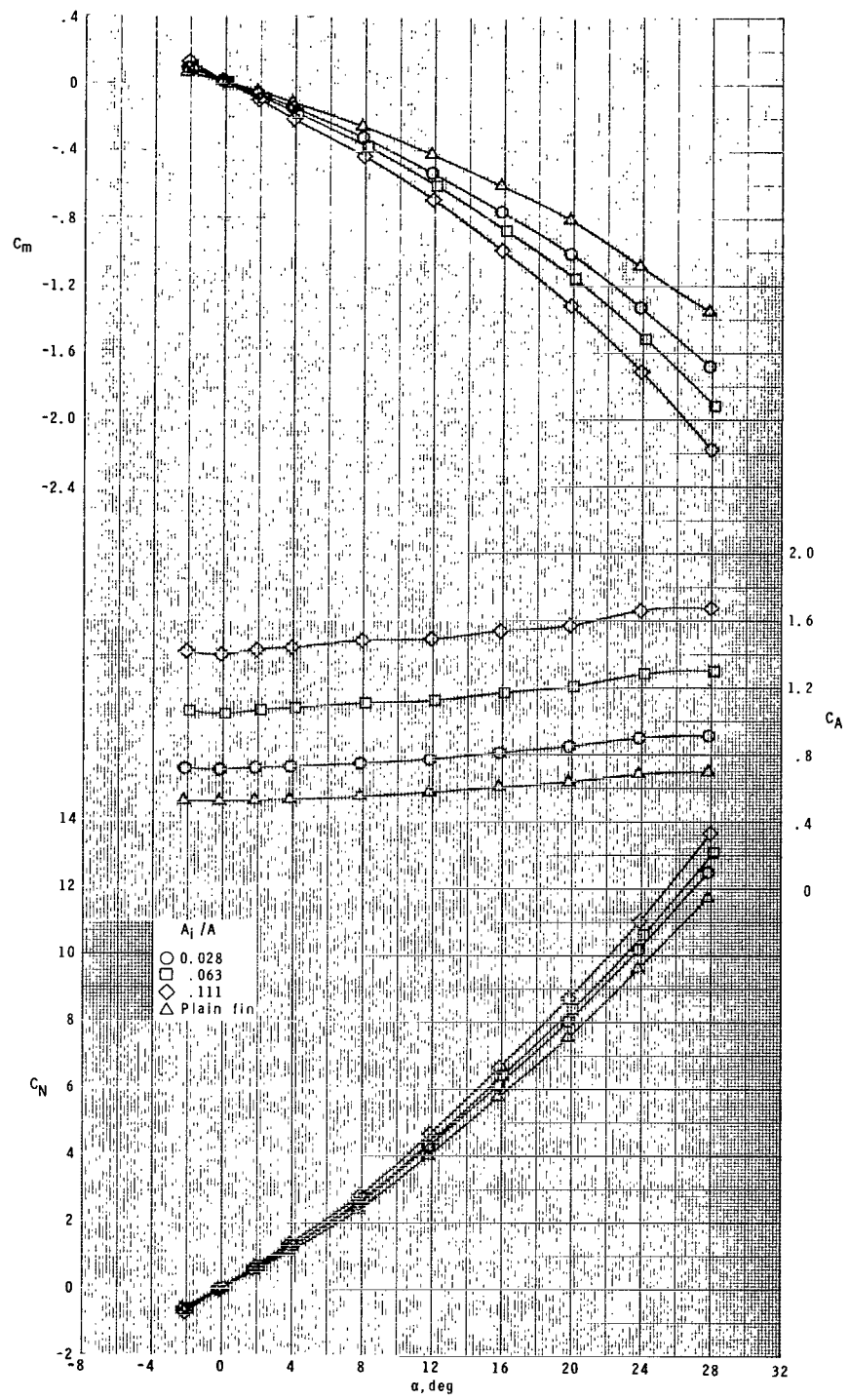
(b)  $M = 2.16.$

Figure 25.- Continued.



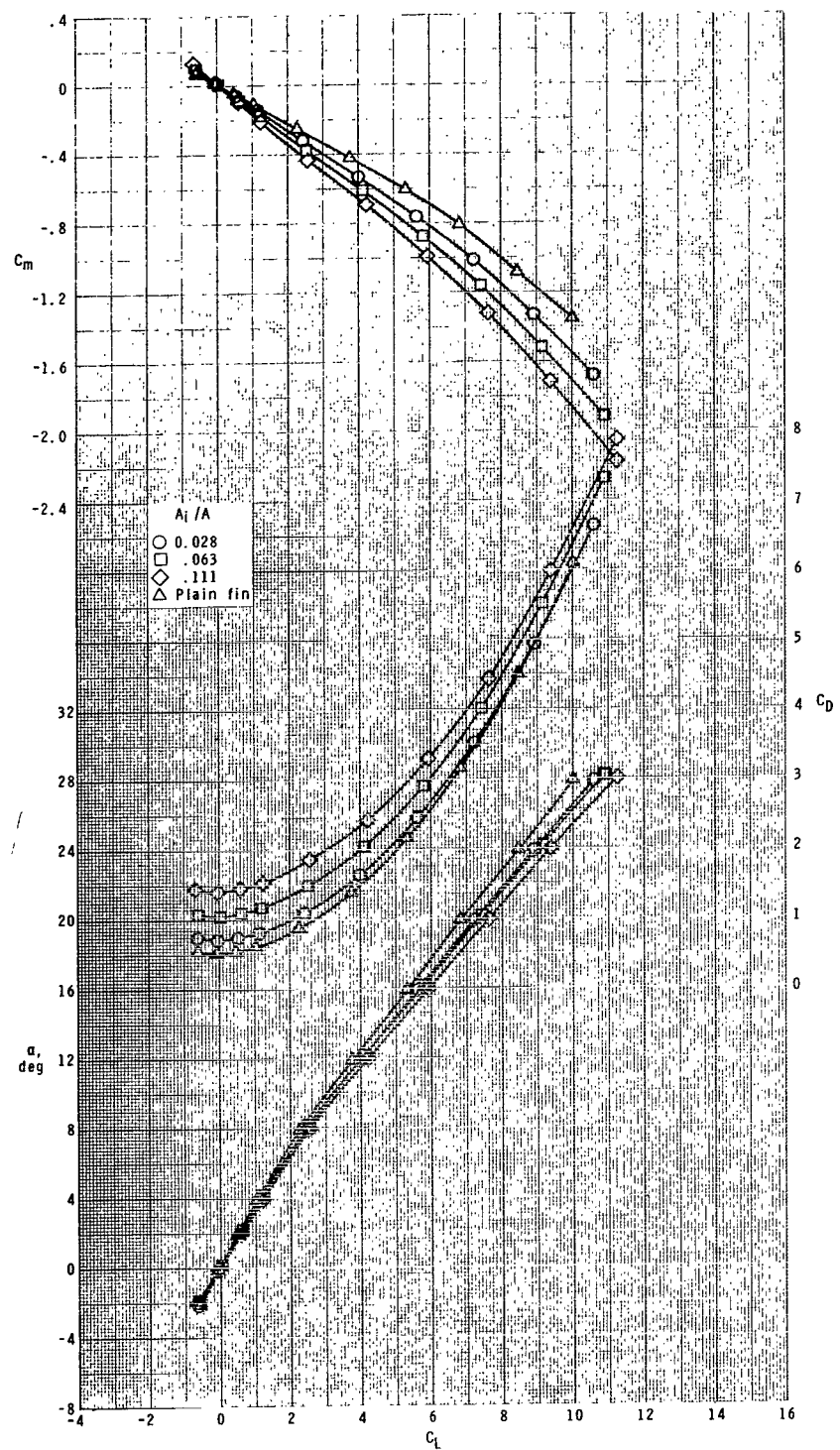
(b) Concluded.

Figure 25.- Continued.



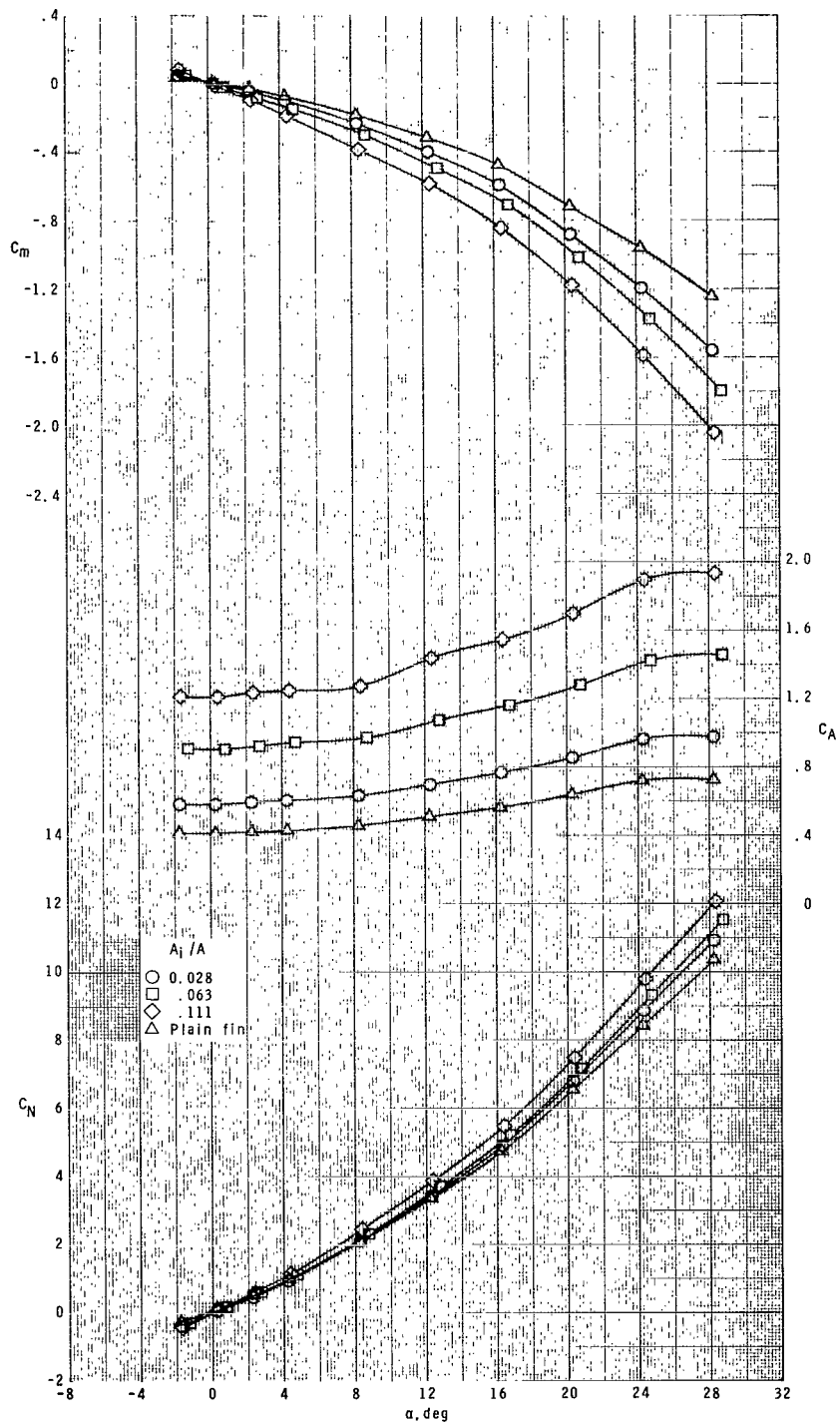
(c)  $M = 2.96.$

Figure 25.- Continued.



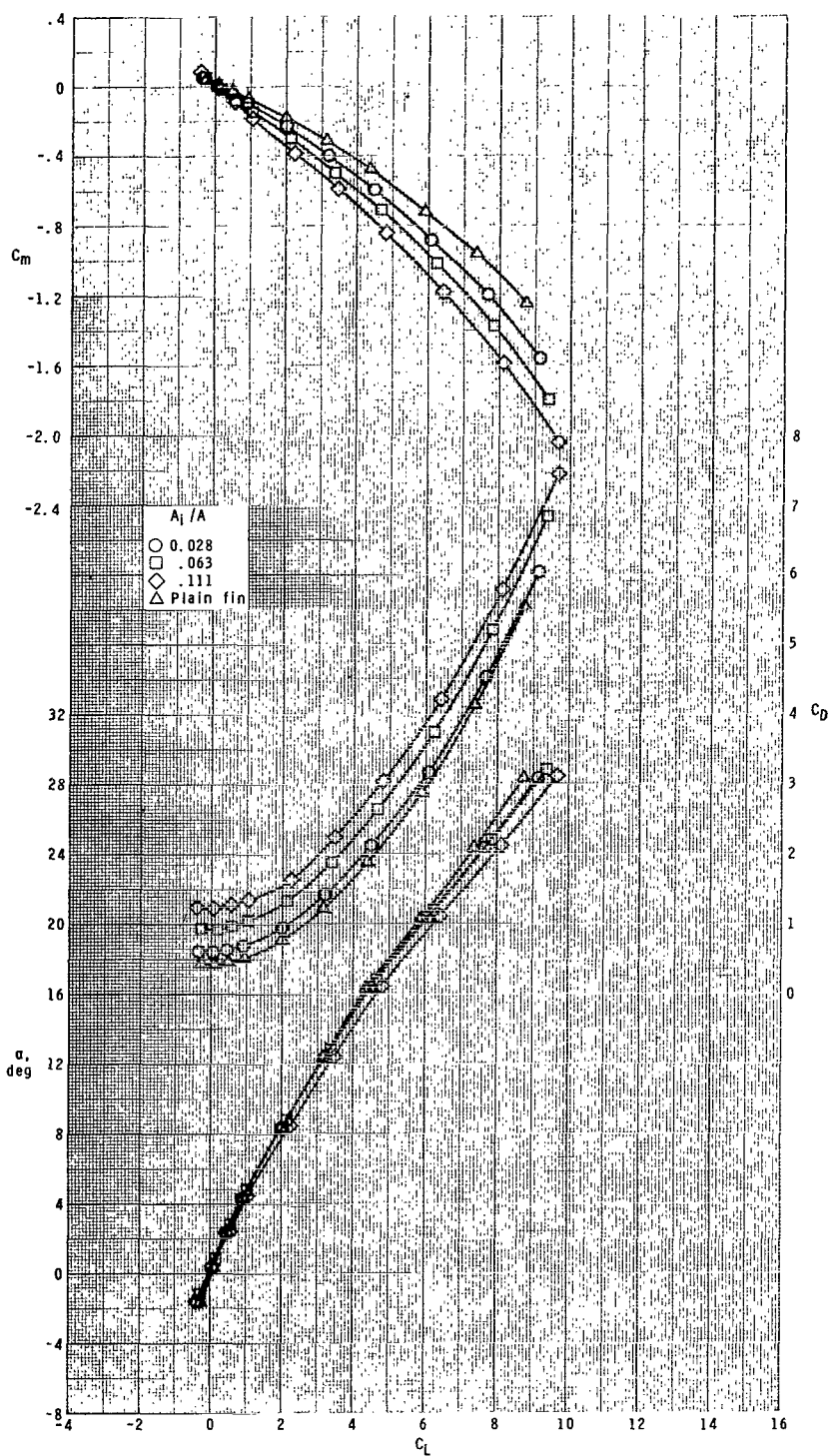
(c) Concluded.

Figure 25.- Continued.



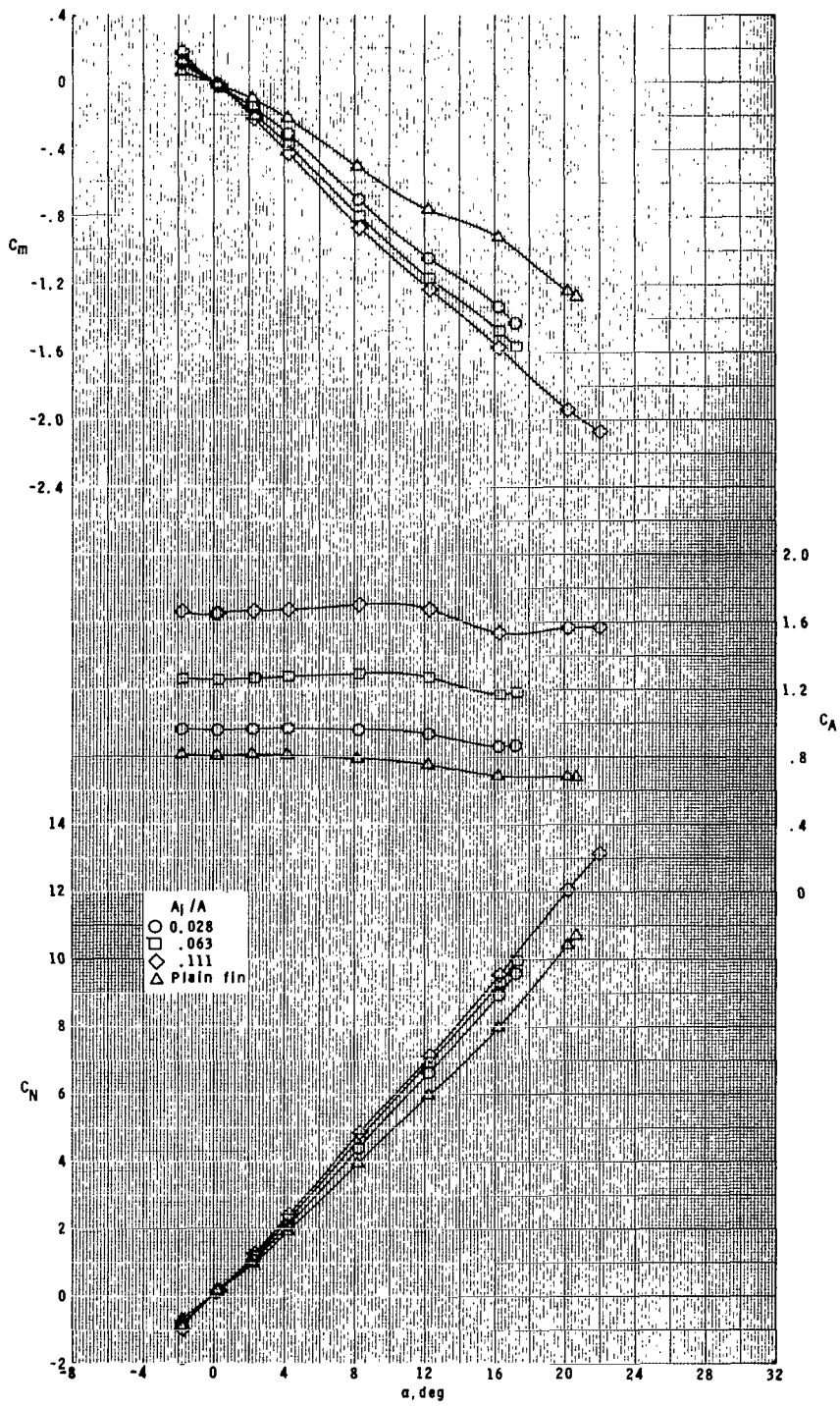
(d)  $M = 4.63.$

Figure 25.- Continued.



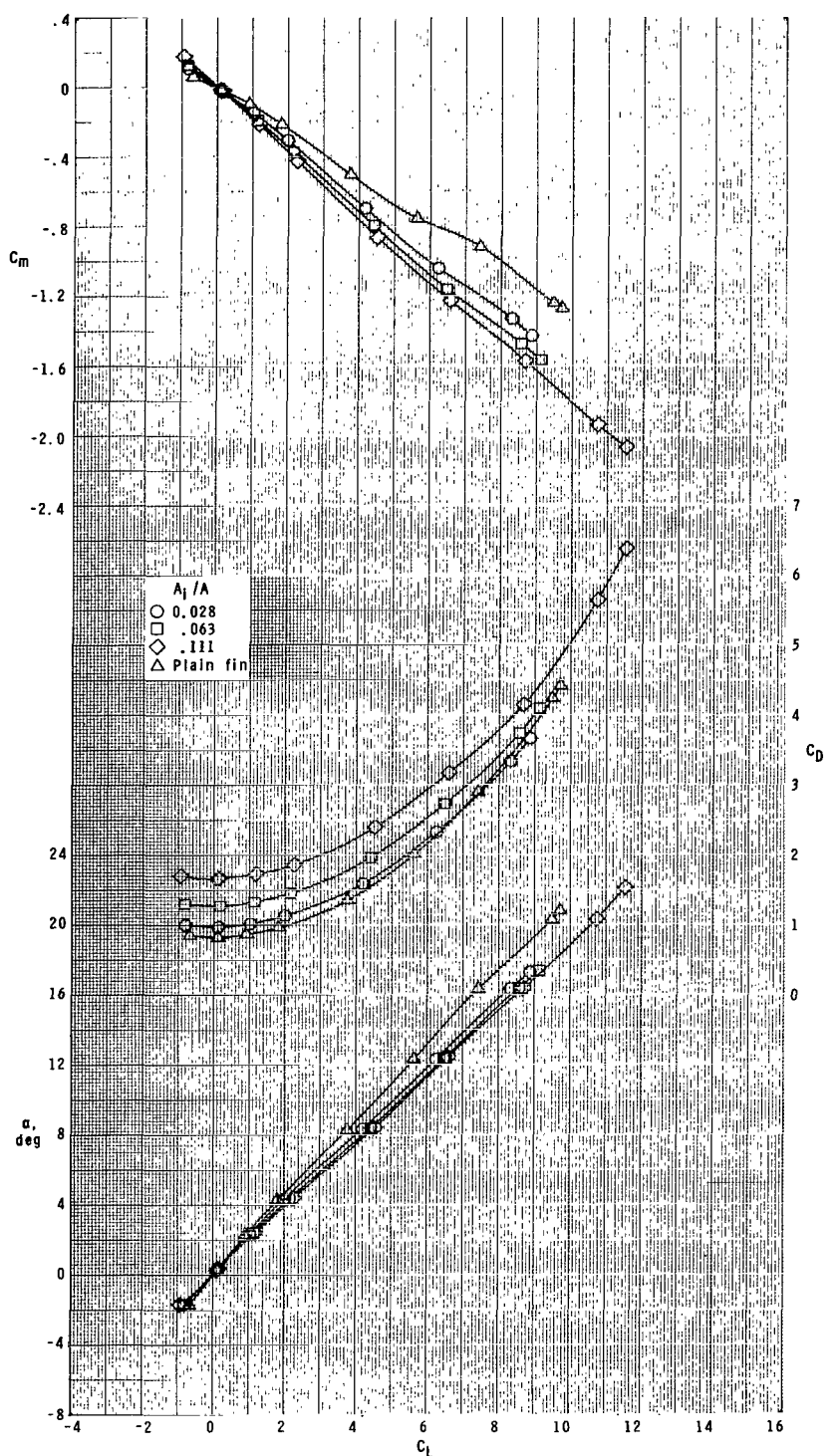
(d) Concluded.

Figure 25.- Concluded.



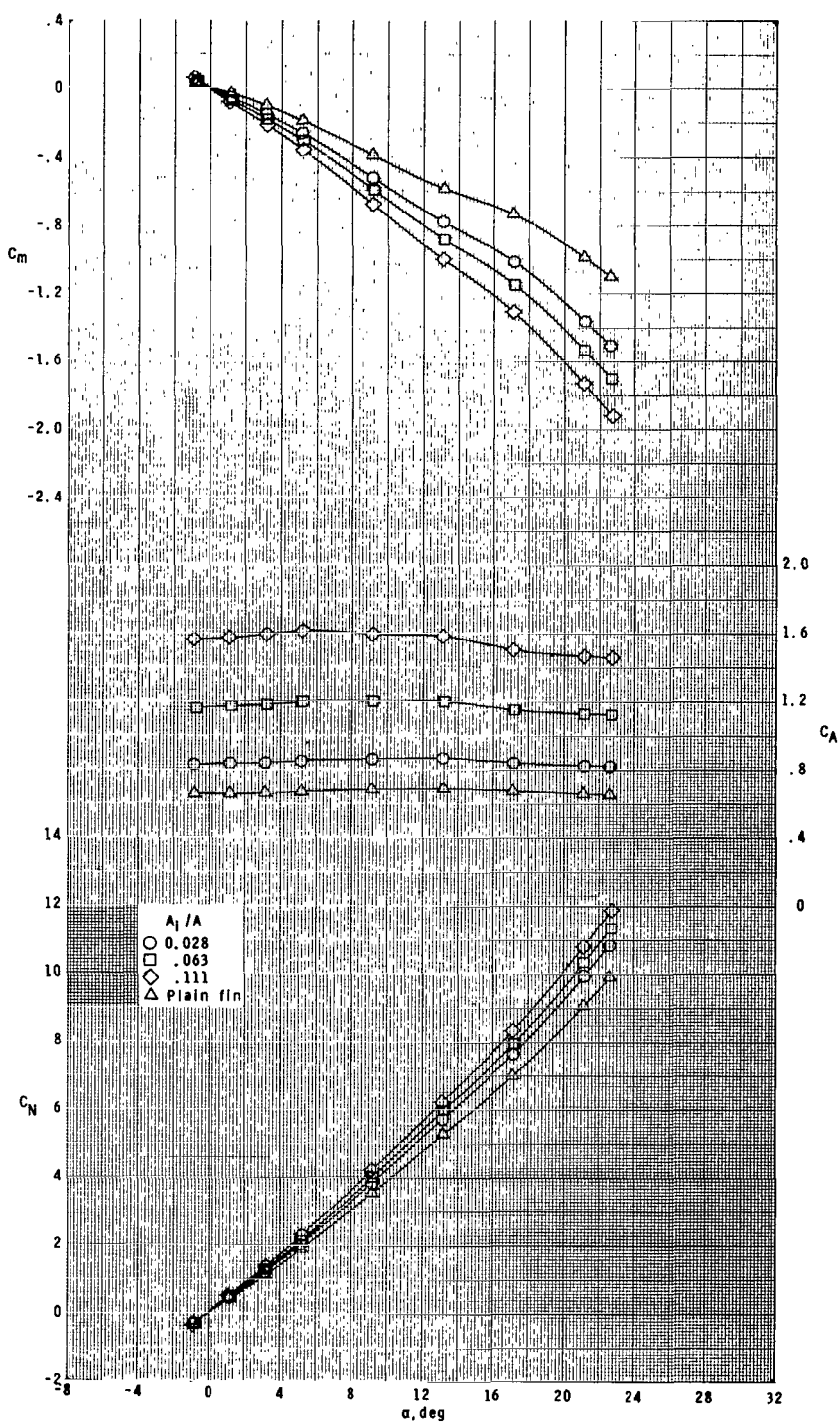
(a)  $M = 1.60.$

**Figure 26.-** Effect of inlet size and fin thickness on longitudinal aerodynamic characteristics of model with flow-through nacelle ram-air-spoiler and plain tail fins at  $\phi = 45^\circ$ .



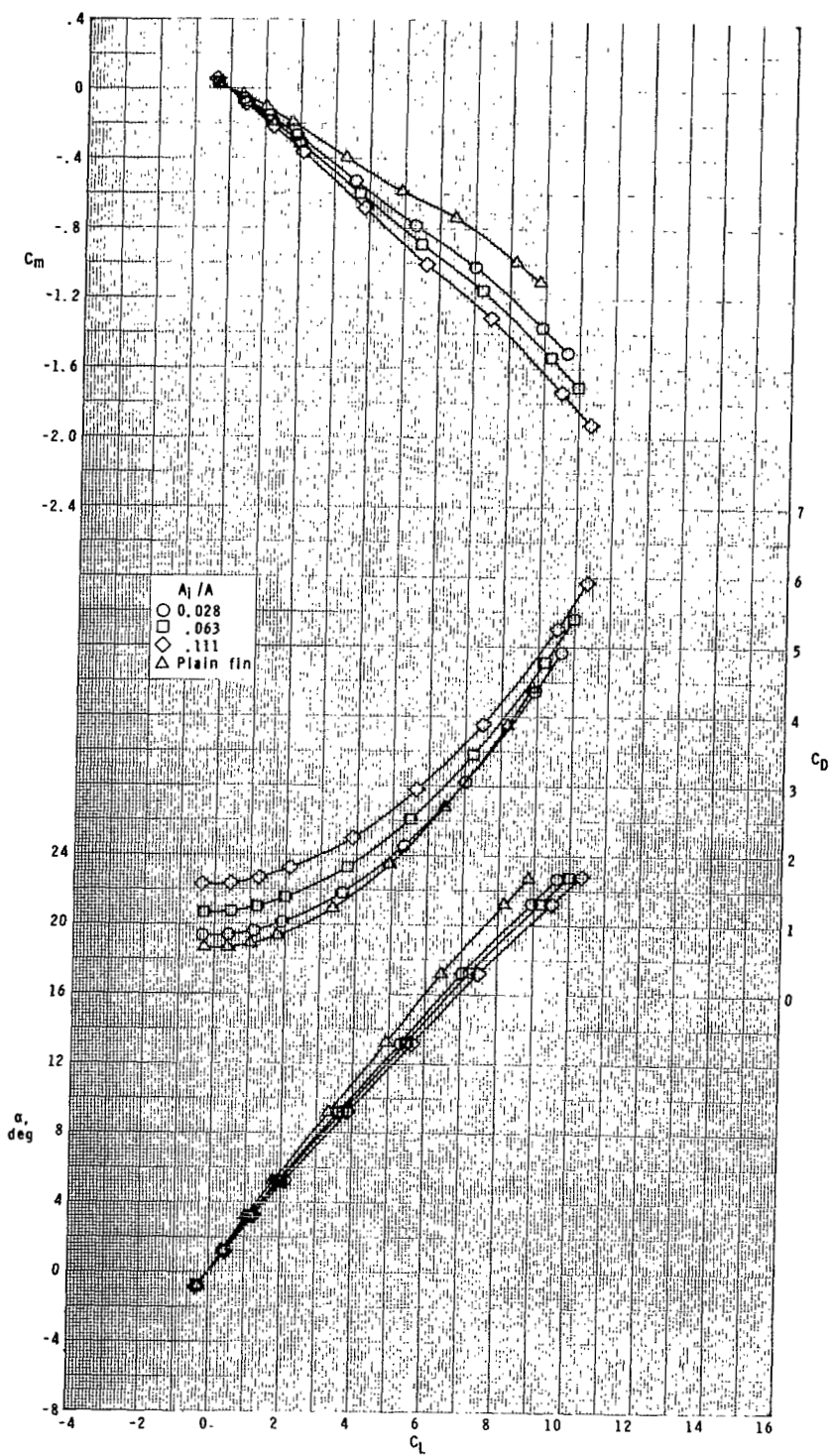
(a) Concluded.

Figure 26.- Continued.



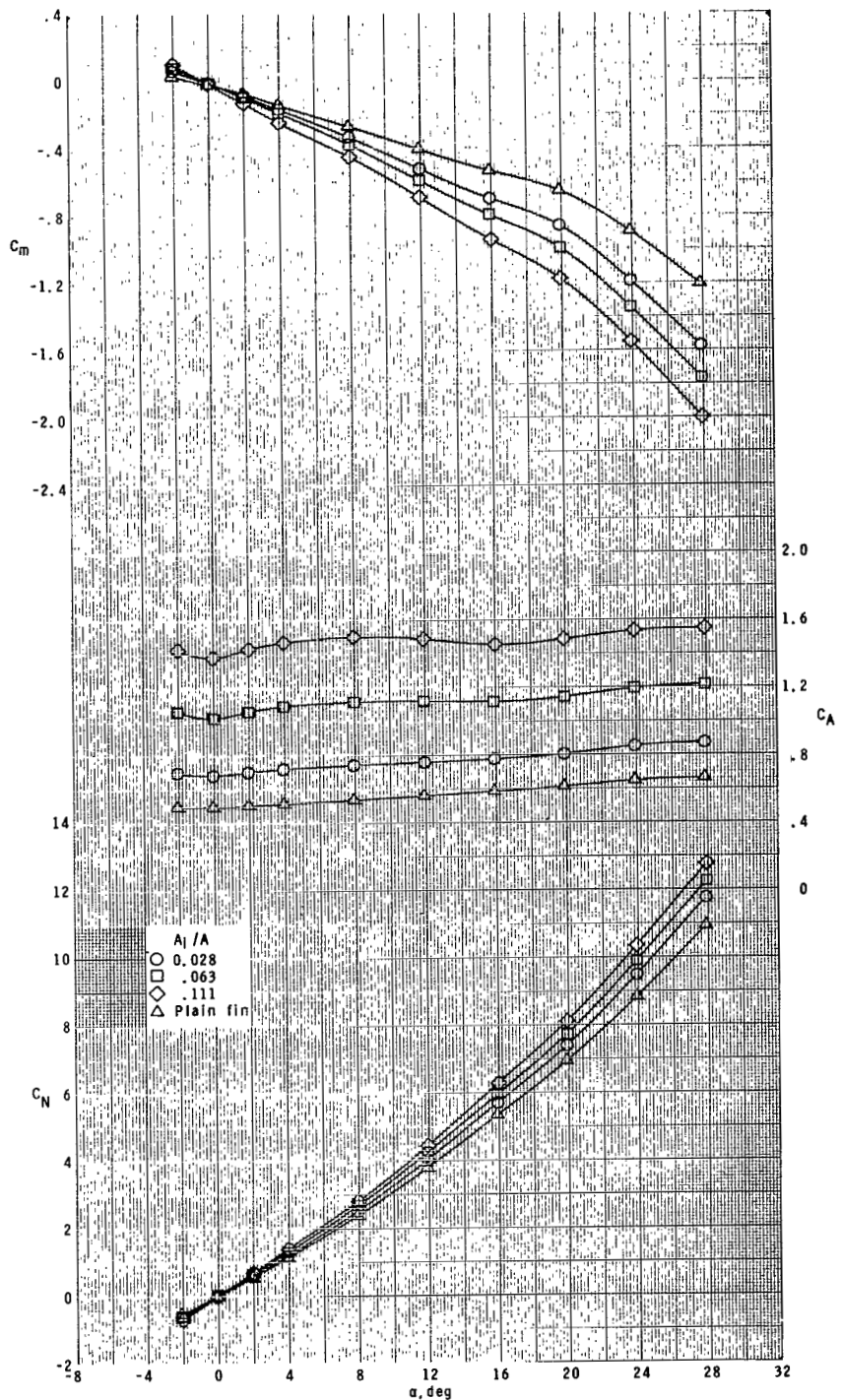
(b)  $M = 2.16.$

**Figure 26.- Continued.**



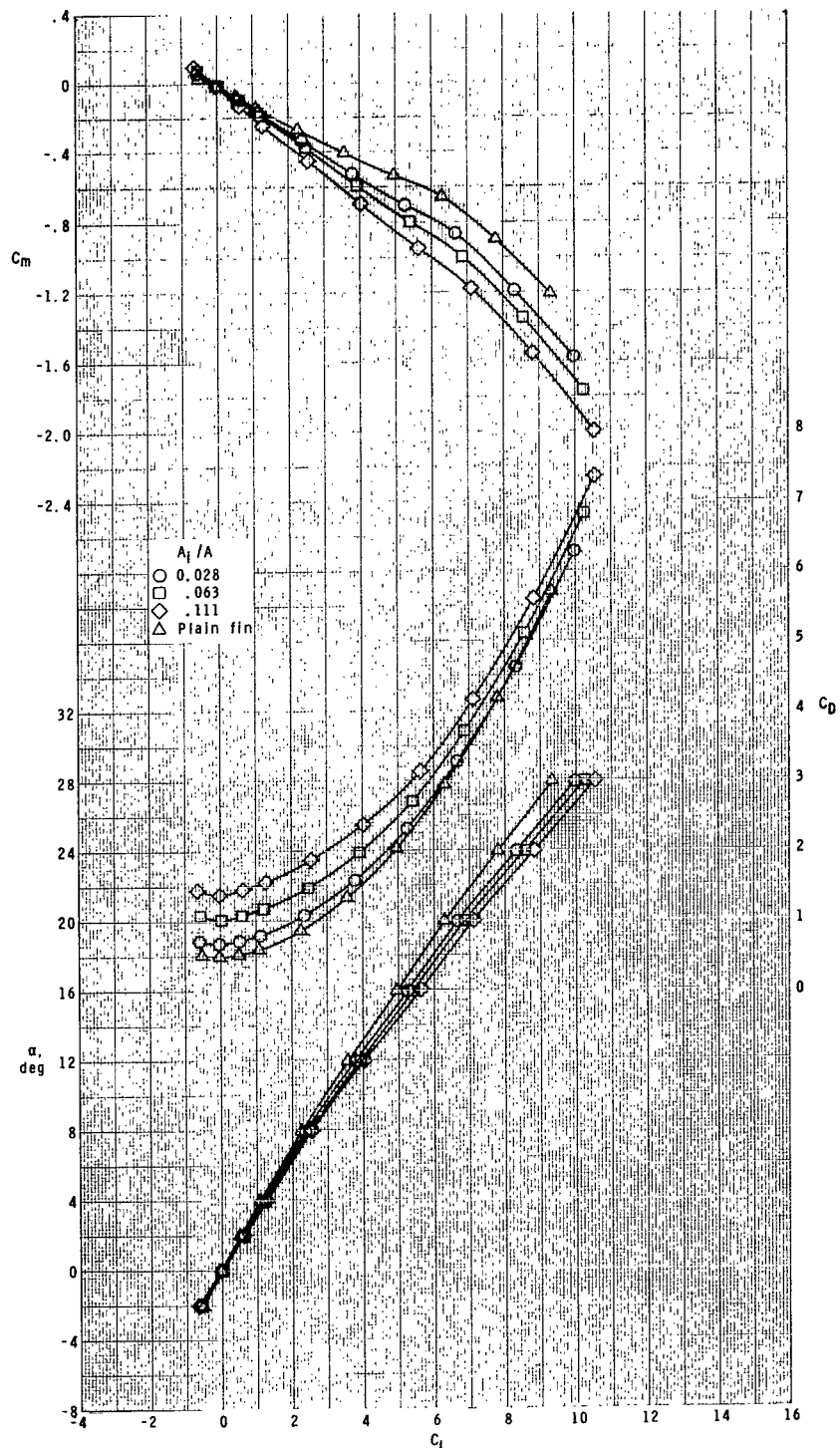
(b) Concluded.

Figure 26.- Continued.



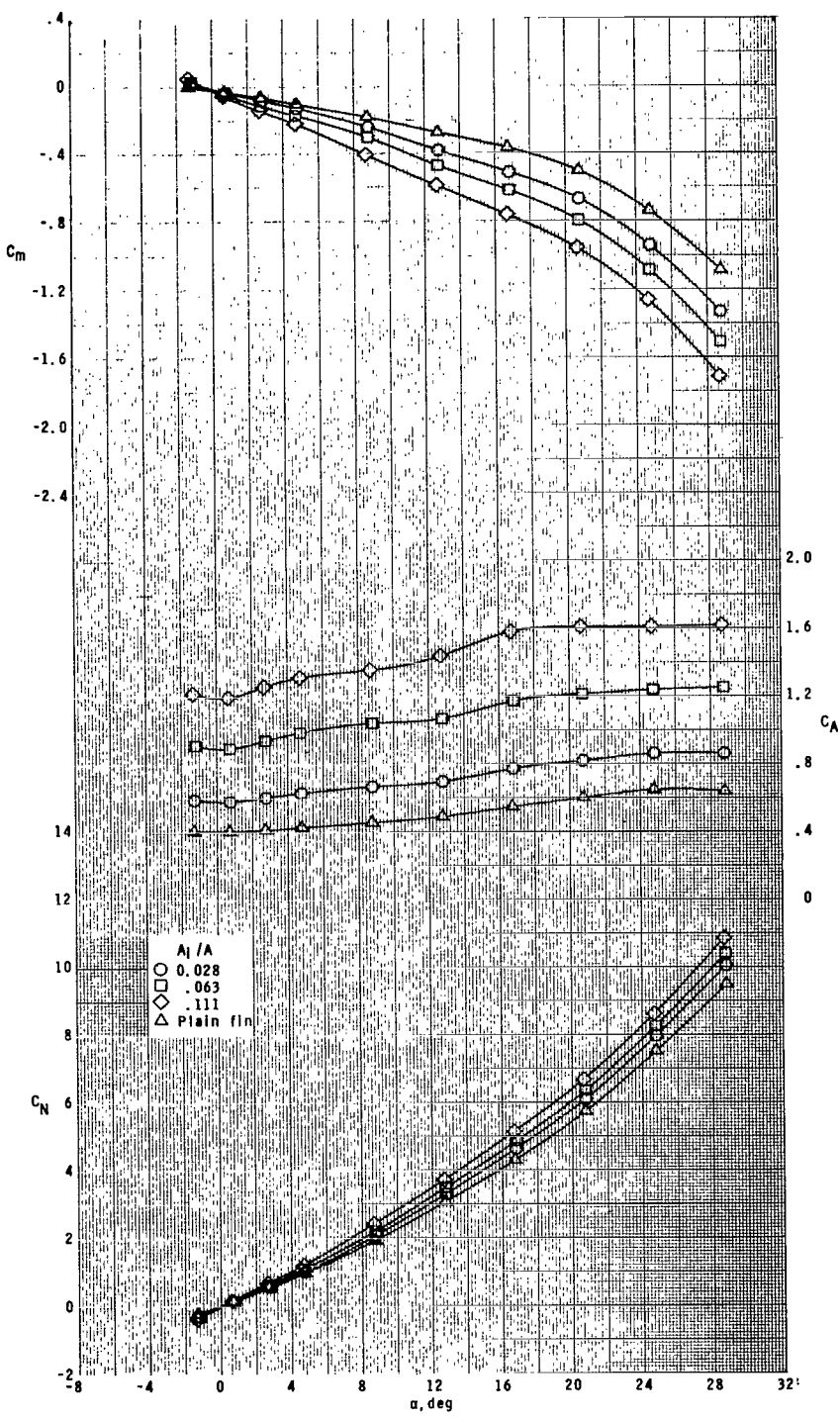
(c)  $M = 2.96.$

Figure 26.- Continued.



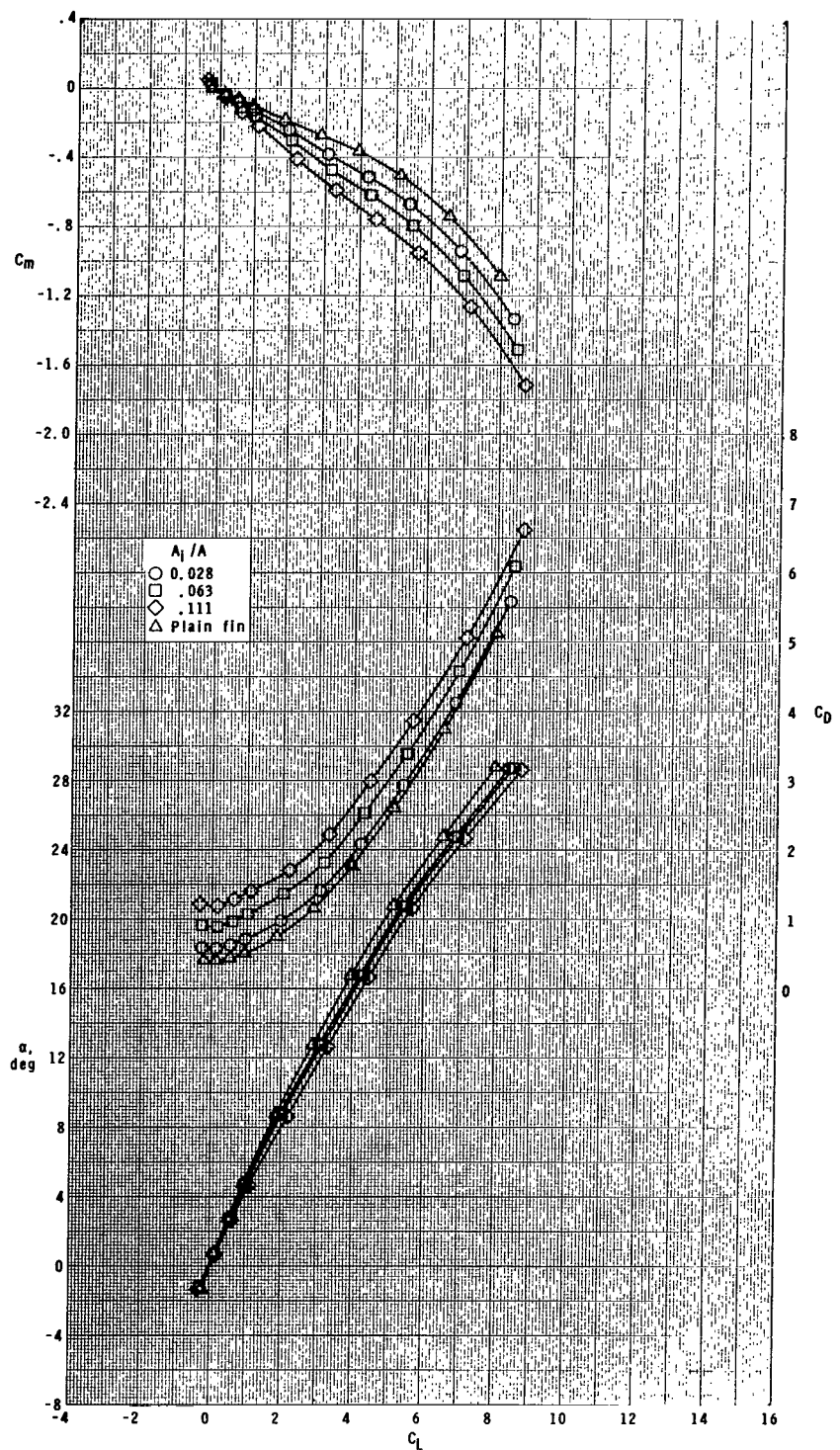
(c) Concluded.

Figure 26.- Continued.



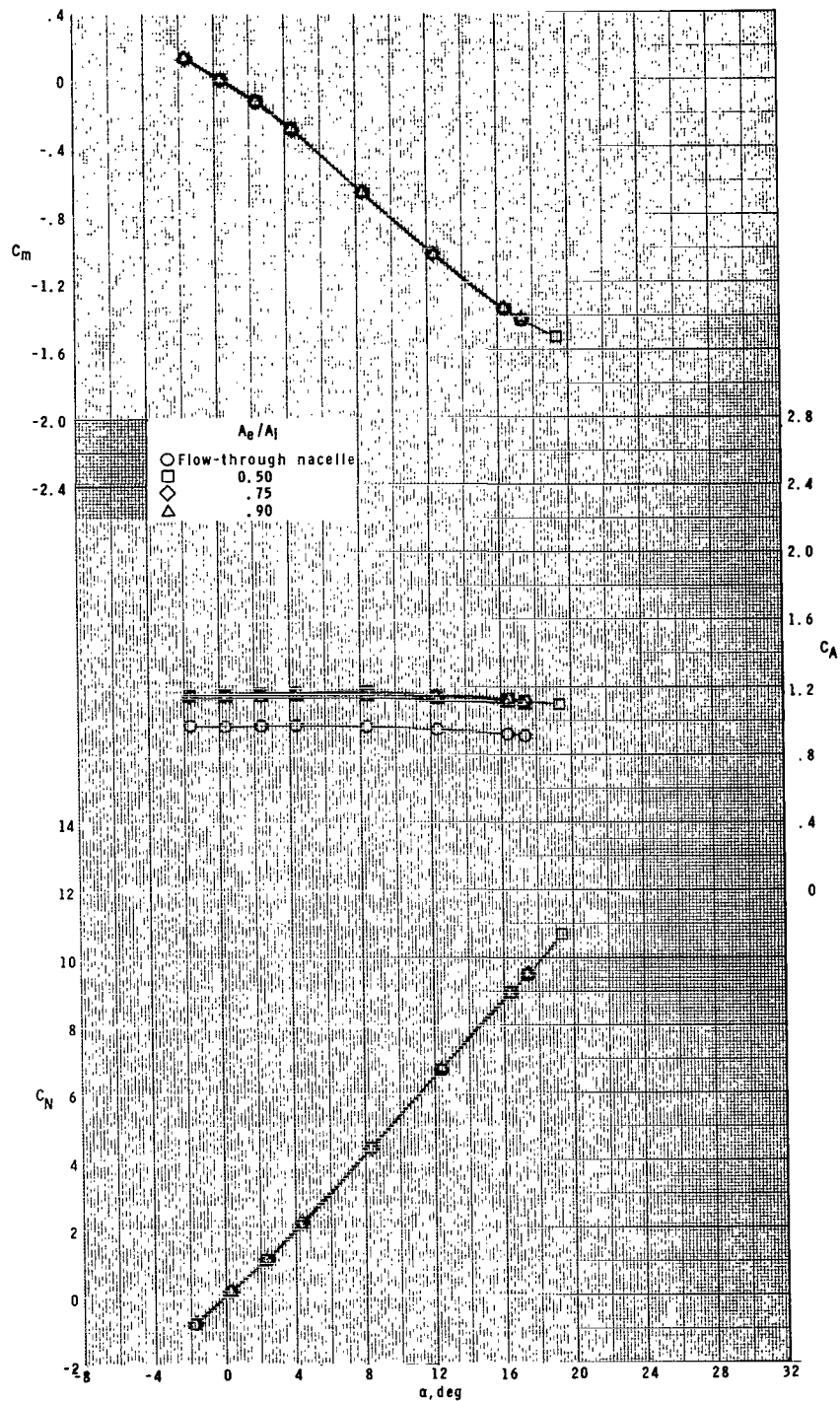
(d)  $M = 4.63.$

Figure 26.- Continued.



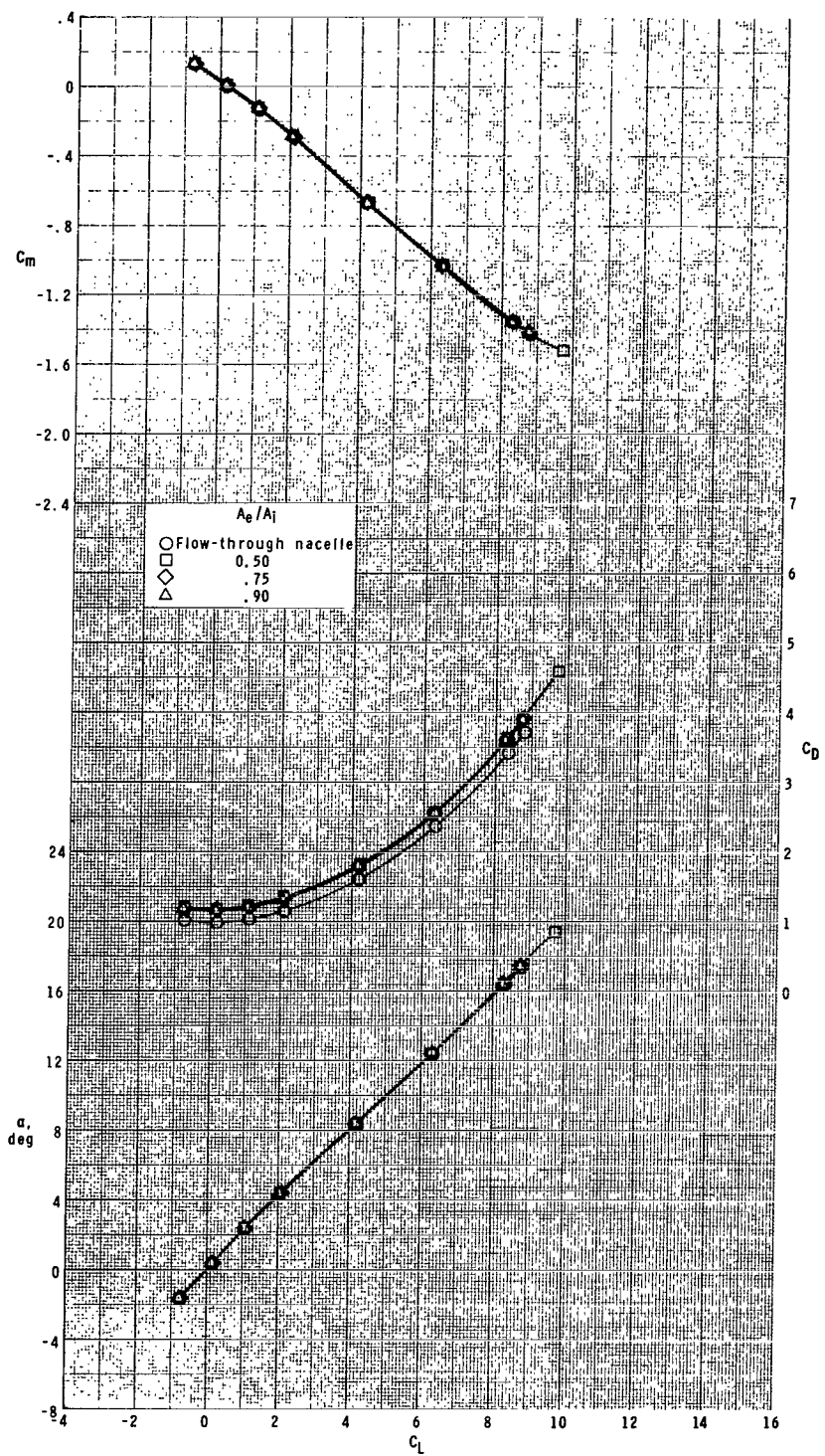
(d) Concluded.

Figure 26.- Concluded.



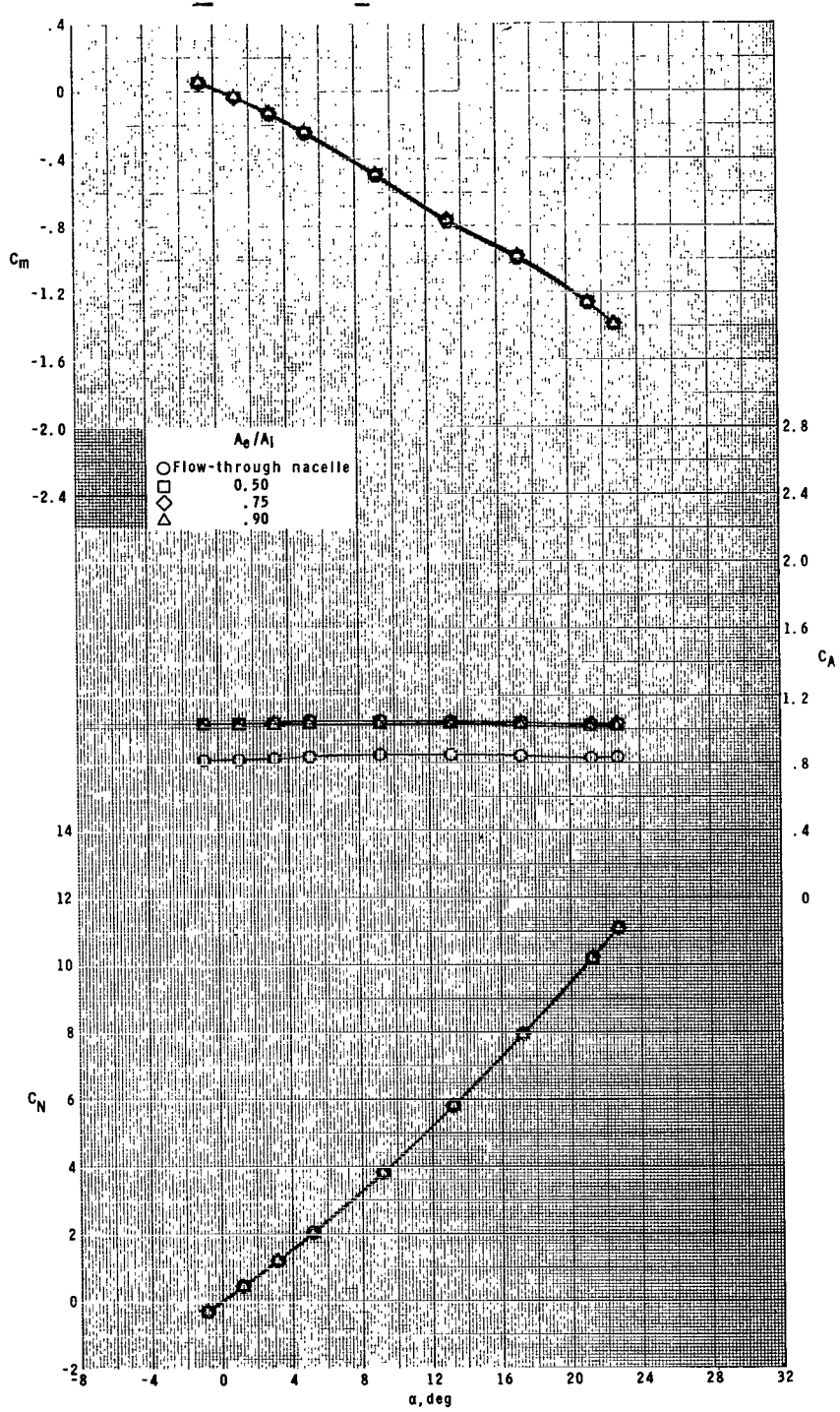
(a)  $M = 1.60.$

**Figure 27.- Effect of ratio of plenum exit area to inlet area for roll control on longitudinal aerodynamic characteristics of model with ram-air-spoiler tail fins for  $A_i/A = 0.028$  at  $\phi = 0^\circ$ .**



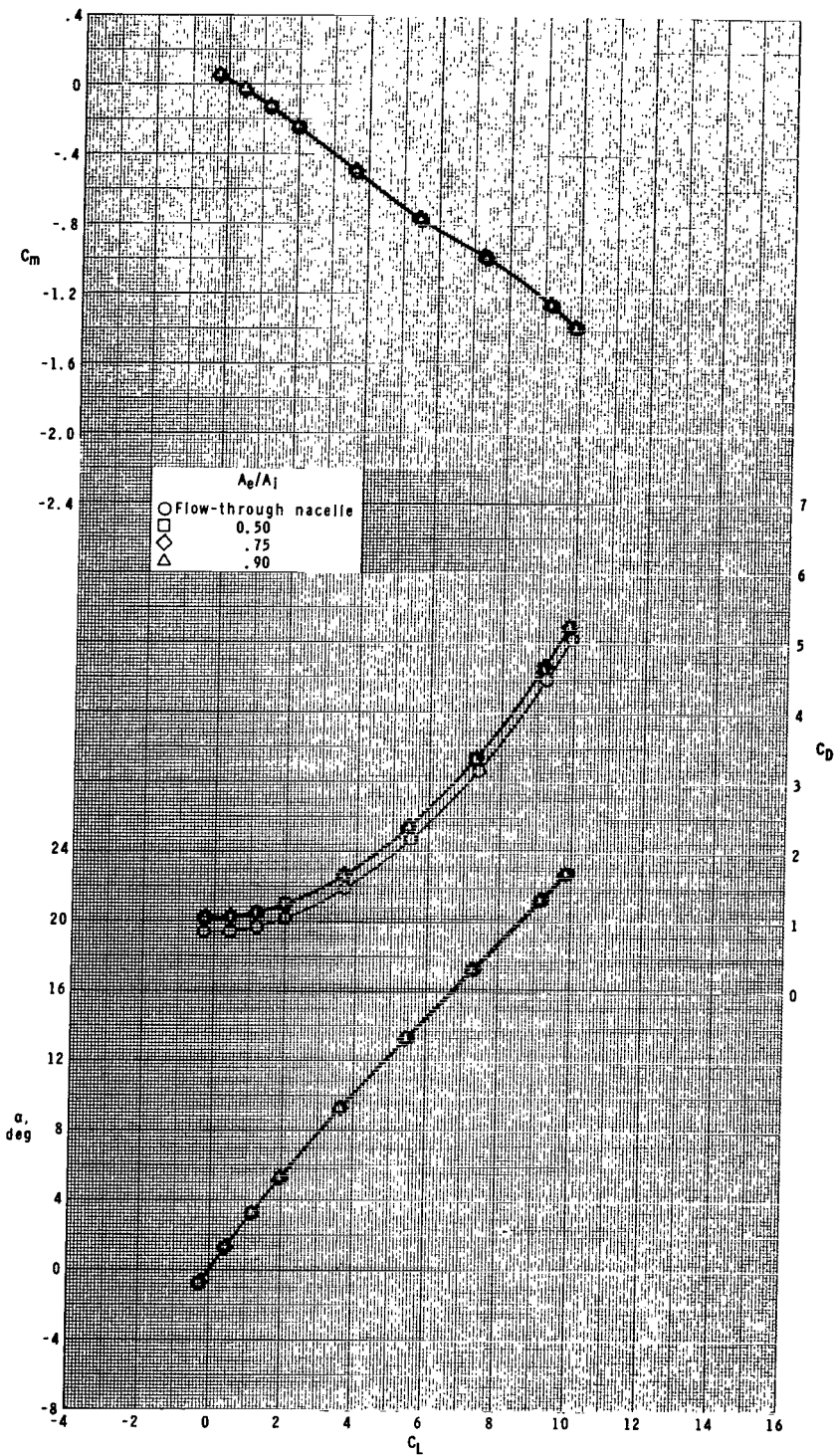
(a) Concluded.

Figure 27.- Continued.



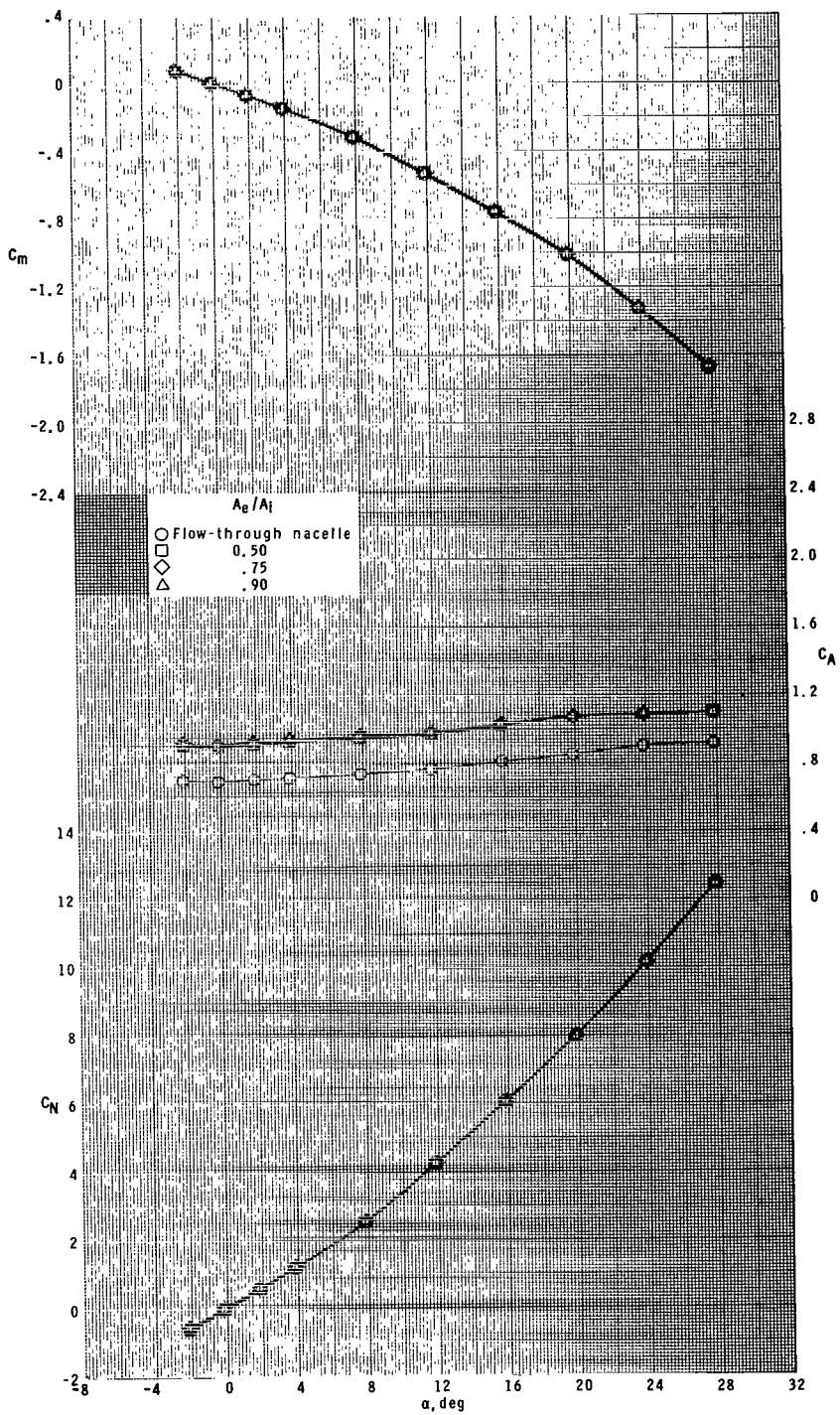
(b)  $M = 2.16$ .

Figure 27.- Continued.



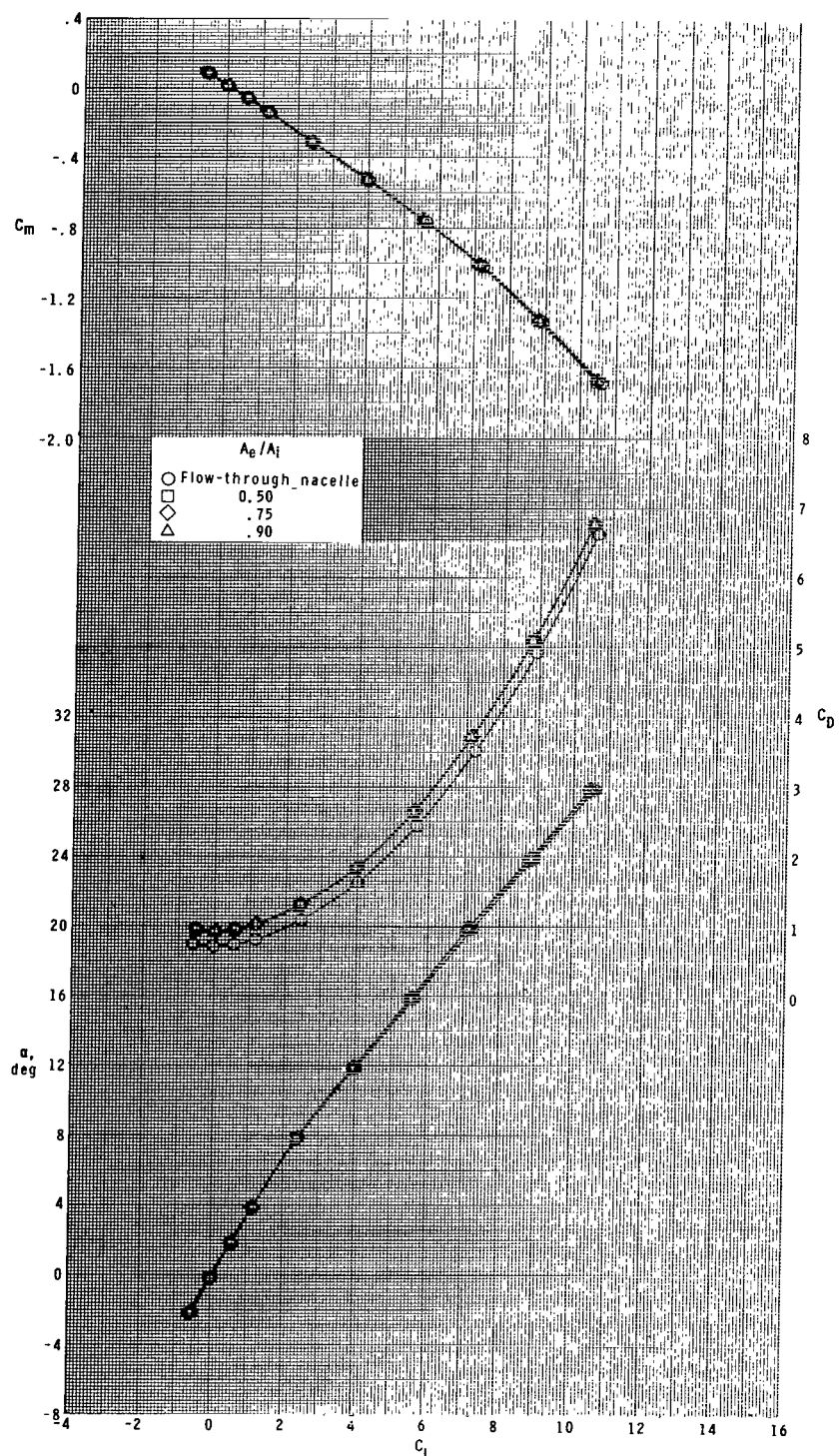
(b) Concluded.

Figure 27.- Continued.



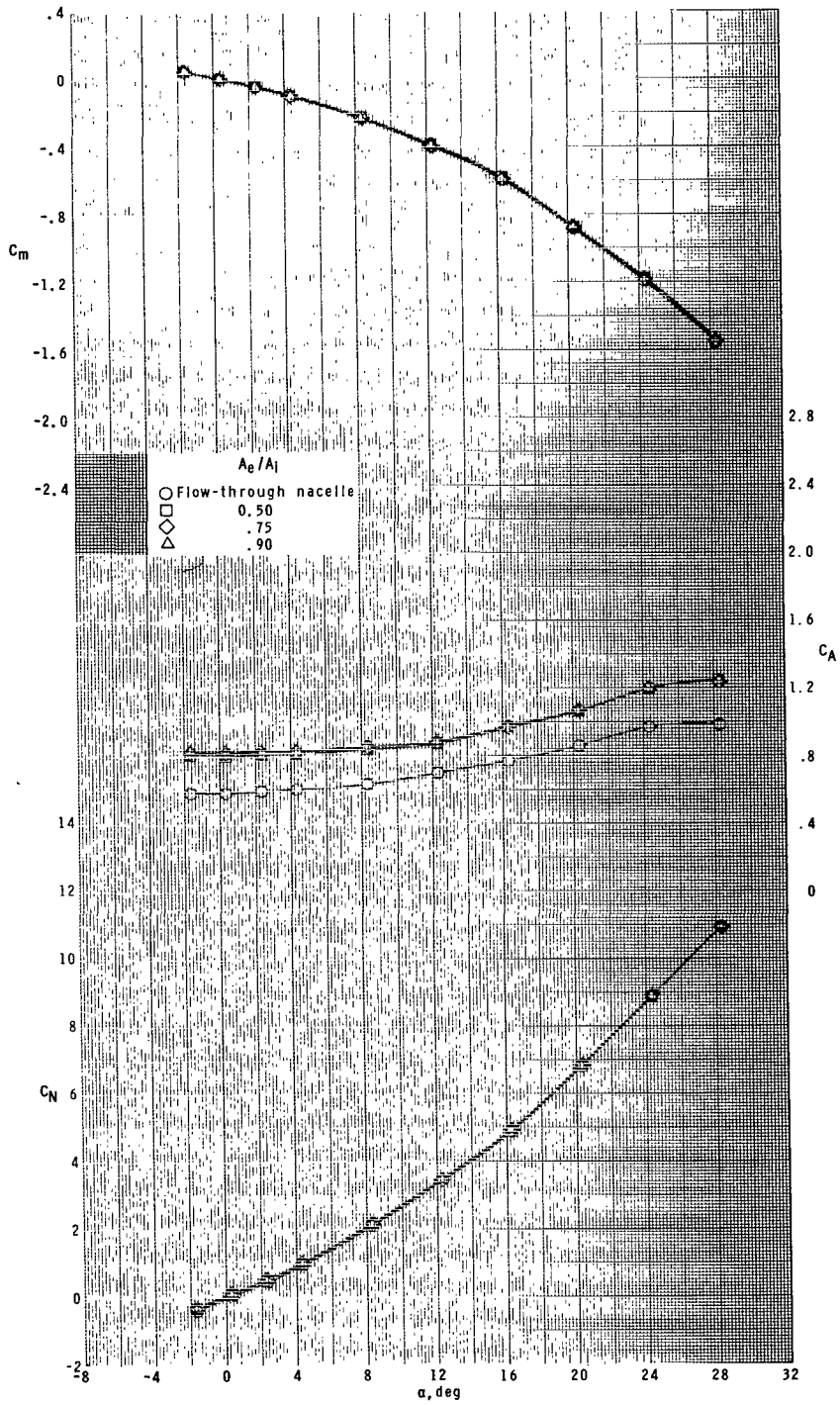
(c)  $M = 2.96.$

Figure 27.- Continued.



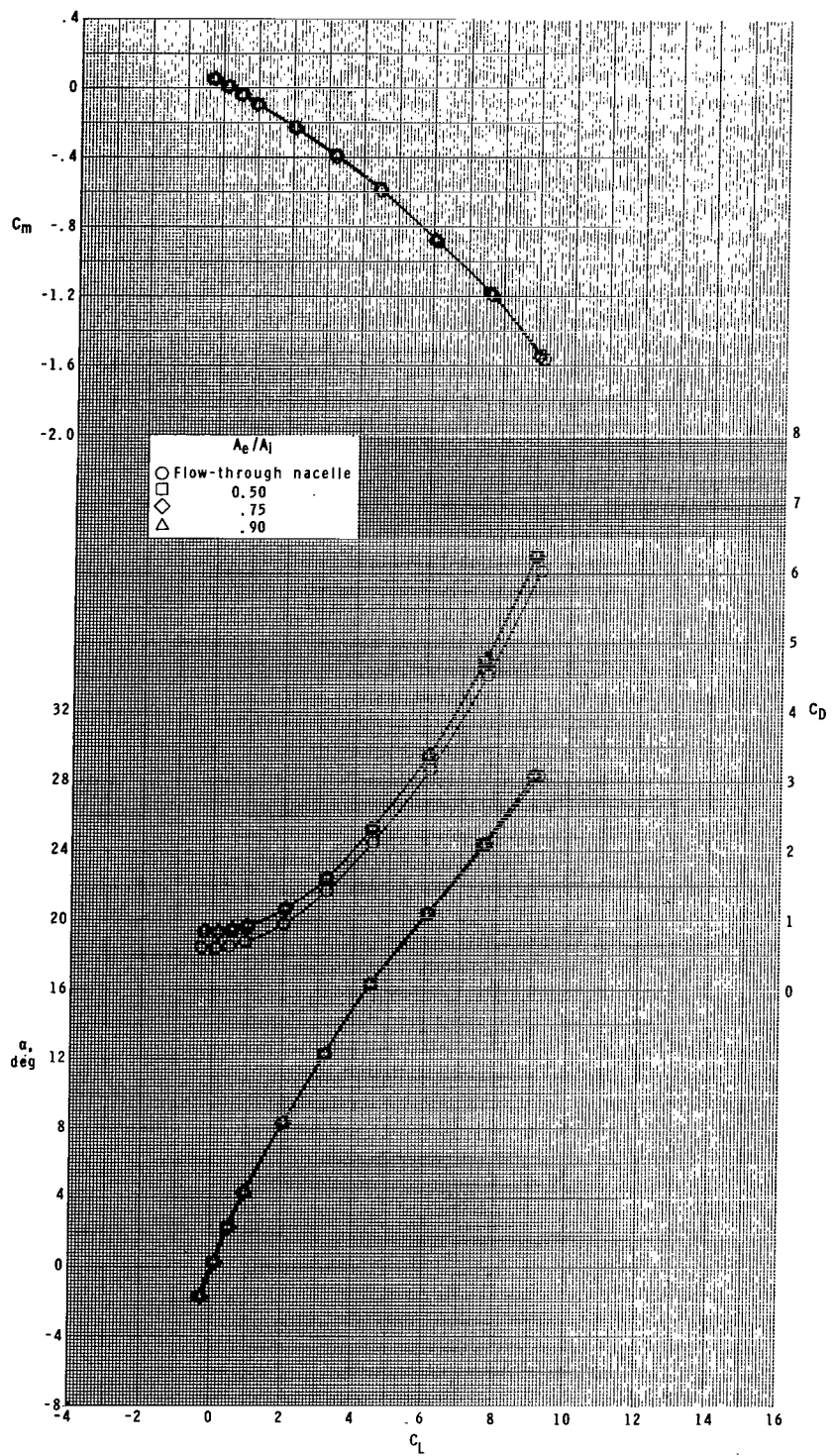
(c) Concluded.

Figure 27.- Continued.



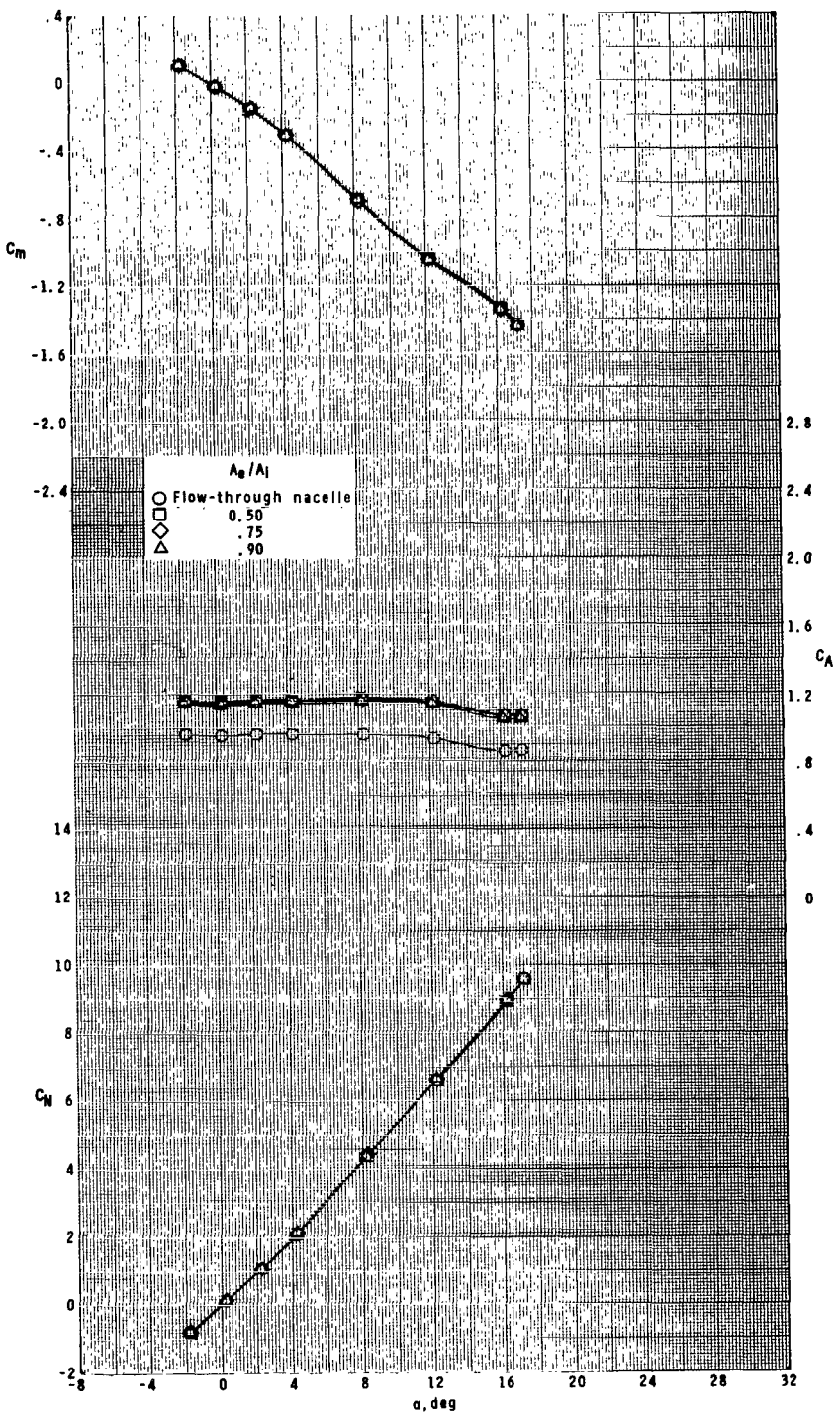
(d)  $M = 4.63.$

Figure 27.- Continued.



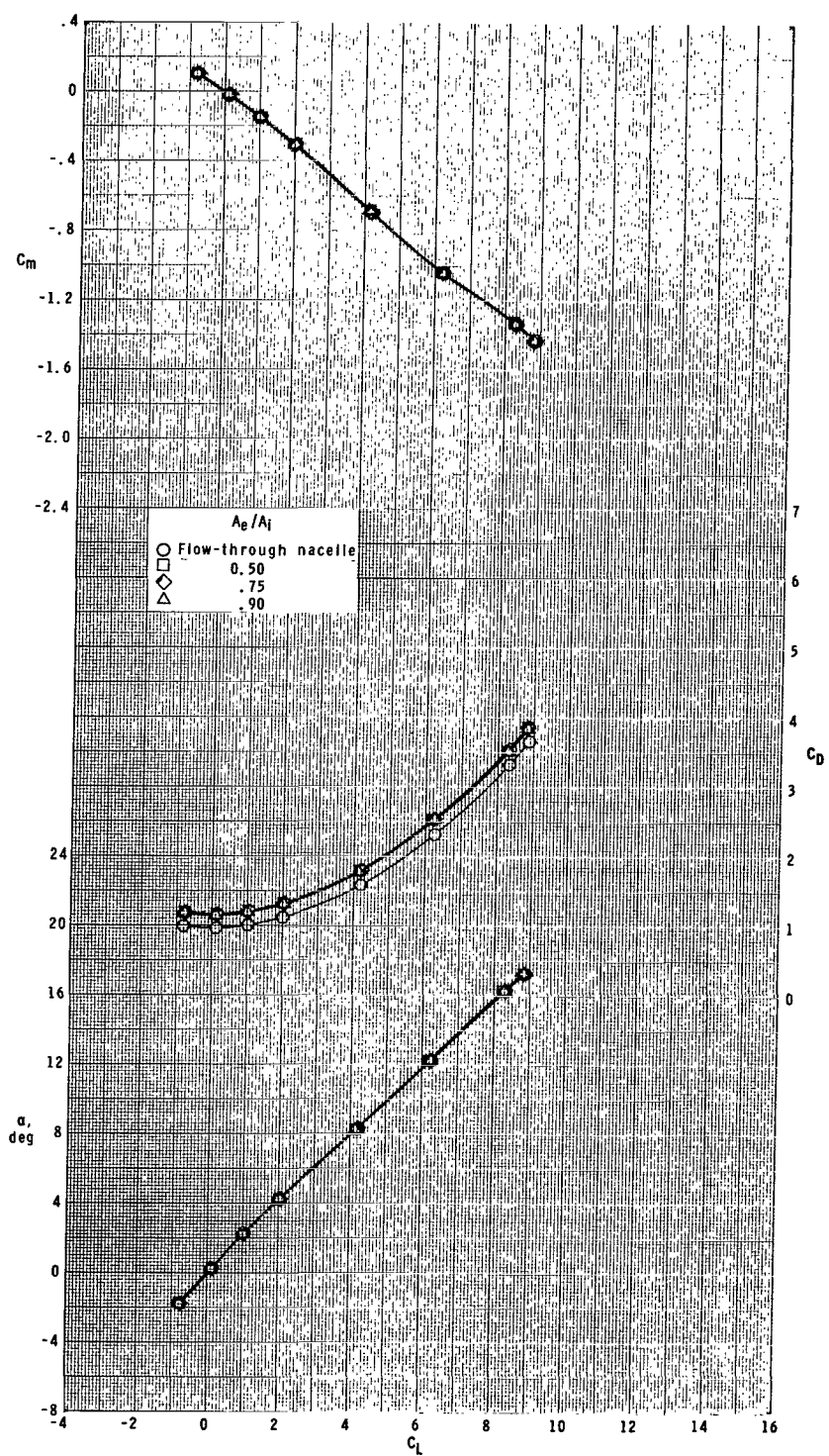
(d) Concluded.

Figure 27.- Concluded.



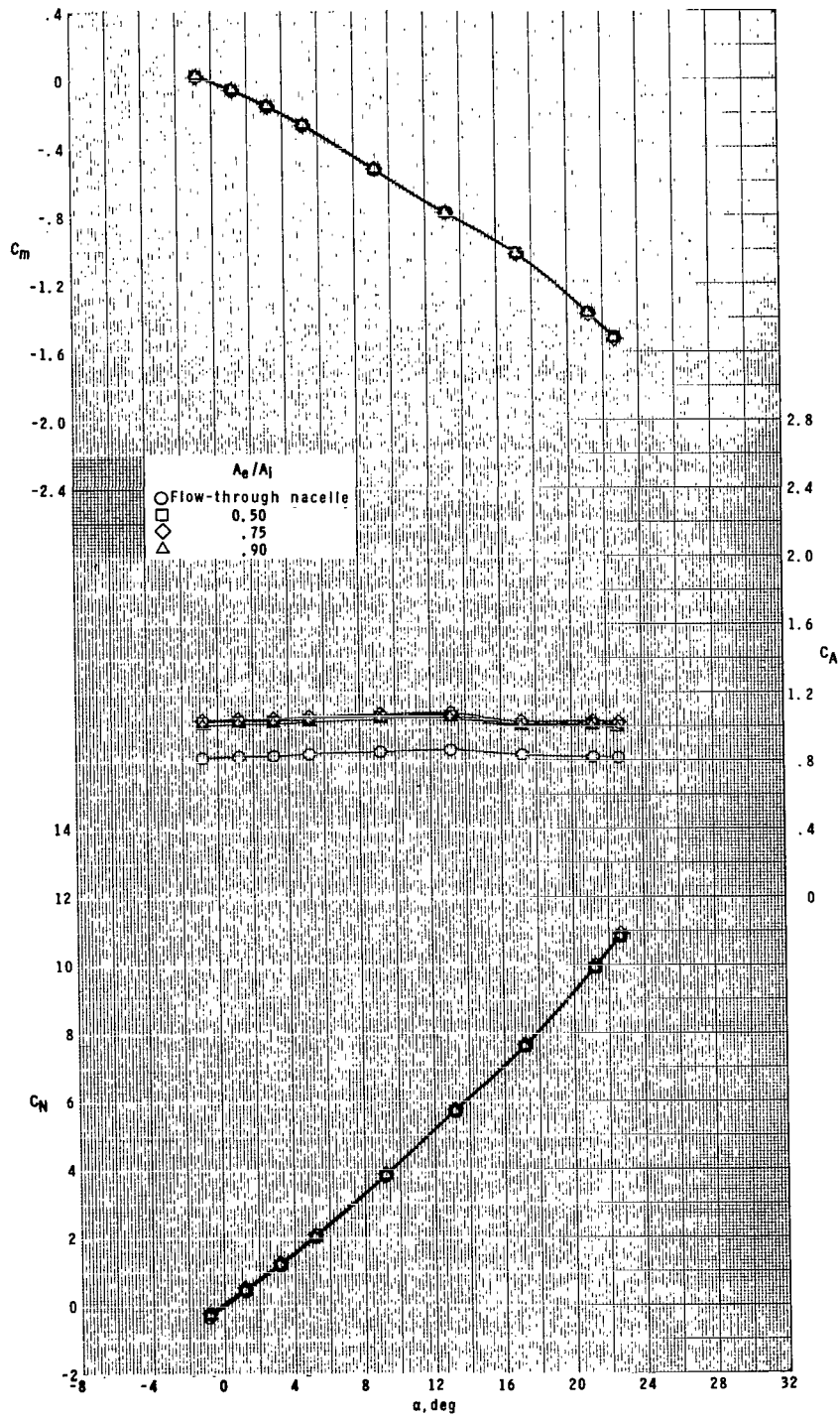
(a)  $M = 1.60.$

**Figure 28.- Effect of ratio of plenum exit area to inlet area for roll control on longitudinal aerodynamic characteristics of model with ram-air-spoiler tail fins for  $A_p/A = 0.028$  at  $\phi = 45^\circ$ .**



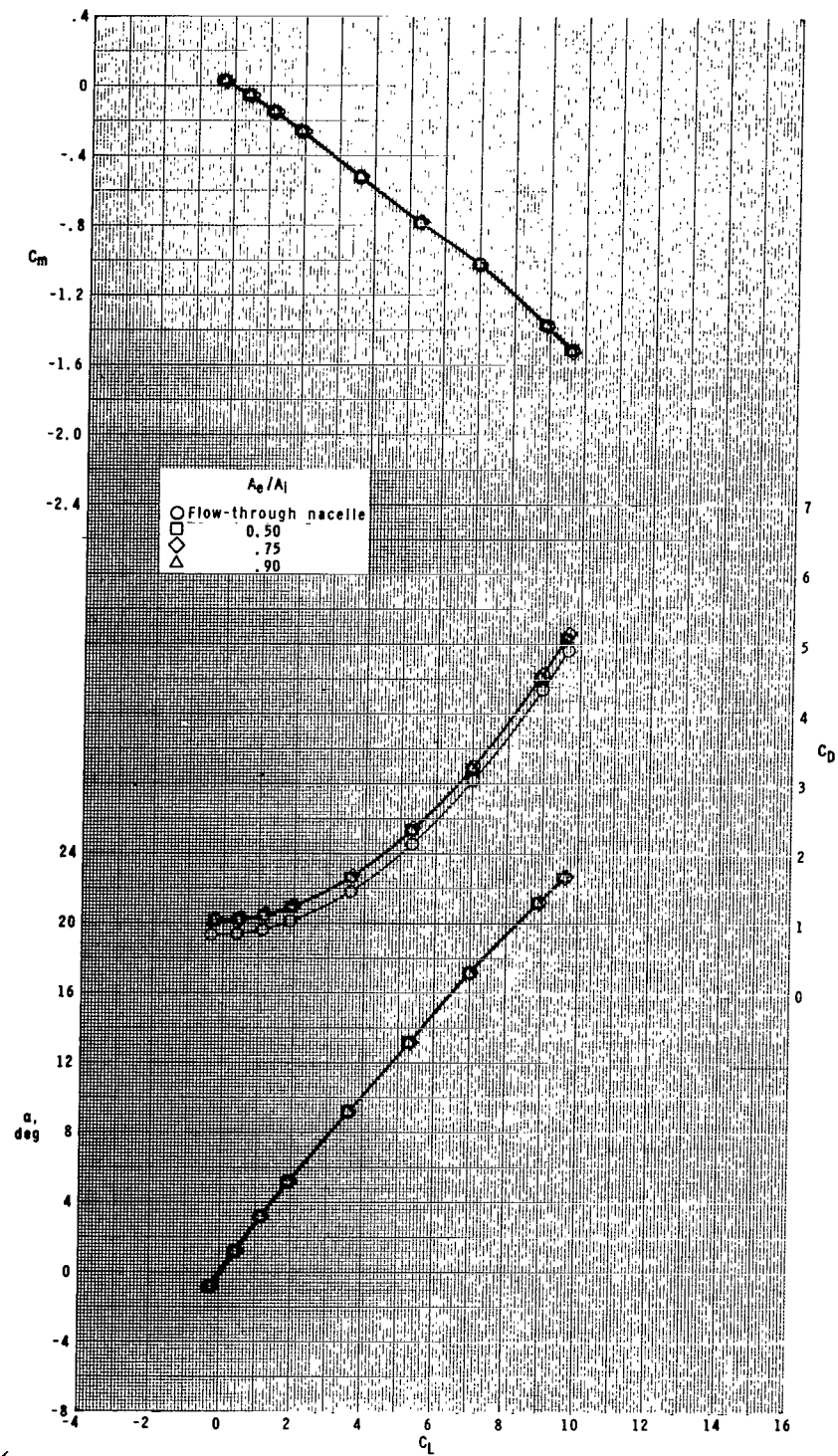
(a) Concluded.

Figure 28.- Continued.



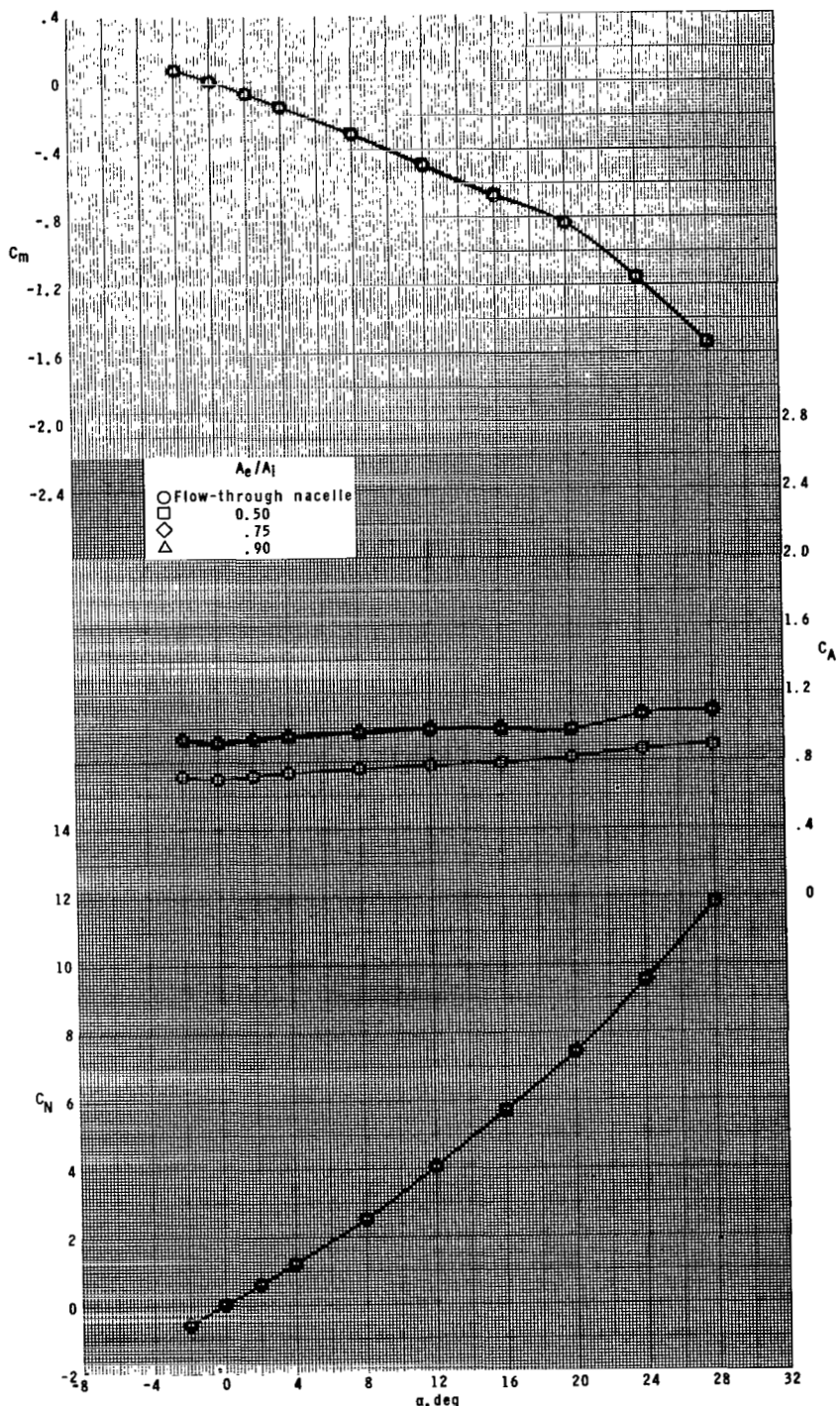
(b)  $M = 2.16.$

Figure 28.- Continued.



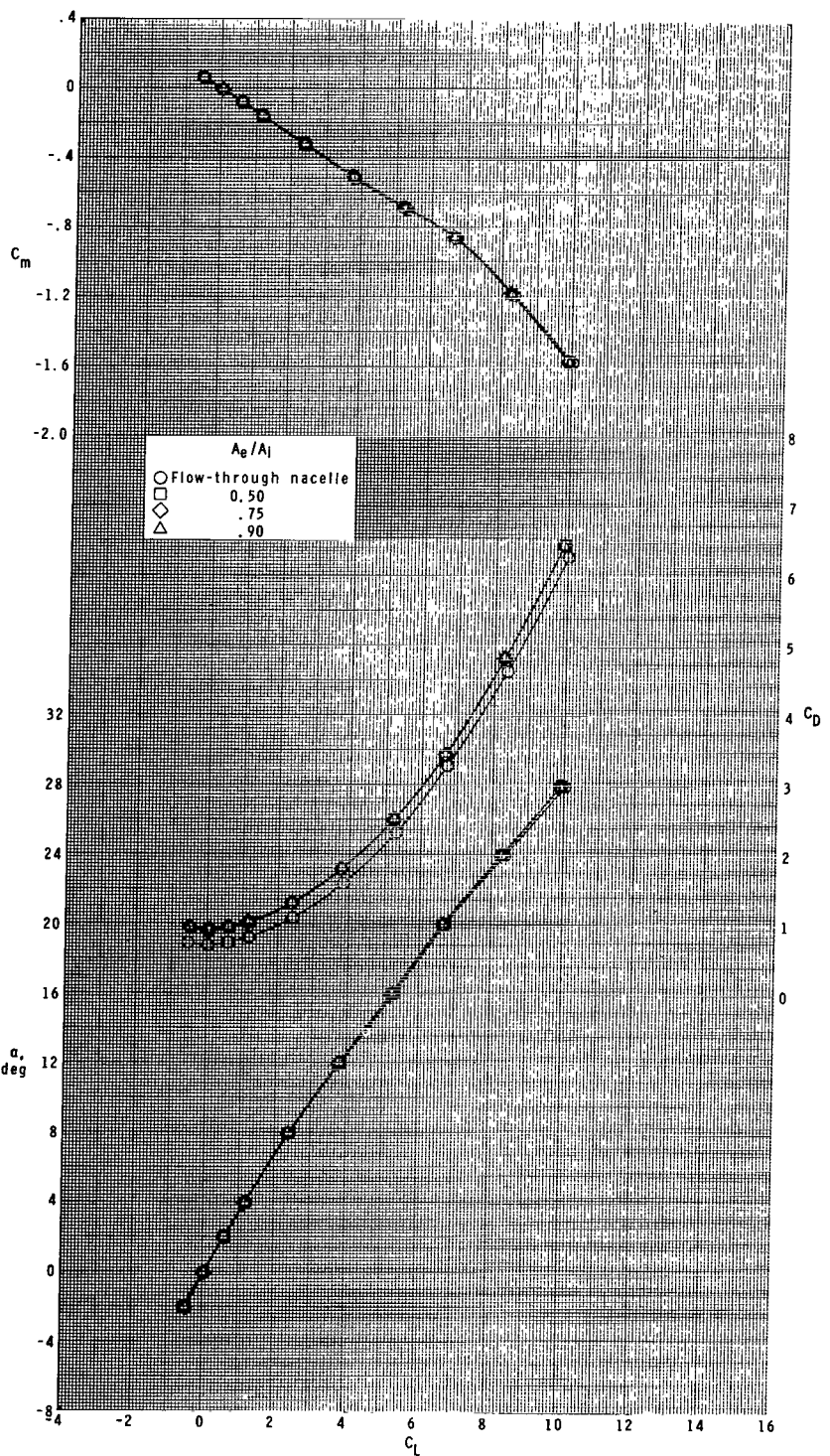
(b) Concluded.

Figure 28.- Continued.



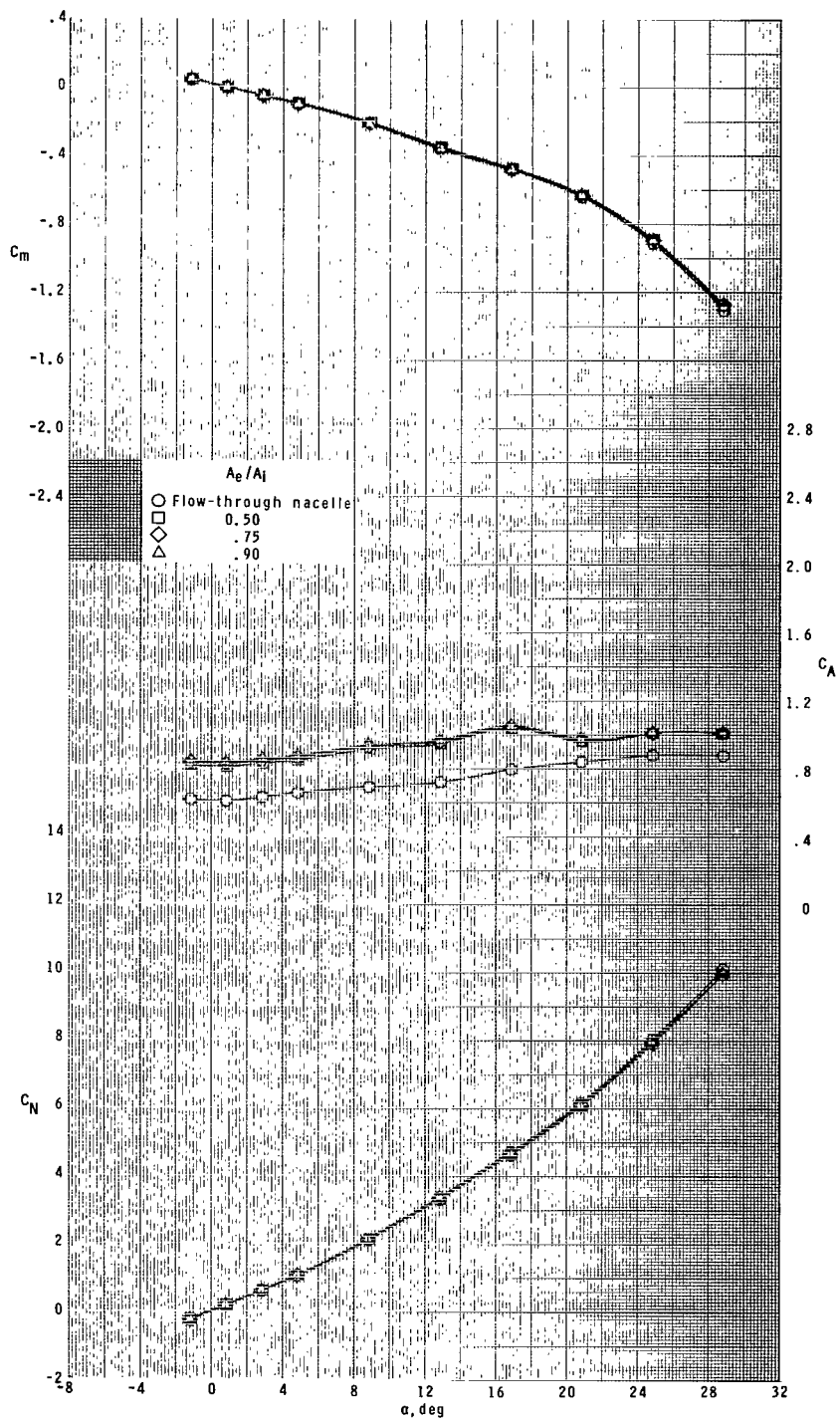
(c)  $M = 2.96.$

Figure 28.- Continued.



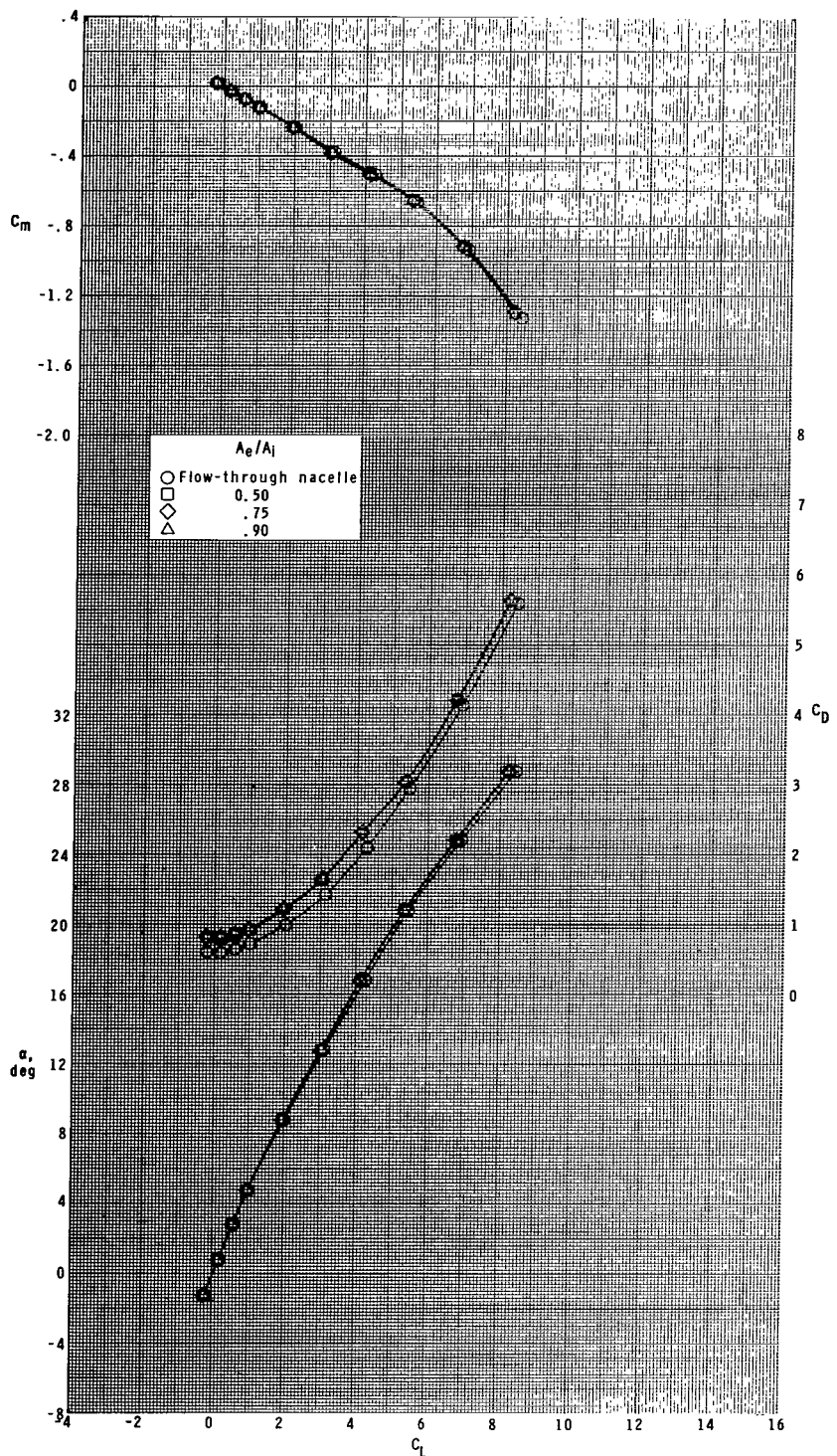
(c) Concluded.

Figure 28.- Continued.



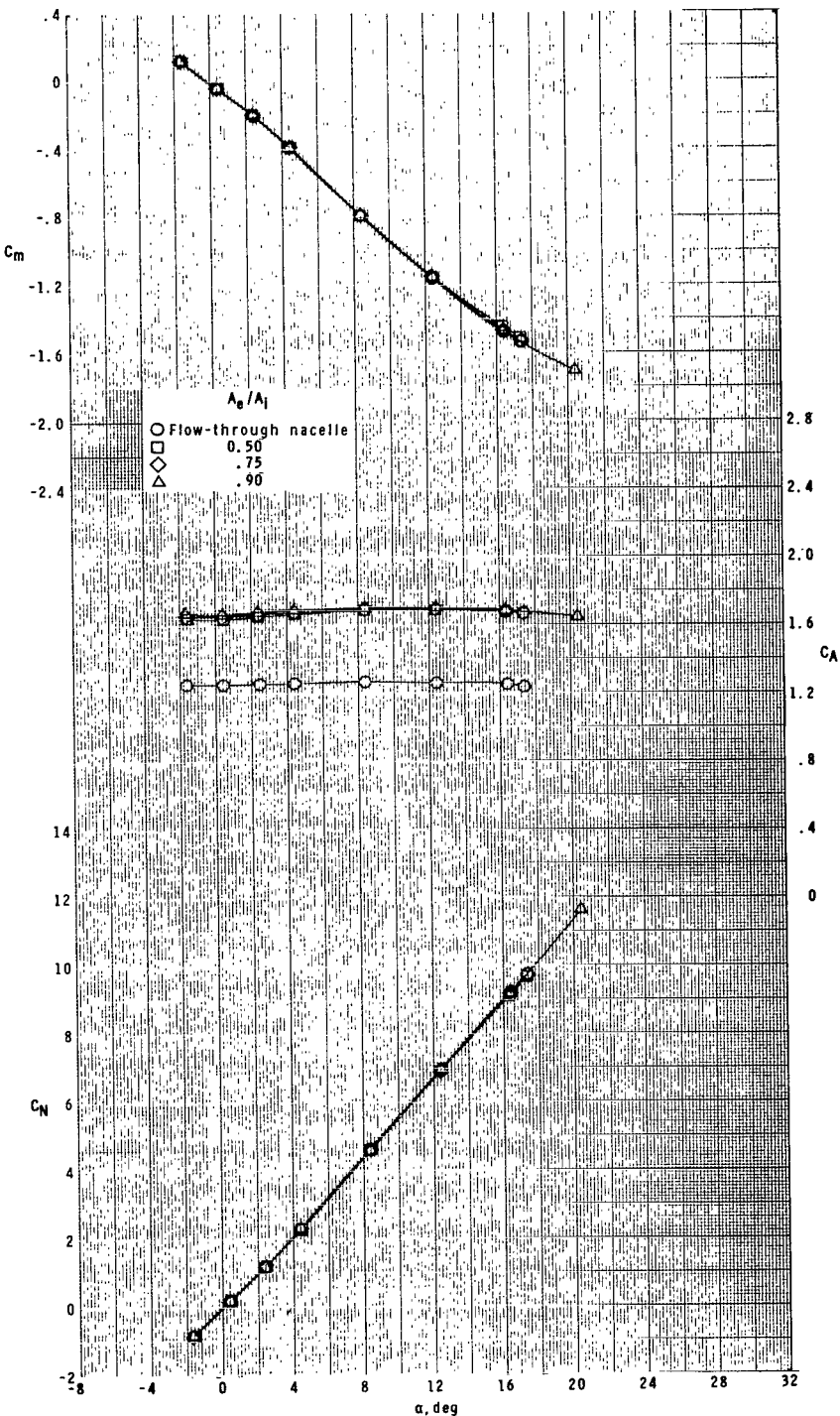
(d)  $M = 4.63.$

Figure 28.- Continued.



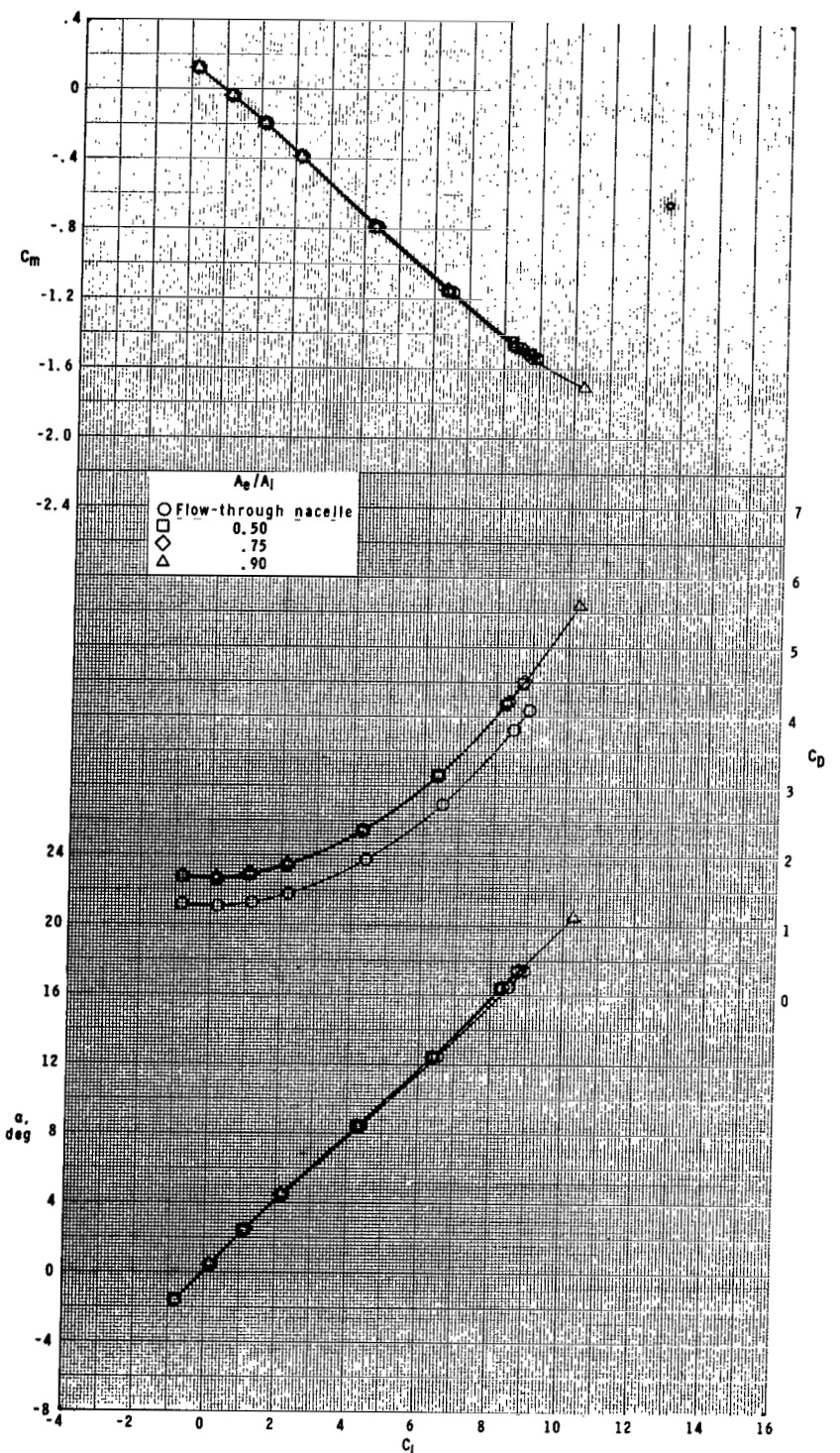
(d) Concluded.

Figure 28.- Concluded.



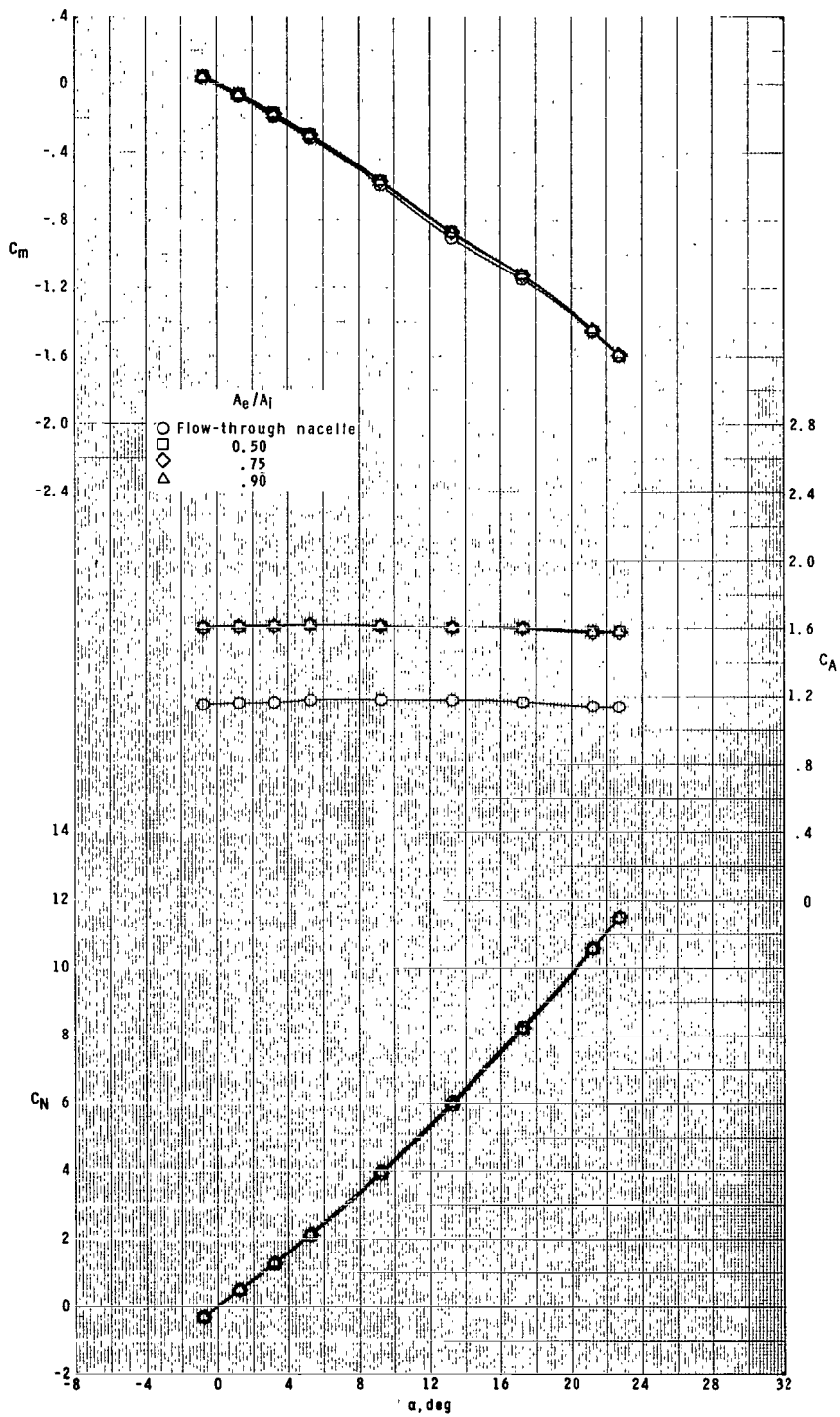
(a)  $M = 1.60.$

Figure 29.- Effect of ratio of plenum exit area to inlet area for roll control on longitudinal aerodynamic characteristics of model with ram-air-spoiler tail fins for  $A_i/A = 0.063$  at  $\phi = 0^\circ$ .



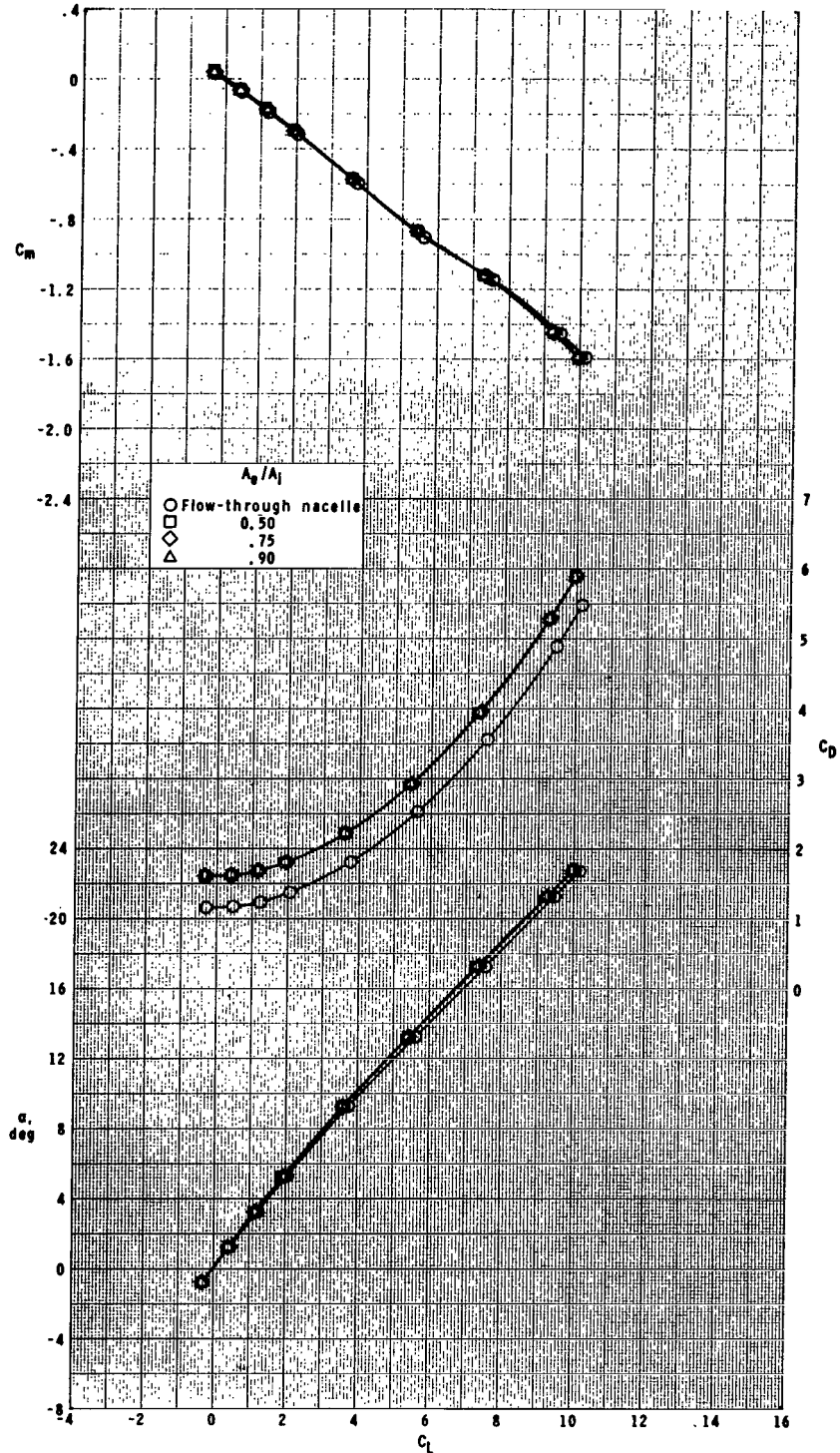
(a) Concluded.

Figure 29.- Continued.



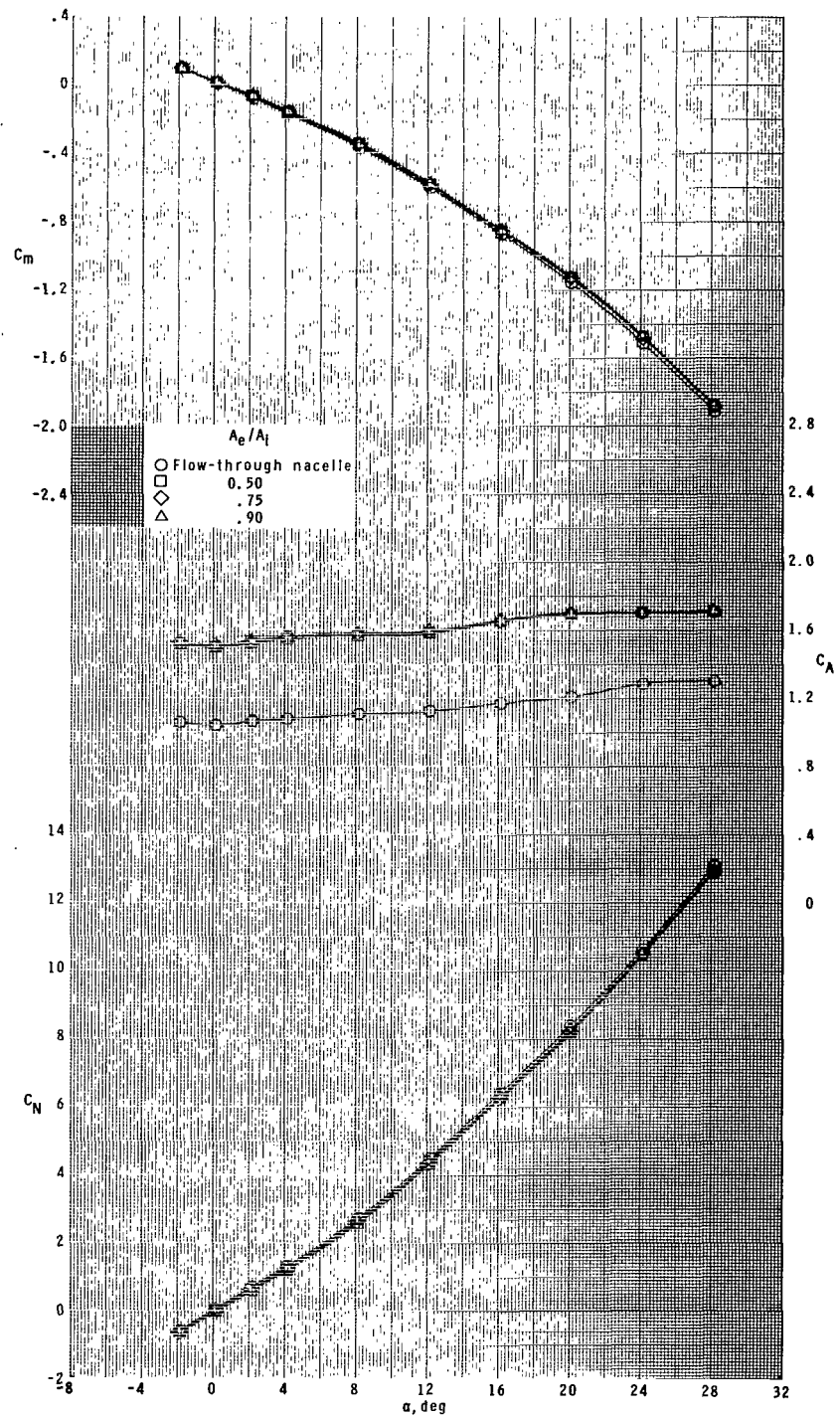
(b)  $M = 2.16.$

Figure 29.- Continued.



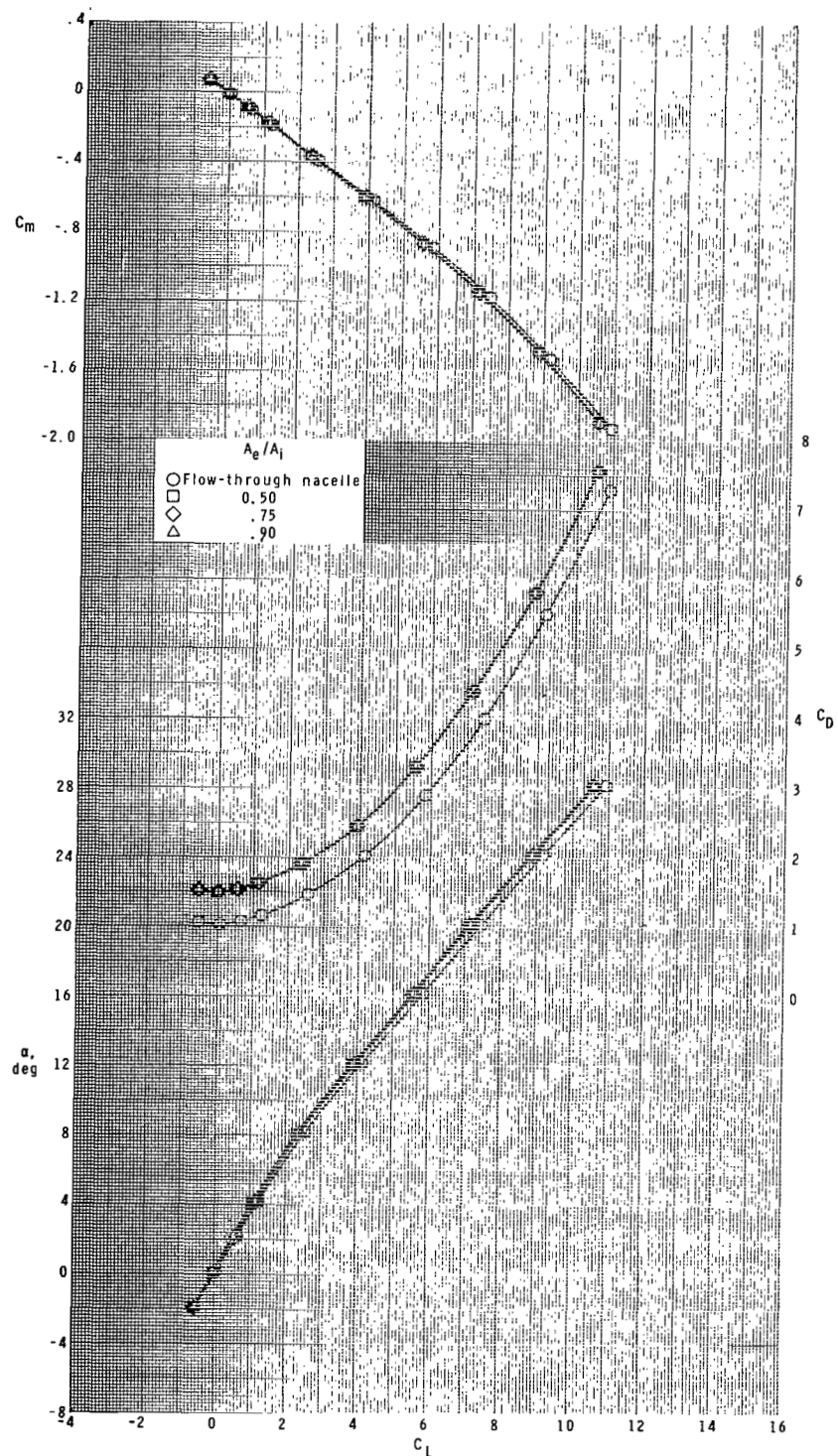
(b) Concluded.

Figure 29 .- Continued.



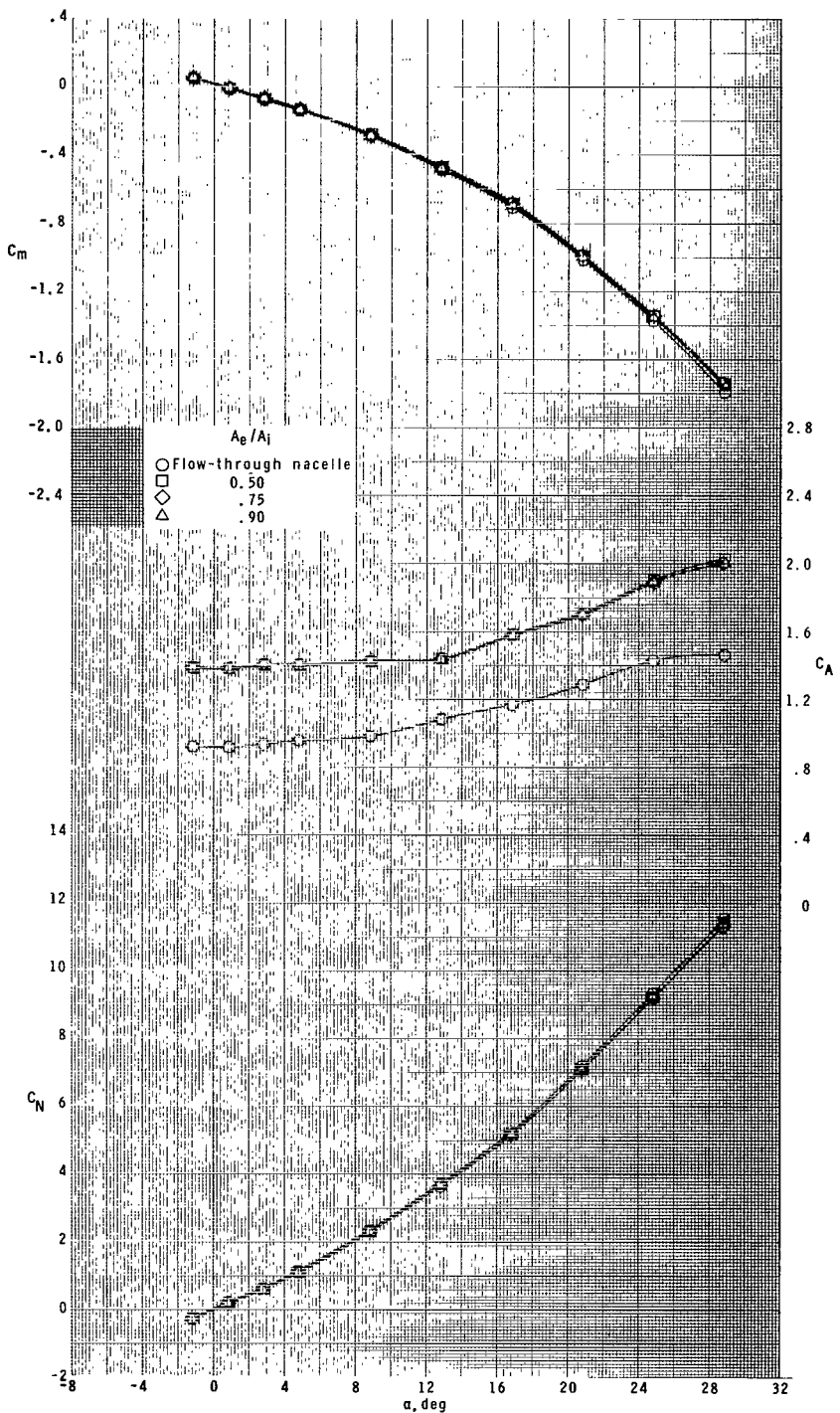
(c)  $M = 2.96.$

Figure 29.- Continued.



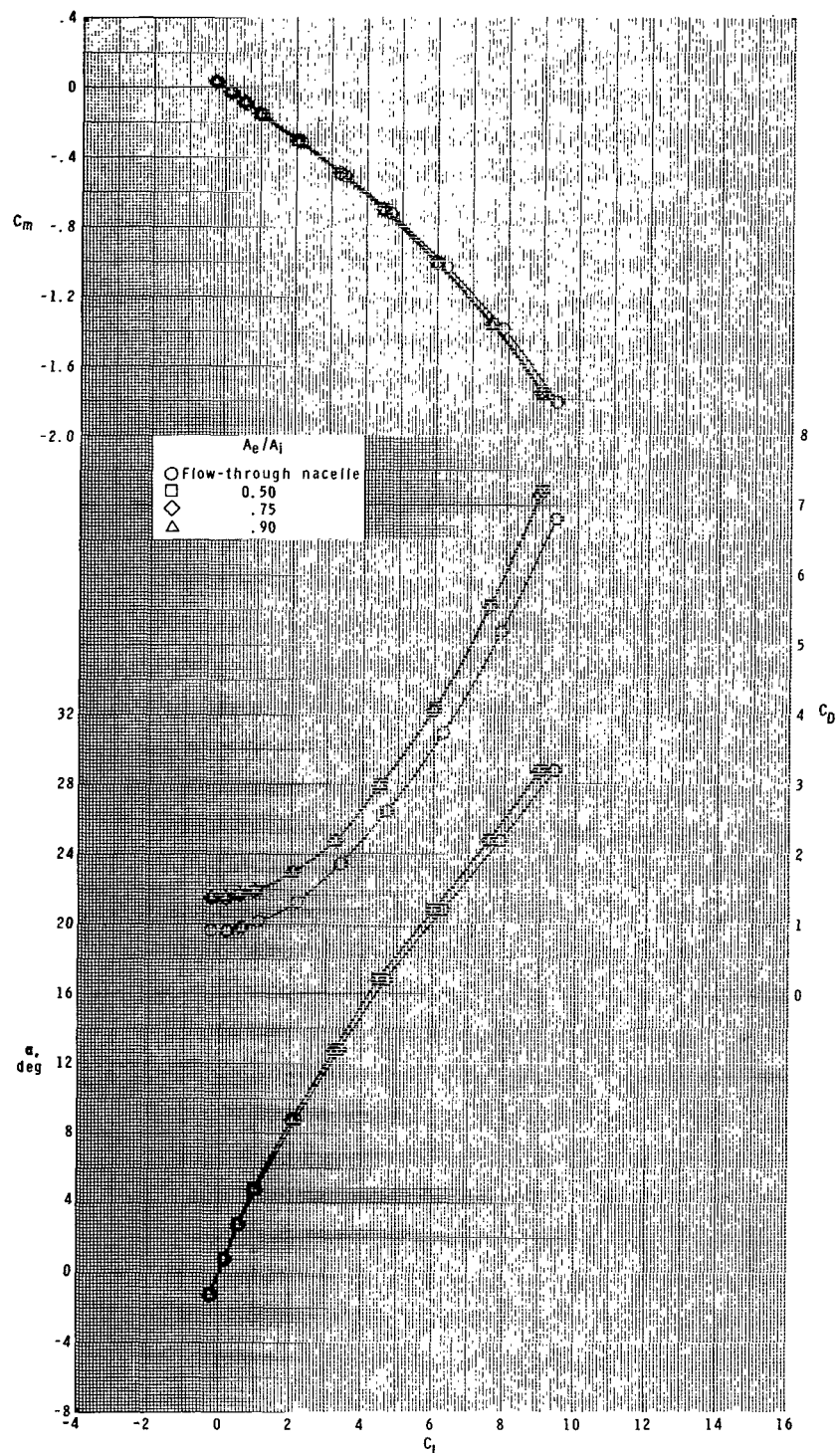
(c) Concluded.

Figure 29.- Continued.



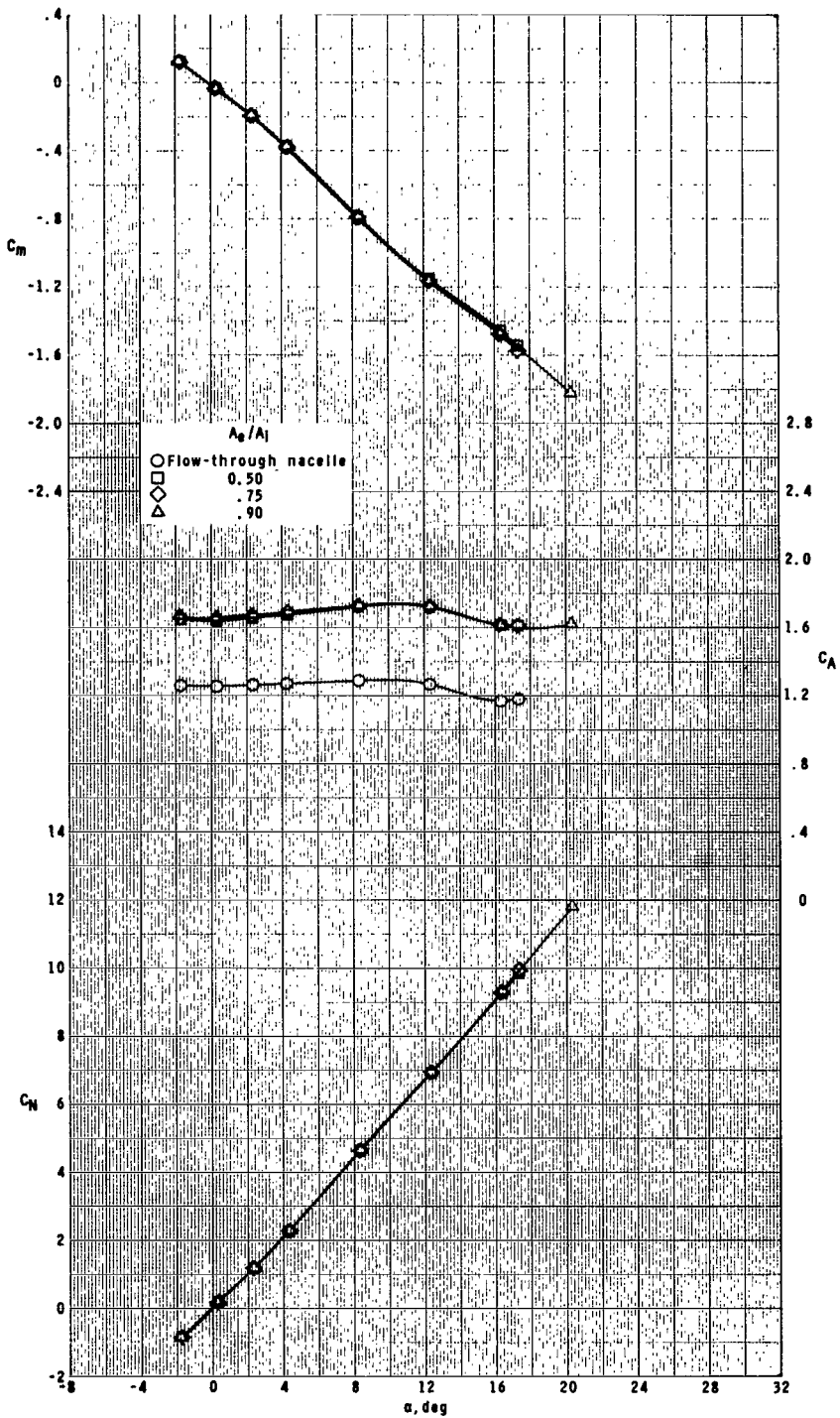
(d)  $M = 4.63.$

Figure 29.- Continued.



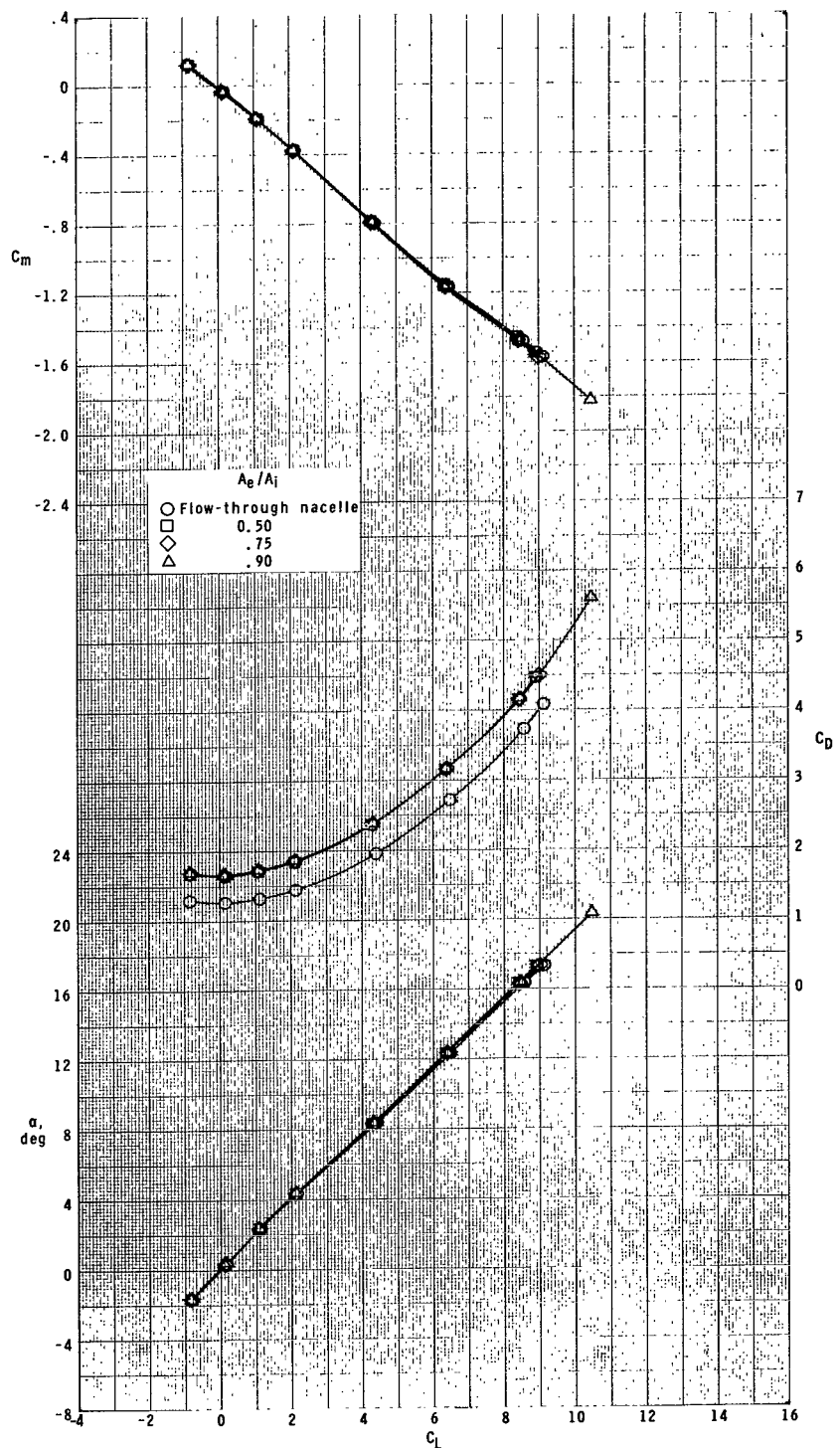
(d) Concluded.

Figure 29.- Concluded.



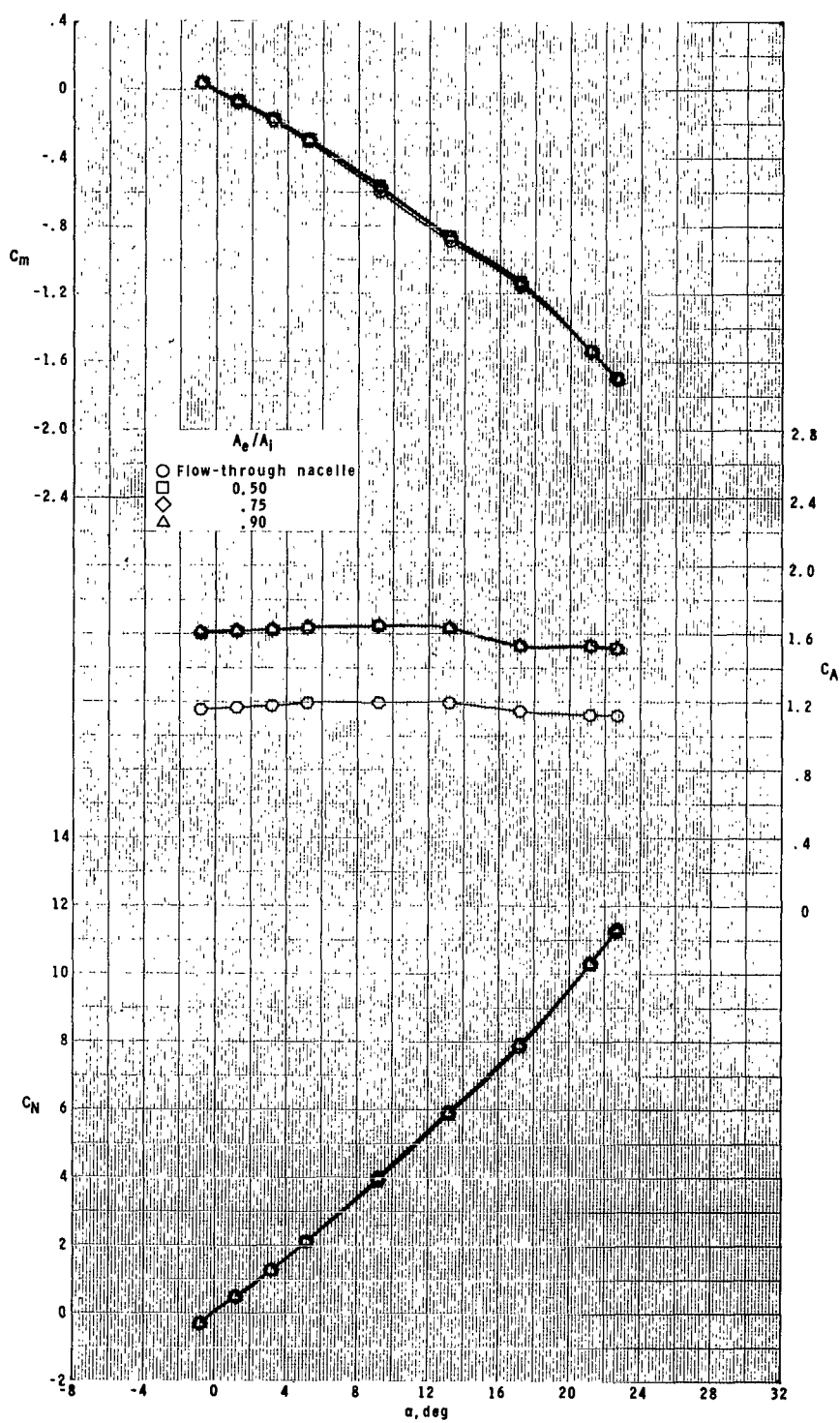
(a)  $M = 1.60$ .

**Figure 30.- Effect of ratio of plenum exit area to inlet area for roll control on longitudinal aerodynamic characteristics of model with ram-air-spoiler tail fins for  $A_p/A = 0.063$  at  $\phi = 45^\circ$ .**



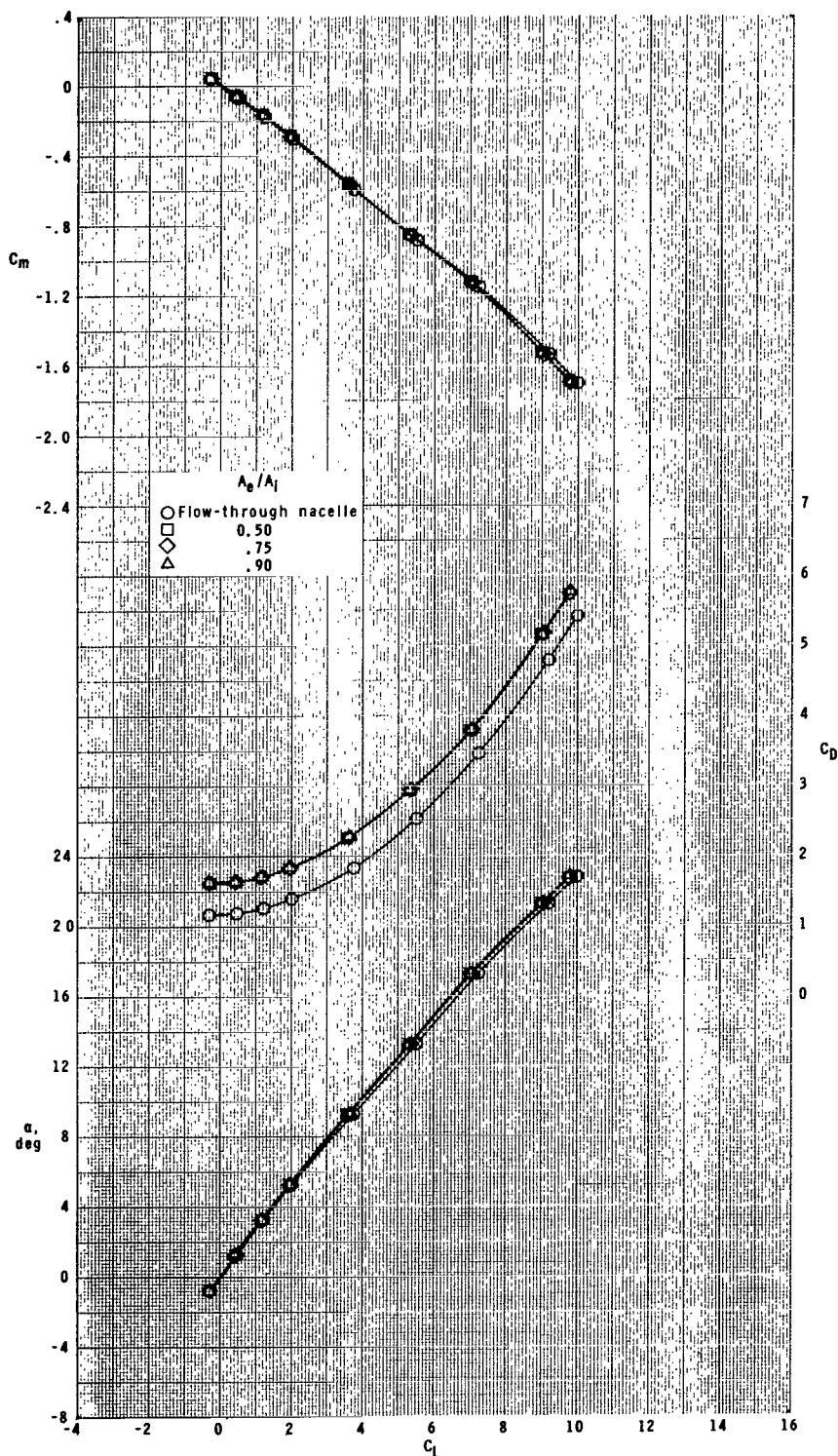
(a) Concluded.

Figure 30.- Continued.



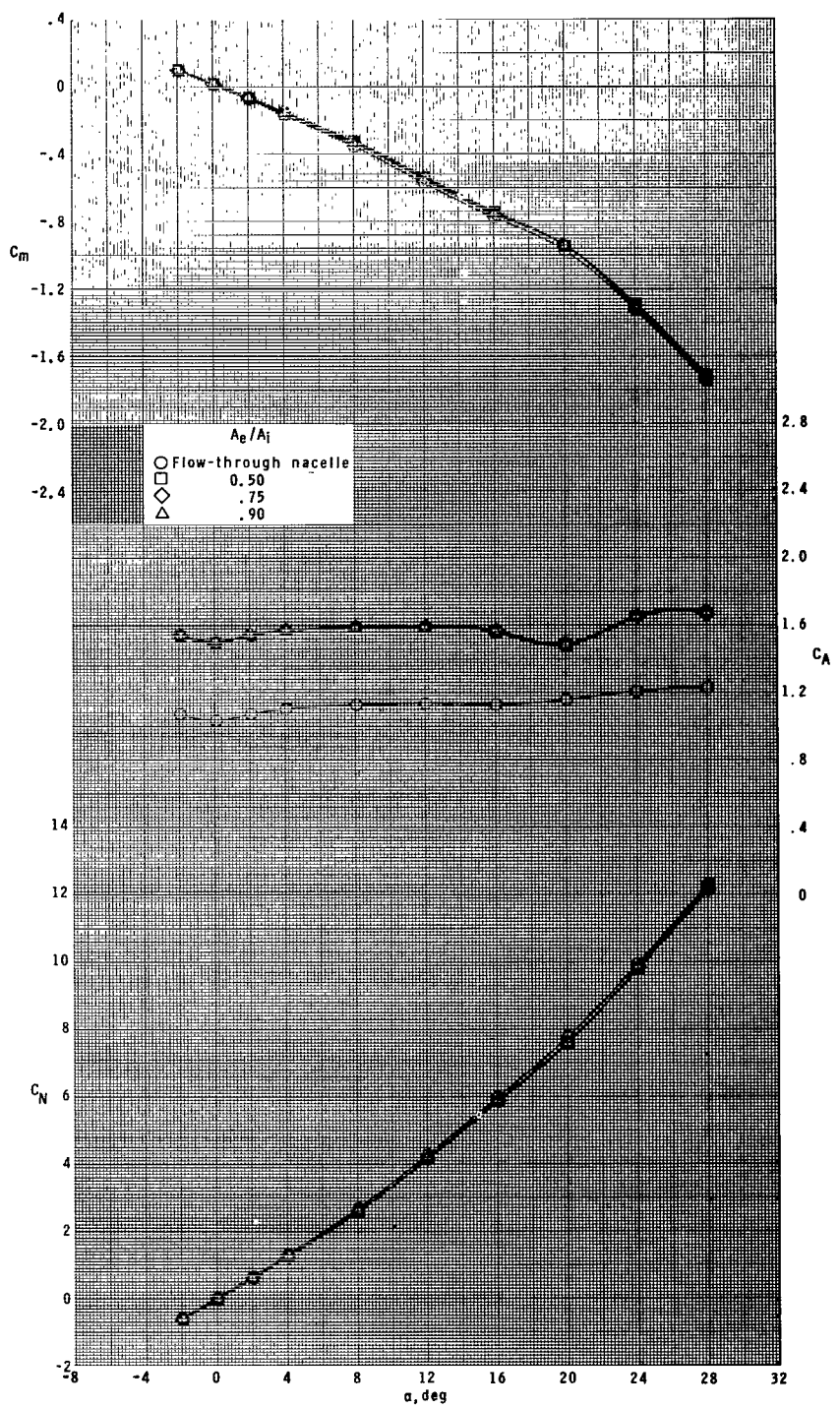
(b)  $M = 2.16.$

Figure 30.- Continued.



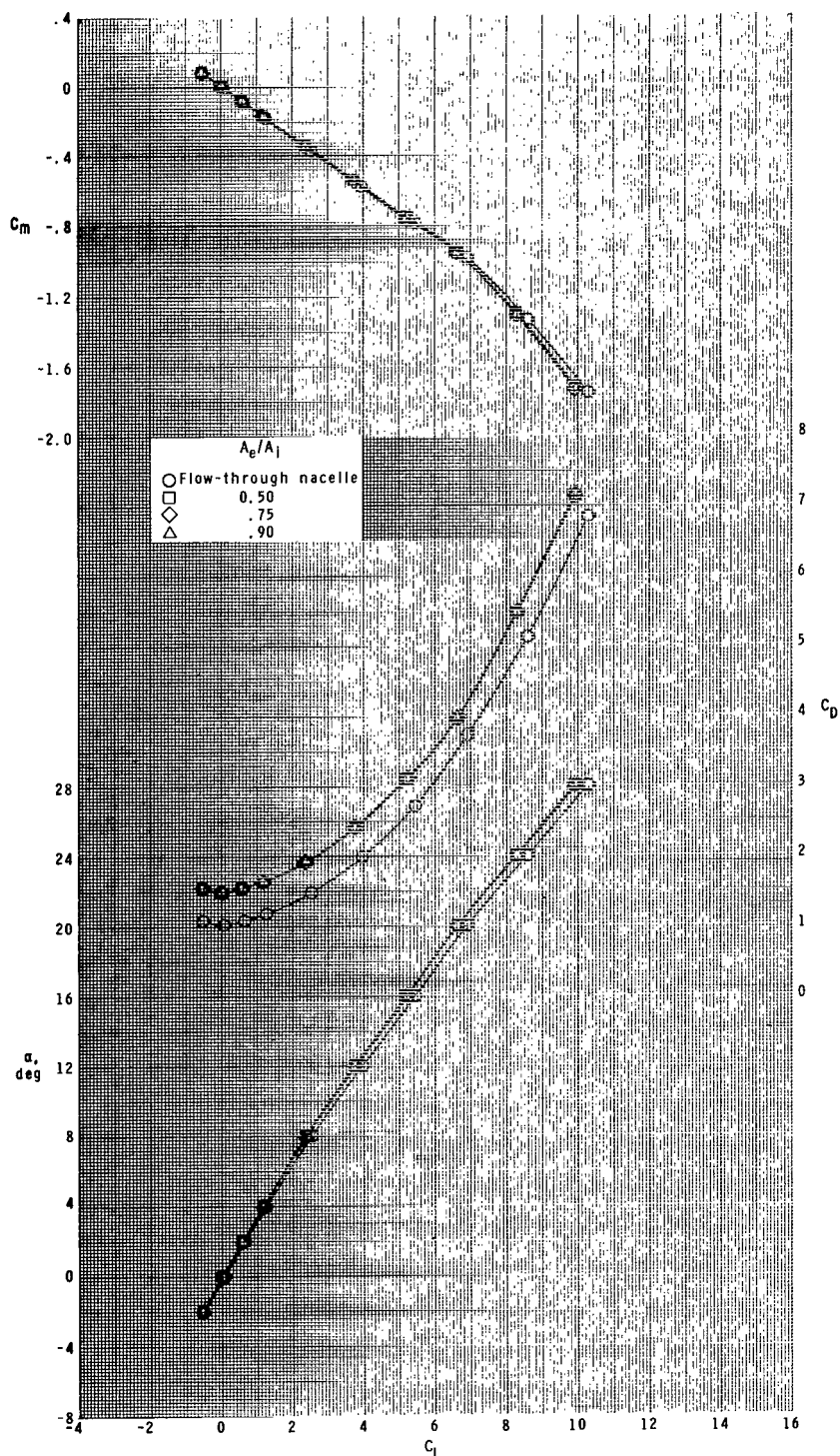
(b) Concluded.

Figure 30.- Continued.



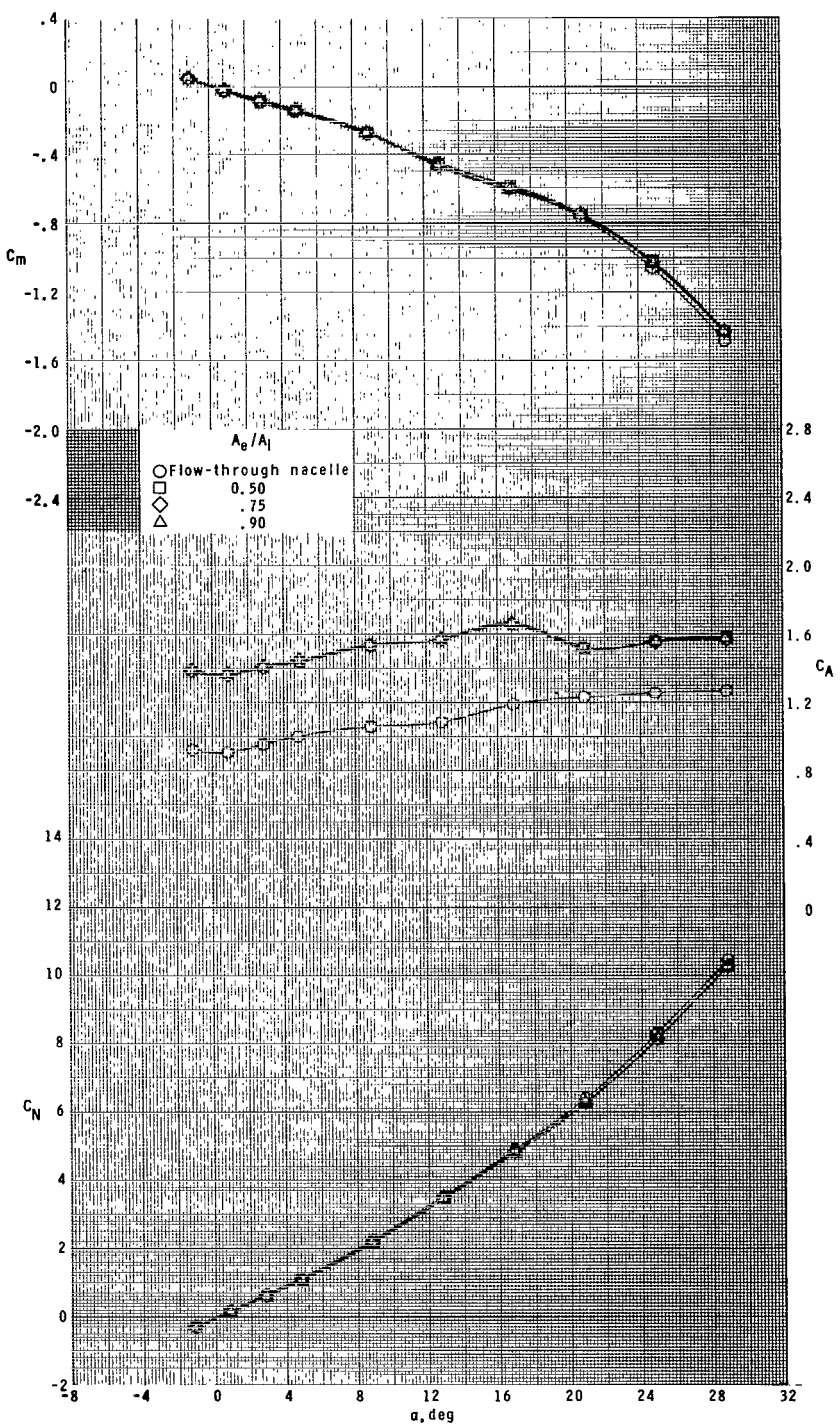
(c)  $M = 2.96.$

Figure 30.- Continued.



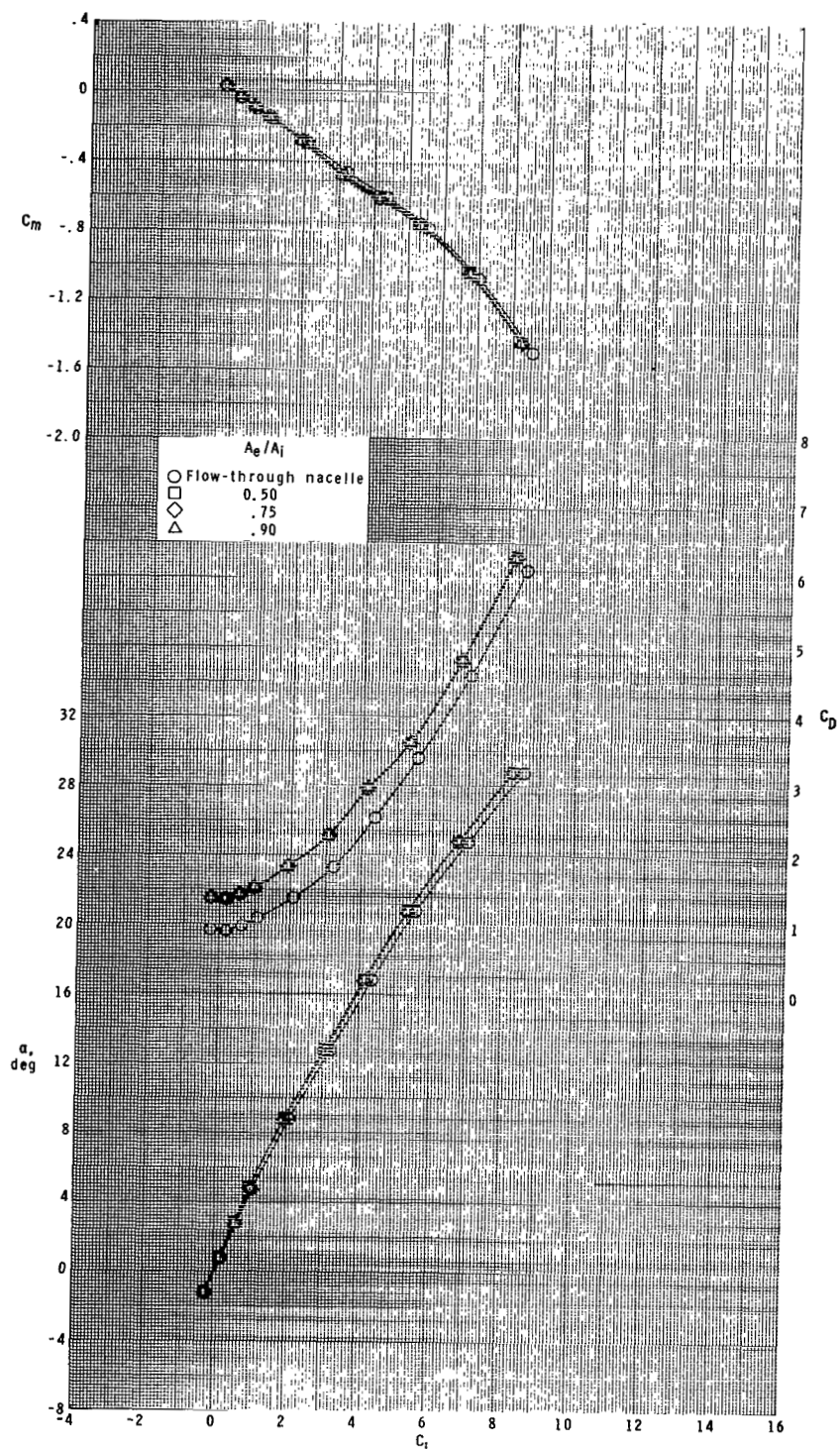
(c) Concluded.

Figure 30.- Continued.



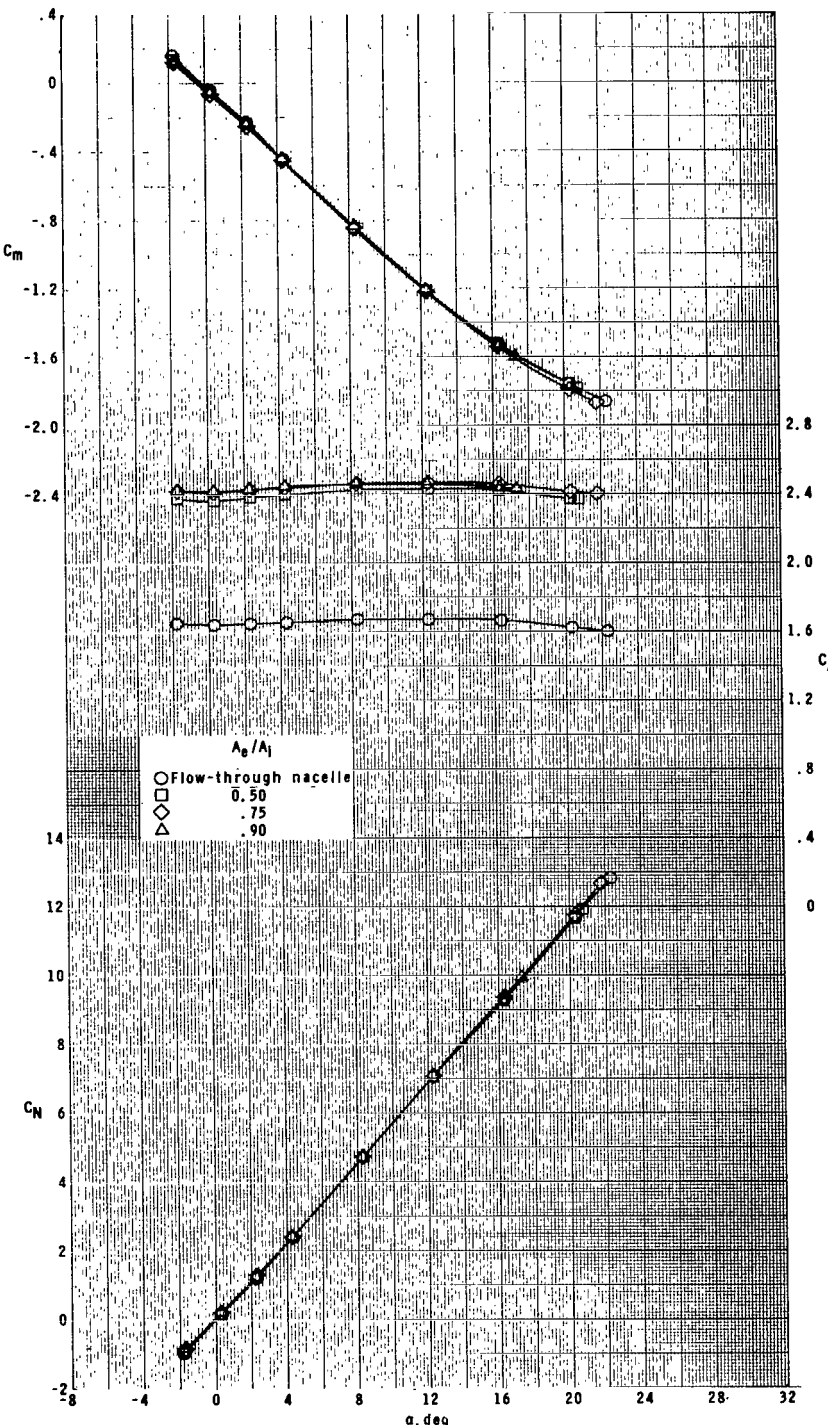
(d)  $M = 4.63.$

Figure 30.- Continued.



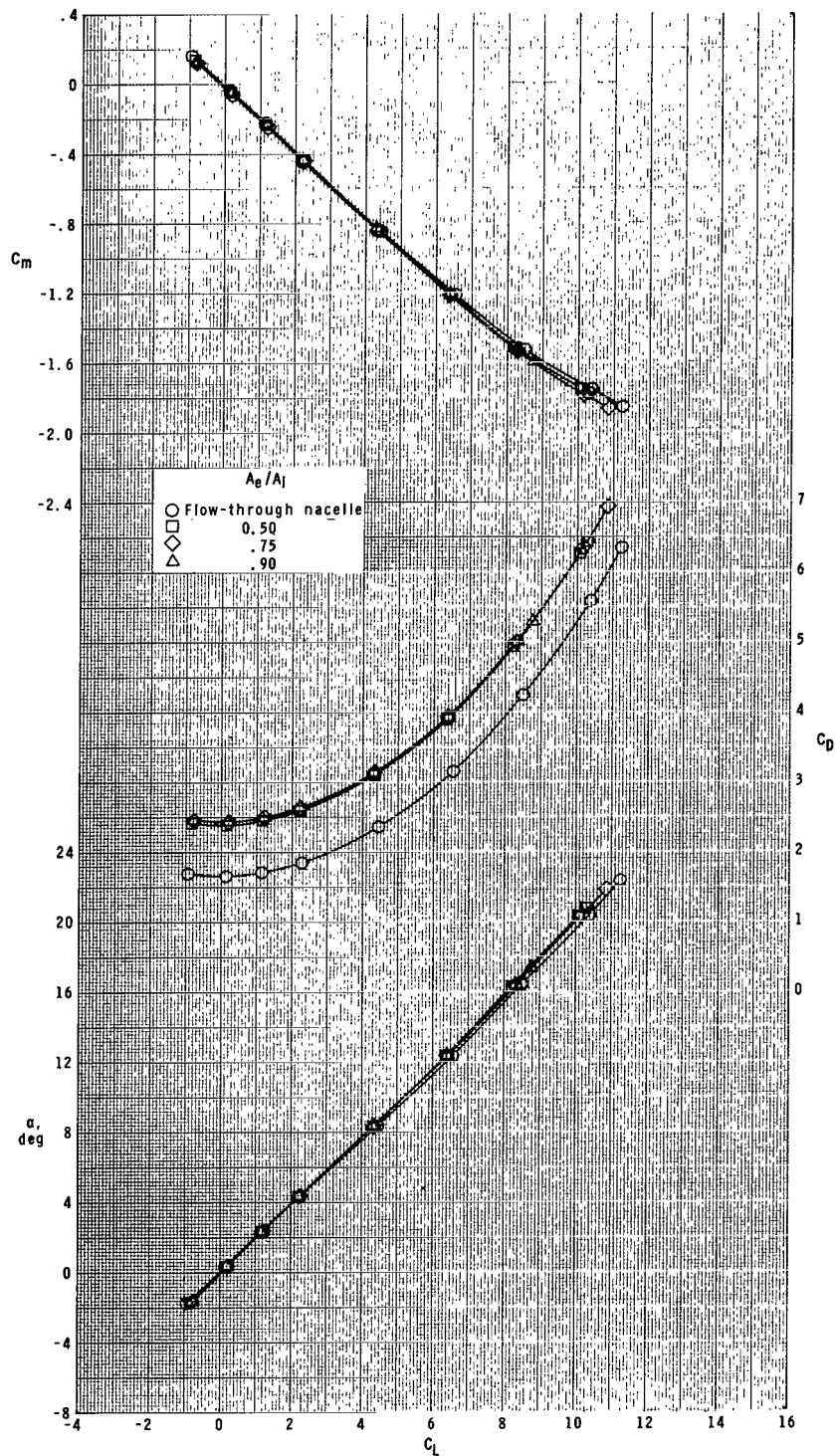
(d) Concluded.

Figure 30.- Concluded.



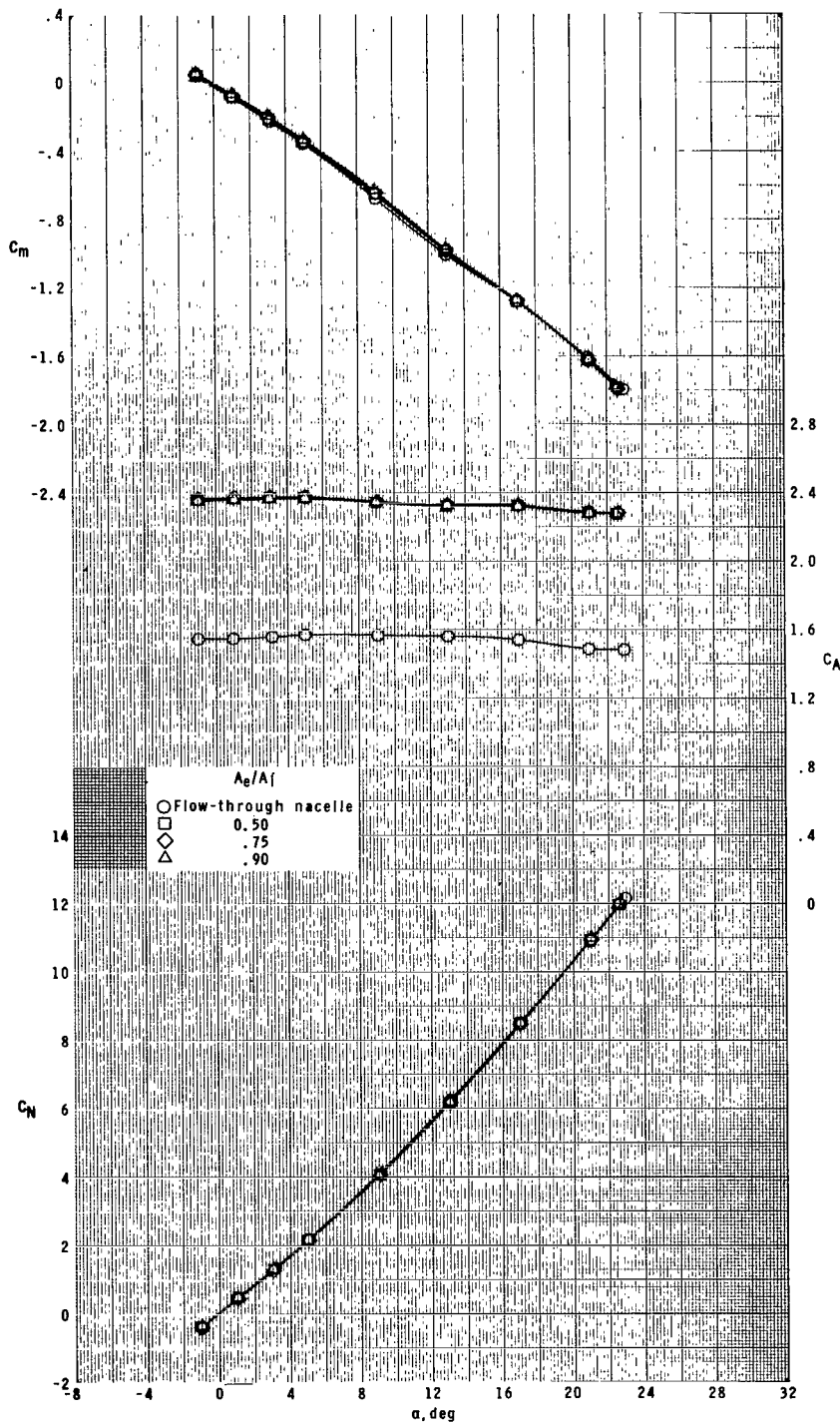
(a)  $M = 1.60$ .

Figure 31.- Effect of ratio of plenum exit area to inlet area for roll control on longitudinal aerodynamic characteristics of model with ram-air-spoiler tail fins for  $A_i/A = 0.111$  at  $\phi = 0^\circ$ .



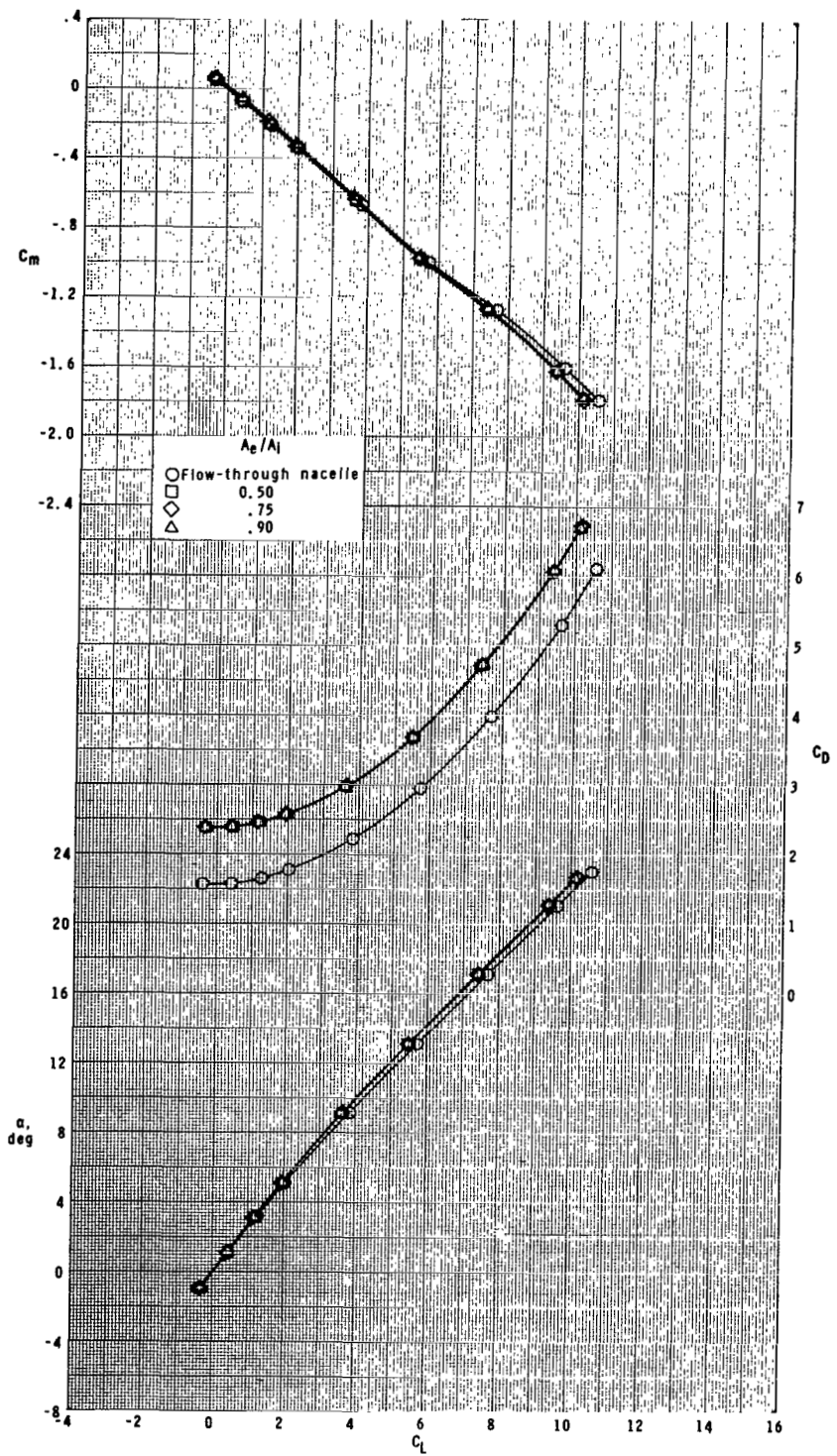
(a) Concluded.

Figure 31.- Continued.



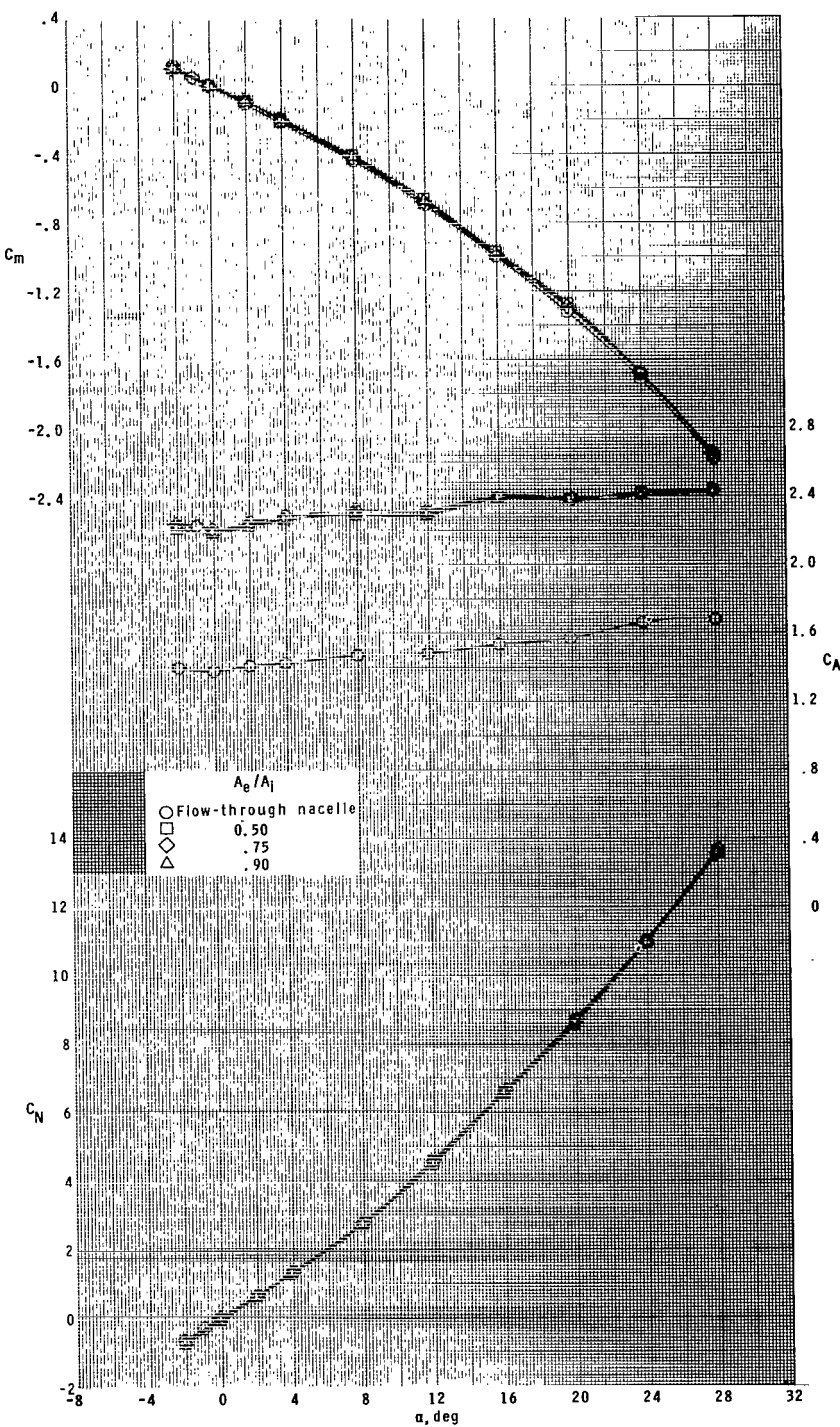
(b)  $M = 2.16.$

Figure 31.- Continued.



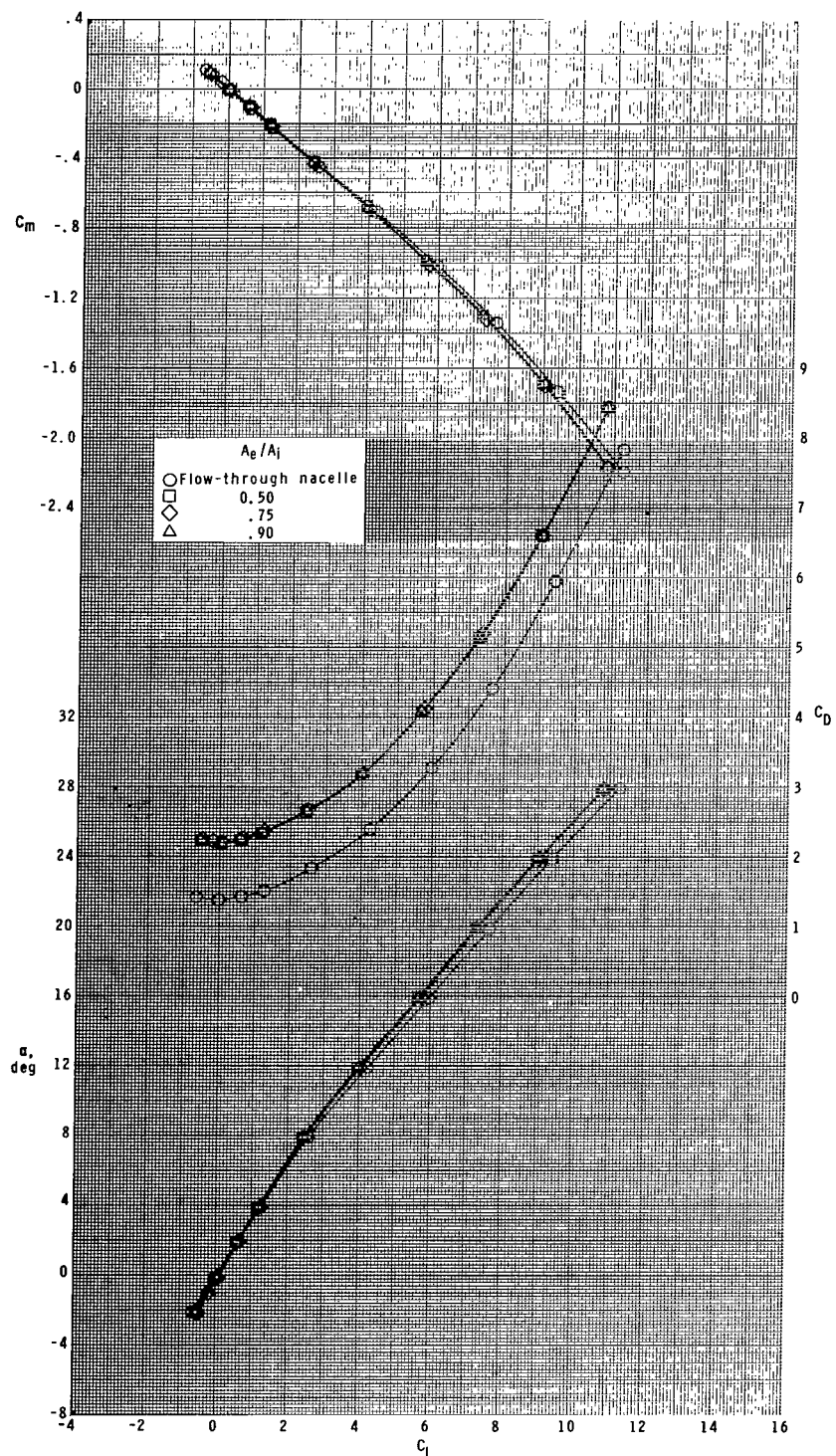
(b) Concluded.

Figure 31.- Continued.



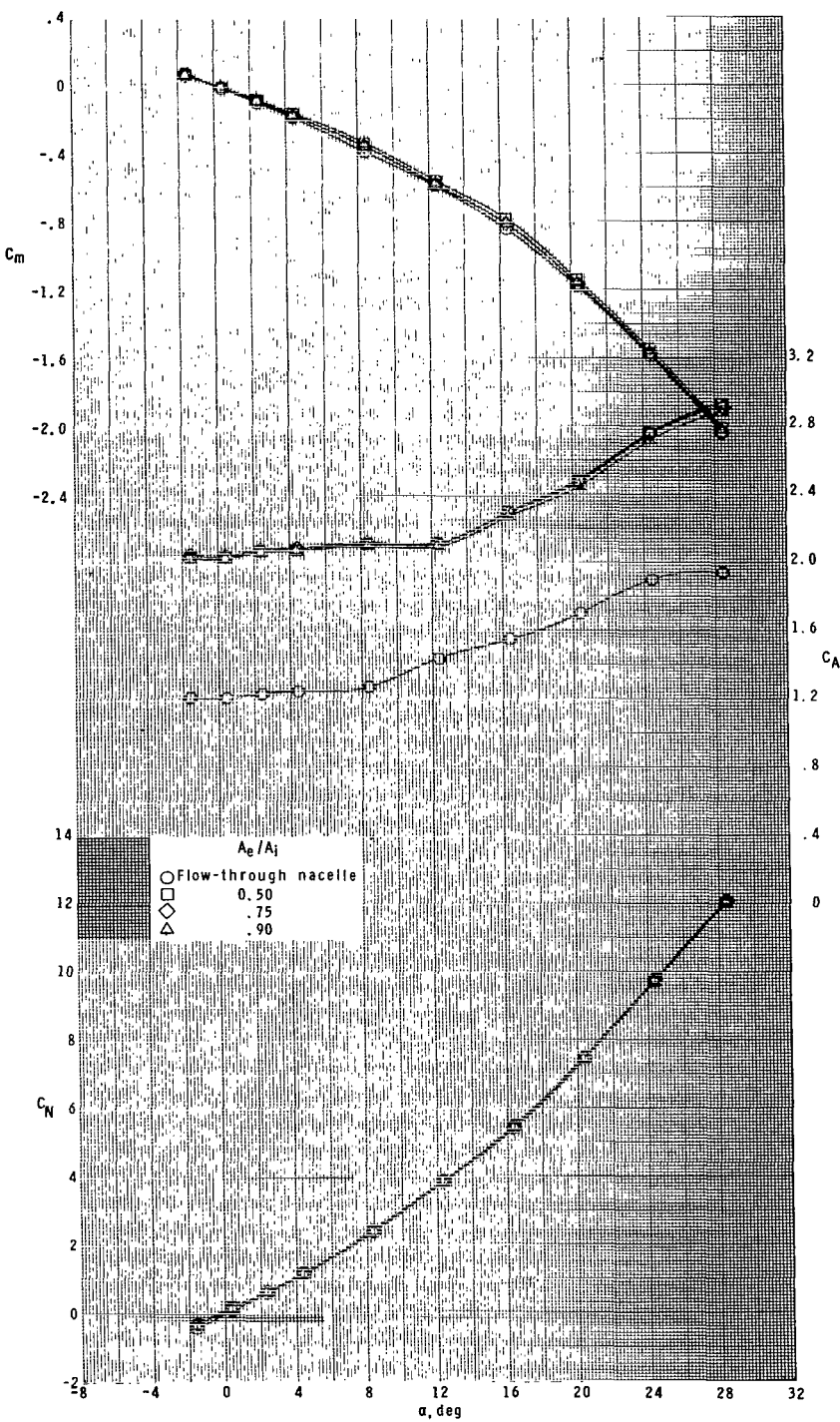
(c)  $M = 2.96$ .

Figure 31.- Continued.



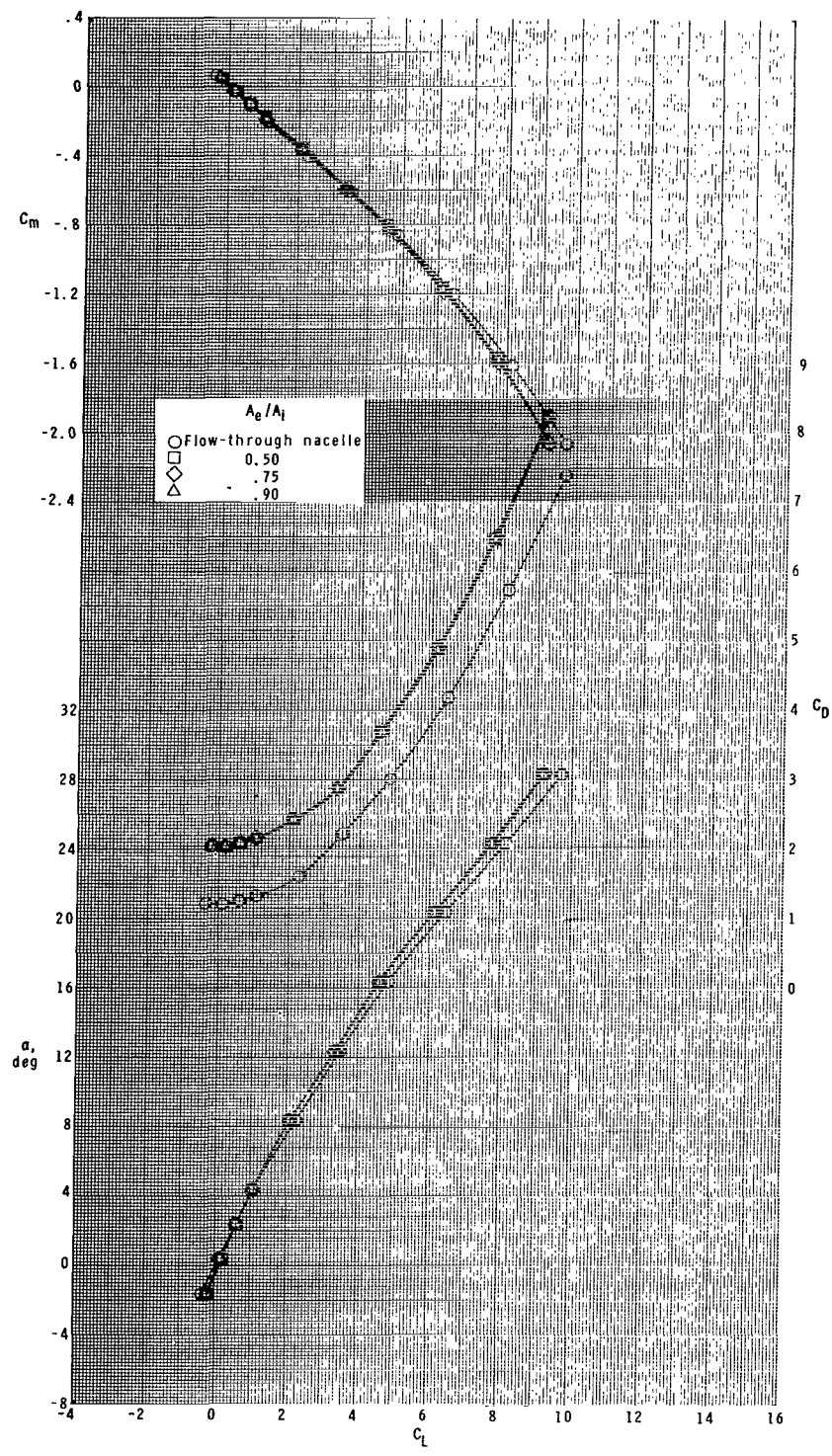
(c) Concluded.

Figure 31.- Continued.



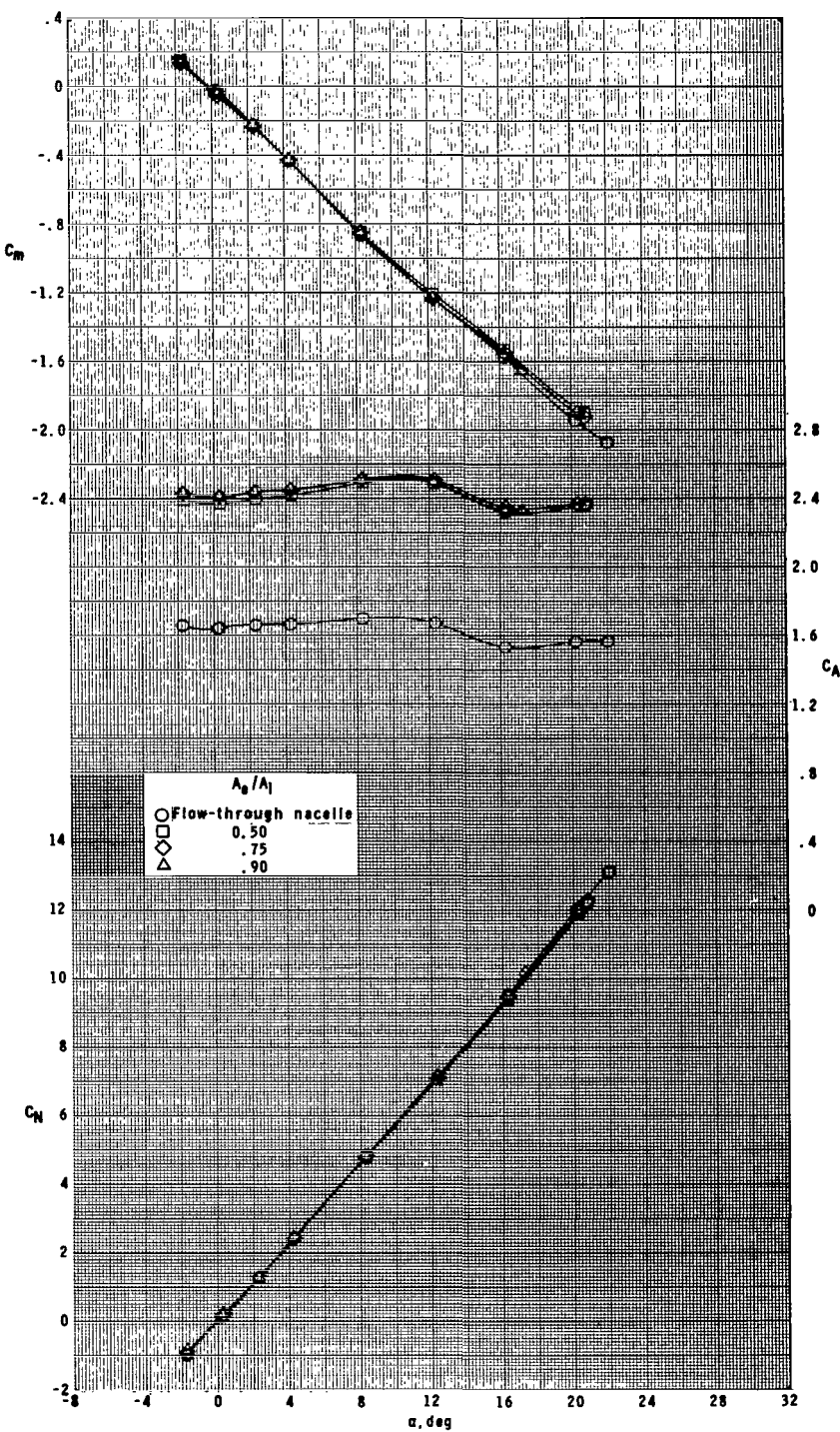
(d)  $M = 4.63.$

Figure 31.- Continued.



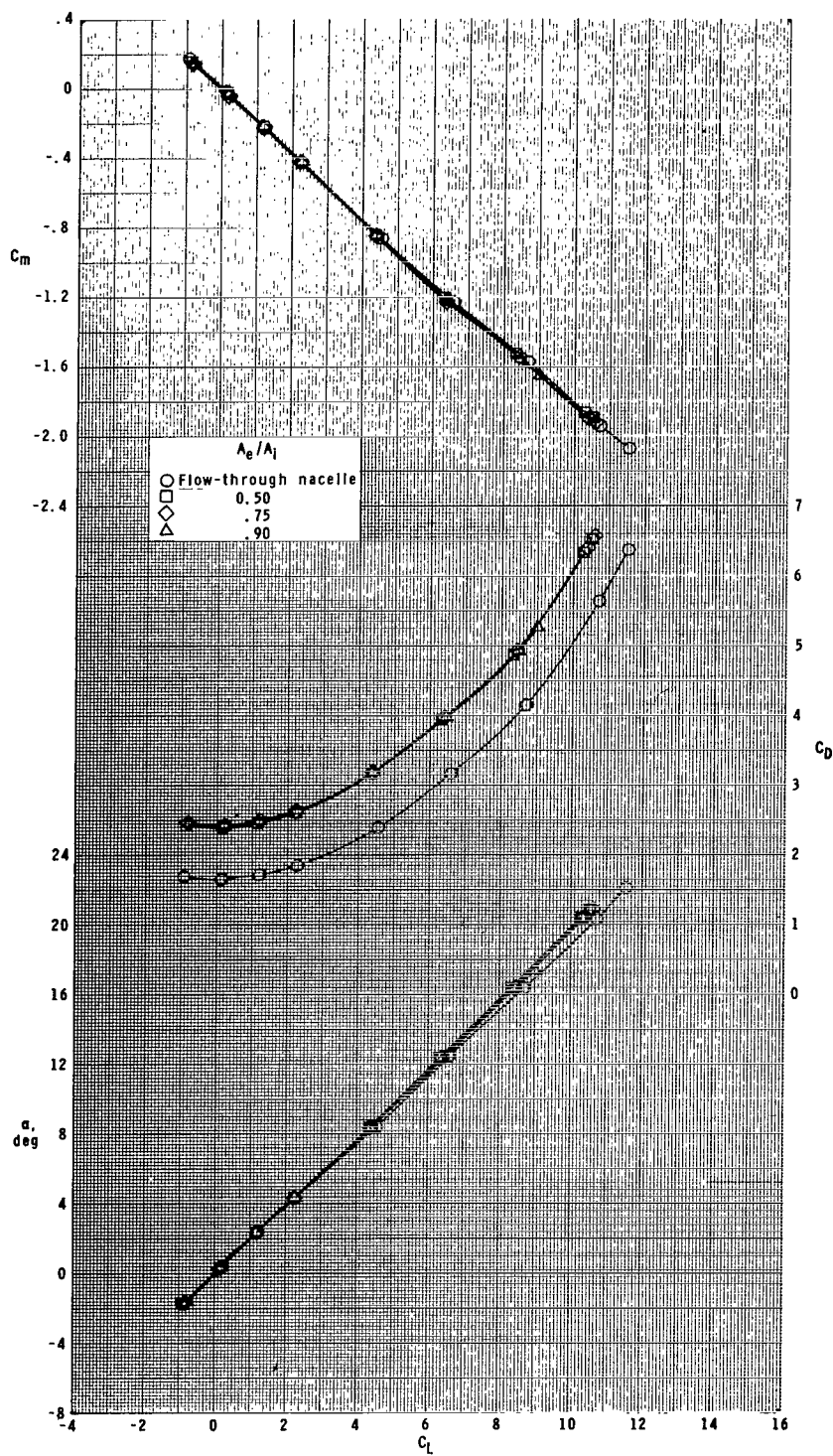
(d) Concluded.

Figure 31.- Concluded.



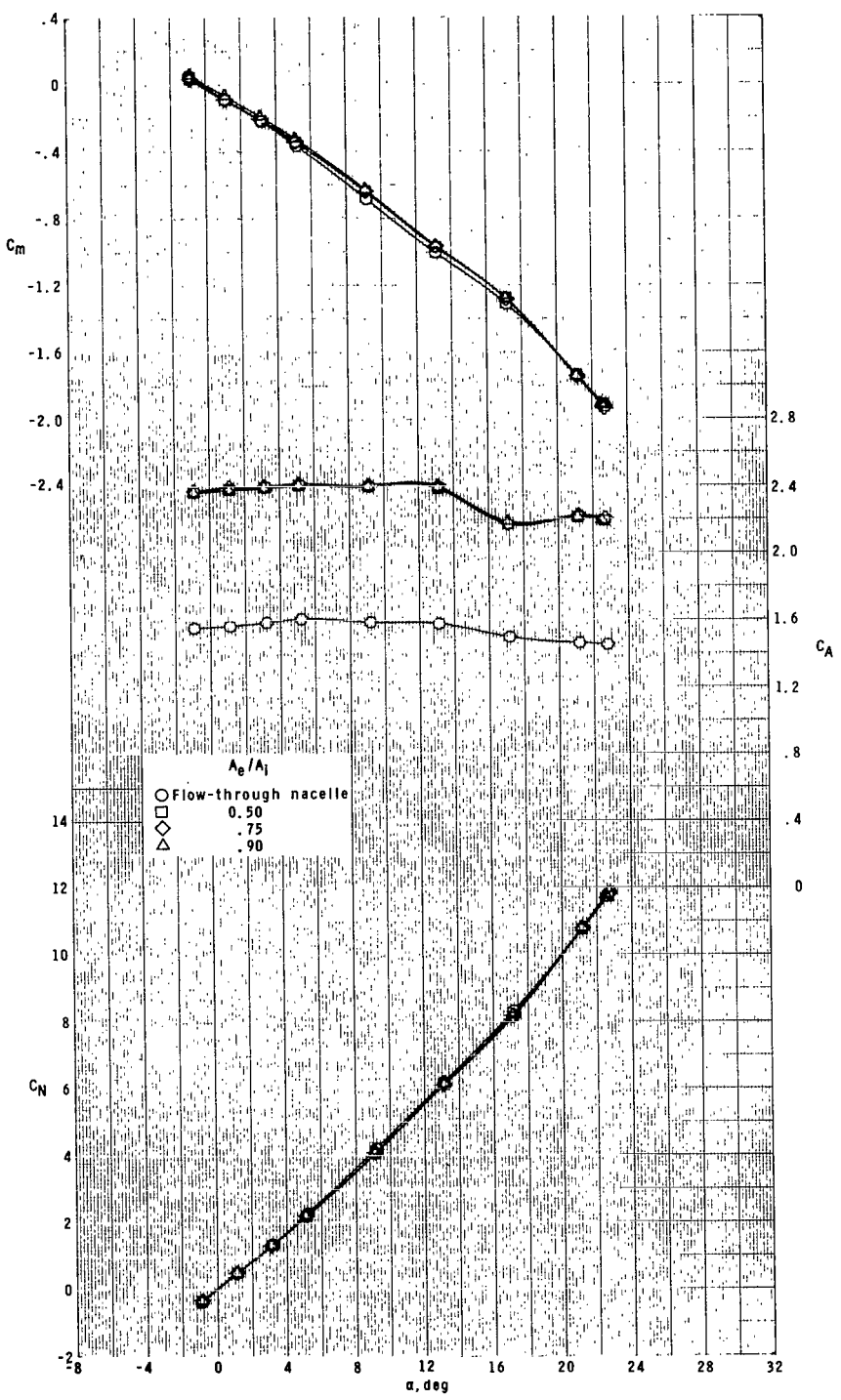
(a)  $M = 1.60.$

**Figure 32.- Effect of ratio of plenum exit area to inlet area for roll control on longitudinal aerodynamic characteristics of model with ram-air-spoiler tail fins for  $A_j/A = 0.111$  at  $\phi = 45^\circ$ .**



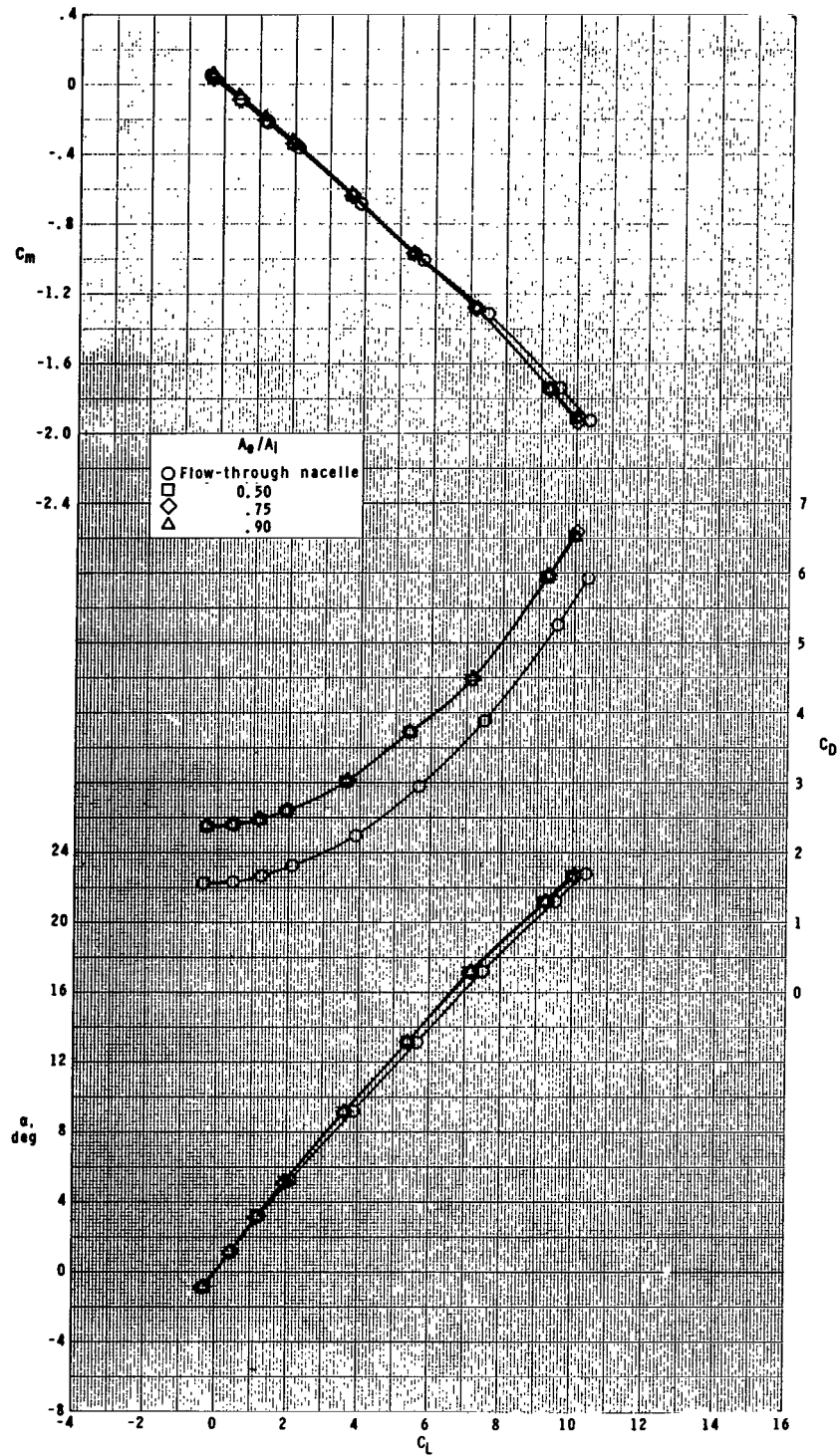
(a) Concluded.

Figure 32.- Continued.



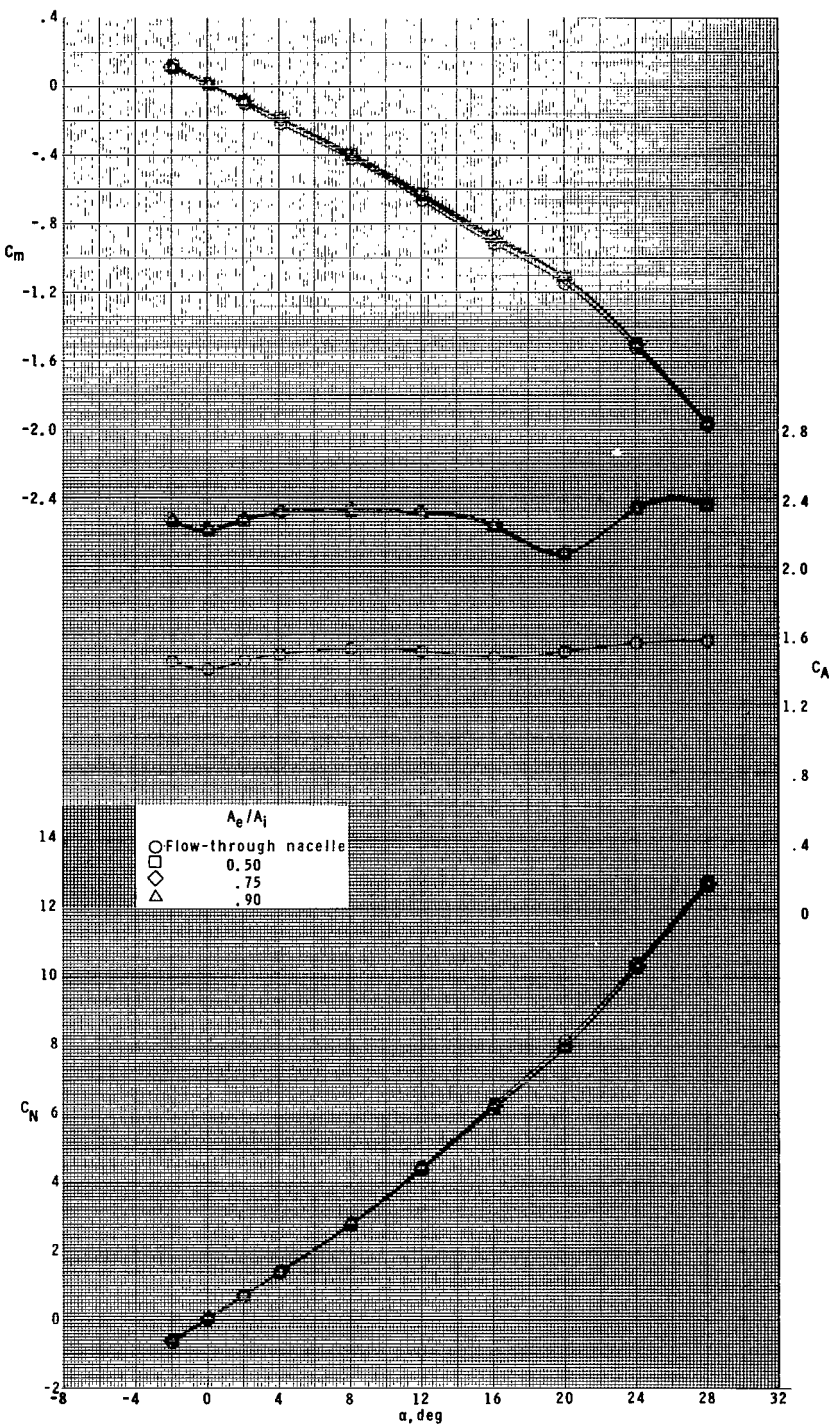
(b)  $M = 2.16.$

Figure 32.- Continued.



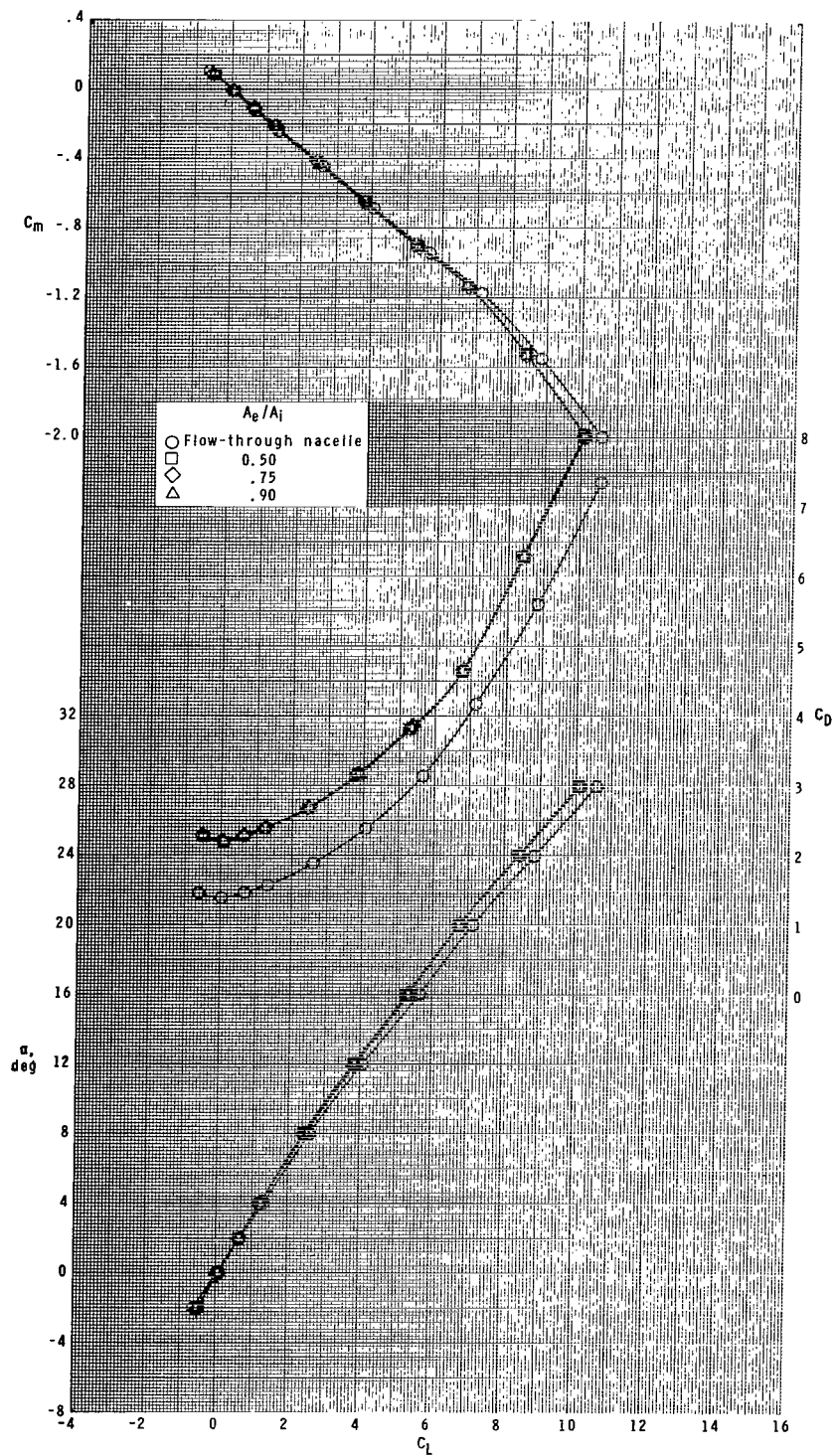
(b) Concluded.

Figure 32.- Continued.



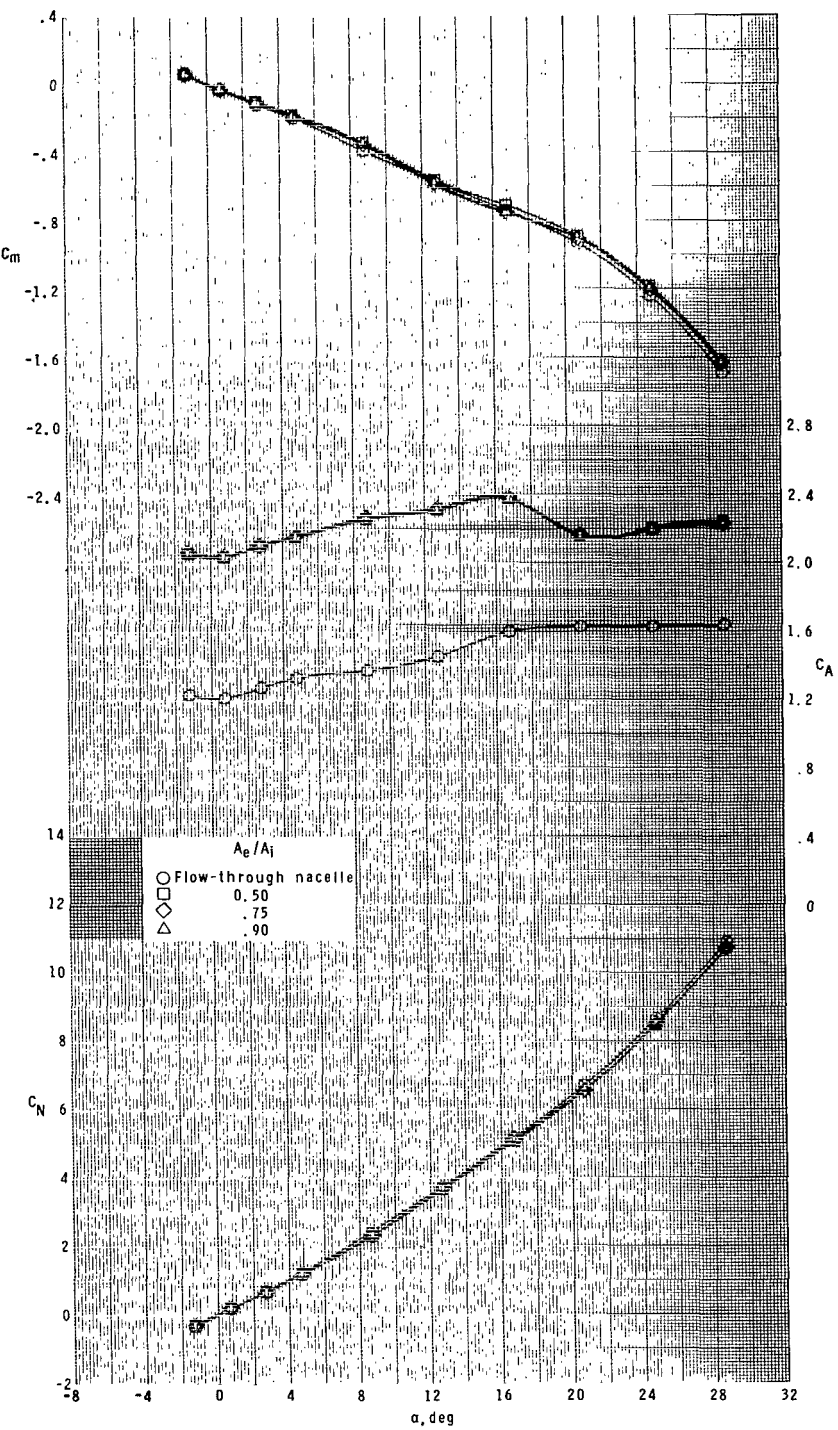
(c)  $M = 2.96.$

Figure 32.- Continued.



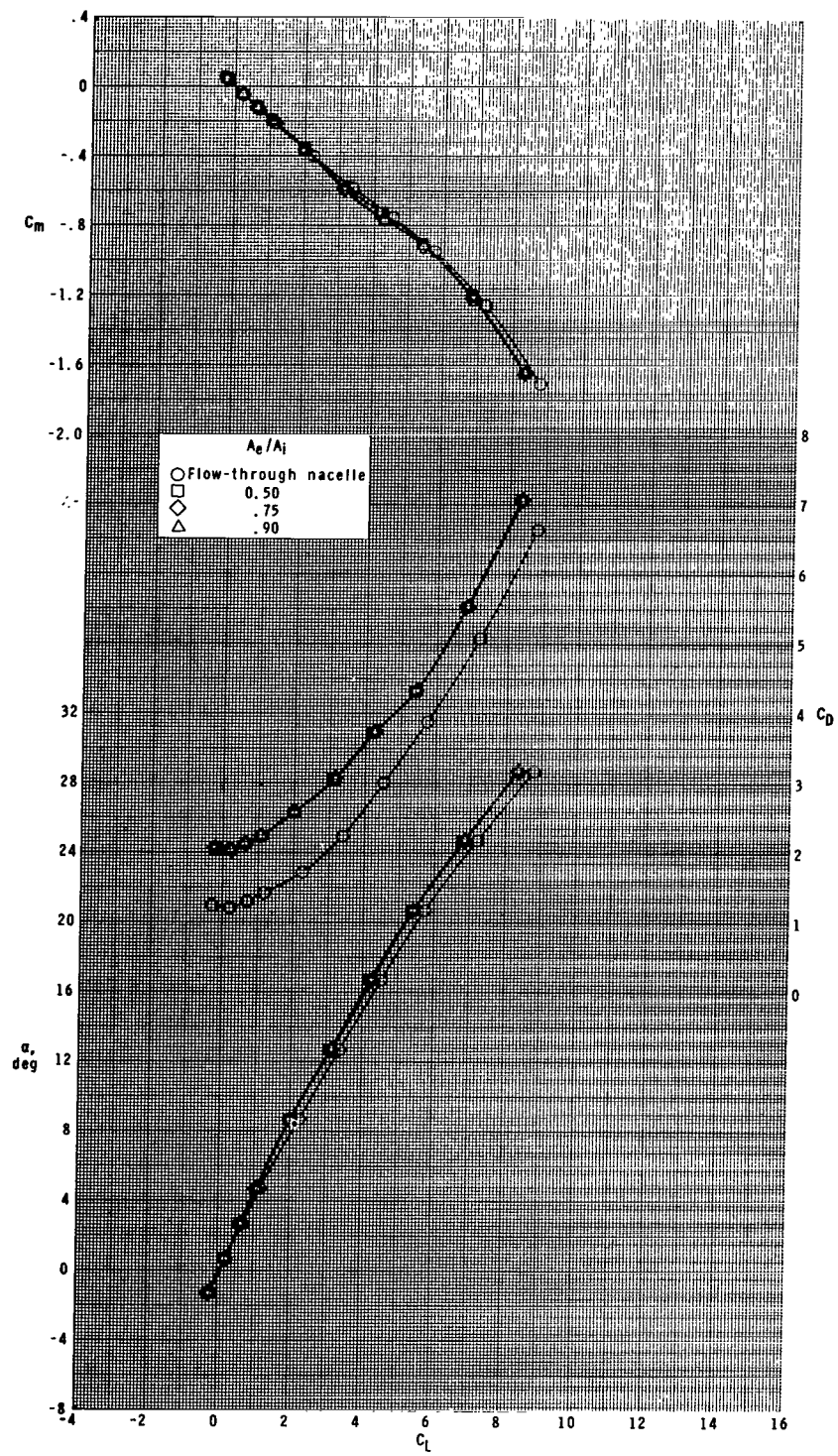
(c) Concluded.

Figure 32.- Continued.



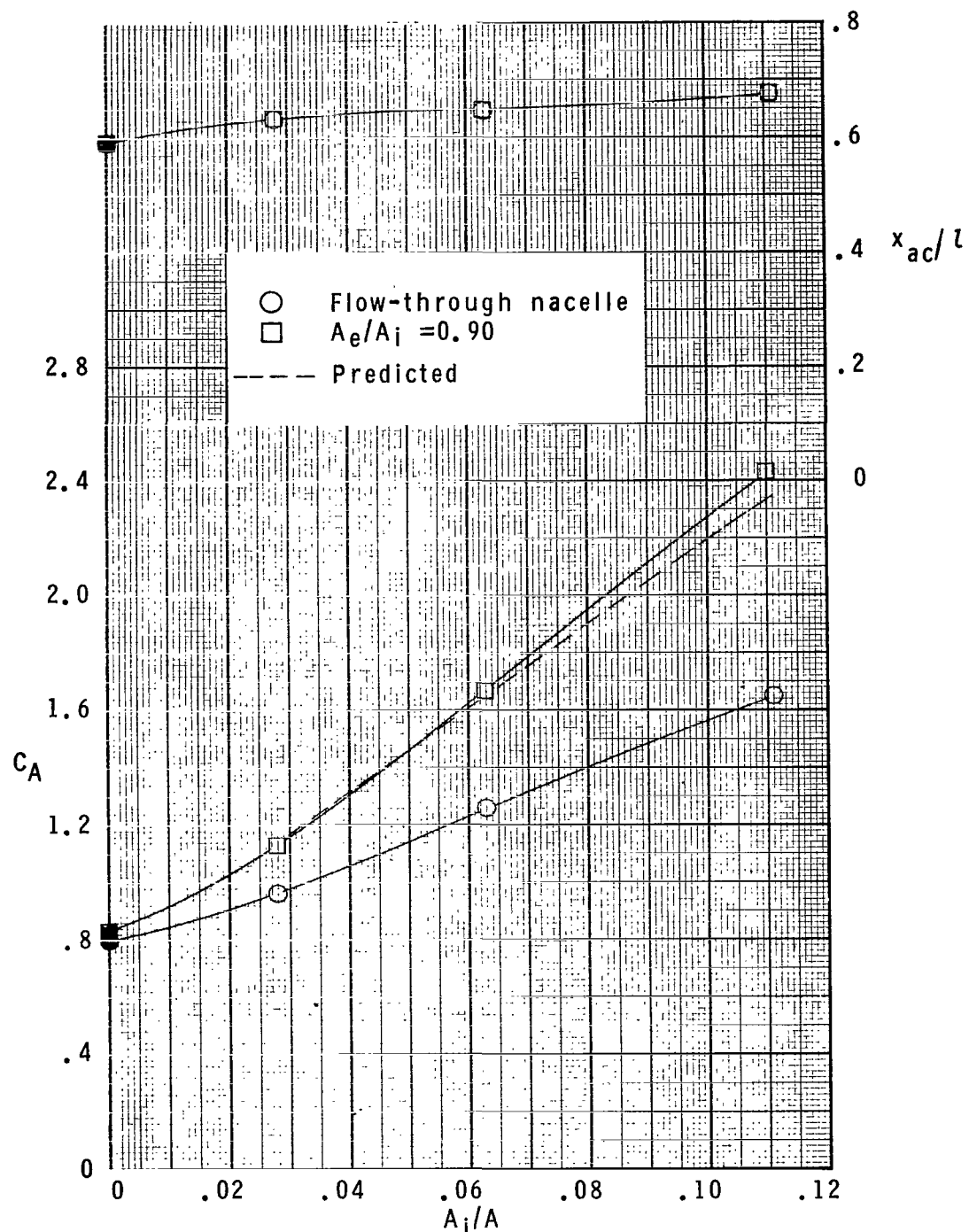
(d)  $M = 4.63.$

Figure 32.- Continued.



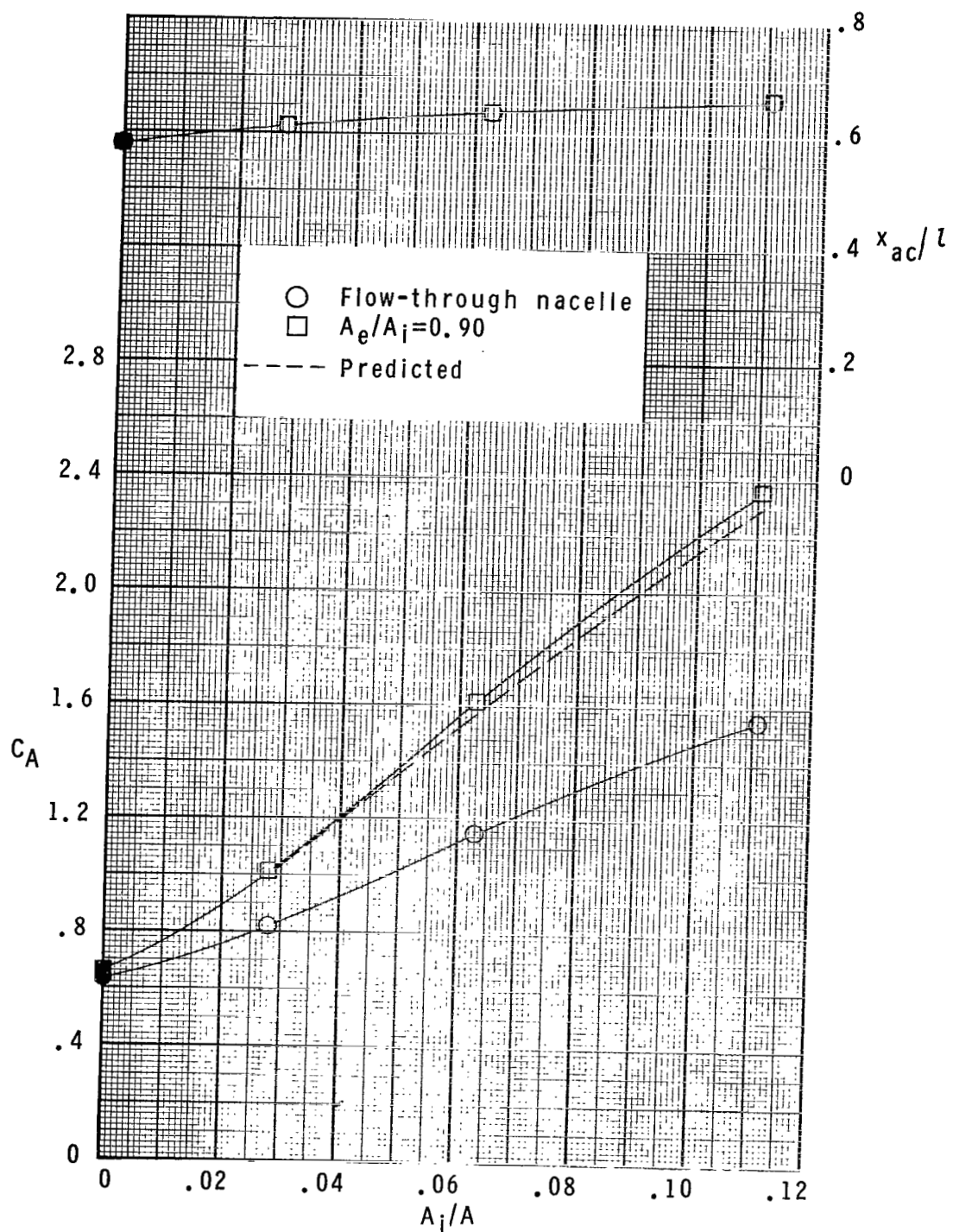
(d) Concluded.

Figure 32.- Concluded.



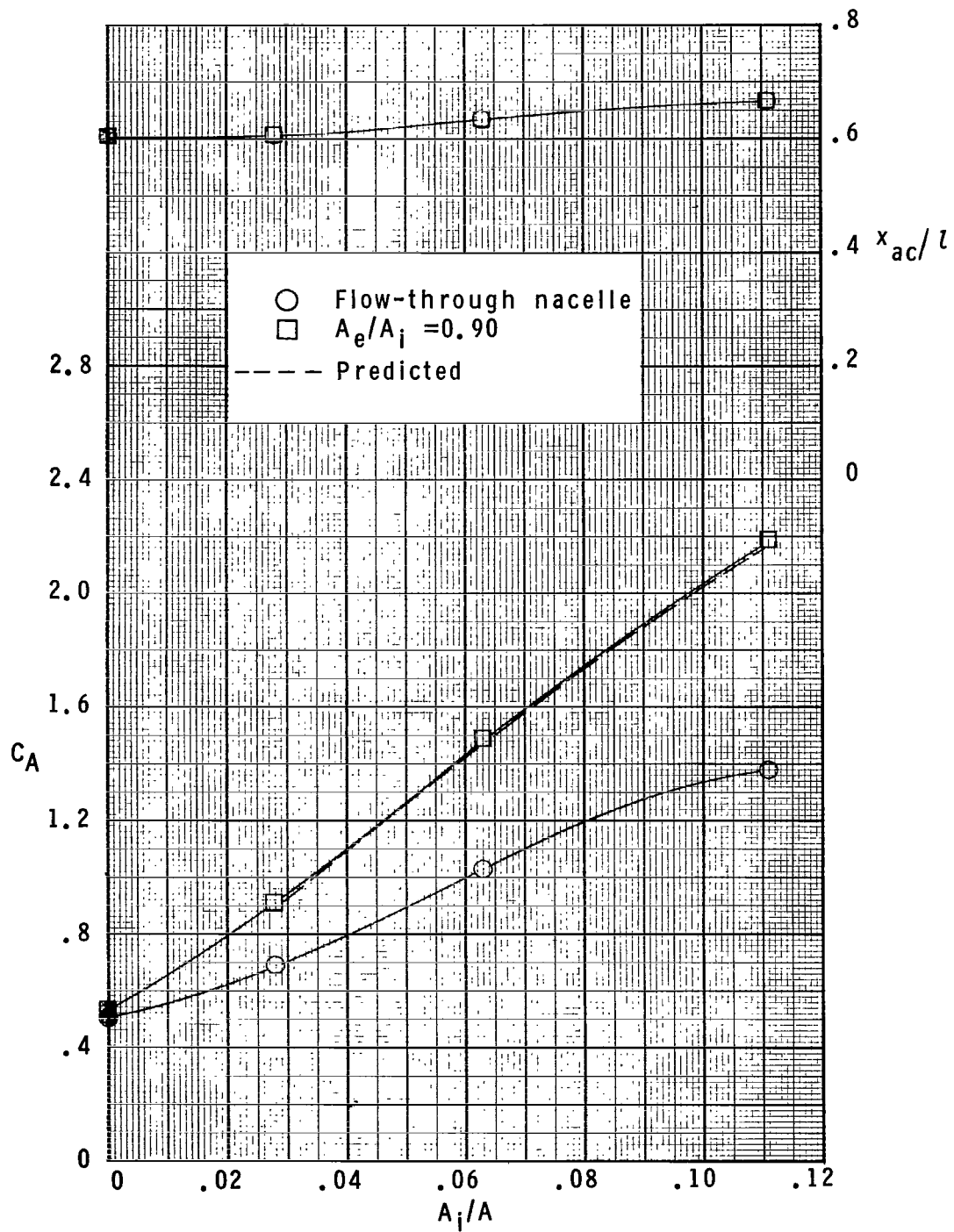
(a)  $M = 1.60.$

Figure 33.- Summary comparison of total axial-force coefficients and aerodynamic-center locations for each ram-air-spoiler and plain tail-fin configuration with and without roll control at  $\phi = 0^\circ$  and  $\alpha = 0^\circ$ .



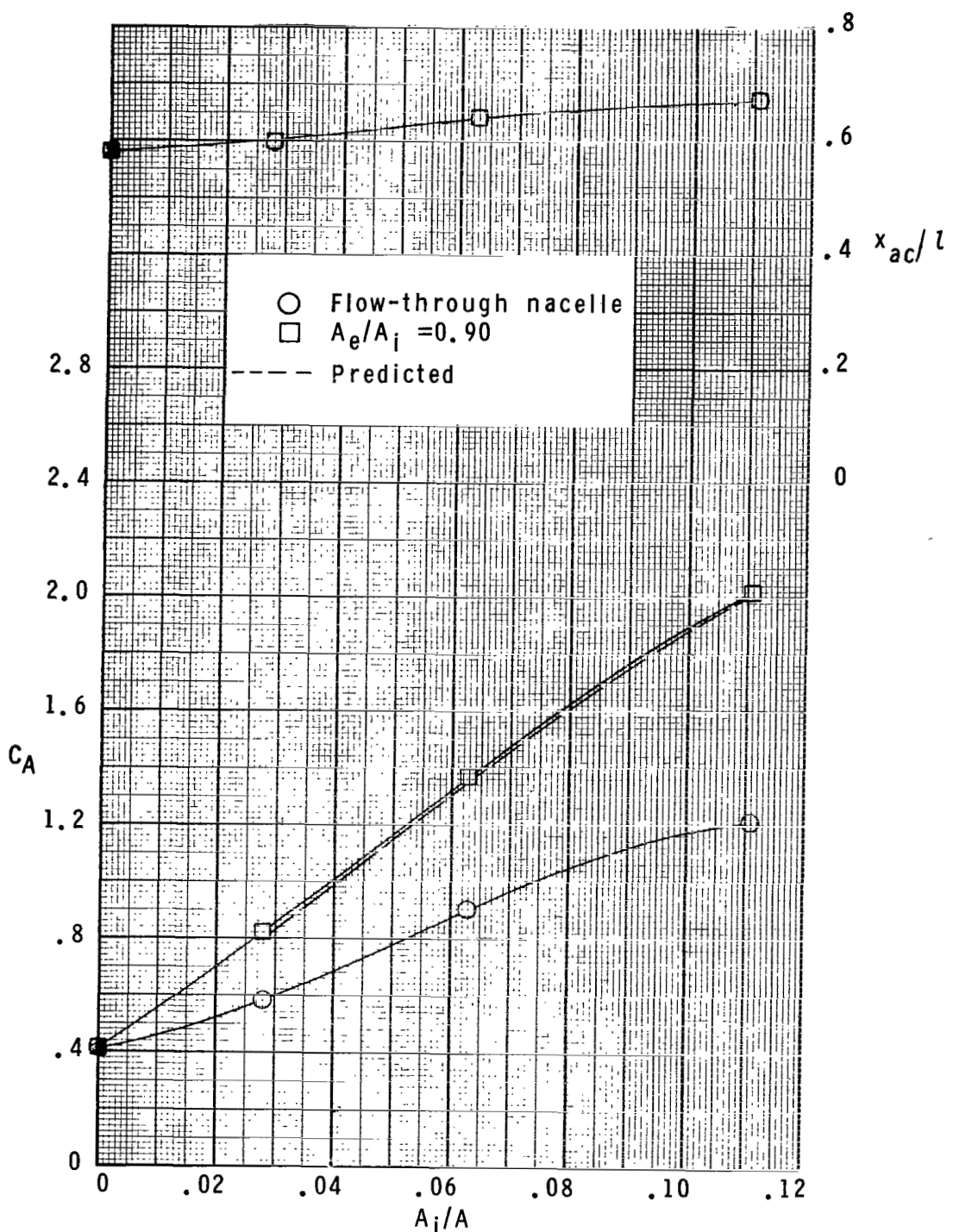
(b)  $M = 2.16.$

Figure 33.- Continued.



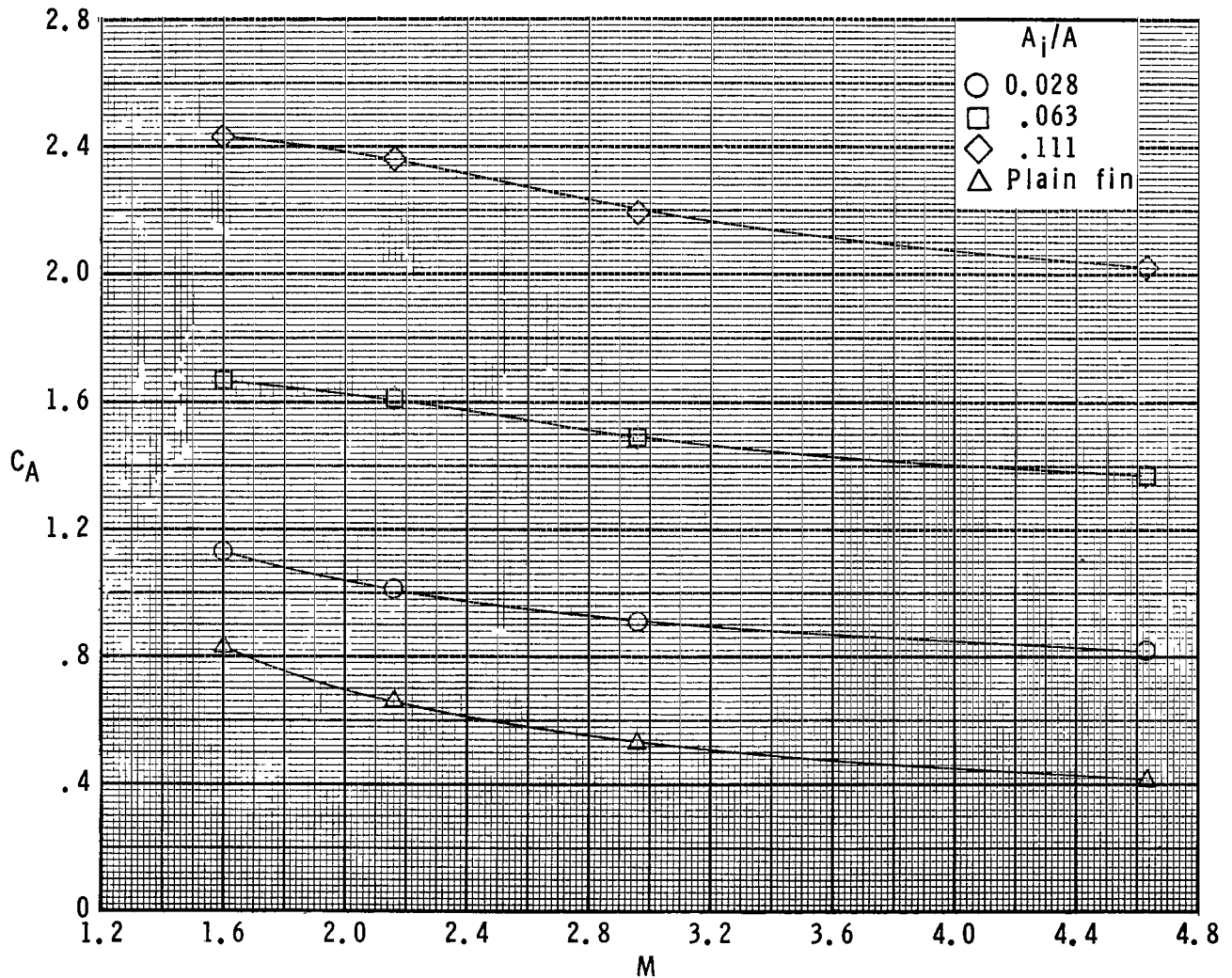
(c)  $M = 2.96$ .

Figure 33.- Continued.



(d)  $M = 4.63.$

Figure 33.- Concluded.



(a)  $A_e/A_i = 0.90$  and  $\delta_{roll} = 10^\circ$ .

**Figure 34.-** Summary of Mach number effects on total axial-force coefficients and aerodynamic-center locations for each ram-air-spoiler and plain tail-fin configuration with and without roll control at  $\phi = 0^\circ$  and  $\alpha = 0^\circ$ .

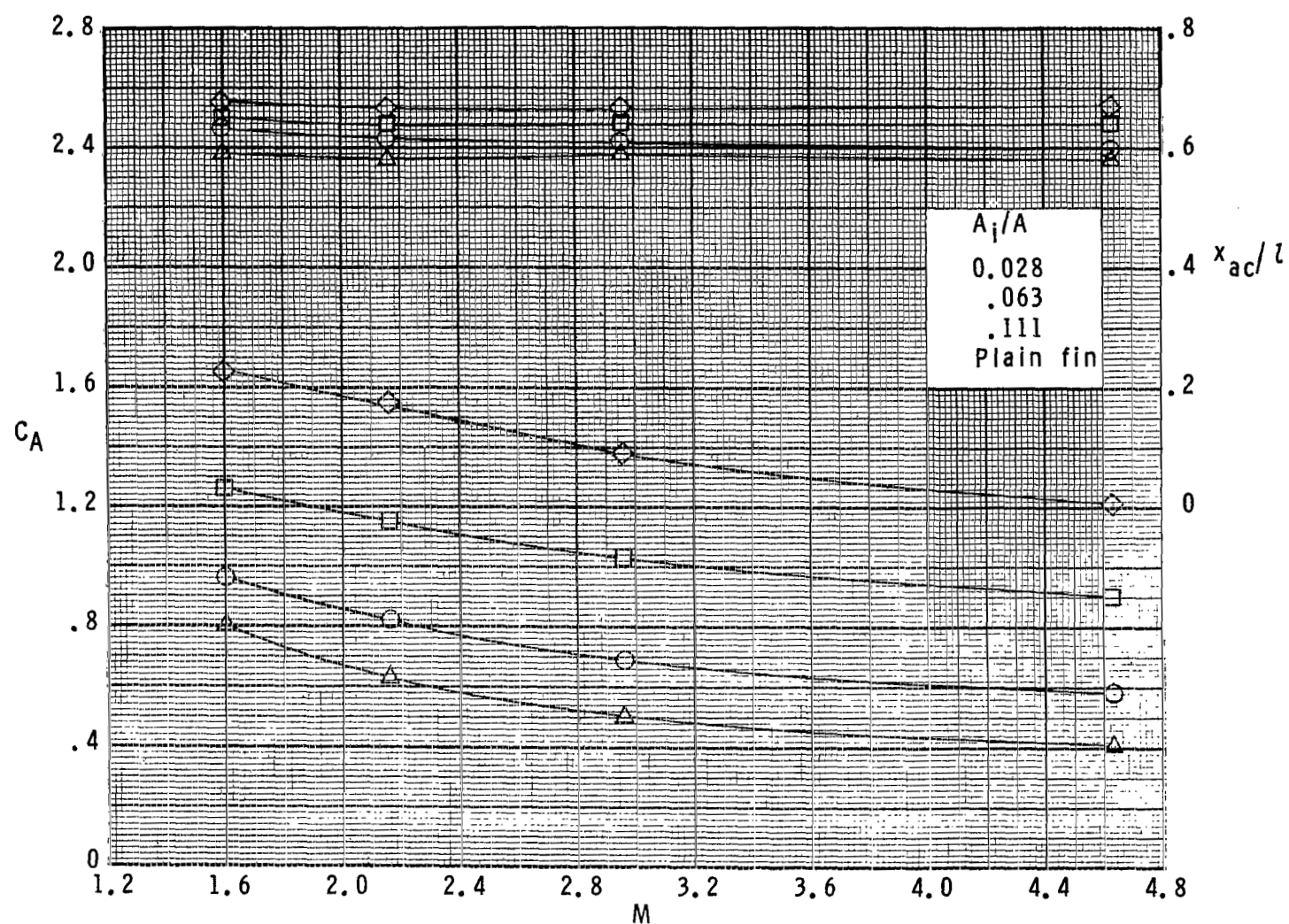
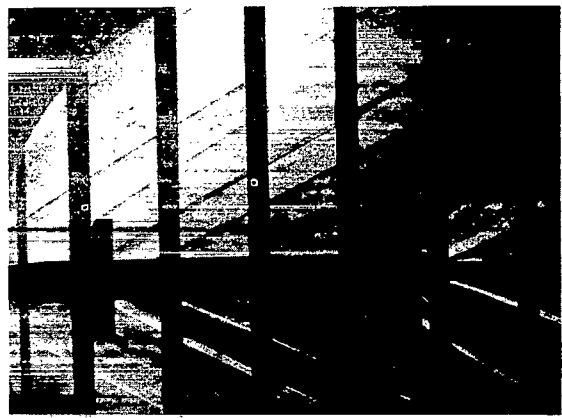
(b) Flow-through nacelle and  $\delta_{roll} = 0^\circ$ .

Figure 34.- Concluded.



M = 1.60;  $\alpha$  = 0.4°



M = 2.16;  $\alpha$  = 1.2°



M = 1.60;  $\alpha$  = 8.4°



M = 2.16;  $\alpha$  = 9.2°



M = 1.60;  $\alpha$  = 20.5°



M = 2.16;  $\alpha$  = 21.2°

(a)  $A_e/A_i = 0.90$ .

L-78-132

Figure 35.- Schlieren photographs of  $A_i/A = 0.063$  ram-air-spoiler tail-fin configuration at  $\phi = 0^\circ$ .



$M = 1.60; \alpha = 0.4^\circ$



$M = 2.16; \alpha = 1.2^\circ$



$M = 1.60; \alpha = 8.4^\circ$



$M = 2.16; \alpha = 9.3^\circ$



$M = 1.60; \alpha = 17.4^\circ$

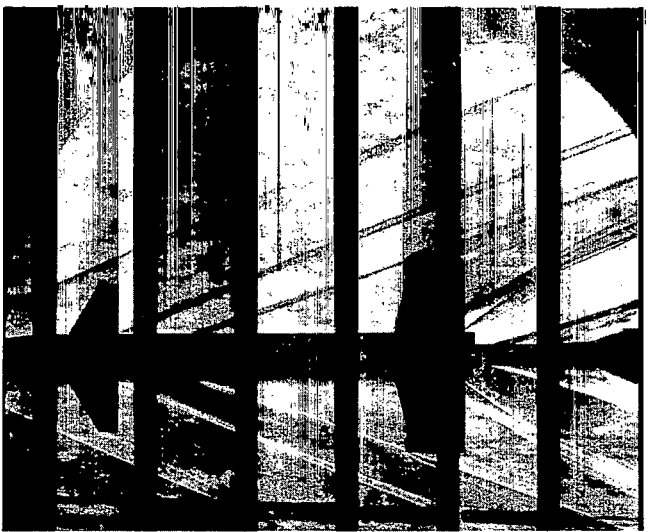


$M = 2.16; \alpha = 21.2^\circ$

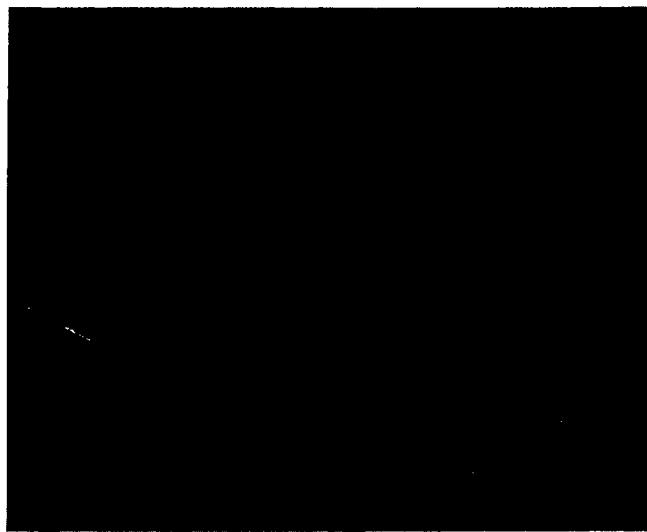
(b) Flow-through nacelle.

L-78-133

Figure 35.- Continued.



M = 2.96;  $\alpha = 0.1^\circ$



M = 2.96;  $\alpha = 8.1^\circ$



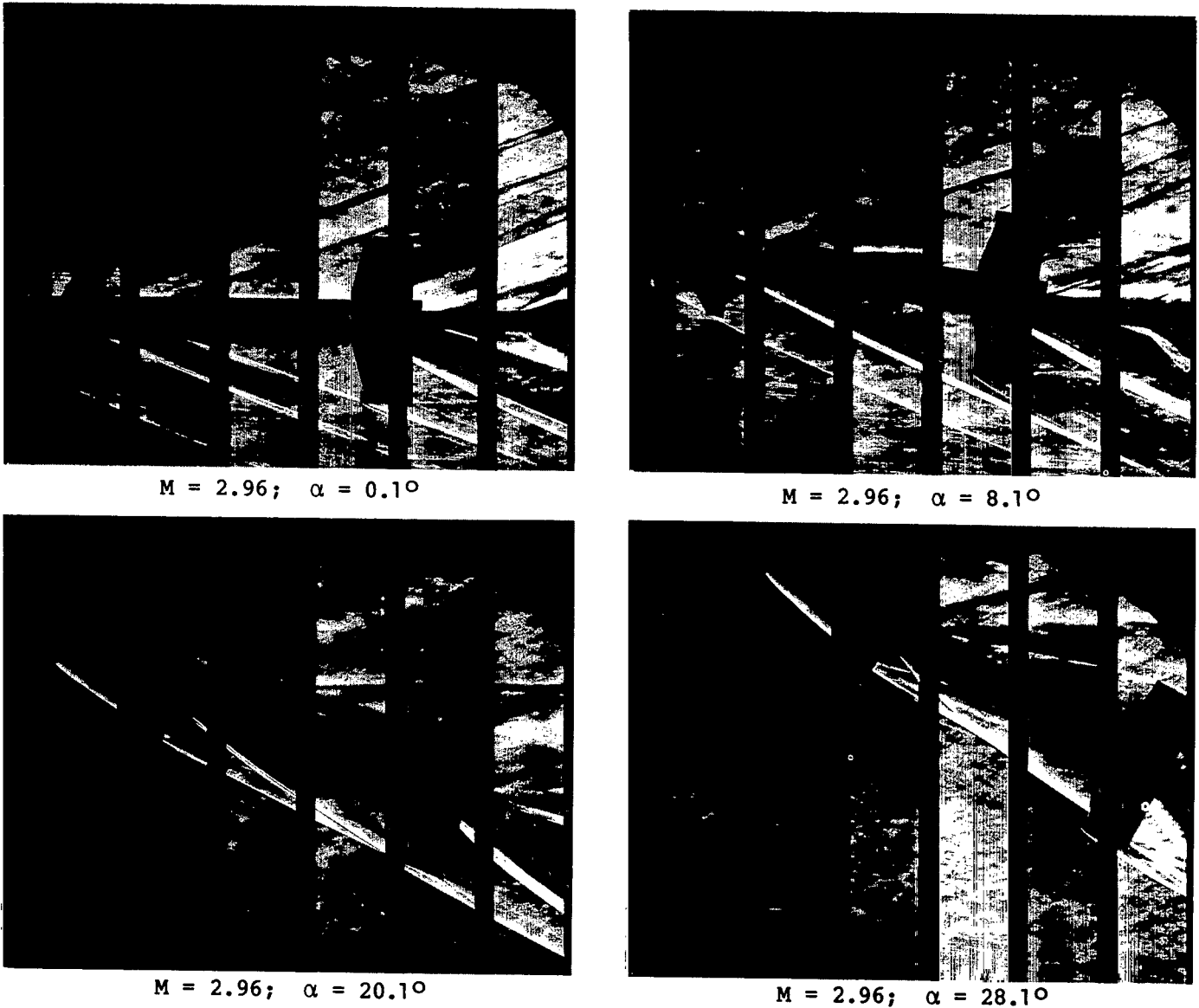
M = 2.96;  $\alpha = 20.1^\circ$



M = 2.96;  $\alpha = 28.1^\circ$

(c)  $A_e/A_i = 0.90.$

L-78-134



(d) Flow-through nacelle.

L-78-135

Figure 35.- Continued.



$M = 4.63; \alpha = 0.8^\circ$



$M = 4.63; \alpha = 8.8^\circ$



$M = 4.63; \alpha = 20.8^\circ$

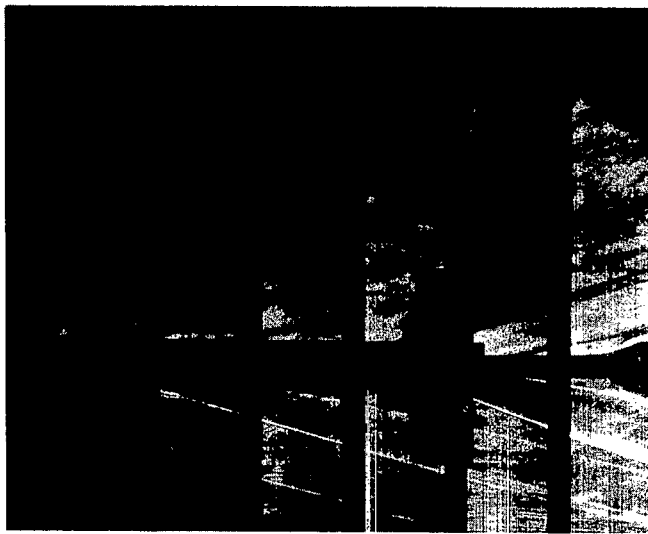


$M = 4.63; \alpha = 28.8^\circ$

(e)  $A_e/A_i = 0.90$ .

L-78-136

Figure 35.- Continued.



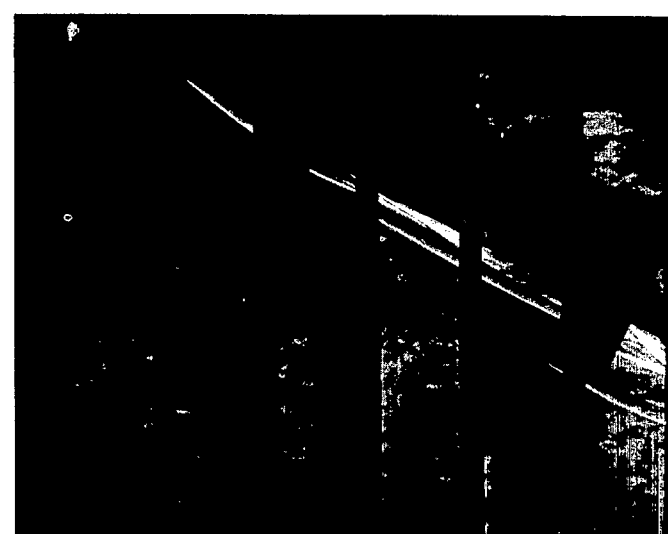
M = 4.63;  $\alpha$  = 0.8°



M = 4.63;  $\alpha$  = 8.8°



M = 4.63;  $\alpha$  = 20.8°



M = 4.63;  $\alpha$  = 28.8°

L-78-137

(f) Flow-through nacelle.

Figure 35.- Concluded.

1. Report No. NASA TP-1353	2. Government Accession No.	3. Recipient's Catalog No.		
4. Title and Subtitle  AN EXPERIMENTAL WIND-TUNNEL INVESTIGATION OF A RAM-AIR-SPOILER ROLL-CONTROL DEVICE ON A FORWARD-CONTROL MISSILE AT SUPERSONIC SPEEDS		5. Report Date December 1978		
7. Author(s)  A. B. Blair, Jr.	6. Performing Organization Code			
9. Performing Organization Name and Address  NASA Langley Research Center Hampton, VA 23665		8. Performing Organization Report No.  L-12518		
12. Sponsoring Agency Name and Address  National Aeronautics and Space Administration Washington, DC 20546		10. Work Unit No.  505-11-23-03		
11. Contract or Grant No.				
13. Type of Report and Period Covered  Technical Paper				
14. Sponsoring Agency Code				
15. Supplementary Notes				
16. Abstract  A parametric experimental wind-tunnel investigation has been made at supersonic Mach numbers to provide design data on a ram-air-spoiler roll-control device that is to be used on forward-control cruciform missile configurations. The results indicate that the ram-air-spoiler tail fin is an effective roll-control device and that roll control is generally constant with vehicle attitude and Mach number unless direct canard and/or forebody shock impingement occurs. The addition of the ram-air-spoiler tail fins resulted in only small changes in aerodynamic-center location. For the ram-air-spoiler configurations tested, there are large axial-force coefficient effects associated with the increased fin thickness and ram-air momentum loss.				
17. Key Words (Suggested by Author(s))  Ram-air-jet spoiler Cruciform missiles Canard-controlled missiles Missile aerodynamics Roll-control device Jet interaction		18. Distribution Statement  Unclassified - Unlimited		
19. Security Classif. (of this report) Unclassified		20. Security Classif. (of this page) Unclassified	21. No. of Pages 188	22. Price* \$9.00
Subject Category 02				

National Aeronautics and  
Space Administration

Washington, D.C.  
20546

Official Business

Penalty for Private Use, \$300

SPECIAL FOURTH CLASS MAIL  
BOOK

Postage and Fees Paid  
National Aeronautics and  
Space Administration  
NASA-451



20 1 1U,A, 010879 S00903DS  
DEPT OF THE AIR FORCE  
AF WEAPONS LABORATORY  
ATTN: TECHNICAL LIBRARY (SUL)  
KIRTLAND AFB NM 87117



POSTMASTER: If Undeliverable (Section 158  
Postal Manual) Do Not Return